RATIONAL DESIGN OF 2,4-DISUBSTITUTED QUINAZOLINE SMALL MOLECULES TO INHIBIT THE INFLAMMATORY CYTOKINE ONCOSTATIN M

by

Riley Olsen

A thesis

submitted in partial fulfillment

of the requirements for the degree of

Master of Science in Chemistry

Boise State University

December 2020

© 2020

Riley Olsen

ALL RIGHTS RESERVED

BOISE STATE UNIVERSITY GRADUATE COLLEGE

DEFENSE COMMITTEE AND FINAL READING APPROVALS

of the thesis submitted by

Riley Olsen

Thesis Title: Rational Design of 2,4-Disubstituted Quinazoline Small Molecules to Inhibit the Inflammatory Cytokine Oncostatin M

Date of Final Oral Examination: 18 August 2020

The following individuals read and discussed the thesis submitted by student Riley Olsen and they evaluated their presentation and response to questions during the final oral examination. They found that the student passed the final oral examination.

Don Warner, Ph.D.	Chair, Supervisory Committee
Matthew King, Ph.D.	Member, Supervisory Committee
Lisa Warner, Ph.D.	Member, Supervisory Committee
Cheryl Jorcyk, Ph.D.	Member, Supervisory Committee

The final reading approval of the thesis was granted by Don Warner, Ph.D., Chair of the Supervisory Committee. The thesis was approved by the Graduate College.

DEDICATION

I would like to dedicate this thesis to my parents, Don and Kimberly Olsen. I would like to thank them for inspiring my curiosity at a young age and for always supporting me and encouraging me to pursue my dreams and do things that I am passionate about. I would also like to thank them for their endless patience with me, as I was not always the most angelic child.

ACKNOWLEDGMENTS

I would like to thank my advisor and my mentor, Dr. Don Warner, for graciously allowing me to work in his lab throughout both my undergraduate and graduate studies. I am very grateful for his ability to see my potential and his unwavering support, always pushing me to become a better chemist and a better person. I am also very grateful for his critical and honest feedback about my work, helping me to refine my experimental techniques and writing abilities. I would like to thank him for his patience and dedication, often staying up late and working on the weekends to help me succeed. Under his guidance I achieved accomplishments I never thought that I could.

I would like to acknowledge the members of my collaborative lab group for assisting me in my research. Specifically, I would like to thank Joseph Tuccinardi for his help assisting me in countless experiments. Without his help, much of my research would not have been successful. In addition, I would like to thank Cody Wolf for performing *in vitro* experiments and Grace Coughlin for performing fluorimetry assays.

I would like to thank my committee members, Dr. Matthew King, Dr. Lisa Warner, and Dr. Cheryl Jorcyk for always having an open door whenever I had questions and for providing invaluable feedback on my work. Additionally, I would like to thank Dr. Joe Dumais, Dr. Xinzhu Pu, and Dr. Matthew Turner for their assistance characterizing my synthesized compounds and Laura Bond for her assistance with statistical analysis.

Lastly, I would like to thank the Boise State Department of Chemistry and Biochemistry for providing me with a teaching assistantship and the Chemistry and Biochemistry Graduate Program for providing me a research assistantship that allowed me to dedicate my time to the research project to fund my education. The work in this thesis was also supported by the METAvivor Quinn Davis Northwest Arkansas METSqueradeFund, an Institutional Development Awards (IDeA) from the National Institute of General Medical Sciences of the National Institutes of Health under Grants #P20GM103408. Support was also received from the Biomolecular Research Center at Boise State University with funding from the National Science Foundation, Grants #0619793 and #0923535; the MJ Murdock Charitable Trust; and the Idaho State Board of Education.

ABSTRACT

Inflammation is one of the body's most important natural defense mechanisms involved in wound healing. It is usually triggered by a harmful event, such as physical trauma or exposure to external stimuli including bacteria, fungi, viruses, harmful chemicals, or environmental particulates. The inflammatory process brings blood containing inflammatory mediators consisting of leukocytes, hormones, and cytokines to the site of trauma to begin healing. However, the lack of a proper inflammatory response or an overactive response can lead to further progressive tissue damage resulting in chronic inflammatory conditions or death. The cytokine oncostatin M (OSM) is of particular interest due to the pivotal role it plays in chronic inflammatory diseases like rheumatoid arthritis, inflammatory bowel disease, and various forms of cancer. These diseases have a detrimental impact on a person’s quality of life and life expectancy, as well as the economy and health care system.

There is currently no clinically approved treatment targeting OSM. Thus, we propose the development of a small molecule inhibitor (SMI) targeting OSM. Using the known crystal structure of OSM combined with computational methods, a sample of 10,000 randomly selected molecules from online databases were docked in the OSM binding site 3, the site presumably responsible for binding to its receptor. The most energetically favorable binding poses were used to create a weighted density map (WDM) that shows the probability of aromatic carbons, hydrogen bond acceptors, and hydrogen bond donors to bind to OSM at particular locations in site 3. A 2,4-disubstituted quinazoline SMI was rationally designed that constructively overlaid with the WDM and was predicted to bind with high affinity based on computational docking studies.

The SMI and analogs thereof, termed the SMI-27 series, were synthesized using a 4-step reaction sequence to create a small library to be tested against OSM. In order to evaluate the ability of the SMIs to inhibit OSM activity and to determine cytokine binding specificity, enzyme-linked immunosorbent assays (ELISAs) and western blot assays were performed. Fluorescence quenching experiments were used to determine the binding affinity of SMI analogs toward OSM. Finally, chemical shift perturbation NMR experiments were used to identify the important amino acids required for binding of the SMI to OSM.

All of the SMI-27 analogs tested by ELISA inhibited OSM induced pSTAT3 expression below the level of the control. Additionally, SMIs 27B3 and 27B5 showed specific binding to OSM, and not to leukemia inhibitory factor (LIF) or interleukin-6 (IL-6), structurally related cytokines. The fluorescence quenching assays indicate that all SMIs exhibited direct binding to OSM, with 27B12 having a Kd of 5.1 ± 2.7 μM. Finally, the chemical shift perturbation assay identified several amino acids that appear to be involved in SMI binding. Importantly, three of these, tentatively assigned as Arg91, Leu92, and Gly166, are all located in OSM site 3. These experiments support our hypothesis that an SMI can be used to inhibit OSM activity and lay a solid foundation for the development of an SMI drug candidate that would provide a significant advancement in clinical treatments of OSM-related diseases.

TABLE OF CONTENTS

DEDICATION iv

ACKNOWLEDGMENTS v

ABSTRACT vii

LIST OF TABLES xi

LIST OF FIGURES xii

LIST OF ABBREVIATIONS xiv

CHAPTER ONE: INTRODUCTION TO THE INFLAMMATORY CYTOKINE ONCOSTATIN M 1

- Inflammation 1
    - Introduction to Inflammation 1
    - Acute vs. Chronic Inflammation 2
    - Economic Burden of Inflammatory Diseases 3
- The Inflammatory Cytokine Oncostatin M 4
    - Introduction to Cytokines 4
    - Oncostatin M 5
    - OSM in Breast Cancer and Metastasis 5
    - Structure and Function of OSM and LIF 6
- Inhibiting OSM: Targeting a Protein-Protein Interaction 9
    - Introduction to Targeting Proteins 9

Methods for Disrupting Protein-Protein Interactions 11

Summary 16

References 18

CHAPTER TWO: DESIGN AND SYNTHESIS OF SMALL MOLECULES TARGETING OSM 28

Overview of Chapter 28

Prior Work to Identify OSM Binding Sites 28

Prior Work to Identify and Develop SMIs for OSM 33

Computationally Aided Rational Design of SMI-27 39

Synthetic Route and Steps to Form SMI-27 Analogs 46

Summary 48

References 50

CHAPTER THREE: EVALUATION OF SMI-27 ANALOGS TARGETING OSM 52

Overview of Chapter 52

Nomenclature of SMI-27 Analogs 52

Enzyme-Linked Immunosorbent Assay 54

Western Blot Assay 57

Fluorescence Quenching Assay 58

NMR Chemical Shift Perturbation Assay 66

Conclusions and Future Directions 68

References 73

APPENDIX A 75

APPENDIX B 102

LIST OF TABLES

Table 2.1. SMI-27 Generic structure and substituents....42

Table 3.1. SMI-27 Nomenclature....54

Table 3.2. SMI-27 binding data....62

LIST OF FIGURES

Figure 1.1. Signaling cascade of OSM and LIF...7

Figure 1.2. LIF and OSM structures 8

Figure 1.3. Surface model of LIF and OSM. 9

Figure 1.4. Protein mimitics to inhibit Bak/Bcl-x_L complex formation. 13

Figure 1.5. Small molecule inhibitors of IL-2. 16

Figure 2.1. OSM crystal structure and receptor binding sites. 30

Figure 2.2. In silico identification of ligand binding sites on OSM...........................33

Figure 2.3. ELISA results of the top 26 hits from the HTVS. 35

Figure 2.4. Synthesis of SMI-10 analogs 36

Figure 2.5 Synthesis of SMI-26 analogs. 37

Figure 2.6. Structures and Kd values of the top SMI-10 and SMI-26 analogs............38

Figure 2.7. Weighted density maps with respect to OSM site 3................................40

Figure 2.8. Weighted density map and surface model of an SMI-27 analog docked in OSM site 3. 41

Figure 2.9. Amino acids predicted to be important for OSM/SMI binding. 43

Figure 2.10. Predicted OSM/SMI stabilizing binding interactions..............................44

Figure 2.11. General synthesis of SMI-27..47

Figure 2.12. Meerwein cyclization mechanism. 48

Figure 3.1. Enzyme-linked immunosorbent assay of SMI-27 analogs. 56

Figure 3.2. Western blot assays of SMI 27B3 and 27B5. 58

Figure 3.3. Fluorescence quenching assay for Kd determination. 59

Figure 3.4. Kd values of SMI-27 analogs. 60

Figure 3.5. Chemical shift perturbation assay. 68

Figure 3.6. Alternative synthesis of 2,4-disubstituted quinazolines. 70

Figure 3.7. Synthesis of 2,4-disubstituted pyrimidines. 71

Figure 3.8. Synthesis of 2,4-disubstituted pyrazolopyrimidines.................................72

LIST OF ABBREVIATIONS

AKT	Protein kinase B
CSP	Chemical shift perturbation
CTC	Circulating tumor cells
ELISA	Enzyme linked immunosorbent assay
FQ	Fluorescence quenching
gp130	Glycoprotein 130
hGH	Human growth hormone
hGHbp	Human growth hormone binding protein
HSQC	Heteronuclear single quantum correlation
HTVS	High-throughput virtual screen/screening
IBD	Inflammatory bowel disease
IL-6	Interleukin-6
JAK	Janus kinase
Kd	Disassociation constant
LIF	Leukemia inhibitory factor
LIFR	Leukemia inhibitory factor receptor
mAb	Monoclonal antibody
MAPK	Mitogen-activated protein kinase
OSM	Oncostatin M

OSMR	Oncostatin M receptor
PI3K	Phosphoinositide 3-kinase
PPI	Protein-protein interaction
RA	Rheumatoid arthritis
SAR	Structure-activity relationship
SELEX	Systematic evolution of ligands by exponential enrichment
SMI	Small molecule inhibitor
STAT	Signal transduction and activator of transcription
VEGF	Vascular endothelial growth factor
WDM	Weighted density map

CHAPTER ONE: INTRODUCTION TO THE INFLAMMATORY CYTOKINE ONCOSTATIN M

Inflammation

Introduction to Inflammation

Inflammation is a non-specific immune response that plays a central role in the complex bodily response to various stimuli.[1] It is usually triggered by some kind of harmful event, such as physical trauma, cellular damage, and exposure to irritants including bacteria, fungi, viruses, harmful chemicals or environmental particulates.[1-3] Inflammation will typically present itself on the surface of the skin in the form of swelling, redness, and heat near the site of the injury or irritation, causing pain and potential loss of function.[2] Inflammation also occurs internally and the manifestation is often less apparent inside the joints, intestines, and breast tissue.[4]

Inflammation has both positive and negative benefits for humans and other organisms. Inflammation is necessary for healing wounds, but the lack of a proper inflammatory response or an overactive response can lead to further progressive tissue damage resulting in chronic conditions or death.[1] The inflammation process begins by increasing blood flow to the affected area, carrying and allowing the release of inflammatory mediators into the body at the site of trauma to begin the healing process. These mediators include leukocytes, hormones, pro- and anti-inflammatory cytokines, and many others.[2, 3, 5, 6] Since inflammation is usually associated with pain, swelling, injury, or disease, it is often viewed as detrimental. However, it is one of the body's most important natural defense mechanisms.[1] The inflammation process helps the body to target and remove foreign or harmful stimuli. Additionally, swelling naturally stabilizes the injury and pain alerts the body to protect the injury in order to prevent any further damage.

Acute vs. Chronic Inflammation

There are two types of inflammation: acute and chronic.[1, 3] Acute inflammation is a short-term inflammation that occurs as a result of tissue trauma and appears almost immediately, ranging from seconds to hours following exposure to harmful stimuli.[3] A few examples of stimuli that induce an acute inflammatory response are minor scratches and cuts, exposure to irritating chemical agents, allergic reactions, lacerations, and blunt force trauma. Symptoms of acute inflammation are typically short-lived and generally last on the order of a few days to weeks.[3]

While acute inflammation mediates the recovery of the body in response to injury, sustained inflammation may result in the onset of chronic inflammation that may have deleterious effects on one’s health if not properly treated.[4] Chronic inflammation, frequently a causative factor in multiple disease types, is a long-term inflammation that can last for months, years, and in some cases a person’s entire life.[2] Chronic inflammation can pose a serious health risk, as it is associated with the onset of cardiovascular diseases, diabetes, rheumatoid arthritis (RA), chronic obstructive pulmonary disease, allergies, inflammatory bowel disease (IBD), ulcerative colitis, Crohn’s disease, and various forms of cancer, among others.[1, 5]

Chronic inflammatory diseases can significantly increase the risk of certain cancers, which is also considered an inflammatory disease. For example, inflammation in the gastrointestinal tract, as in ulcerative colitis and Crohn’s disease, greatly increases the risk of a person developing colon or prostate cancer.[7] Similarly, inflammation of the breasts due to traumatic injury or surgical modifications has also been associated with an increased risk of breast cancer.[8] A cancerous tumor can be thought of as a wound that continuously tries to heal itself but fails to do so.[9] This means that the attempted healing process continuously occurs and biological healing agents are sent to the site of the tumor, which leads to uncontrolled cell proliferation, and the cycle continues as the tumor/wound never actually heals. Such chronic conditions tend to frequently lead to early death, and mitigation of chronic inflammation is thought to be one of the primary reasons for an increase in life expectancy.[10]

Economic Burden of Inflammatory Diseases

Chronic inflammation affects more than a person’s quality of life and life expectancy; it also detrimentally impacts the economy and the health care system.[11] It causes people to be unable to perform simple everyday tasks and go into work, leading to lost wages and economic production. Additionally, treating inflammatory diseases incurs excessive costs for the person affected, as well as the health care system. It is estimated that over 60% of Americans have at least one chronic condition, over 40% have at least two, and over 12% have five or more.[12] Notably, Americans with five or more chronic conditions account for over 40% of the total health care spending in the United States.[12] The overall financial burden attributed to chronic inflammatory diseases is difficult to estimate given their prevalence. However, for some conditions the cost incurred by patients is well-documented. For example, nearly 1.6 million Americans have rheumatoid arthritis, which costs approximately $6200 per patient each year.[11] The average yearly expense to 1.3 million Americans with psoriatic arthritis is estimated to be $3600 per patient per year.[11] Over 54 million Americans are affected by some form of arthritis, which is almost 25% of all Americans. At an estimated loss of $164 billion in yearly wages, arthritis is thought to be the leading cause of Americans missing work.[13] The same study found that arthritis is responsible for over $140 billion per year in healthcare costs, indicating a total financial burden in the United States of over $300 billion per year. Cancer, the second leading cause of deaths of Americans, is estimated to cost over $170 billion per year for medical treatment.[14] The number of deaths and the extraneous cost associated with chronic inflammatory-related diseases highlights a serious need for prevention and better treatment.

The Inflammatory Cytokine Oncostatin M

Introduction to Cytokines

To better treat inflammatory diseases, the cause of the diseases must be further studied and understood. Cytokines are small proteins involved in cell signaling and have a role in inflammation.[15] Specifically, The interlukin-6 (IL-6) family cytokines, sometimes referred to as the glycoprotein 130 (gp130) cytokine family, are associated with multiple inflammatory diseases including rheumatoid arthritis, inflammatory bowel disease, and the progression of a variety of cancers.[16-18] All IL-6 cytokines initiate cell signaling by forming a heterodimeric complex with gp130 as a common receptor and a second receptor that is selective for the given cytokine. The IL-6 family cytokine Oncostatin M (OSM) is of particular relevance as its activity has been directly linked to many of the previously mentioned diseases. OSM is found to be highly overexpressed in synovial tissue and fluids in RA patients, intestinal mucosa in IBD patients, and serum levels of breast cancer patients compared to healthy individuals.[17, 19, 20]

Oncostatin M

OSM was first identified and characterized using U937 macrophage cells in 1986 and gained attention after showing antiproliferative effects among various human cancer cell lines, including the A375 melanoma and A549 lung carcinoma cell lines.[21, 22] Since then, it has been shown to play a pleiotropic role in cell differentiation, bone and skeletal tissue metabolism, liver function, inflammatory responses, and many other biological functions.[23-26] A variety of cell populations secrete OSM, including macrophages, monocytes, neutrophils, T cells, and a variety of cancer cells.[27-30] Secreted OSM levels increase in the event of acute and chronic inflammation.[17, 31] Despite all the attention OSM has received, much remains unclear as to how it binds to its receptor, OSMR, and its extensive role throughout the body.[32]

OSM in Breast Cancer and Metastasis

The role of OSM in facilitating breast cancer metastasis is a primary driver of the research described herein. While OSM was first shown to have antiproliferative effects against certain cancer cell lines, the Jorcyk lab have several reports that show that OSM increases the metastatic potential of breast and other types of cancers.[33, 34] They found, for example, that OSM initiates angiogenesis, tumor cell detachment, and correlates to an increased number of circulating tumor cells (CTCs).[34-37] The migration of CTCs though the circulatory system allows for metastasis to occur in distant organs, such as the lungs and bones.[35, 38] Recently, Tawara et al. found that high levels of OSM correlated with high levels of IL-6 in serum of breast cancer patients when compared to healthy patients.[20] This is important because high levels of OSM and IL-6 in breast cancer patients is correlated with a reduction of patient survival and high levels of OSM were also shown to increase the potential for breast cancer metastasis.[20]

Structure and Function of OSM and LIF

The cytokine most closely related to OSM in structure and function is the IL-6 family member leukemia inhibitory factor (LIF). Their commonality is believed to have arisen from a gene duplication event on human chromosome 22.[39] OSM and LIF signaling cascades are remarkably similar but use slightly different receptors and oppositely recruits the receptors (Figure 1.1). LIF signals through heterodimeric LIFR-gp130 complex by first binding to LIF receptor (LIFR) and then recruiting gp130.[32, 40] OSM, in contrast, first binds to gp130 and then OSMR is recruited to make a complete complex.[41] After creating the ligand-receptor complex, various signaling cascades are activated by phosphorylation. Both LIF and OSM activate the Janus kinase/signal transduction and activator of transcription (JAK/STAT) pathway, resulting in the activation of STAT proteins, most notably STAT3, that are associated with a variety of immune responses.[42] Both cytokines also activate the phosphoinositide 3-kinases/protein kinase B (PI3K/AKT) and mitogen-activated protein kinase (MAPK) signaling pathways, crucial for cell survival and differentiation.[42, 43]

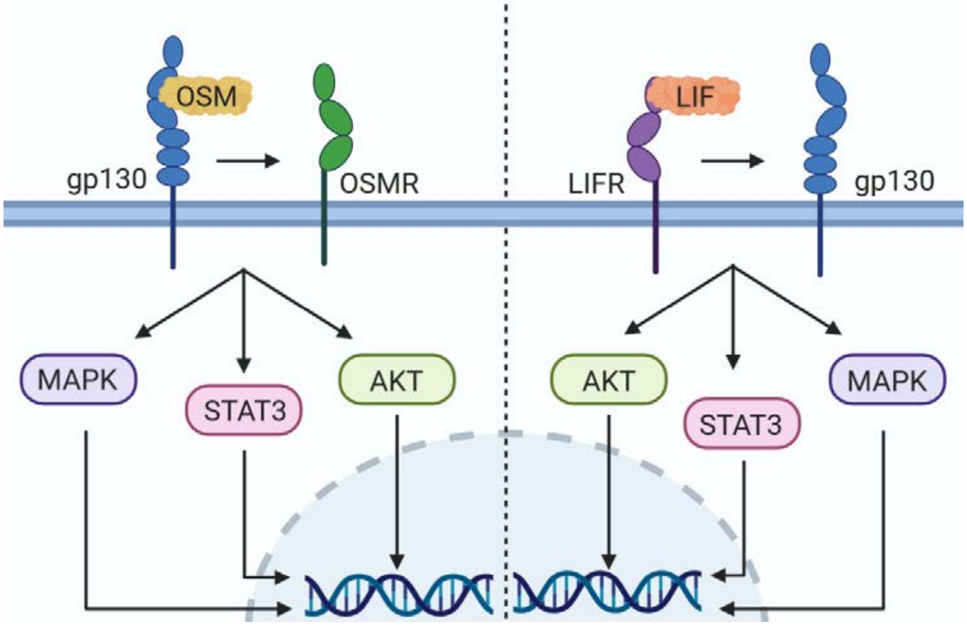

Figure 1.1. Signaling cascade of OSM and LIF.
OSM first binds to gp130 and recruits OSMR to create a complete receptor complex. LIF, in contrast, binds to LIFR and recruits gp130. Both activate similar pathways, including JAK/STAT, MAPK, and AKT pathways, that result in changes in gene expression.

The redundancy in OSM and LIF signaling is explained by their similarity in structure. Both are composed of a four helical bundle (Figure 1.2).[44, 45] Interestingly, while LIF can only bind to LIFR, OSM can bind to both OSMR and LIFR. All IL-6 family cytokines that bind to LIFR contain a conserved phenylalanine and lysine amino acid residue pair.[44] The conserved residues of OSM are Phe160 and Lys163, whereas in LIF they are Phe157 and Lys159 (Figure 1.3). Studies show that when either of these residues are mutated in OSM or LIF, cell signaling dramatically decreases.[45] This suggests that targeting the domain around Phe160 and Lys163 in OSM with a therapeutic would block it from binding to OSMR and inhibit its cell signaling ability. However, due to the close structural similarities, LIF must always be considered to ensure specific binding to OSM and not LIF.

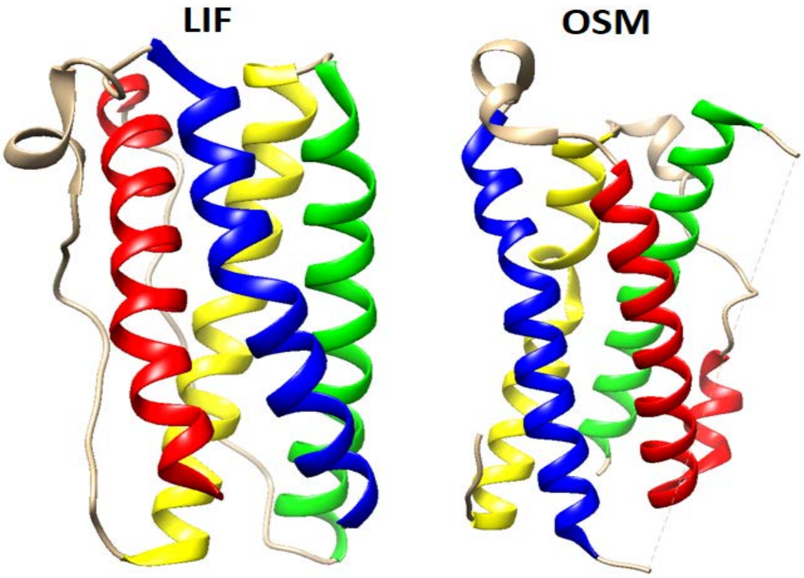

Figure 1.2. LIF and OSM structures
The four alpha helical bundles that compose LIF (left) and OSM (right)**.**

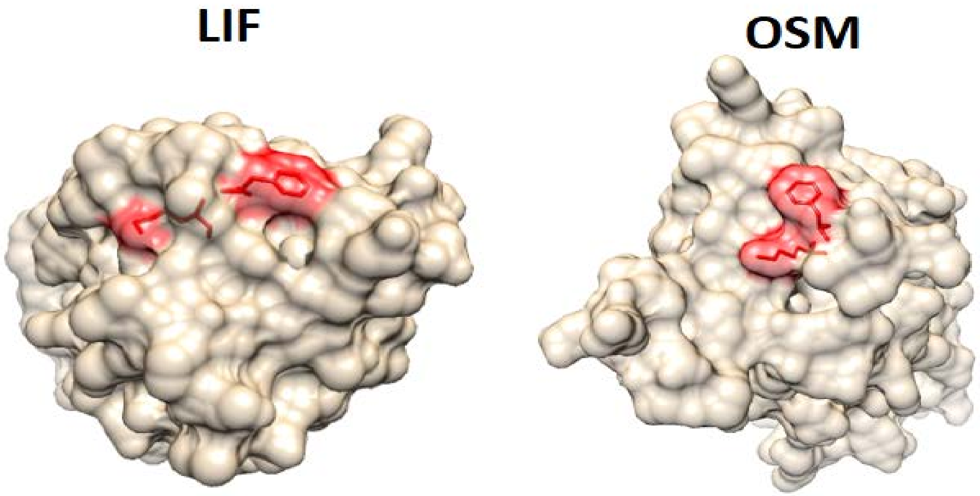

Figure 1.3. Surface model of LIF and OSM.
A surface model of LIF (left) and OSM (right) with phenylalanine and lysine residues (shown in red) thought to be responsible for binding to LIFR. The residues on LIF are Phe157 and Lys159. On OSM, they are Phe160 and Lys163.

Inhibiting OSM: Targeting a Protein-Protein Interaction

Introduction to Targeting Proteins

The field of targeting and disrupting protein-protein interactions (PPIs) is an interesting and challenging field, with the potential to create novel therapeutics for diseases previously thought to be untreatable or incurable. Protein-protein interactions account for a large portion of protein-based biology within and outside of cells and play a role in many diseases.[46] Proteins such as OSM and LIF bind to their receptors located on the outside of the cell surface and have proven particularly difficult to disrupt.[40] This is due in part to the crystal structure of OSMR being unknown, providing little to no information on how to best mimic the receptor to effectively compete with OSM binding to OSMR. In addition, OSM and LIF are very similar in structure, making it difficult to design a therapeutic that will selectively bind to one and not the other. This section will discuss methods and examples of targeting proteins and disrupting PPIs.

In theory, targeting a protein is as simple as the child's game of placing the correct shape block into the correct shape hole (i.e., a square block into a square hole, a triangle block into a triangle hole, etc.), however, it is not always that simple. In most cases, before you can design the drug (the block), you must first identify the target protein active site (the hole). There has been a great success in the field of designing therapeutics that inhibit enzymes (i.e., proteins that catalyze biological chemical reactions). Enzymes are relatively easy to target due to the nature of their active site shape and activity, which is almost always a deep and well-defined pocket that is shielded from exposure to the surrounding solvent.[47] The native substrate the enzyme performs its catalytic function on can often provide an excellent template for a drug.[47] Frequently, drugs can be designed to resemble the native substrate but are less easily metabolized, allowing for inhibition of the target enzyme.

In contrast, designing therapeutics targeting proteins that participate in PPIs is not nearly as simple and has seen much less success due to several different factors. Most protein surfaces involved in PPIs are relatively featureless—flat and without deep, well-defined binding pockets. Typically, there are no native substrates to build templates from, and the amino acid residues responsible for binding are frequently not identified. Furthermore, the region of the protein responsible for binding is often large and discontinuous and interacts with other large and discontinuous protein surfaces. These interactions often occur through multiple points of contact, rendering it difficult for a small molecule to disrupt.[47]

The functional epitope, or the active binding site of a protein responsible for binding to its receptor, is often referred to as a “hot spot”. A common method of revealing hot spots is through alanine scanning mutagenesis experiments that involve systematically replacing each amino acid in the protein with an alanine and observing the change in binding free energy or biological activity of each mutant structure.[48, 49] A classic example of using this technique for identifying residues important for protein-protein interactions was conducted in 1989 by Cunningham and Wells in their work with human growth hormone (hGH) and its receptor human growth hormone binding protein (hGHbp).[48] It was found that of the 31 side chains on the binding surface, eight amino acid residues accounted for nearly 85% of the binding energy, and over half of the amino acid residues on the surface played no part in the binding interaction at all.[49] This pivotal research shows that a relatively small set of residues are responsible for hGH-hGHbp binding, suggesting that the interaction could be disrupted using a small molecule that mimics the binding epitope of either the protein or its receptor.[49, 50] Since then, many studies have used alanine scanning to identify protein hot spots, including OSM.[32, 45, 51, 52]

Methods for Disrupting Protein-Protein Interactions

Given the significant structural, topological, and functional differences of PPIs compared with other targets, disrupting PPIs requires a modified approach relative to traditional drug discovery and design. Some approaches that have proven successful in the past include the use of RNA aptamers, structures that mimic protein secondary structures, monoclonal antibodies, and synthetic small molecule inhibitors.[53-55] Each of these methods are briefly described below.

The drug Pegaptanib is an example of an RNA aptamer that successfully blocked a PPI. Brought to market by Pfizer in 2004, it is the first RNA aptamer approved by the FDA for clinical use.[53] Pegaptanib disrupts the protein vascular endothelial growth factor (VEGF) from binding to its receptors VEGFR1 and VEGFR2, which play a role in angiogenesis, age-related macular degeneration, and diabetic macular edema.[56-58] RNA aptamers were first isolated in the early 1990s from randomized pools of RNA using a method called Systematic Evolution of Ligands by Exponential Enrichment, commonly referred to as SELEX.[59, 60] They are composed of a chain of nucleic acids, usually 56-120 nucleotides long, and typically contain a variable region and two constant regions. The variable region is located in the middle, and the constant regions are located at both ends.[61] RNA aptamers bind with high affinity, high specificity, show relatively low immunogenicity, and have a long half-life, making them excellent candidates for drugs to target PPIs.[61]

A protein mimetic has been used to disrupt the Bak/Bcl-x_L complex that is highly overexpressed in many forms of cancer.[54] This is important because this complex prevents mutated cells from undergoing apoptosis even when apoptotic signals are generated by chemotherapy.[62] To determine the best secondary structure to mimic, a combination of the crystal structure of Bak/Bcl-x_L complex along with alanine scanning experiments were performed.[63] It was concluded that Val74, Leu78, Ile81, and Ile85 of Bak were involved in key binding interactions. Molecules that contained alkyl or aryl substituents such as isobutyl, isopropyl, and naphthalenemethylene were chosen to best mimic those hydrophobic residues of Bak (Figure 1.4). Suzuki-Miyaura coupling reactions were used to link together the individual molecules, creating a synthetic alpha helix with carboxylic acids on both ends of the molecule.[54] A Kd of 2.09 μM was obtained using only alkyl groups (Figure 1.4B). However, when the isopropyl group was changed to a naphthalenemethylene group binding affinity was dramatically improved and a Kd of 114 nM was obtained (Figure 1.4C). These results illustrate the impact minor changes to a molecule can significantly change its binding affinity.

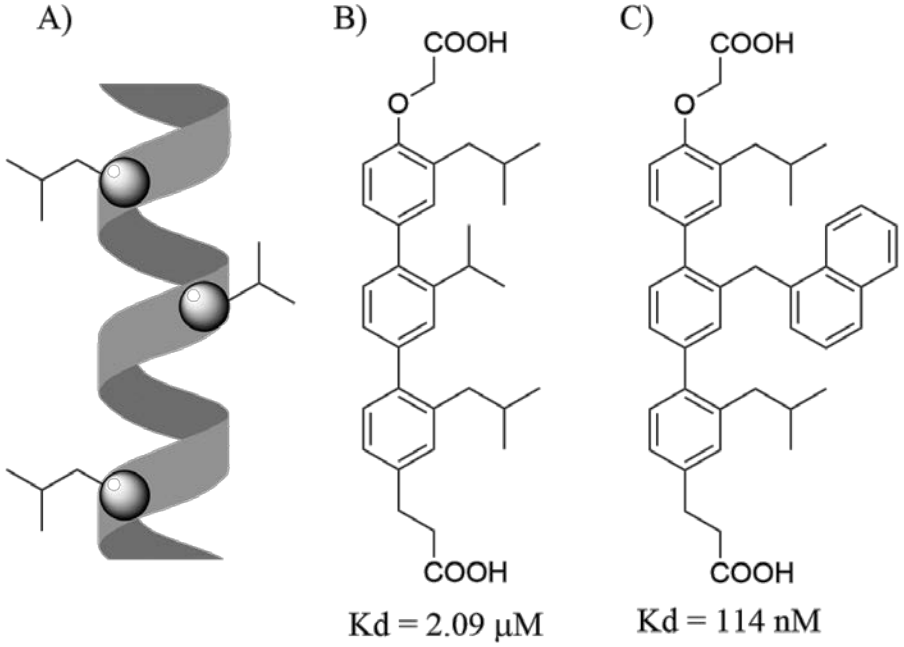

Figure 1.4. Protein mimitics to inhibit Bak/Bcl-x$_L$ complex formation. A) Helical structure that mimics the shape of a protein alpha helix. B) Synthetic protein alpha helix mimetic that contains only alkyl groups and has a Kd of 2.09 μM. C) Similar structure to compound "B" but replaces the isopropyl group with an aromatic naphthalene resulting in a 30-fold improvement of Kd to 114 nM.

Monoclonal antibodies (mAbs) have also proven successful in disrupting PPIs. Typically, mAbs are derived from antibodies in rodents and then humanized.[64] This process is performed by first taking the target protein and injecting it into a rodent. When the rodent has an immune response to the human antigen, its DNA is extracted. The rodent complementarity-determining region loop is transplanted to a human antibody framework and cloned. The cloned DNA is commonly expressed using Chinese hamster ovary cells or E.coli to obtain the mAb.[64, 65] The mAb can then be further engineered for higher specificity.[66] An example of using a mAb to disrupt a PPI is “anti-Tac” developed by Biogen and Abbvie and sold under the trade name Daclizumab, which inhibits interleukin-2 (IL-2) from binding to one of its receptors (IL-2Rα).[67] Anti-Tac has been used to treat adult T-cell leukemia in humans, providing a significant clinical advancement in the treatment of cancer.[68]

While mAbs can be beneficial for treating certain diseases, they also have their downsides. Daclizumab serves to illustrate the potential drawbacks of using mAbs as therapeutics. In March of 2018, Daclizumab was voluntarily withdrawn off the market due to immune-mediated disorders and the risk of liver injury.[69] Many mAbs have shown to be immunosuppressive compounds and have a very long half-life.[70] This could be problematic for a patient contracting an infection that requires an immediate immune response, as well as if a patient suffering an injury that requires an inflammatory response involving the targeted protein. Other disadvantages of mAbs include a short shelf-life (requiring refrigeration), not being orally bioavailable requiring parenteral administration, and high cost associated with development.[71, 72]

Synthetic small molecules inhibitors (SMIs) serve as another method to disrupt PPIs. An SMI targeting the disruption of the IL-2/IL-2Rα complex was originally developed by Roche in 1997.[55] The structure of IL-2 was elucidated by combining X-ray crystallography and NMR experiments. Next, site-directed mutagenesis was used to identify the amino acid residues Lys35, Arg38, Thr41, Phe42, Lys43, Tyr45, Glu62, and

Leu72 that are responsible for binding interactions between IL-2 and its receptor IL-2Rα.[73] Using structure-based drug design mimicking the Arg38-Phe42 region, a first-generation SMI was developed and had a Kd of 3 μM at biological pH (Figure 1.5A). This milestone study is the first example of an SMI that interrupts a cytokine/cytokine-receptor interaction.[55]

Attempts to make an even more potent second-generation SMI to disrupt IL-2/IL-2Rα complex formation uses “tethering”, a fragment-based method.[74] In this approach, fragments with low to mild binding affinities are tethered together to produce a compound with an even higher binding affinity than the individual fragments. Fragments are discovered using thiol containing molecules and introducing them to a modified protein structure containing cysteine under reductive conditions. If they come in contact with the protein surface and the cysteine, they form a disulfide bond with the protein. The fragments are then identified by obtaining a mass spectrum of the protein/fragment complex and subtracting the mass of the protein. It was found that small aromatic carboxylic acids were preferential.[75] Twenty analogs containing aromatic carboxylic acids were synthesized and eight of them had nanomolar binding dissociation constants, with the best analog having a Kd of 60 nM (Figure 1.5B). This shows that SMIs with μM binding affinity can be modified to obtain optimized compounds with low nM binding affinity and effectively disrupt cytokine/cytokine receptor interactions.

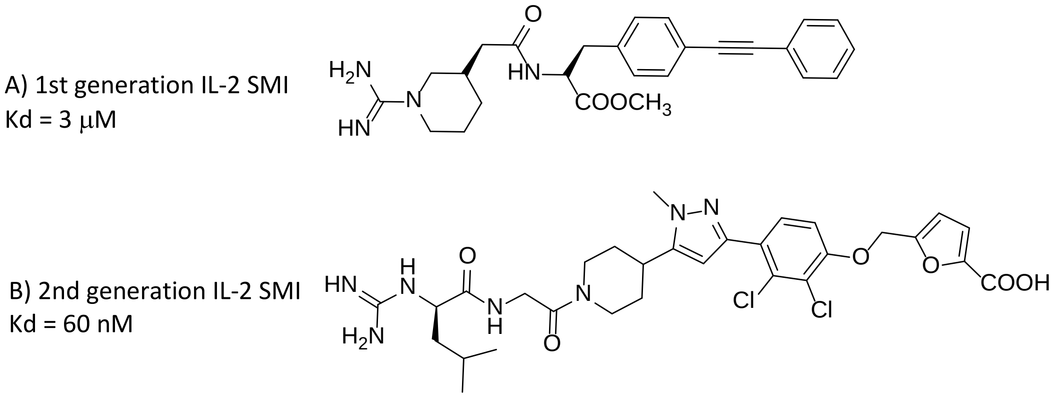

Figure 1.5. Small molecule inhibitors of IL-2.
A) The first-generation small molecule inhibitor of IL-2 with a 3 μM Kd. B) Second-generation small molecule inhibitor of IL-2 developed using a fragment-based method and exhibited a Kd of 60 nM, showing a significant improvement from the first-generation molecule.

Summary

Inflammatory diseases have a detrimental impact on both a person's health and the economy, highlighting the need for the development of new therapeutics to treat these diseases. Several methods to develop therapeutics that disrupt PPIs have shown to be successful. Some PPIs, such as IL-2/IL2Rα, have been disrupted using both mAbs and SMIs. Inhibiting OSM is of particular relevance due to it playing a known role in inflammatory diseases such as IBD, RA, and various cancers. To date, there are no clinically approved therapeutics targeting OSM. A mAb developed by GlaxoSmithKline targeting OSM was studied but ended up failing in phase 2 trials due to poor binding affinity. [76, 77] A higher binding affinity mAb is currently undergoing phase 2 trials.[78] Given that no SMIs targeting OSM have been reported and because small molecules are expected to have longer shelf-lives, shorter half-lives, and are expected to be orally bioavailable in comparison to mAbs, we sought to develop a novel SMI to inhibit OSM, as described in the next chapter.[71, 72]

References

1. Pahwa, R.; Goyal, A.; Bansal, P. Chronic Inflammation. *StatPearls* [Online]: **2020,** https://www.ncbi.nlm.nih.gov/books/NBK493173/#_NBK493173_pubdet_ (accessed Aug 21, 2020).
2. What is an inflammation? *Institute for Quality and Efficiency in Health Care (IQWiG)* [Online] **2010**, https://www.ncbi.nlm.nih.gov/books/NBK279298/#_NBK279298_pubdet_ (accessed on Aug 21, 2020)
3. Anderson, J. M., Inflammation, Wound Healing, and the Foreign-Body Response. *Biomaterials Science: An Introduction to Materials in Medicine*, 3rd Edition; Elsevier: **2013**; pp 503-512.
4. Chen, L.; Deng, H.; Cui, H.; Fang, J.; Zuo, Z.; Deng, J.; Li, Y.; Wang, X.; Zhao, L., Inflammatory responses and inflammation-associated diseases in organs. *Oncotarget* **2018,** *9* (6), 7204-7218.
5. Coussens, L. M.; Werb, Z., Inflammation and cancer. *Nature* **2002,** *420* (6917), 860-7.
6. Curcic, S.; Holzer, M.; Frei, R.; Pasterk, L.; Schicho, R.; Heinemann, A.; Marsche, G., Neutrophil effector responses are suppressed by secretory phospholipase A2 modified HDL. *Biochim Biophys Acta* **2015,** *1851* (2), 184-93.
7. Dennis, L. K.; Lynch, C. F.; Torner, J. C., Epidemiologic association between prostatitis and prostate cancer. *Urology* **2002,** *60* (1), 78-83.
8. Cahan, A. C.; Ashikari, R.; Pressman, P.; Cody, H.; Hoffman, S.; Sherman, J. E., Breast cancer after breast augmentation with silicone implants. *Ann Surg Oncol* **1995,** *2* (2), 121-5.
9. Dvorak, H. F., Tumors: wounds that do not heal. Similarities between tumor stroma generation and wound healing. *N Engl J Med* **1986,** *315* (26), 1650-9.

10. Crimmins, E. M.; Finch, C. E., Infection, inflammation, height, and longevity. *Proc Natl Acad Sci U S A* **2006,** *103* (2), 498-503.

11. Williams, J. P.; Meyers, J. A., Immune-mediated inflammatory disorders (I.M.I.D.s): the economic and clinical costs. *Am J Manag Care* **2002,** *8* (21), 664-81.

12. Buttorff, C.; Ruder, T.; Bauman, M., Multiple Chronic Conditions in the United States. RAND Corporation: Santa Monica, CA, **2017**.

13. Murphy, L. B.; Cisternas, M. G.; Pasta, D. J.; Helmick, C. G.; Yelin, E. H., Medical Expenditures and Earnings Losses Among US Adults With Arthritis in 2013. *Arthritis Care Res (Hoboken)* **2018,** *70* (6), 869-876.

14. Mariotto, A. B.; Yabroff, K. R.; Shao, Y.; Feuer, E. J.; Brown, M. L., Projections of the cost of cancer care in the United States: 2010-2020. *J Natl Cancer Inst* **2011,** *103* (2), 117-28.

15. Dinarello, C. A., Historical insights into cytokines. *Eur J Immunol* **2007**, *37*, 34-45.

16. Alam, J.; Jantan, I.; Bukhari, S. N. A., Rheumatoid arthritis: Recent advances on its etiology, role of cytokines and pharmacotherapy. *Biomed Pharmacother* **2017,** *92*, 615-633.

17. West, N. R.; Hegazy, A. N.; Owens, B. M. J.; Bullers, S. J.; Linggi, B.; Buonocore, S.; Coccia, M.; Görtz, D.; This, S.; Stockenhuber, K.; Pott, J.; Friedrich, M.; Ryzhakov, G.; Baribaud, F.; Brodmerkel, C.; Cieluch, C.; Rahman, N.; Müller-Newen, G.; Owens, R. J.; Kühl, A. A.; Maloy, K. J.; Plevy, S. E.; Keshav, S.; Travis, S. P. L.; Powrie, F.; Bailey, A.; Barnes, E.; Bird-Lieberman, B.; Brain, O.; Braden, B.; Collier, J.; East, J.; Howarth, L.; Klenerman, P.; Leedham, S.; Palmer, R.; Rodrigues, A.; Simmons, A.; Sullivan, P.; Uhlig, H., Oncostatin M drives intestinal inflammation and predicts response to tumor necrosis factor–neutralizing therapy in patients with inflammatory bowel disease. *Nature Medicine* **2017,** *23*, 579-589.

18. García-Tuñón, I.; Ricote, M.; Ruiz, A.; Fraile, B.; Paniagua, R.; Royuela, M., OSM, LIF, its receptors, and its relationship with the malignance in human breast carcinoma (in situ and in infiltrative). *Cancer Invest* **2008,** *26* (3), 222-9.

19. Fearon, U.; Mullan, R.; Markham, T.; Connolly, M.; Sullivan, S.; Poole, A. R.; FitzGerald, O.; Bresnihan, B.; Veale, D. J., Oncostatin M induces angiogenesis and cartilage degradation in rheumatoid arthritis synovial tissue and human cartilage cocultures. *Arthritis Rheum* **2006,** *54* (10), 3152-62.

20. Tawara, K.; Scott, H.; Emathinger, J.; Wolf, C.; LaJoie, D.; Hedeen, D.; Bond, L.; Montgomery, P.; Jorcyk, C., HIGH expression of OSM and IL-6 are associated with decreased breast cancer survival: Synergistic induction of IL-6 secretion by OSM and IL-1β. *Oncotarget* **2019,** *10* (21), 2068-2085.

21. Zarling, J. M.; Shoyab, M.; Marquardt, H.; Hanson, M. B.; Lioubin, M. N.; Todaro, G. J., Oncostatin M: A growth regulator produced by differentiated histiocytic lymphoma cells. *Proc Natl Acad Sci USA* **1986**, *83*, 9739-9743

22. Malik, N.; Kallestad, J. C.; Gunderson, N. L.; Austin, S. D.; Neubauer, M. G.; Ochs, V.; Marquardt, H.; Zarling, J. M.; Shoyab, M.; Wei, C.-M.; Linsley, P. S.; Rose, T. M. Molecular Cloning, Sequence Analysis, and Functional Expression of a Novel Growth Regulator, Oncostatin. M. *Mol Cell Biol* **1989**, *9* (7), 2847-2853.

23. Modur, V.; Feldhaus, M. J.; Weyrich, A. S.; Jicha, D. L.; Prescott, S. M.; Zimmerman, G. A.; McIntyre, T. M., Oncostatin M is a proinflammatory mediator: In vivo effects correlate with endothelial cell expression of inflammatory cytokines and adhesion molecules. *J Clin Invest* **1997,** *100* (1), 158-168.

24. Minehata, K. I.; Takeuchi, M.; Hirabayashi, Y.; Inoue, T.; Donovan, P. J.; Tanaka, M.; Miyajima, A., Oncostatin M maintains the hematopoietic microenvironment and retains hematopoietic progenitors in the bone marrow. *Int J Hematol* **2006,** *84* (4), 319-327.

25. Miyajima, A.; Kinoshita, T.; Tanaka, M.; Kamiya, A.; Mukouyama, Y.; Hara, T., Role of oncostatin M in hematopoiesis and liver development. *Cytokine Growth Factor Rev* **2000**, *11* (3), 177-183.

26. Heinrich, P. C.; Behrmann, I.; Haan, S.; Hermanns, H. M.; Müller-Newen, G.; Schaper, F., Principles of interleukin (IL)-6-type cytokine signalling and its regulation. *Biochem J* **2003,** *374* (Pt 1), 1-20.

27. Tanaka, M.; Miyajima, A., Oncostatin M, a multifunctional cytokine. *Rev Physiol Biochem Pharmacol*. **2003** *149*, 39-52.

28. Grenier, A.; Dehoux, M.; Boutten, A.; Arce-Vicioso, M.; Durand, G.; Gougerot-Pocidalo, M. A.; Chollet-Martin, S., Oncostatin M production and regulation by human polymorphonuclear neutrophils. *Blood* **1999,** *93* (4), 1413-21.

29. Grenier, A.; Combaux, D.; Chastre, J.; Gougerot-Pocidalo, M. A.; Gibert, C.; Dehoux, M.; Chollet-Martin, S., Oncostatin M Production by Blood and Alveolar Neutrophils during Acute Lung Injury. *Laboratory Investigation* **2001,** *81* (2), 133-141.

30. Hurst, S. M.; McLoughlin, R. M.; Monslow, J.; Owens, S.; Morgan, L.; Fuller, G. M.; Topley, N.; Jones, S. A., Secretion of oncostatin M by infiltrating neutrophils: regulation of IL-6 and chemokine expression in human mesothelial cells. *J Immunol* **2002,** *169* (9), 5244-51.

31. Jones, S. A.; Jenkins, B. J., Recent insights into targeting the IL-6 cytokine family in inflammatory diseases and cancer. *Nat Rev Immunol* **2018,** *18* (12), 773-789.

32. Adrian-Segarra, J. M.; Schindler, N.; Gajawada, P.; Lörchner, H.; Braun, T.; Pöling, J., The AB loop and D-helix in binding site III of human Oncostatin M (OSM) are required for OSM receptor activation. *J Biol Chem* **2018,** *293* (18), 7017-7029.

33. Ryan, R. E.; Martin, B.; Mellor, L.; Jacob, R. B.; Tawara, K.; McDougal, O. M.; Oxford, J. T.; Jorcyk, C. L., Oncostatin M binds to extracellular matrix in a bioactive conformation: implications for inflammation and metastasis. *Cytokine* **2015,** *72* (1), 71-85.

34. Jorcyk, C. L.; Holzer, R. G.; Ryan, R. E., Oncostatin M induces cell detachment and enhances the metastatic capacity of T-47D human breast carcinoma cells. *Cytokine* **2006,** *33* (6), 323-336.

35. Tawara, K.; Bolin, C.; Koncinsky, J.; Kadaba, S.; Covert, H.; Sutherland, C.; Bond, L.; Kronz, J.; Garbow, J. R.; Jorcyk, C. L., OSM potentiates preintravasation events, increases CTC counts, and promotes breast cancer metastasis to the lung. *Breast Cancer Res* **2018,** *20* (1), 53.

36. Holzer, R. G.; Ryan, R. E.; Tommack, M.; Schlekeway, E.; Jorcyk, C. L., Oncostatin M stimulates the detachment of a reservoir of invasive mammary carcinoma cells: role of cyclooxygenase-2. *Clin Exp Metastasis* **2004,** *21* (2), 167-76.

37. Queen, M. M.; Ryan, R. E.; Holzer, R. G.; Keller-Peck, C. R.; Jorcyk, C. L., Breast cancer cells stimulate neutrophils to produce oncostatin M: potential implications for tumor progression. *Cancer Res* **2005,** *65* (19), 8896-904.

38. Bolin, C.; Tawara, K.; Sutherland, C.; Redshaw, J.; Aranda, P.; Moselhy, J.; Anderson, R.; Jorcyk, C. L., Oncostatin m promotes mammary tumor metastasis to bone and osteolytic bone degradation. *Genes Cancer* **2012,** *3* (2), 117-30.

39. Rose, T. M.; Lagrou, M. J.; Fransson, I.; Werelius, B.; Delattre, O.; Thomas, G.; de Jong, P. J.; Todaro, G. J.; Dumanski, J. P., The genes for oncostatin M (OSM) and leukemia inhibitory factor (LIF) are tightly linked on human chromosome 22. *Genomics* **1993,** *17* (1), 136-40.

40. Skiniotis, G.; Lupardus, P. J.; Martick, M.; Walz, T.; Garcia, K. C., Structural Organization of a Full-Length gp130/LIF-R Cytokine Receptor Transmembrane Complex. *Molecular Cell* **2008,** *31* (5), 737-748.

41. Liu, J.; Hadjokas, N.; Mosley, B.; Estrov, Z.; Spence, M. J.; Vestal, R. E., Oncostatin M-specific receptor expression and function in regulating cell proliferation of normal and malignant mammary epithelial cells. *Cytokine* **1998**, *10* (4), 295-302.

42. Korzus, E.; Nagase, H.; Rydell, R.; Travis, J., The mitogen-activated protein kinase and JAK-STAT signaling pathways are required for an oncostatin M-responsive element-mediated activation of matrix metalloproteinase 1 gene expression. *J Biol Chem* **1997,** *272* (2), 1188-96.

43. Starr, R.; Willson, T. A.; Viney, E. M.; Murray, L. J.; Rayner, J. R.; Jenkins, B. J.; Gonda, T. J.; Alexander, W. S.; Metcalf, D.; Nicola, N. A.; Hilton, D. J., A family of cytokine-inducible inhibitors of signalling. *Nature* **1997,** *387* (6636), 917-21.

44. Robinson, R. C.; Grey, L. M.; Staunton, D.; Vankelecom, H.; Vernallis, A. B.; Moreau, J. F.; Stuart, D. I.; Heath, J. K.; Jones, E. Y., The crystal structure and biological function of leukemia inhibitory factor: Implications for receptor binding. *Cell* **1994,** *77* (7), 1101-1116.

45. Deller, M. C.; Hudson, K. R.; Ikemizu, S.; Bravo, J.; Jones, E. Y.; Heath, J. K., Crystal structure and functional dissection of the cytostatic cytokine oncostatin M. *Structure* **2000,** *8* (8), 863-874.

46. Gonzalez, M. W.; Kann, M. G., Chapter 4: Protein interactions and disease. *PLoS Comput Biol* **2012,** *8* (12), e1002819.

47. Yin, H.; Hamilton, A. D., Strategies for targeting protein-protein interactions with synthetic agents. *Angew Chem Int Ed Engl* **2005,** *44* (27), 4130-63.

48. Cunningham, B. C.; Wells, J. A., High-resolution epitope mapping of hGH-receptor interactions by alanine-scanning mutagenesis. *Science* **1989,** *244* (4908), 1081-5.

49. Cunningham, B. C.; Wells, J. A., Comparison of a structural and a functional epitope. *J Mol Biol* **1993,** *234* (3), 554-63.

50. Clackson, T.; Wells, J. A., A hot spot of binding energy in a hormone-receptor interface. *Science* **1995,** *267* (5196), 383-6.

51. Du, Q.; Qian, Y.; Xue, W., Molecular Simulation of Oncostatin M and Receptor (OSM-OSMR) Interaction as a Potential Therapeutic Target for Inflammatory Bowel *Disease. Front Mol Biosci.*, **2020,** 7, 29.

52. DeLano, W. L., Unraveling hot spots in binding interfaces: progress and challenges. *Curr Opin Struct Biol* **2002,** *12* (1), 14-20.

53. Ng, E. W.; Adamis, A. P., Anti-VEGF aptamer (pegaptanib) therapy for ocular vascular diseases. *Ann N Y Acad Sci* **2006,** *1082*, 151-71.

54. Kutzki, O.; Park, H. S.; Ernst, J. T.; Orner, B. P.; Yin, H.; Hamilton, A. D., Development of a potent Bcl-x(L) antagonist based on alpha-helix mimicry. *J Am Chem Soc* **2002,** *124* (40), 11838-9.

55. Tilley, J.; Chen, L.; Fry, D.; Emerson, S.; Powers, G.; Biondi, D.; Varnell, T.; Trilles, R.; Guthrie, R.; Mennona, F.; Kaplan, G.; LeMahieu, R.; Carson, M.; Han, R.; Liu, C.; Palermo, R.; Ju, G., Identification of a small molecule inhibitor of the IL-2/IL-2R alpha receptor interaction which binds to IL-2. *J Am Chem Soc* **1997,** *119* (32), 7589-7590.

56. Senger, D. R.; Galli, S. J.; Dvorak, A. M.; Perruzzi, C. A.; Harvey, V. S.; Dvorak, H. F., Tumor cells secrete a vascular permeability factor that promotes accumulation of ascites fluid. *Science* **1983,** *219* (4587), 983-5.

57. Leung, D. W.; Cachianes, G.; Kuang, W. J.; Goeddel, D. V.; Ferrara, N., Vascular endothelial growth factor is a secreted angiogenic mitogen. *Science* **1989,** *246* (4935), 1306-9.

58. Ferrara, N., Vascular endothelial growth factor: basic science and clinical progress. *Endocr Rev* **2004,** *25* (4), 581-611.

59. Ellington, A. D.; Szostak, J. W., In vitro selection of RNA molecules that bind specific ligands. *Nature* **1990,** *346* (6287), 818-22.

60. Tuerk, C.; Gold, L., Systematic evolution of ligands by exponential enrichment: RNA ligands to bacteriophage T4 DNA polymerase. *Science* **1990,** *249* (4968), 505-10.

61. Germer, K.; Leonard, M.; Zhang, X., RNA aptamers and their therapeutic and diagnostic applications. *Int J Biochem Mol Biol* **2013,** *4* (1), 27-40.

62. Reed, J. C., Apoptosis-regulating proteins as targets for drug discovery. *Trends Mol Med* **2001,** *7* (7), 314-9.

63. Muchmore, S. W.; Sattler, M.; Liang, H.; Meadows, R. P.; Harlan, J. E.; Yoon, H. S.; Nettesheim, D.; Chang, B. S.; Thompson, C. B.; Wong, S. L.; Ng, S. L.; Fesik, S. W., X-ray and NMR structure of human Bcl-xL, an inhibitor of programmed cell death. *Nature* **1996,** *381* (6580), 335-41.

64. Mallbris, L.; Davies, J.; Glasebrook, A.; Tang, Y.; Glaesner, W.; Nickoloff, B. J., Molecular Insights into Fully Human and Humanized Monoclonal Antibodies: What are the Differences and Should Dermatologists Care? *J Clin Aesthet Dermatol* **2016,** *9* (7), 13-5.

65. Skerra, A.; Plückthun, A., Assembly of a functional immunoglobulin Fv fragment in Escherichia coli. *Science* **1988,** *240* (4855), 1038-41.

66. Igawa, T.; Tsunoda, H.; Kuramochi, T.; Sampei, Z.; Ishii, S.; Hattori, K., Engineering the variable region of therapeutic IgG antibodies. *MAbs* **2011,** *3* (3), 243-52.

67. Waldmann, T. A.; White, J. D.; Goldman, C. K.; Top, L.; Grant, A.; Bamford, R.; Roessler, E.; Horak, I. D.; Zaknoen, S.; Kasten-Sportes, C., The interleukin-2 receptor: a target for monoclonal antibody treatment of human T-cell lymphotrophic virus I-induced adult T-cell leukemia. *Blood* **1993,** *82* (6), 1701-12.

68. Waldmann, T. A., The structure, function, and expression of interleukin-2 receptors on normal and malignant lymphocytes. *Science* **1986,** *232* (4751), 727-32.

69. Daclizumab withdrawn from the market worldwide. *Drug Ther Bull* **2018,** *56* (4), 38.

70. Ryman, J. T.; Meibohm, B., Pharmacokinetics of Monoclonal Antibodies. *CPT Pharmacometrics Syst Pharmacol* **2017,** *6* (9), 576-588.

71. Mócsai, A.; Kovács, L.; Gergely, P., What is the future of targeted therapy in rheumatology: Biologics or small molecules? *BMC Medicine* **2014,** *12,* 43.

72. Blackstone, E. A.; Joseph, P. F., The economics of biosimilars. *Am Health Drug Benefits* **2013,** *6* (8), 469-78.

73. Sauvé, K.; Nachman, M.; Spence, C.; Bailon, P.; Campbell, E.; Tsien, W. H.; Kondas, J. A.; Hakimi, J.; Ju, G., Localization in human interleukin 2 of the binding site to the alpha chain (p55) of the interleukin 2 receptor. *Proc Natl Acad Sci USA* **1991,** *88* (11), 4636-40.

74. Erlanson, D.; Braisted, A.; Raphael, D.; Randal, M.; Stroud, R.; Gordon, E.; Wells, J., Site-directed ligand discovery. *Proc Natl Acad Sci USA* **2000,** *97* (17), 9367-9372.

75. Braisted, A.; Oslob, J.; Delano, W.; Hyde, J.; McDowell, R.; Waal, N.; Yu, C.; Arkin, M.; Raimundo, B., Discovery of a potent small molecule IL-2 inhibitor through fragment assembly. *J Am Chem Soc* **2003,** *125* (13), 3714-3715.

76. Plater-Zyberk, C.; Buckton, J.; Thompson, S.; Spaull, J.; Zanders, E.; Papworth, J.; Life, P. F., Amelioration of arthritis in two murine models using antibodies to oncostatin M. *Arthritis Rheum* **2001,** *44* (11), 2697-2702

77. Choy, E. H.; Bendit, M.; McAleer, D.; Liu, F.; Feeney, M.; Brett, S.; Zamuner, S.; Campanile, A.; Toso, J., Safety, tolerability, pharmacokinetics and pharmacodynamics of an anti- oncostatin M monoclonal antibody in rheumatoid arthritis: Results from phase II randomized, placebo-controlled trials. *Arthritis Res Ther* **2013**, *15* (5), 132

78. Reid, J.; Zamuner, S.; Edwards, K.; Rumley, S. A.; Nevin, K.; Feeney, M.; Zecchin, C.; Fernando, D.; Wisniacki, N., In vivo affinity and target engagement in skin and blood in a first-time-in-human study of an anti-oncostatin M monoclonal antibody. *Br J Clin Pharmacol* **2018,** *84* (10), 2280-2291.

CHAPTER TWO: DESIGN AND SYNTHESIS OF SMALL MOLECULES TARGETING OSM

Overview of Chapter

Given OSM's significant role in various inflammatory diseases, and the fact that there is no clinically approved therapeutic targeting OSM, the goal of this research is to develop a novel SMI that inhibits OSM signaling. Studies in the literature to identify hotspots as probable sites for SMIs to bind and disrupt OSM/OSMR complex formation and signaling have been evaluated to guide the design of SMIs. Prior work within our collaborative research team comprised of Dr. Cheryl Jorcyk, Dr. Lisa Warner, Dr. Don Warner, Dr. Matt King, and Dr. Danny Xu (now at Idaho State University Meridian), and their students has been performed to develop SMIs for OSM. Using high-throughput virtual screenings, 26 potential SMIs of OSM were identified. Two of the potential SMIs, 10 and 26, were chosen to be further optimized for increased activity and drug likeness. The focus of this research, however, differentiates from prior work done in our lab group and uses computational methods to rationally design a new potential SMI of OSM, called SMI-27. The design and the synthesis of SMI-27 analogs are described herein.

Prior Work to Identify OSM Binding Sites

A fundamental piece of literature that first elucidated the crystal structure of OSM and identified hotspots responsible for OSM binding to its receptors was published in

2000 by Deller et al.[1] The crystal structure was determined by expressing OSM from *E.coli*, purifying it using high-resolution gel filtration, growing crystals by vapor diffusion from hanging drops, and then subjecting crystals to x-ray diffraction. The potential receptor binding sites of OSM, shown in Figure 2.1, were named based on analogy to the receptor binding sites in human growth hormone, which similar to OSM and other IL-6 family cytokines, is a four-helical bundle with two unique binding sites for both of its receptors.[2] Site-directed alanine mutagenesis experiments investigated hotspots responsible for binding.[1] When amino acid residues Phe160 and Lys163, located in “site 3”, were mutated, activity was dramatically decreased, as determined by a Ba/F3-OSMR/gp130 assay. This assay relies upon Ba/F3 murine cells that have been transfected with hOSMR and hgp130 cDNA such that the cells co-express hOSMR and hgp130. The assay then evaluates the ability of the OSM mutants to facilitate proliferation of the Ba/F3 cells. Compared to native hOSM, a decrease in cell proliferation implies that the mutant OSM does not bind to its receptors. These results demonstrated that Phe160 and Lys163 are essential for the formation of the OSM/OSMR/gp130 heterodimeric complex and, importantly, identified potential binding sites that enabled future drug-discovery research focused on OSM.

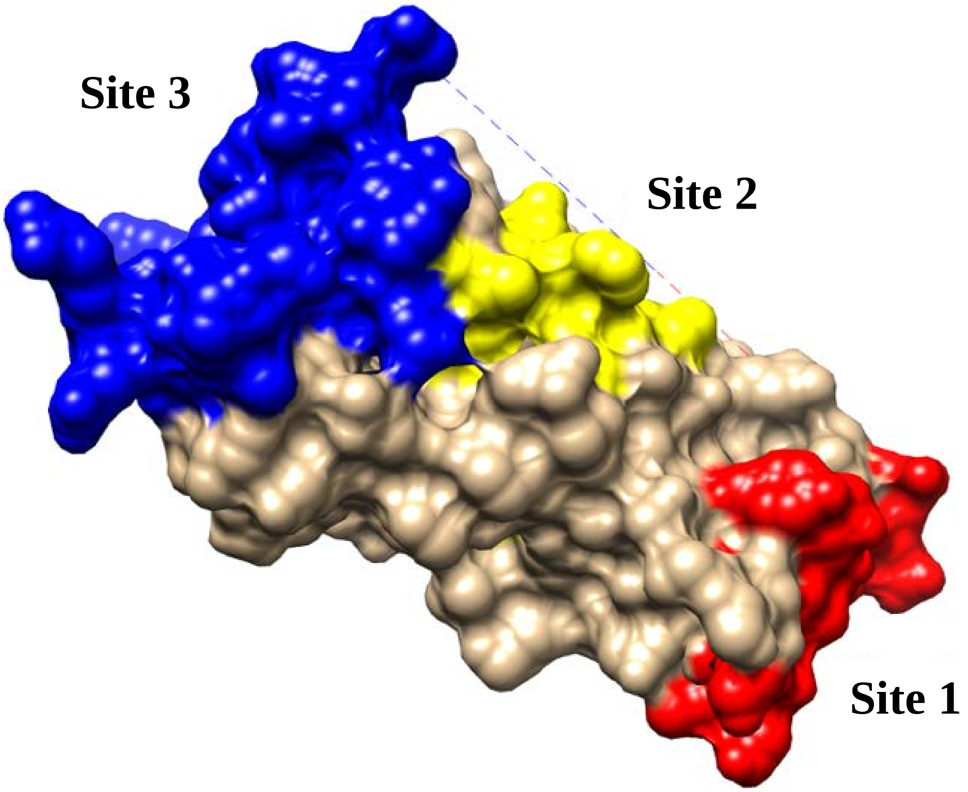

Figure 2.1. OSM crystal structure and receptor binding sites.
Surface model of OSM crystal structure (PDB: EV1S) with the receptor binding sites 1, 2, and 3 shown.

It was not until the report of Adrian-Segarra et al. in 2018 that additional residues in site 3 responsible for OSM specifically binding to OSMR were determined.[3] Similar to Deller et al., site-directed alanine mutagenesis experiments focused in site 3 confirmed the importance of Phe160 and Lys163 residues, termed the FXXK motif, for OSM biding to OSMR. Additionally, Tyr34, Gln38, Gly39, Leu45, and Pro153 were found to play an important role in OSM binding to OSMR but did not have a significant effect on OSM binding to LIFR, while mutations of Leu40 and Cys49 had a major impact on OSM binding to both OSMR and LIFR. It is hypothesized that mutation of Gly39 and Pro153, typically found in turns of protein secondary structures, causes the protein to undergo a conformational change that renders it unable to bind to OSMR. These results were experimentally confirmed by an immunoblot assay in which the phosphorylation of Tyr705 on STAT3 was quantified after being electrophoresed in NuPAGE gel. These findings help to further the knowledge of amino acids responsible for OSM binding to OSMR.

Recently, in March 2020, Du et al. aimed to further elucidate residues involved in the binding of OSM to OSMR using computational methods.[4] Per-residue binding free energy decomposition and computational alanine scanning experiments to predict hot-spots were performed. The per-residue binding free energy decomposition experiments successfully predicted the residues previously mentioned by Adrian-Segarra et al., as well as seven new residues: Arg36, Asp41, Val42, Arg100, Leu103, Gln161, and Leu164. Given that the crystal structure of the OSM/OSMR complex remains unknown, a homology model of OSMR was constructed using LIFR. Next, computational methods were used to predict the binding free energy of amino acids at the OSM/OSMR interface. Based on the per-residue binding free energy decomposition results, all residues exhibiting more than 1 kcal/mol binding free energy were subjected to computational alanine scanning. The residues Arg100, Leu103, Phe160, and Gln161 all exhibited binding free energy of more than 2 kcal/mol, suggesting these amino acids are of significant importance in OSM/OSMR complex formation. This computational work in congruence with other previously mentioned experimental results clearly indicate which amino acid residues should be targeted for the development of therapeutics to treat OSM-related diseases.

Within our collaborative research team, the potential ligand binding sites on OSM were predicted by Danny Xu and Matt King using ligand shape matching and the utilization of 3-dimensional templates coupled with site geometry searches for clefts/pockets. Using the human OSM crystal structure (PDB ID: 1EVS), the AutoLigand program[5] scanned the protein surface for potential SMI binding sites.[6, 7] Calculations produced three primary SMI binding sites on the OSM surface with favorable energy/volume ratios (Figure 2.2). The volume of site 3, on the order of molecular volumes of SMIs, indicated this region to be the preferred SMI binding site on OSM and should be targeted for the development of new SMI compounds. Importantly, the computational experiments agreed with the aforementioned literature reports that identified site 3 as a hot spot and important for OSM signaling.

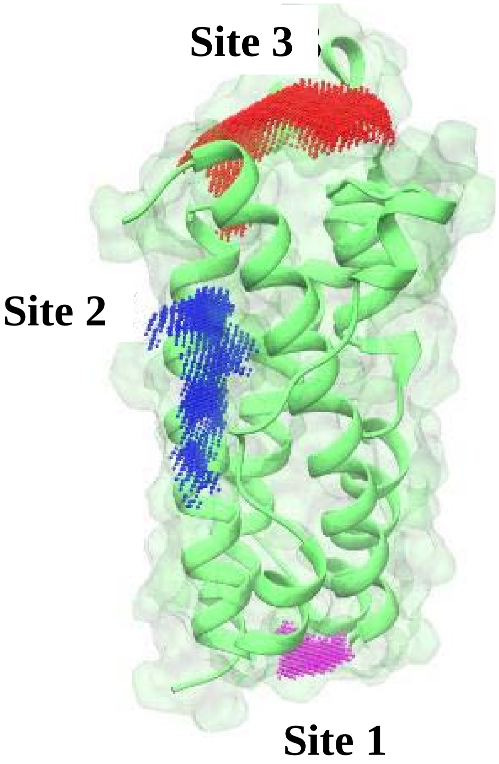

	Volume	E/V
Site 1	77.9	-2.41
Site 2	162.5	-2.41
Site 3	315.6	-2.45

Figure 2.2. In silico identification of ligand binding sites on OSM. Site 3 was found to have the largest pocket volume and greatest energy to volume ratio (E/V), indicating this the most likely spot for an SMI to bind. Volumes are in units of Å^3, and E/V ratios in kcal mol^{-1} Å^{-3}. (Image courtesy of Dr. Matt King)

Prior Work to Identify and Develop SMIs for OSM

The literature evidence demonstrating the importance of site 3 for OSM binding to OSMR, in combination with work done by our collaborative research group suggesting that site 3 would be the optimal site for a SMI to bind, prompted us to identify possible SMIs that target site 3 and disrupt OSM from binding to its receptor. Using ~1.65 million compounds from online databases (ZINC15 and NIH NCBI), a high-throughput virtual screen (HTVS) was performed by Dr. Danny Xu and Dr. Matt King. From the screening results, 26 different lead compounds were identified and obtained from commercial sources. Next, the 26 lead compounds were subjected to an enzyme-linked immunosorbent assay (ELISA) conducted by members of the Jorcyk lab (Figure 2.3). OSM turns on the JAK/STAT3 signaling pathway, wherein JAK phosphorylates STAT3 to pSTAT3 that can be measured by ELISA. In this ELISA, T47D cells were treated with and without exogenous OSM. When OSM is present, the induced level of pSTAT3 is normalized to 1.0 and used as a positive control. Background level of pSTAT3 without any added OSM is used as a baseline value. Cells are then treated with OSM and SMIs to identify which compounds best inhibit OSM induced pSTAT3 expression below the baseline value. Although several compounds displayed promising activity, compounds 10 and 26 have received the most attention due to their inhibitory activity, their synthetic accessibility, and the ease with which analogs could be generated. Currently, small libraries of each of these SMIs are being prepared and tested to increase potency and drug likeness.

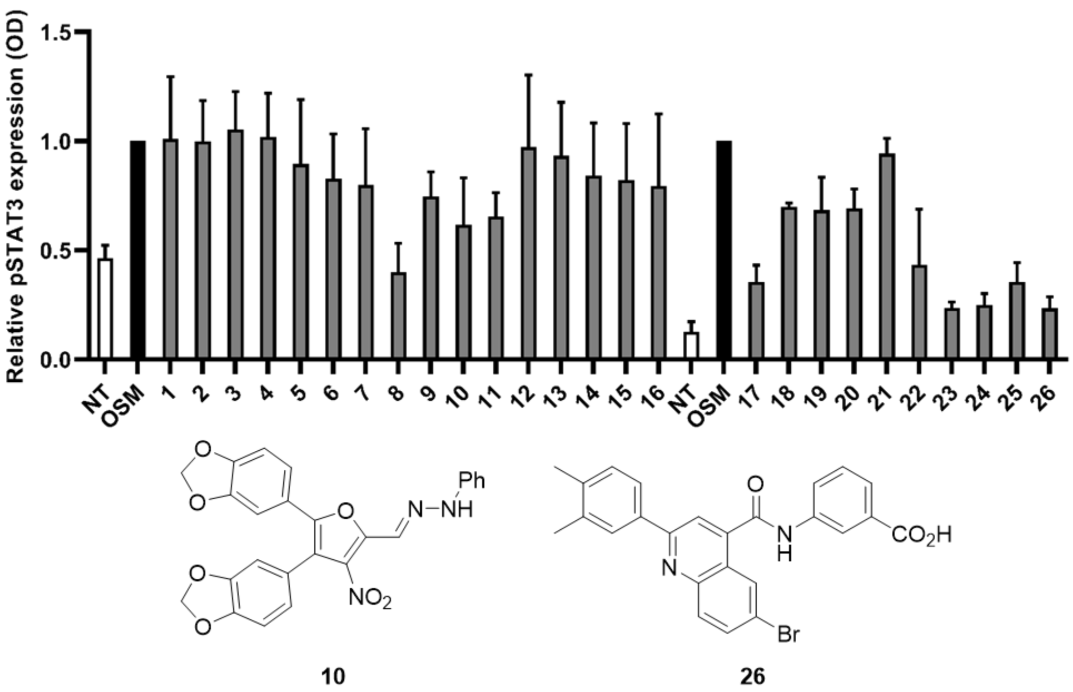

Figure 2.3. ELISA results of the top 26 hits from the HTVS.
The inhibition of OSM induced pSTAT3 expression of the top 26 hits from the HTVS. The two compounds, 10 and 26, were selected for optimization due to their ease of synthesis and diversification.

Despite the parent structure of SMI-10 being a promising lead candidate, it possessed some problematic functional groups. Given that nitro-containing aromatic compounds are often carcinogenic and mutagenic,[8] this functional group is not desirable. Dr. Don Warner's lab found the phenylhydrazone group to be labile, and its decomposition generates a potentially reactive electrophile that would complicate biological activity. Fortunately, computational modeling of SMI-10 demonstrated that the nitro group is solvent exposed and served little to no role in binding to OSM, suggesting it could be removed without negatively impacting binding. It was also proposed that the phenylhydrazone group could be replaced with a more stable aryl amide or a propionic acid. The general synthetic scheme of SMI-10 analogs, starting from commercially available materials, is shown in Figure 2.4.

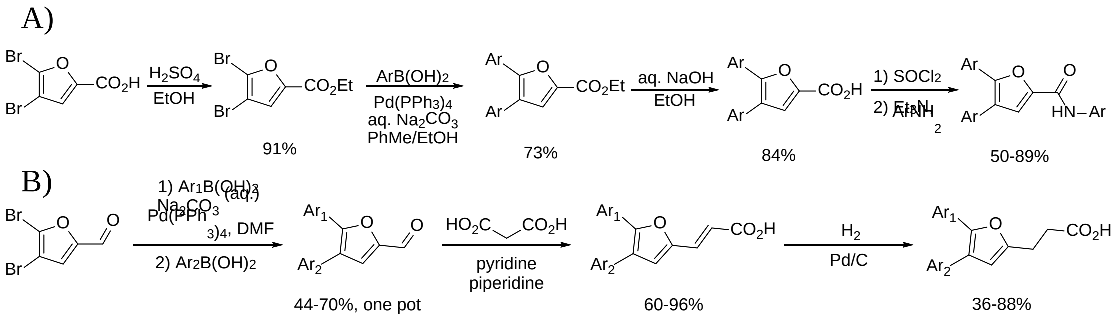
A)
H2SO4
EtOH
91%
ArB(OH)2
Pd(PPh3)4
aq. Na2CO3
PhMe/EtOH
73%
aq. NaOH
EtOH
84%
1) SOCl2
2) Et3N, ArNH2
50-89%
B)
1) Ar1B(OH)2
Na2CO3 (aq.)
Pd(PPh3)4, DMF
2) Ar2B(OH)2
44-70%, one pot
HO2C CO2H
pyridine
piperidine
60-96%
H2
Pd/C
36-88%

Figure 2.4. Synthesis of SMI-10 analogs
General synthetic route of SMI-10 analogs starting with commercially available materials to form A) aryl amide and B) propionic acid analogs.

The parent structure of SMI-26 did not possess any inherently toxic functional groups and also appeared to be a relatively stable molecule. Efforts to generate more potent analogs of SMI-26 relied on a “Topliss tree”[9] analysis. This approach systematically optimizes drugs containing substituted benzene rings for maximum binding affinity by following patterns observed when the lipophilic, electrostatic, and steric properties of the benzene rings are changed. As shown in Figure 2.5, SMI-26 analogs were synthesized using a 3-step general reaction sequence that started with a Pfitzinger reaction[10] that was followed by an amidation reaction and then a saponification (in the case of final SMIs that contained a carboxylic acid in the R_2 position). This short process allowed for a small library of analogs to be generated very quickly from commercial materials.

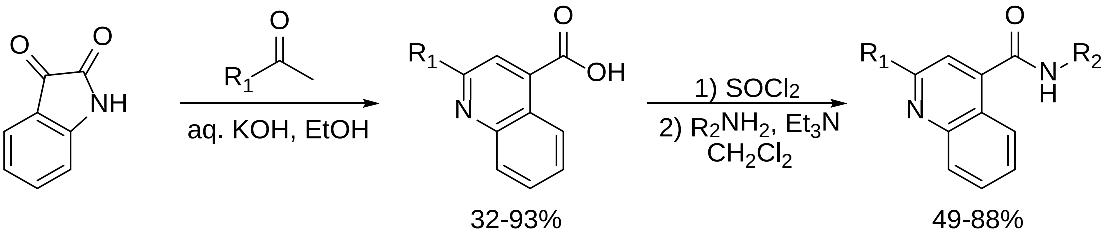

Figure 2.5 Synthesis of SMI-26 analogs.
General synthetic route of SMI-26 analogs using commercially available materials.

To test the binding affinity of the small library of the 10 and 26 analogs toward OSM, a fluorimetry quenching (FQ) assay was performed.[11] The FQ assay works by exciting an exposed aromatic residue on a protein at a certain wavelength, then recording the intensity of the fluorescent wavelength emitted. This assay was chosen because OSM has an exposed tryptophan amino acid, Trp187, that will fluoresce at 350 nm when excited at 280 nm. Upon addition and binding of the SMI to OSM, a reduction in the fluorescence intensity of the emitted wavelength was observed. The signal intensity was plotted against the amount of SMI added and fit to Stern-Volmer equation to determine Kd of the SMI. All FQ assays were performed in triplicate. Several compounds showed Kd values of less than 10 μM, with the best being 2.5 μM (Figure 2.6). These results provide encouragement that with further optimization, an SMI can be developed with a binding affinity toward OSM in the nM range.

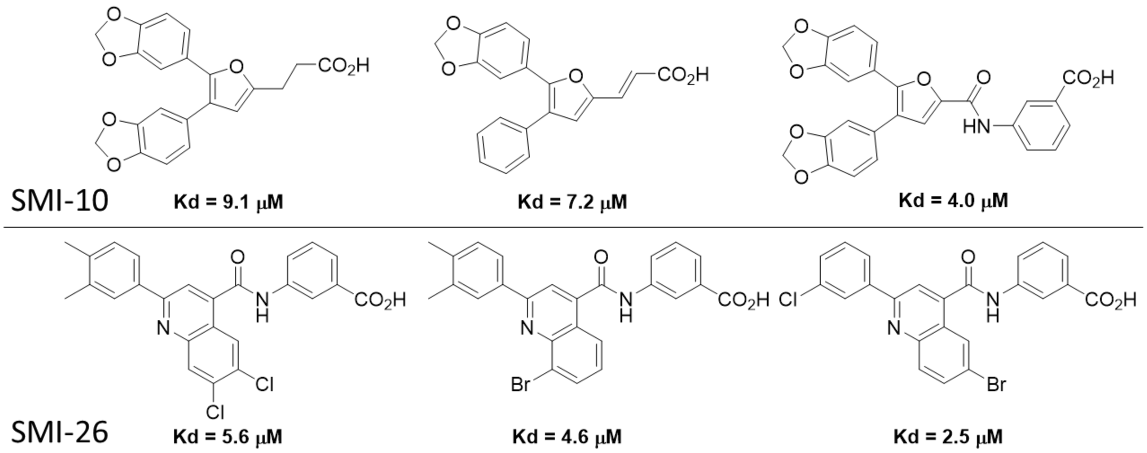
SMI-10
Kd = 9.1 μM
Kd = 7.2 μM
Kd = 4.0 μM
SMI-26
Kd = 5.6 μM
Kd = 4.6 μM
Kd = 2.5 μM
O
CO2H
HN
N
H
Cl
Br

Figure 2.6. Structures and Kd values of the top SMI-10 and SMI-26 analogs. Top performing SMI-10 and SMI-26 analogs based of Kd values as determined by fluorescence quenching assays run in triplicate.

Computationally Aided Rational Design of SMI-27

The research conducted as part of this project takes the computational approach one step further. Specifically, computational methods were used to aid in the rational design of a new candidate, SMI-27. To accomplish this, a subset of 10,000 small molecules randomly selected from a ~22M compound library (ZINC15) were docked in OSM site 3 using AutoDock 4.2.[12] Using the resulting lowest-energy docking pose of each molecule, the spatial distributions of pharmacophore atom types, including aromatic carbons, hydrogen bond acceptors, and hydrogen bond donors were mapped with respect to OSM site 3. To construct weighted density maps (WDM) of the pharmacophore and to create a visual representation of important binding features, a 3-dimensional density grid was generated about the OSM site 3 binding pocket with a grid resolution of 0.1 Å cubed (Figure 2.7). The size of the “blobs” represents the probability of finding a specific atom type of an SMI bound in that location. For example, in Figure 2.7A there are large dark gray regions, which indicate a large number of aromatic hydrocarbons prefer to orient in those areas. The same process was repeated for hydrogen bond acceptors (blue: nitrogen, red: oxygen, yellow: sulfur, green: halogen) (Figure 2.7B), and hydrogen bond donors (OH, NH, SH) (Figure 2.7C).

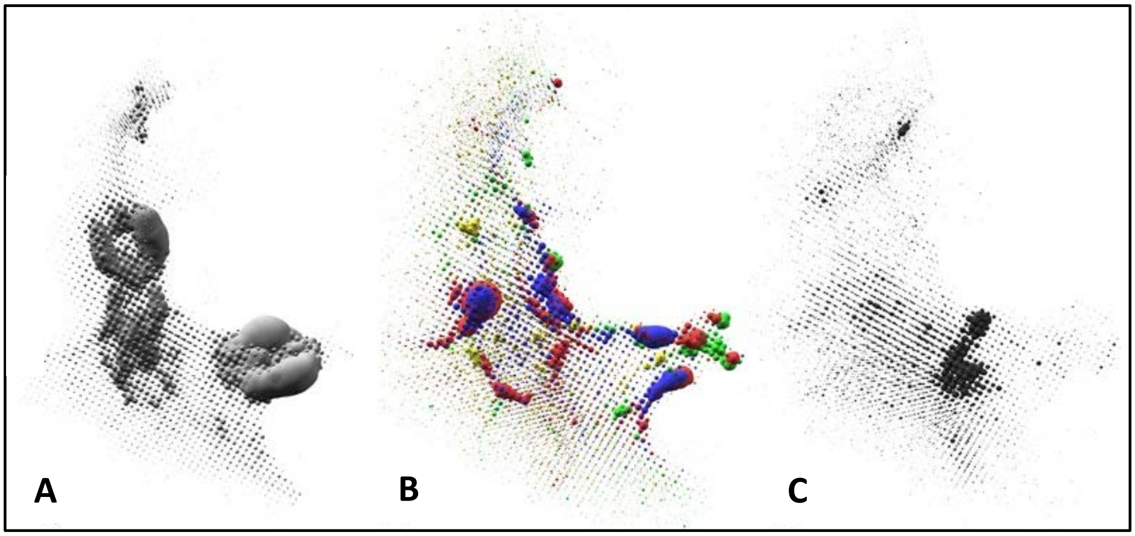

Figure 2.7. Weighted density maps with respect to OSM site 3.
Weighted density maps of pharmacophore features extracted from randomly selected docking results of 10,000 small-molecule ligands to OSM. The figures represent A) aromatic hydrocarbons, B) hydrogen bond acceptors (blue: nitrogen, red: oxygen, yellow: sulfur, green: halogen), and C) hydrogen bond donors (OH, NH, SH). (Image courtesy of Dr. Matt King).

To help rationally design SMI-27, the WDM was then overlaid with site 3 of OSM, as shown in Figure 2.8. Using the visual representation, several molecules were designed so that the atoms of each SMI best overlaid with the WDM. This would, in theory, maximize stabilizing binding interactions between amino acid residues in the putative binding of OSM and the SMI. The designed compounds were prioritized based on how constructively they overlaid with the WDM and their ease of synthesis. After those factors were considered, a 2,4-disubstituted quinazoline core with a hydrophobic aryl group in the 2-position (referred to as R_1) and an aryl group appended by an amide linker to the 4-position (referred to as R_2) was selected for synthesis, shown in Table 2.1. Using various combinations of R_1 and R_2 groups, a small library of 24 potential inhibitors of OSM was synthesized.

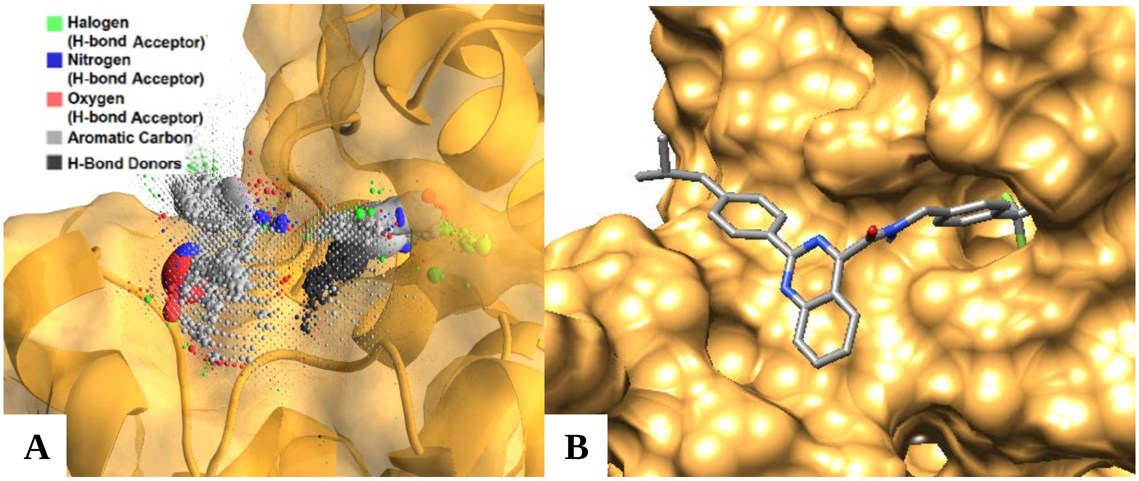
Halogen
(H-bond Acceptor)
Nitrogen
(H-bond Acceptor)
Oxygen
(H-bond Acceptor)
Aromatic Carbon
H-Bond Donors
A
B

Figure 2.8. Weighted density map and surface model of an SMI-27 analog docked in OSM site 3.

A) Weighted probability map constructed from docking results of ~10,000 small molecules overlaid in OSM site 3. Colored regions show the probability of finding a specific atom type of a small molecule bound in that region. B) An SMI-27 analog docked against OSM site 3 visualizes its predicted binding pose.

Table 2.1. SMI-27 Generic structure and substituents
SMI-27, consisting of a 2,4-disubstituted quinazoline core with a hydrophobic aryl group in the 2-position and an aryl or alkyl group appended to the 4-position by an amide linker, was selected for synthesis. A small library of 24 SMIs was constructed using various combinations of R1 and R2.

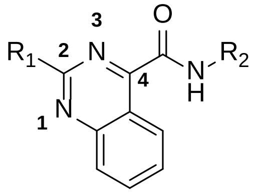

R_1	R_2			
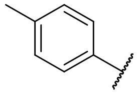	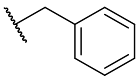	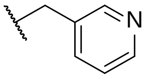	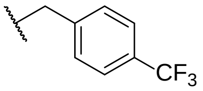	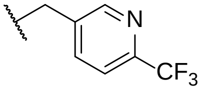
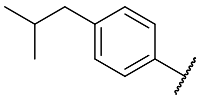	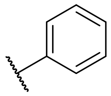	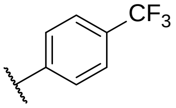	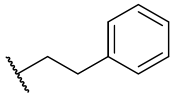	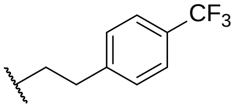
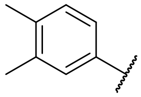	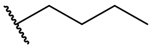	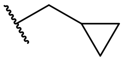	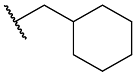	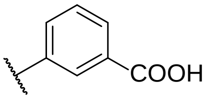

Before the small molecules were synthesized, they were computationally modeled and docked against OSM in site 3 to estimate their binding energy. Any binding score lower than -6.0 kcal/mol was selected for synthesis to be further tested *in vitro*. Docking studies were performed using UCSF Chimera molecular modeling software[13] in combination with Autodock Vina.[14] Images from the docking studies of rationally designed SMI-27 analogs were visually examined to predict amino acid residues involved in binding the SMI to OSM (Figure 2.9).

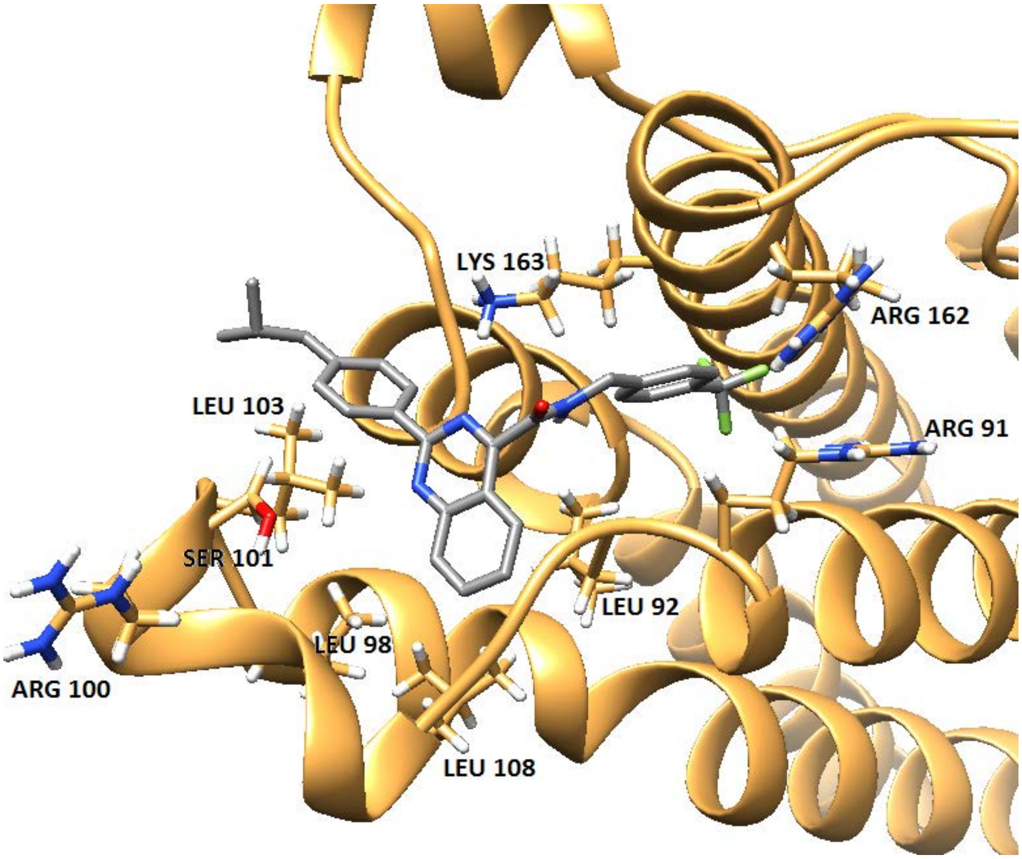

Figure 2.9. Amino acids predicted to be important for OSM/SMI binding. An SMI-27 analog docked in OSM site 3 with amino acid residues shown that are thought to play in important role in binding between the small molecule and the target protein.

The most important predicted stabilizing binding interactions are depicted in Figure 2.10. Hydrogen bonding interactions were predicted to occur between the quinazoline nitrogen in the 1-position with Arg100 and Ser101, as well as between the quinazoline nitrogen in the 3-position and amide oxygen with Lys163. Hydrophobic interactions were expected to occur between the R_1 aryl group and Leu103, while the aromatic carbons on the bottom of the quinazoline ring were predicted to fit into a hydrophobic groove and interact with Leu92, Leu98, and Leu108. The R_2 aryl group was predicted to participate in cation-pi interactions with positively charged Arg93 and

Arg162 residues that reside deep in a hydrophobic pocket of OSM site 3. Similarly, the nitrogen atom of the picolyl group and electron withdrawing groups on R_2 were predicted to have electrostatic/hydrogen bonding interactions with the same arginine residues.

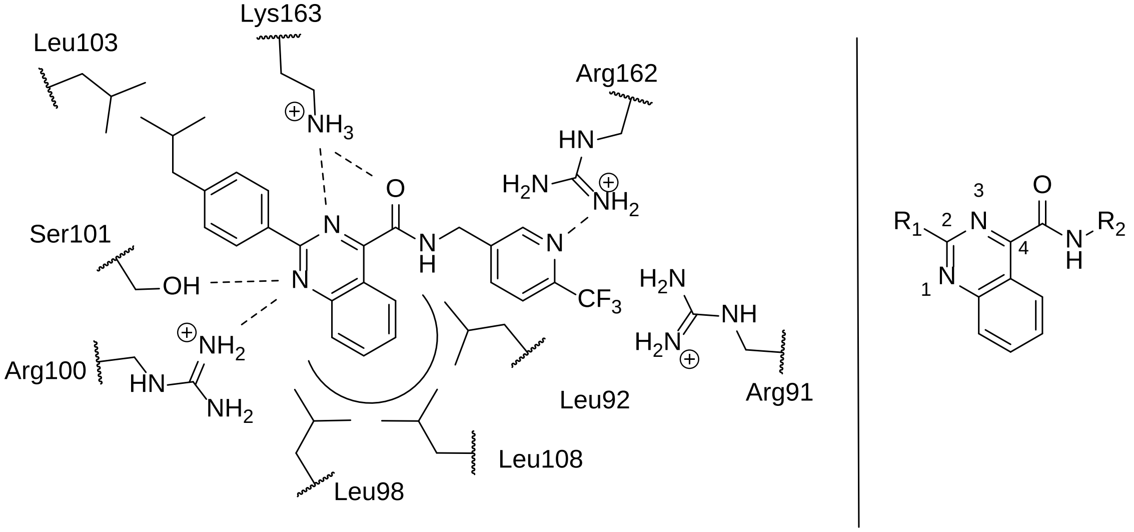

Figure 2.10. Predicted OSM/SMI stabilizing binding interactions.
The most important predicted stabilizing binding interactions between SMI-27 and OSM in site 3. Hydrogen bonds are shown by dashed lines. A hydrophobic groove is shown by the half-circle.

The WDM computational predictions suggested that hydrophobic interactions were the most important for R_1. So, the SMIs that were designed always consisted of an R_1 phenyl ring that contained additional attached hydrophobic groups. When holding R_2 constant and changing R_1, the binding studies suggested that the shorter and less hydrophobic 4-methylphenyl group would increase binding affinity by about -0.3 kcal/mol over the longer and more hydrophobic 4-isobutylphenyl group, which also has additional sp^3 character. While -0.3 kcal/mol is not a significant difference in binding affinity, the docking studies treated OSM as a rigid structure and did not take into account its dynamic flexibility.[15] However, in reality, OSM might adapt and allow for additional hydrophobic interactions to take place with the isobutyl group. Therefore, 4-methylphenyl, 3,4-dimethylphenyl, and 4-isobutylphenyl were chosen for synthesis to assess the following questions: A) Does additional sp^3 character of R_1 increase flexibility and allow for more hydrophobic interactions to occur? and B) Does increasing the number of hydrophobic carbon atoms of R_1 result in more hydrophobic interactions with OSM and result in a higher binding affinity?

Computational docking studies where R_1 was held constant and R_2 was changed produced differences in binding affinity of up to -2.6 kcal/mol. This suggests that the most important SMI/OSM interactions are due to the R_2 group, which is predicted to stick deep within a pocket located in OSM's binding site 3 and potentially participating in cation/pi stacking interactions with the positively charged Arg91 and Arg162 residues. As such, this portion of the scaffold was prioritized to introduce molecular diversity. The R_2 groups varied in carbon chain length, hydrophobicity, electron withdrawing groups, and aromaticity to assess the following questions: A) Does a longer chain length allow R_2 too much flexibility and result in binding poses that do not inserted into the deep pocket or does a shorter, less flexible chain length force the R_2 group into the pocket?, B) Does placing a heteroatom in the R_2 aryl ring make it more soluble, and/or allow for a stabilizing hydrogen bonding interactions?, C) Does an electron withdrawing group on R_2 pull more electron density toward that side of the molecule and allow for stabilizing electrostatic interactions?, and D) Can a non-aromatic alkyl R_2 group achieve the same binding affinity without the predicted cation-pi interactions?

Synthetic Route and Steps to Form SMI-27 Analogs

Although a synthesis for the exact 2-arylquinazoline-4-carboxamide compounds was not present in the literature, a protocol for the preparation of closely related compounds with antiproliferative properties was present in the patent literature (WO 2014143960).[16] An adaptation of this protocol was chosen to access a carboxylic acid precursor that upon coupling with various amines would allow for convergent introduction of diverse amide groups (Figure 2.11). The first step of the synthesis converted commercially available alkyl-substituted benzoic acids to an acid chloride using thionyl chloride. Next, without any purification, the acid chloride was treated with aniline to yield a variety of N-phenyl benzamides. Next, the key reaction, a Meerwein cyclization,[17] assembled the quinazoline core in a one-pot, two-step sequence. In this transformation, the amide moiety was converted to an imidoyl chloride using PCl_5, which was then treated with ethyl cyanoformate and $SnCl_4$. Acting as a Lewis acid, the $SnCl_4$ mediates the formation of the quinazoline core between the resulting acyl nitrilium ion and the aniline phenyl ring. The quinazoline ethyl ester product obtained from this sequence was smoothly saponified using 6M NaOH/ethanol at room temperature to afford the desired carboxylic acid precursor. Finally, similar to the first step, the resultant carboxylic acid was treated with thionyl chloride to form an acid chloride and various amines were introduced to achieve the desired diversity.

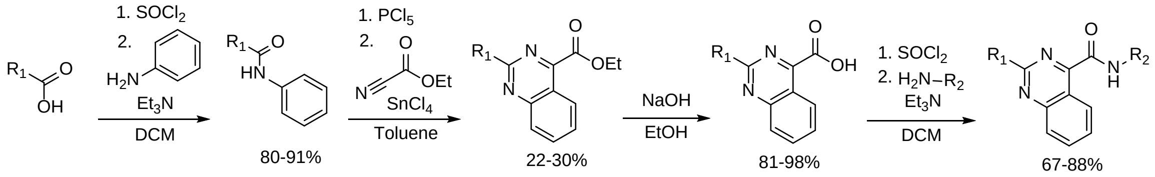

Figure 2.11. General synthesis of SMI-27
General synthetic scheme of the 2,4-disubstituted quinazoline small molecule, SMI-27 analogs.[16]

The proposed mechanism for the key Meerwein cyclization step, shown in Figure 2.12, is thought to proceed through a five-membered Lewis acid chelate that enhances the electrophilicity of the nitrilium carbon.[17] The increased reactivity allows cyclization to occur in a favorable 6-endo-dig fashion that, upon re-aromatization, generates the final products in yields ranging from 22% to 30%. While somewhat disappointing, the low yields are acceptable given the significant structural changes that occurred in the one-pot transformation. Future work should include an effort to improve the yields of this transformation, especially considering the high reactivity of the imidoyl chloride, low nucleophilicity of the arene required for cyclization, and difficulty in isolating the product from the back tar produced following aqueous workup. Even though overall yields of the entire 7-step process were as low as 10%, a small library of 24 different compounds were produced using this general synthetic route.

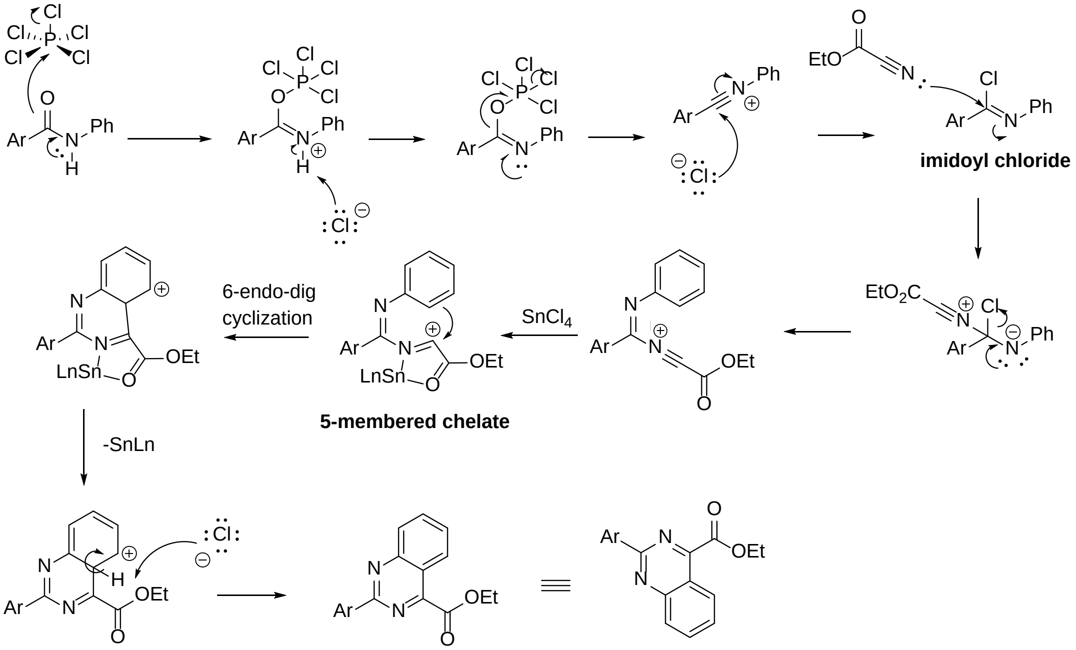

Figure 2.12. Meerwein cyclization mechanism.
Proposed mechanism for the Meerwein cyclization reaction to form the quinazoline core of SMI-27.[17]

Summary

Using computational methods, a WDM was generated using 10,000 randomly selected compounds docked in OSM site 3. Then, the WDM was used to create a visual representation, aiding in the rational design of new SMI candidates. A 2,4-disubstituted quinazoline small molecule, called SMI-27, overlaid well with the WDM and could be prepared by a short synthetic sequence. Thus, SMI-27 was selected for optimization via the synthesis of a small library of analogs. The synthesis involves four steps to access final analogs, involving a Meerwein cyclization in the second step that was key to affording the quinazoline core. Using various combinations of R_1 and R_2, the synthesized library consisted of 24 different analogs in total. As described in the next chapter, the compounds were evaluated for their ability to inhibit OSM induced pSTAT3 expression, as well as binding affinity toward OSM.

References

1. Deller, M. C.; Hudson, K. R.; Ikemizu, S.; Bravo, J.; Jones, E. Y.; Heath, J. K., Crystal structure and functional dissection of the cytostatic cytokine oncostatin M. *Structure* **2000,** *8* (8), 863-74.

2. de Vos, A. M.; Ultsch, M.; Kossiakoff, A. A., Human growth hormone and extracellular domain of its receptor: crystal structure of the complex. *Science* **1992,** *255* (5042), 306-12.

3. Adrian-Segarra, J. M.; Schindler, N.; Gajawada, P.; Lörchner, H.; Braun, T.; Pöling, J., The AB loop and D-helix in binding site III of human Oncostatin M (OSM) are required for OSM receptor activation. *J Biol Chem* **2018,** *293* (18), 7017-7029.

4. Du, Q.; Qian, Y.; Xue, W., Molecular Simulation of Oncostatin M and Receptor (OSM-OSMR) Interaction as a Potential Therapeutic Target for Inflammatory Bowel Disease. *Front Mol Biosci.*, **2020**. *7*, 29

5. Harris, R.; Olson, A. J.; Goodsell, D. S., Automated prediction of ligand-binding sites in proteins. *Proteins* **2008,** *70* (4), 1506-17.

6. Chollangi, S.; Mather, T.; Rodgers, K. K.; Ash, J. D., A unique loop structure in oncostatin M determines binding affinity toward oncostatin M receptor and leukemia inhibitory factor receptor. *J Biol Chem* **2012,** *287* (39), 32848-59.

7. Durrant, J. D.; Votapka, L.; Sørensen, J.; Amaro, R. E., POVME 2.0: An Enhanced Tool for Determining Pocket Shape and Volume Characteristics. *J Chem Theory Comput* **2014,** *10* (11), 5047-5056.

8. Purohit, V.; Basu, A. K., Mutagenicity of nitroaromatic compounds. *Chem Res Toxicol* **2000,** *13* (8), 673-92.

9. Topliss, J. G., Utilization of operational schemes for analog synthesis in drug design. *J Med Chem* **1972,** *15* (10), 1006-11.

10. Shvekhgeimer, M. G., The Pfitzinger Reaction. *Chem Heterocycl Compd* **2004**, *40* (3), 257-294.

11. Charlier, H. A.; Plapp, B. V., Kinetic cooperativity of human liver alcohol dehydrogenase γ2. *J Biol Chem* **2000**. *257*, 11569-11575.

12. Morris, G. M.; Huey, R.; Lindstrom, W.; Sanner, M. F.; Belew, R. K.; Goodsell, D. S.; Olson, A. J., AutoDock4 and AutoDockTools4: Automated docking with selective receptor flexibility. *J Comput Chem* **2009,** *30* (16), 2785-91.

13. Pettersen, E. F.; Goddard, T. D.; Huang, C. C.; Couch, G. S.; Greenblatt, D. M.; Meng, E. C.; Ferrin, T. E., UCSF Chimera--a visualization system for exploratory research and analysis. *J Comput Chem* **2004,** *25* (13), 1605-12.

14. Trott, O.; Olson, A. J., AutoDock Vina: improving the speed and accuracy of docking with a new scoring function, efficient optimization, and multithreading. *J Comput Chem* **2010,** *31* (2), 455-61.

15. Arkin, M.; Randal, M.; DeLano, W.; Hyde, J.; Luong, T.; Oslob, J.; Raphael, D.; Taylor, L.; Wang, J.; McDowell, R.; Wells, J.; Braisted, A., Binding of small molecules to an adaptive protein-protein interface. *Proc Natl Acad Sci USA* **2003,** *100* (4), 1603-1608.

16. Young BL, J. M., Deog; JK, C.-H. A. Tetrahydroisoquinolin-2-yl-(quinazolin-4-yl)methanone compounds as cancer cell growth inhibitors. World Patent WO2014143960, **2015**.

17. Danijel, K.; N., R.; Helmut, R.; Frank, S., Hetarenes III (Six-Membered Rings and Larger Hetero-Rings with Maximum Unsaturation), *Houben-Weyl Methods of Organic Chemistry, 4th Edition;* Georg Thieme Verlag: **2014**; Vol. E 9b/2, pp 550.

CHAPTER THREE: EVALUATION OF SMI-27 ANALOGS TARGETING OSM

Overview of Chapter

OSM has been shown to play a role in rheumatoid arthritis, inflammatory bowel disease, various forms of cancer, and other inflammatory diseases.[1-4] OSM is responsible for initiating the activation of several cell signaling proteins.[5-7] One of the first is STAT3, which is phosphorylated to pSTAT3 as part of the JAK/STAT signaling pathway. In order to assess SMI-27 analogs' ability to inhibit OSM activity, we evaluated inhibition of OSM-induced pSTAT3 expression using an enzyme-linked immunosorbent assay (ELISA). To determine SMI binding specificity and cytokine cross-reactivity, western blot assays were also performed with multiple related cytokines. Fluorescence quenching assays were used to determine the binding affinity of SMI analogs toward OSM. Finally, NMR chemical shift perturbation (CSP) experiments were used to validate binding experiments and identify the important amino acids required for binding of the SMI to OSM.[8] These experiments and their results, along with new and potentially improved SMIs and their proposed syntheses are described herein.

Nomenclature of SMI-27 Analogs

A discussion of the biological activity of the SMI-27 analogs first requires an explanation of the systematic nomenclature of the analogs, which is based on the functional groups appended at two particular sites, referred to as R_1 and R_2, as shown in

Table 3.1. For example, in the case of 27A1, the first numeric indicator “27” refers to the quinazoline core with an amide at the 4-position, the alphabetical indicator “A” refers to a given aromatic group (R_1) appended to the 2-position, and the second numerical indicator “1” refers to the group appended to the amide (R_2) at the 4-position. In addition, when an analog is referred to as a member of the “A-series”, the R_1 group is held constant while the R_2 groups are changed. Likewise, when referring to the “1-series”, the R_2 substituent “1” (i.e., a benzyl group) is held constant while the substituents at R_1 are changed. Lastly, SMI-27 analogs, such as 27A1, will often be shortened to just “A1”. A library of 24 SMI-27 analogs was synthesized using various combinations of R_1 (A-C) and R_2 (1-12), as denoted in Table 3.1.

Table 3.1. SMI-27 Nomenclature

SMI-27 structures are named based on the R_1 and R_2 groups placed at the 2-position and 4-position, respectively. The example of 27A1 is shown with R_1 equaling "A" and R_2 equaling "1".

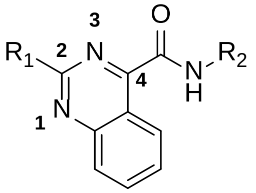

Generic SMI-27

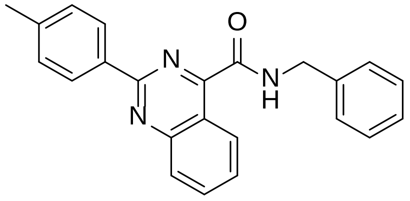

27A1

R_1	**R_2**			
A 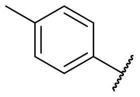	**1** 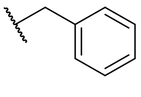	**2** 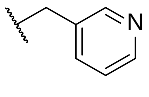	**3** 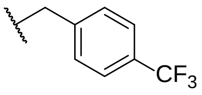	**4** 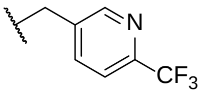
B 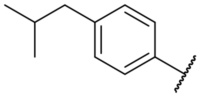	**5** 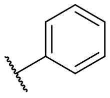	**6** 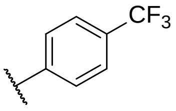	**7** 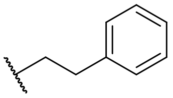	**8** 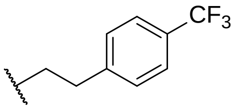
C 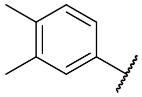	**9** 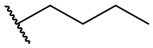	**10** 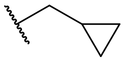	**11** 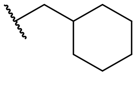	**12** 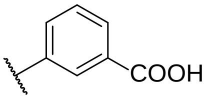

Enzyme-Linked Immunosorbent Assay

Upon forming a complex with its receptors, OSM initiates a signaling cascade that induces the phosphorylation of several signaling proteins, one of which is STAT3.[5] Specifically, Tyr705 on STAT3 is phosphorylated by receptor-associated Janus kinases (JAK) to form phosphorylated STAT3 (pSTAT3). To assess SMI-27 analogs' ability to inhibit OSM cell signaling, a sandwich ELISA was performed by Cody Wolf, a doctoral graduate student in the Jorcyk lab (Figure 3.1). In short, T47D human breast cancer cells were treated with OSM and SMI, the cells were lysed, and then the cell lysates were treated with a "capture" antibody specific for binding to pSTAT3. A "detection" antibody, which is selective for the capture antibody, relies upon chemiluminescence and absorbance to quantify the extent of pSTAT3 expression. When there is no exogenous OSM present (no treatment, NT), the expression of pSTAT3 in the cell is minimal. When cells are treated with OSM (10 ng/mL), a significant amount of pSTAT3 is observed and this amount is used as a positive control and normalized to one (i.e., 1.0). To evaluate the inhibitory activity of each SMI, twenty-one of the SMI-27 analogs were pre-incubated with OSM before adding it to the cells. The resultant pSTAT3 expression is then compared to the positive control, where an optimal SMI would fully inhibit pSTAT3 expression, returning expression to no treatment levels.

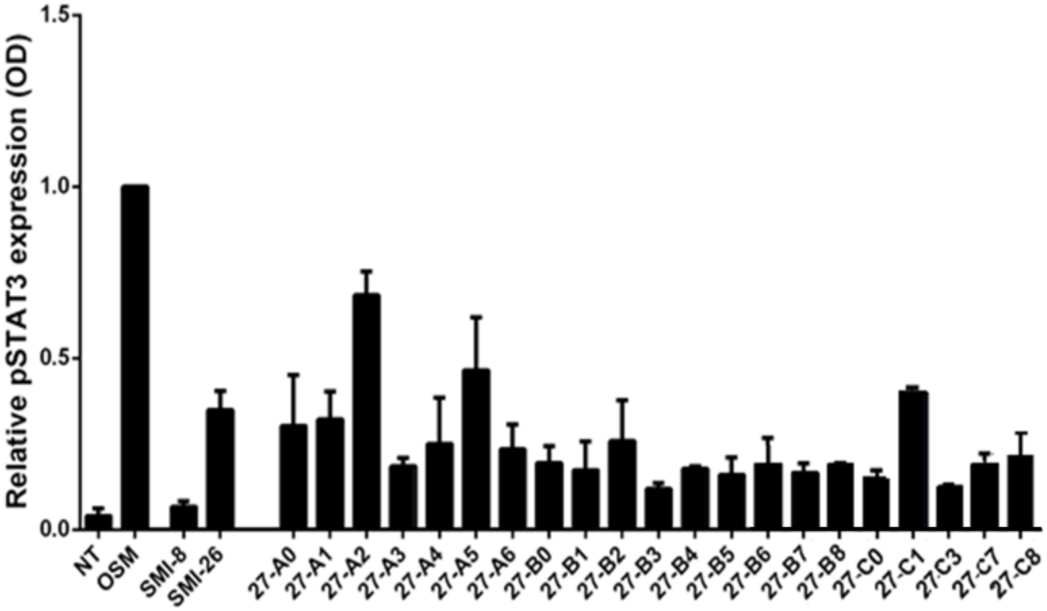

Figure 3.1. Enzyme-linked immunosorbent assay of SMI-27 analogs.
A lower relative pSTAT3 expression level suggests that SMI-27 analogs bind to OSM and inhibit its ability to initiate cell signaling. All SMI-27 analogs tested inhibit pSTAT3 expression below the control. SMI-8 and SMI-26, analogs discovered using a high-throughput virtual screening, are shown for comparison. All experiments were run in triplicate (n = 3) (Data obtained by Cody Wolf, Jorcyk lab)

The results obtained from the ELISA allow for preliminary structure-activity relationships to be determined. Regarding the R_2 group, the 3-series, each with a 4-trifluoromethylbenzyl group, were the best performers of each analog set (A, B, and C). The 4-series always performed worse than the 3-series, presumably due to the conversion of a CH group to an sp^2 hybridized nitrogen atom in the R_2 aryl ring (i.e., a picolyl group) given that this is the only difference between the two. Interestingly, this is in direct contrast to computational docking predictions, where the 4-series were predicted to be the best performers of all SMI-27 analogs. Similarly, in contrast to the computational prediction, the 2-series with an unsubstituted picolyl group at R_2 always performed worse than the 1-series with an unsubstituted benzyl group at R_2. Thus, incorporation of a nitrogen into the R_2 aryl ring reduces the ability of the SMI to inhibit OSM signaling. As such, no additional analogs containing a picolyl group were prepared.

The ELISA experiments also suggest a trend with respect to the R_1 group. Specifically, every B-series, which has an isobutylphenyl group at R_1, performs better than the corresponding 4-methylphenyl A-series and 3,4-dimethylphenyl C-series. This suggests that molecules with more hydrophobic and rotationally flexible alkyl groups attached to the benzene ring at R_1 better inhibit OSM induced pSTAT3 expression. While this was not predicted by the computational docking studies, it was speculated that the adaptive nature of the protein binding pocket combined with a more flexible SMI might allow more SMI-protein interactions to occur.[9] The ELISA data show promising evidence that all the rationally designed SMI-27 analogs that were tested inhibit OSM cell signaling, as indicated by the decrease of induced pSTAT3 expression below the level of the control.

Western Blot Assay

Cytokines similar in structure to OSM, such as IL-6 and LIF, that bind to heterodimeric complexes of gp130 and their respective receptors can also induce pSTAT3 expression.[6] In order to determine if inhibition of pSTAT3 expression is attributable to specific binding of SMIs to OSM and not related cytokines, a western blot assay was conducted by Cody Wolf (Jorcyk lab) using SMIs 27B3 and 27B5, two of the better performing analogs in the ELISA study. Similar to an ELISA, T47D human breast cancer cells were treated with OSM, IL-6, or LIF in the presence and absence of the SMIs. Next, the cells were lysed and electrophoresed on an SDS-PAGE gel. The gel was then transferred to a nitrocellulose membrane and treated with pSTAT3 specific antibodies. One of the antibodies is fluorescently tagged that allows for quantification of pSTAT3 expression. If the signal (band color intensity) decreases, it demonstrates that the SMI is inhibiting the cell signaling induced by that particular cytokine.

The western blot experiments, presented in Figure 3.2, show that both 27B3 and 27B5 only decrease the signal of the OSM band to a great extent, meaning that they specifically bind to OSM, with reduced or no binding to IL-6 or LIF. These data also imply that SMIs 27B3 and 27B5 are not inhibiting pSTAT3 production through binding to receptors such as gp130 or LIFR, IL-6 and LIF still induce pSTAT3 expression in the presence of SMI.

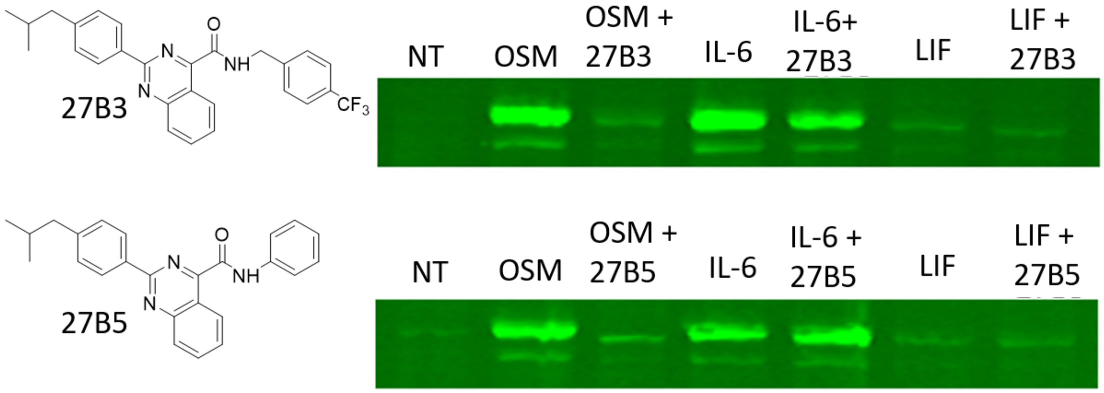

Figure 3.2. Western blot assays of SMI 27B3 and 27B5.
The western blot assay shows that both 27B3 and 27B5 inhibit pSTAT3 expression induced by OSM, as indicated by the decreased band intensity. The SMIs do not significantly inhibit induction of pSTAT3 by IL-6 or LIF. (Data obtained from Cody Wolf, Jorcyk lab)

Fluorescence Quenching Assay

The ELISA results demonstrated that the SMI-27 analogs inhibit OSM-induced expression of pSTAT3. Further, the western blot assays suggested that the inhibition occurred via disruption of the binding of OSM to its receptors. However, we desired to investigate the direct binding of SMI-27 analogs to OSM. To achieve this, fluorescence quenching (FQ) assays were employed, using an adaptation of a protocol previously described by Charlier and Plapp to investigate human liver alcohol dehydrogenase.[10] This assay was chosen because OSM has a tryptophan amino acid residue, Trp187, that will fluoresce at 350 nm when excited at 280 nm. Upon binding of the SMI to OSM, a reduction, or quenching, of the fluorescence intensity of the emitted wavelength is observed (Figure 3.3A). The quantified signal is then plotted against SMI concentration and the data is fit to a modified Stern-Volmer function to calculate a dissociation constant, Kd (Figure 3.3B).

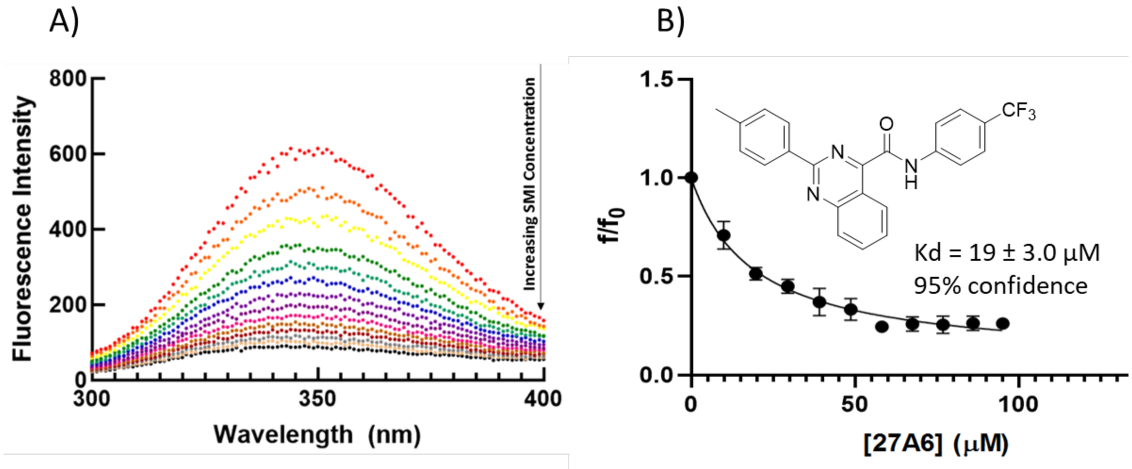

Figure 3.3. Fluorescence quenching assay for Kd determination.
A) Fluorescence signal intensity quenched with each addition of an SMI. B) Fluorescence signal intensity plotted against concentration of SMI-27A6, with a Stern-Vollmer function applied to determine a Kd of 19 ± 3.0 μM. Samples were run in triplicate along with a DMSO blank.

Data obtained from the FQ experiments provide important structure-activity relationships (SAR) for the SMIs based on how well they bind. In regard to changing the

R_1 group and holding R_2 constant, no clear and absolute trends in binding affinity are observed, as shown in Figure 3.4. This can potentially be explained by the fact that all the R_1 groups are structurally very similar, with each being an alkyl-substituted benzene ring. This was expected because, as mentioned in chapter 2, the R_1 groups were not computationally predicted to have a major impact on binding affinity. It is hypothesized that investigation of groups with varying steric, electron withdrawing, and electron donating properties would allow for further determination of SAR and improved binding affinity.

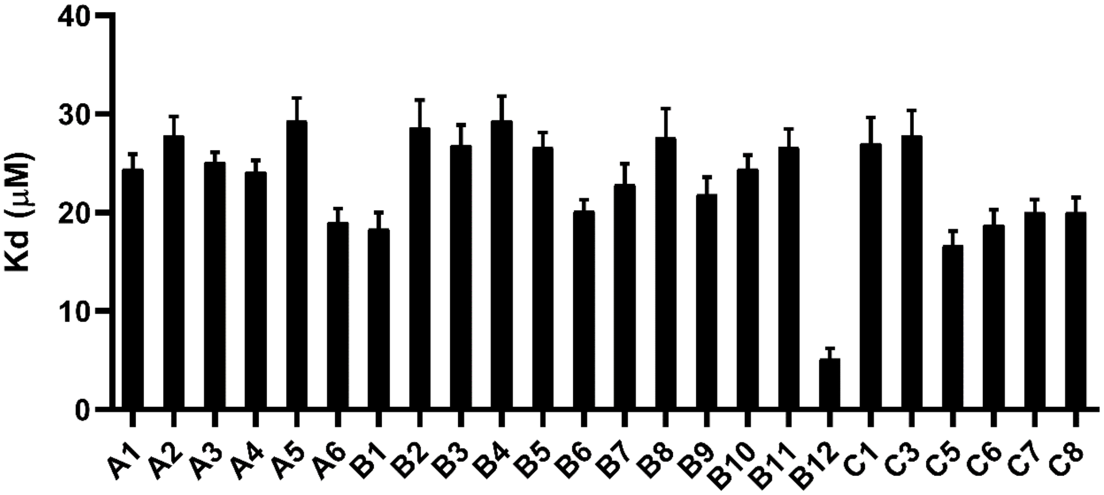

Figure 3.4. Kd values of SMI-27 analogs.
Kd values for SMI-27 analogs ranging from 29.3 to 5.1 μM obtained from fluorescence quenching assays. Each sample was run in triplicate along with a DMSO blank.

Changing the R_2 group was computationally predicted to have a greater effect on binding affinity, thus received more focus than R_1 for introducing diversity to the SMI-27 analogs and several trends are observed. When examining the effect a nitrogen heteroatom in the R_2 aryl ring has on binding affinity, a clear trend occurs. First, the 1-series that contained an unsubstituted benzyl group had an increased binding affinity over the 2-series, which contained an unsubstituted picolyl group. Similarly, B3 which has a 4-trifloromethylbenzyl group, performed better than B4, which differs only by the conversion of a CH group to an sp^2 hybridized nitrogen atom in the R_2 aryl ring. These results are is consistent with the ELISA data, but are inconsistent with computational predictions. Further, B4, with a binding energy of -8.7 kcal/mol, was predicted to be one of the best predicted analogs. In the FQ assay, it actually was the worst performing SMI-27 analog, with a Kd of 29.3 ± 5.6 μM (Table 3.2). These discrepancies might be explained by the picolyl nitrogen and its increased electronegativity compared to the whole carbon analogs, which would decrease aromatic ring electron density and thus weaken potential cation/pi interactions with positively charged amino acids.

Table 3.2. SMI-27 binding data

SMI-27 names, susbtituents, binding affinities, and predicted binding energies.

	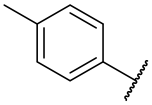	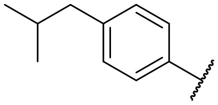	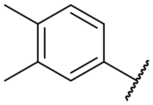
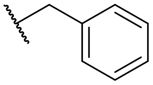	**27A1**	**27B1**	**27C1**
	Kd = 24.4 ± 3.2	Kd = 18.3 ± 3.7	Kd = 27.0 ± 5.6
	$E_{rel} = -7.3$	$E_{rel} = -7.0$	$E_{rel} = -7.4$
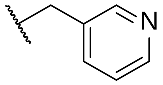	**27A2**	**27B2**	Not synthesized
	Kd = 27.8 ± 4.3	Kd = 28.6 ± 6.1	
	$E_{rel} = -7.5$	$E_{rel} = -7.3$	
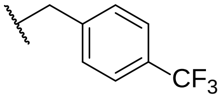	**27A3**	**27B3**	**27C3**
	Kd = 25.1 ± 2.2	Kd = 26.8 ± 4.5	Kd = 27.8 ± 5.6
	$E_{rel} = -8.8$	$E_{rel} = -8.4$	$E_{rel} = -8.7$
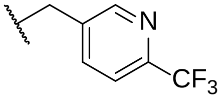	**27A4**	**27B4**	Not synthesized
	Kd = 24.1 ± 2.5	Kd = 29.3 ± 5.6	
	$E_{rel} = -9.1$	$E_{rel} = -8.7$	
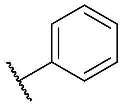	**27A5**	**27B5**	**27C5**
	Kd = 29.3 ± 4.9	Kd = 26.6 ± 3.0	Kd = 16.6 ± 3.5
	$E_{rel} = -7.5$	$E_{rel} = -7.3$	$E_{rel} = -7.6$
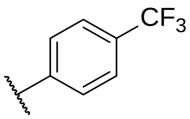	**27A6**	**27B6**	**27C6**
	Kd = 19.0 ± 3.0	Kd = 20.1 ± 2.3	Kd = 18.7 ± 3.5
	$E_{rel} = -6.9$	$E_{rel} = -7.1$	$E_{rel} = -7.2$

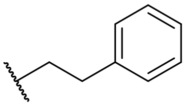	Not synthesized	**27B7** Kd = 22.8 ± 4.8 E_{rel} = -7.2	**27C7** Kd = 20.0 ± 2.7 E_{rel} = -7.3
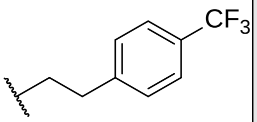	Not synthesized	**27B8** Kd = 27.6 ± 6.7 E_{rel} = -8.3	**27C8** Kd = 20.0 ± 3.4 E_{rel} = -8.4
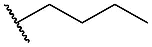	Not synthesized	**27B9** Kd = 21.8 ± 3.9 E_{rel} = -6.5	Not synthesized
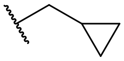	Not synthesized	**27B10** Kd = 24.4 ± 3.0 E_{rel} = -6.5	Not synthesized
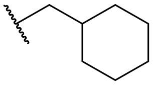	Not synthesized	**27B11** Kd = 26.6 ± 4.1 E_{rel} = -6.7	Not synthesized
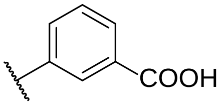	Not synthesized	**27B12** Kd = 5.1 ± 2.7 E_{rel} = -7.7	Not synthesized

Kd values are expressed in μM as determined by fluorescence quenching assays.

E_{rel} values are expressed in kcal/mol as predicted by computational docking studies.

The chain length of the R_2 group that links it to the amide presents another observable trend. The shorter aniline derivatives tend to have higher binding affinities for every series (A, B, and C) compared to the longer benzyl and phenethyl groups at R_2. Possibly, the shorter and less flexible bond linking the aniline to the amide might force the aniline group into the pocket of OSM site 3, which contains positively charged Arg91/Arg162 residues. These groups are predicted to be involved in cation/pi interactions and play a major factor in binding affinity. Benzyl and phenethyl groups have increased rotational freedom, allowing them to adopt different binding poses outside the pocket containing the Arg91/Arg162 residues critical for binding. Further, the aromatic rings of the aniline analogs are more electron rich due to direct conjugation with the amide nitrogen. This would allow for stronger cation/pi interactions, in contrast to the non-conjugated benzyl and phenethyl groups.

Next, electron withdrawing groups were placed on the R_2 aryl ring to investigate their effect on binding affinity. It can be observed that the 6-series, containing a 4-triflouromethyl aniline, tend to perform better than the 5-series, containing a non-substituted aniline. This trend compliments both the computational predictions and the ELISA results. It is hypothesized that placing an electron withdrawing group on the R_2 group pulls electron density towards that side of the molecule making it electron rich, allowing for electrostatic interactions with the positively charged Arg91/Arg162 residues deep in a pocket of OSM site 3. This hypothesis is further reinforced in light of the increased binding affinity of B12, a 3-carboxyaniline derivative with a Kd of 5.1 ± 2.7 μM, that substantially outperforms all other SMI-27 analogs. This is likely due to the carboxylic acid having a formal negative charge at physiological pH that allows for strong interactions with the positively charged Arg91/Arg162 residues. However, having an electron withdrawing group on the R_2 aryl ring does not always increase binding affinity, as shown by a comparison of the 1-series to the 3-series. For these groups, the absence (1-series) or presence (3-series) of a 4-trifluoromethyl substituent on the benzyl group is the only difference. The minimal impact of the electron withdrawing group could be due to the benzyl group having an additional degree of rotational freedom. As previously described, this would allow for different binding poses to occur outside the deep binding pocket in OSM site 3 that would not participate in electrostatic interactions with the Arg91/Arg162 residues.

To investigate the effect of cation/pi interaction between the positively charged Arg91/Arg162 residues and aromatic R_2 groups, non-aromatic groups were introduced at R_2. Analog B1, containing an aromatic benzyl group, binds with higher affinity than B11, which has a non-aromatic cyclohexylmethyl group. The improved affinity implies that cation/pi interactions are, in fact, important.

In summary, the FQ assays demonstrated that all SMI-27 analogs exhibited direct binding to OSM, with Kd values ranging from 29.3 to 5.1 μM. The analog with the worst binding affinity is 27B4, which has a 4-triflouromethylpicolyl R_2 group. The best performing analog is 27B12 that contains a 3-carboxylic aniline at R_2. However, there are gaps in the analog library, so additional compounds must be synthesized and tested in order to obtain a complete SAR profile.

A 2-way ANOVA statistical analysis was performed by Laura Bond on the Kd values obtained from the FQ assay to determine if any significant differences occurred. The analysis confirmed that B12, containing a 3-carboxylic acid aniline at R_2, was in fact the best performing analog. All other R_2 series values are not significantly different, where comparisons can be made. Also, when holding R_2 constant and changing R_1, the

C-series, on average, had improved Kd values compared to the A- and B-series. This result suggests that alkyl substitution at two positions on the R_1 phenyl group, at positions 3 and 4, affords extra stabilizing hydrophobic interactions since both the A-series and the B-series are only substituted at the 4 position. Thus, to a first approximation, the statistical analysis supports the generation of an analog that combines the 3,4-dimethylphenyl group at R_1 (the C-series) and a 3-carboxylic acid aniline at R2 (the 12-series) for future analysis.

NMR Chemical Shift Perturbation Assay

Preliminary NMR experiments were conducted to determine residues involved in binding and the location in which SMIs bind to OSM. Specifically, chemical shift perturbation (CSP) assays were used to accomplish this goal.[8] This experiment involves first recording a $^{15}N/^{1}H$ heteronuclear single quantum correlation (HSQC) NMR spectrum of isotopically enriched OSM and then obtaining another spectrum after addition of increasing concentration of SMI. If the SMI binds to OSM, the HSQC chemical shifts for the amino acid residues involved in binding to the SMI will be perturbed due to a change in the magnetic environment. This experiment relies upon ^{15}N-isotopically enriched OSM, which was obtained from the Boise State Biomolecular Research Center using a protocol developed by Dr. Lisa Warner and co-workers (data unpublished).

SMI 27B5 was chosen for proof-of-concept CSP experiments since it showed a significant reduction of relative pSTAT3 expression in the ELISA, displayed specific binding to OSM by western blot, and had a moderate Kd value based on the fluorescence quenching experiment. As shown in Figure 3.5, HSQC spectra were obtained upon addition of 1 or 2 μL increments of 20 mM SMI stock solution (corresponding to 20, 40, 80, and 120 μM SMI) to 500 μL of a 100 μM solution of OSM. The signals for several residues, highlighted in boxes, shifted upon addition of increasing amounts of the SMI.

The SMI-27 analog perturbed the chemical shift of three amino acids that are also perturbed by an SMI-10 analog. The three amino acids, with chemical shifts at (7.2, 115), (7.0, 122), and (7.7, 106) ppm, have been tentatively assigned as Arg91, Lue92, and Gly166, respectively, based on a minimal chemical shift displacement from previously published NMR chemical shift assignments of a different OSM construct.[11] These results are significant because these three amino acids are all located in OSM site 3, the site at which OSM binds to OSMR. Importantly, SMI-27 and SMI-10 are structurally very different (see Figure 2.3 in Chapter 2 for SMI-10 structure) and were designed to target OSM site 3 using two different computational methods (SMI-10 via a high-throughput virtual screen and SMI-27 via a weighted probability map). Further, this result suggests that our weighted probability map to computationally design SMI-27 analogs that target OSM's site III is a valid approach. Currently, our collaborative team is assigning chemical shifts of the amino acid backbone for this particular construct of OSM, which will allow for the unequivocal identification of the SMI/OSM binding site and will enable the identification of valuable SAR information to help guide the design of more potent analogs.

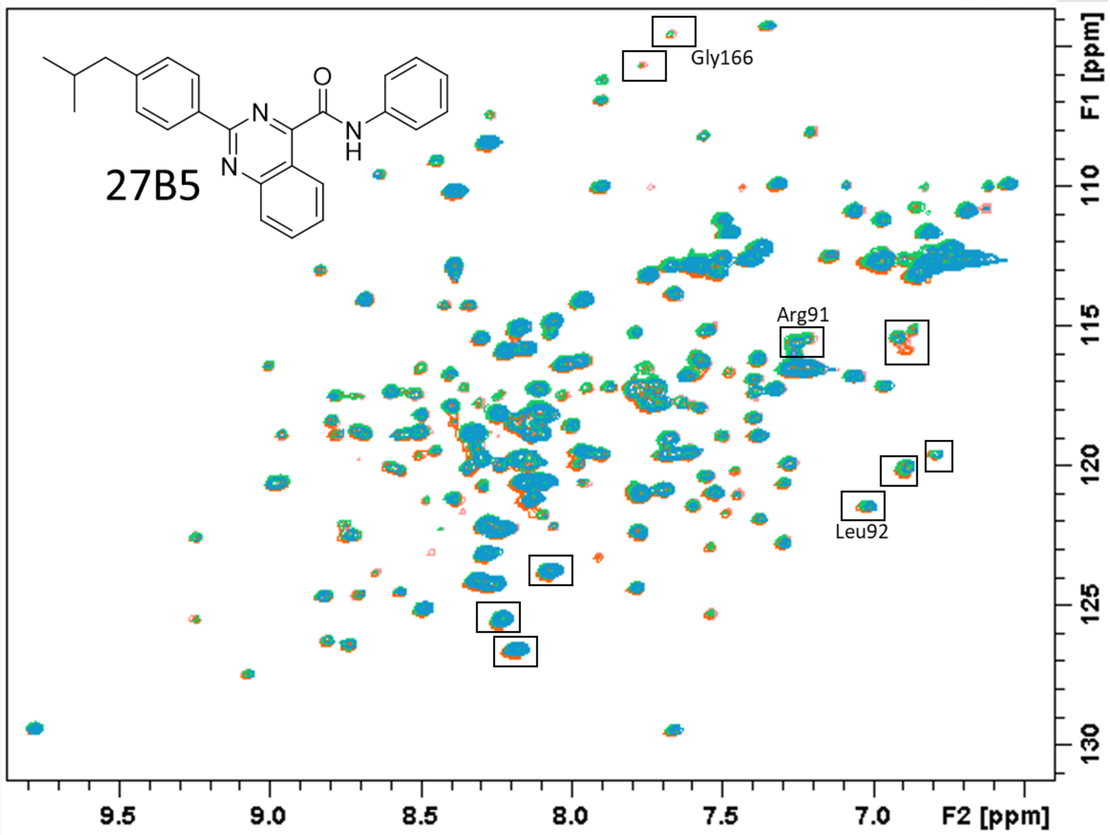

Figure 3.5. Chemical shift perturbation assay.
Ten different residues that shift upon addition of increasing amounts of SMI-27B5 are highlighted by boxes. Notably, Arg91, Lue92, and Gly166, with chemical shifts of (7.2, 115), (7.0, 122), and (7.7, 106) ppm, respectively, are found in OSM binding site 3, which is the targeted binding site.

Conclusions and Future Directions

The current approach used to synthesize SMI-27 analogs and their 2,4-disubstituted quinazoline core has successfully generated a small library of compounds but has several flaws that must be overcome. Specifically, the synthesis is not convergent and amenable to generating diversity at R_1. Currently, incorporation of different groups at this site must be accomplished in the very first step of the sequence, restricting the introduction of significant diversity in subsequent steps. This is problematic since the yield of the second step, involving the cyclization to form the quinazoline core, generates product in particularly low yield, allowing for only a small handful of final analogs to be made due to material constraints. Therefore, new SMIs that are structurally related to SMI-27 but employ a different synthetic route must be designed, synthesized, and evaluated to allow more diversity and create potentially more potent compounds. For this reason, several alternative approaches are suggested below.

Palladium-catalyzed cross-coupling reactions using commercially available 2,4-dichloroquinazoline offer a facile approach to generate a large library of compounds using a convergent synthetic route (Figure 3.6). This sequence relies upon preferential activation of the chlorine at the 4-position over that at the 2-position toward oxidative addition of a palladium (0) catalyst, which is often the rate-limiting step in Suzuki or Stille coupling reactions. Accordingly, literature precedent suggests that there is regioselectivity for coupling at the 4-position over the 2-position.[12] The route proposed in Figure 3.6A provides entry to a variety of amides at R_2 relying on a Stille cross-coupling reaction to install the ethyl ester that is subsequently converted to the R_2-containing amide.[13] Also, diversity at the R_1 position is incorporated using commercially available boronic acids or esters in Suzuki cross-coupling reactions.

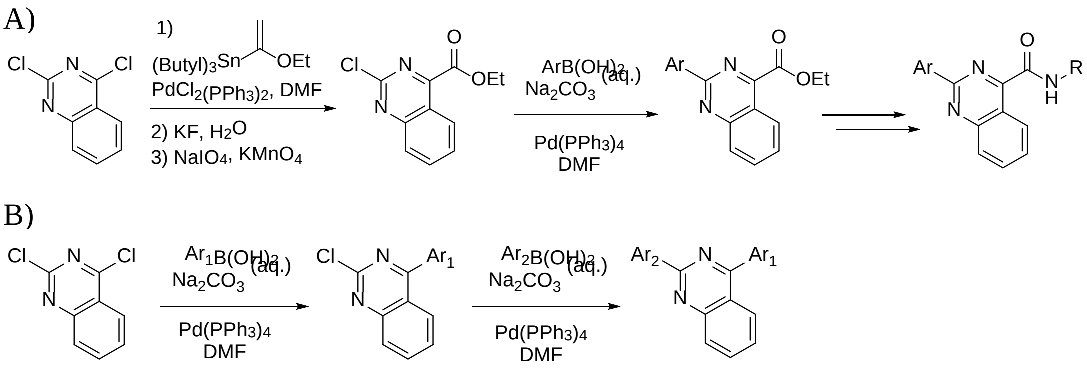

Figure 3.6. Alternative synthesis of 2,4-disubstituted quinazolines.

From the Kd values obtained using FQ assays, increasing the hydrophobicity does not appear to have a significant effect on binding affinity. For that reason, aryl groups containing hetero atoms in the ring, and/or electron withdrawing and donating substituents should be investigated. Similarly, the same starting material will provide access to non-amide functional groups at R_2, using the sequence depicted in Figure 3.6B. In addition to allowing for investigation of the importance of the amide functional group at this position, it will enable for investigation of the effect of heterocycles, aliphatic groups, and other previously inaccessible functional groups. Final compounds will be obtained quickly though a 2-step reaction sequence from commercially available starting materials.

The quinazoline core is rather planar and hydrophobic, which leads to poor solubility in aqueous media and could be problematic when developing a drug that is intended to be orally bioavailable. For this reason, it is also worth considering a pyrimidine core in place of the quinazoline that is present in the SMI-27 analogs. As shown in Figure 3.7, the pyrimidine lacks the bicyclic ring of the quinazoline, increasing the ratio of heteroatoms and sp^2 carbon atoms, which should render it less hydrophobic and more water soluble. Overall, to produce amide-containing (Figure 3.7A) and non-amide containing compounds (Figure 3.7B), reactions previously proposed in Figure 3.6 should be used. Importantly, the schemes presented in Figure 3.7 should produce final compounds in only 2 steps from commercially-available building blocks, allowing for a small library of compounds to be synthesized quickly.

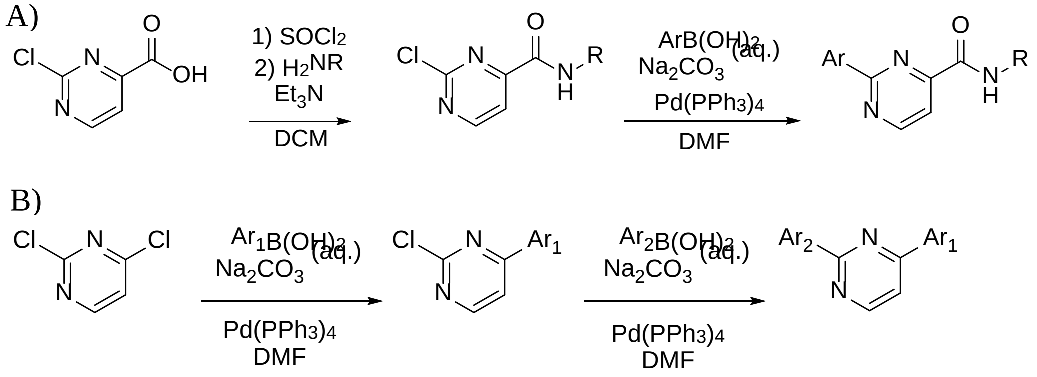

Figure 3.7. Synthesis of 2,4-disubstituted pyrimidines.

Finally, the synthesis of analogs containing a pyrazolo[3,4-d]pyrimidine core is proposed (Figure 3.8). While this moiety retains the bicyclic planar ring system similar to the quinazoline compounds, it increases the number of heteroatoms and a basic nitrogen atoms which should increase aqueous solubility and bioavailability. The compounds can be prepared by first protecting the pyrazole nitrogen and then performing sequential Suzuki coupling reactions as described previously.

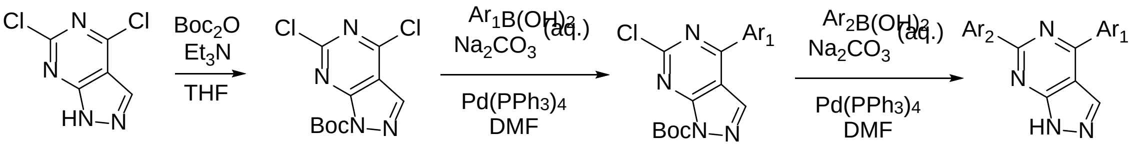
Cl
N
Cl
N
HN–N
Boc2O
Et3N
THF
Cl
N
Cl
N
BocN–N
Ar1B(OH)2 (aq.)
Na2CO3
Pd(PPh3)4
DMF
Cl
N
Ar1
N
BocN–N
Ar2B(OH)2 (aq.)
Na2CO3
Pd(PPh3)4
DMF
Ar2
N
Ar1
N
HN–N

Figure 3.8. Synthesis of 2,4-disubstituted pyrazolopyrimidines.

In summary, all rationally designed and synthesized SMI-27 analogs tested by ELISA exhibited inhibition of OSM signaling. SMIs 27B3 and 27B5 appear to be selective for OSM over the cytokines IL-6 and LIF, as evidenced by western blot assays. This is especially noteworthy given the structural similarity of OSM to LIF. The FQ assays demonstrated direct binding to OSM, with Kd values ranging from 29.3 to 5.1 μM. The SMI 27B12, which contains a carboxylic acid on the R_2 aryl group, has a Kd of 5.1 ± 2.7 μM, which is the best value observed for all the SMI-27 analogs. CSP assays indicate that two structurally distinct SMIs, 27B5 and 10B, both bind in OSM site 3, which helps validate the computational model. This research lays a solid foundation that could help lead to the development of a SMI drug candidate, which would provide a significant advancement in clinical treatments of OSM related diseases.

References

1. Alam, J.; Jantan, I.; Bukhari, S. N. A., Rheumatoid arthritis: Recent advances on its etiology, role of cytokines and pharmacotherapy. *Biomed Pharmacother* **2017,** *92*, 615-633.

2. West, N. R.; Hegazy, A. N.; Owens, B. M. J.; Bullers, S. J.; Linggi, B.; Buonocore, S.; Coccia, M.; Görtz, D.; This, S.; Stockenhuber, K.; Pott, J.; Friedrich, M.; Ryzhakov, G.; Baribaud, F.; Brodmerkel, C.; Cieluch, C.; Rahman, N.; Müller-Newen, G.; Owens, R. J.; Kühl, A. A.; Maloy, K. J.; Plevy, S. E.; Keshav, S.; Travis, S. P. L.; Powrie, F.; Bailey, A.; Barnes, E.; Bird-Lieberman, B.; Brain, O.; Braden, B.; Collier, J.; East, J.; Howarth, L.; Klenerman, P.; Leedham, S.; Palmer, R.; Rodrigues, A.; Simmons, A.; Sullivan, P.; Uhlig, H., Oncostatin M drives intestinal inflammation and predicts response to tumor necrosis factor–neutralizing therapy in patients with inflammatory bowel disease. *Nature Medicine* **2017,** *23,* 579-589.

3. García-Tuñón, I.; Ricote, M.; Ruiz, A.; Fraile, B.; Paniagua, R.; Royuela, M., OSM, LIF, its receptors, and its relationship with the malignance in human breast carcinoma (in situ and in infiltrative). *Cancer Invest* **2008,** *26* (3), 222-9.

4. Royuela, M.; Ricote, M.; Parsons, M. S.; García-Tuñón, I.; Paniagua, R.; De Miguel, M. P., Immunohistochemical analysis of the IL-6 family of cytokines and their receptors in benign, hyperplasic and malignant human prostate. *J Pathol* **2004,** *202* (1), 41-49.

5. Korzus, E.; Nagase, H.; Rydell, R.; Travis, J., The mitogen-activated protein kinase and JAK-STAT signaling pathways are required for an oncostatin M-responsive element-mediated activation of matrix metalloproteinase 1 gene expression. *J Biol Chem* **1997,** *272* (2), 1188-96.

6. Heinrich, P. C.; Behrmann, I.; Haan, S.; Hermanns, H. M.; Müller-Newen, G.; Schaper, F., Principles of interleukin (IL)-6-type cytokine signalling and its regulation. *Biochem J* **2003,** *374* (Pt 1), 1-20.

7. Ryan, R. E.; Martin, B.; Mellor, L.; Jacob, R. B.; Tawara, K.; McDougal, O. M.; Oxford, J. T.; Jorcyk, C. L., Oncostatin M binds to extracellular matrix in a bioactive conformation: implications for inflammation and metastasis. *Cytokine* **2015,** *72* (1), 71-85.

8. Williamson, M. P., Using chemical shift perturbation to characterise ligand binding. *Prog Nucl Magn Reson Spectrosc* **2013,** *73*, 1-16.

9. Arkin, M.; Randal, M.; DeLano, W.; Hyde, J.; Luong, T.; Oslob, J.; Raphael, D.; Taylor, L.; Wang, J.; McDowell, R.; Wells, J.; Braisted, A., Binding of small molecules to an adaptive protein-protein interface. *Proc Natl Acad Sci USA* **2003,** *100* (4), 1603-1608.

10. Charlier, H. A.; Plapp, B. V., Kinetic cooperativity of human liver alcohol dehydrogenase γ2. *J Biol Chem* **2000**. *275*, 11569-11575

11. Hoffman, R. C.; Moy, F. J.; Price, V.; Richardson, J.; Kaubisch, D.; Frieden, E. A.; Krakover, J. D.; Castner, B. J.; King, J.; March, C. J.; Powers, R., Resonance assignments for Oncostatin M, a 24-kDa alpha-helical protein. *J Biomol NMR* **1996,** *7* (4), 273-82.

12. Almond-Thynne, J.; Blakemore, D.; Pryde, D.; Spivey, A., Site-selective Suzuki-Miyaura coupling of heteroaryl halides - understanding the trends for pharmaceutically important classes. *Chemical Science* **2017,** *8* (1), 40-62.

13. Blaquiere, N.; Burch, J.; Castanedo; Georgette; Feng, J. A.; Hu, B.; Lin, X.; Staben, S.; Wu, G.; Yuen, P.-W. Alkynyl alcohols as NIK kinase inhibitors and their preparation. World Patent WO2015025026A, **2015**.

APPENDIX A

Materials and Methods

Biological Evaluation

General procedure for enzyme-linked immunosorbent assays: Inhibition of pSTAT3 was determined by ELISA against T47D human breast cancer cell lines. Cells were serum starved for 4 hours. Small molecules (10 µM in DMSO) and human recombinant OSM (10 ng/mL) were incubated in serum-free RPMI-1640 medium at 37 °C and 5% CO_2. After incubation, the SMI-27 analogs and OSM were added to the serum starved cells for 30 minutes. Cells were lysed using a 1x PathScan Sandwich ELISA Lysis buffer (CST #7018S) for 15 minutes after which the lysates were collected and stored at -20 °C. Lysates were analyzed for pSTAT3 expression using a PathScan Phospho-Stat3 (Tyr705) Sandwich ELISA Antibody Pair kit (CST #7146). pSTAT3 expression was measured with absorbance at 450nm and quantified by comparison relative to OSM-induced pSTAT3 expression.

General procedure for western blot assays T47D cells were plated on 24-well plates at 70-75% confluency and allowed to adhere overnight. Cells were serum starved with serum free RPMI media for 4 h, and subsequently treated with either commercially available OSM (Peprotech; Cat# 300-10T) or a co-incubated solution of OSM and small molecule (10 µM). Afterwards, cell lysates were collected with 1X Cell Lysis Buffer (Cell Signaling Technology; Cat# 7018). Lysates were run on an SDS-PAGE gel and transferred onto a nitrocellulose membrane via semi-dry transfer. Blots were rinsed with Milli-Q H_2O and allowed to dry completely before being blocked with LiCor Odyssey PBS blocking buffer for 1 hour (LiCor; Cat# 927-4000). After blocking, primary antibodies (1:1000) suspended in blocking buffer were applied to the membrane, shaken for 1hr at room temperature, and incubated overnight at 4 °C. Membranes were then washed 6 x 5 min with 1X PBS supplemented with 0.5% Tween and secondary antibodies (1:15,000) suspended in blocking buffer were applied for 45 min. A final wash step of 6 x 5 min with PBS-T, membranes were imaged at 700 nm using the LiCor Odyssey CLx imaging system. Antibodies: phospho-STAT3 (Y705) (Cell Signaling Technology; Cat# 9145), Beta-Actin (Cell Signaling Technologies; Cat# 3700), donkey anti-rabbit IRDye 800CW (LiCor; Cat# 925-32213).

General procedure for fluorescence quenching assays: A solution of recombinant OSM (2 mL, 1 µM) in four separate polymethylmethacrylate cuvettes is prepared by dilution of a concentrated stock solution of recombinant OSM with buffer solution (100 mM sodium chloride, 50 mM sodium phosphate, 100 mM freshly added DTT, pH = 6.6). Three cuvettes are titrated in 10 µM increments using a 2 mM small molecule stock solution in DMSO, and the fourth cuvette is titrated with an equivalent volume of DMSO as a control. A total of 11 titration points are collected (including zero-point blank), not to exceed 5% (v/v) total concentration of DMSO. The fluorescence intensity is recorded at OSM's emission maximum of 350 nm using an excitation wavelength of 280 nm (4 nm slit width) and PMT voltage of 700 V. Each titration point is normalized to OSM's fluorescence intensity in the absence of small molecule and corrected by adding the decrease in fluorescence intensity caused by dilution with DMSO. The average value of the three independent replicates for each point is plotted against concentration of small molecule delivered, and fit to a modified Stern-Volmer function, $\frac{f}{f_0} = \frac{f_1}{1-\frac{[X]}{Kd}} + (1 - f_1)$, originally described by Charlier et al., where $\frac{f}{f_0}$ is the fluorescence signal of the sample with SMI divided by the fluorescence signal of the blank, f_1 is the fluorescence signal of the sample with SMI, [X] is the concentration of the SMI, and Kd is the binding affinity of the SMI toward OSM.[1] Kd values were obtained from the fitting routine and errors are reported as the standard error of the fit with a symmetrical 95% confidence interval. Raw data was analyzed using Microsoft Excel and all curve fitting analysis was performed in *GraphPad Prism 8*.[2]

To conduct a statistical analysis of the dissociation constants, three separate Kd values were obtained from each individual replicate using Graphpad Prism 8. The resulting mean Kd values were subjected to a 2-way analysis of variance (ANOVA), providing model-based estimates of specific R_1 and R_2 combinations that were then explicitly compared to answer the questions of interest. Both raw Kd and logged Kd were evaluated for model fit. Based on residual plots, there was no benefit to using the logged data, so all results are based on the raw Kd values. The analysis of variance model has a highly significant $R_1 \times R_2$ interaction ($p = 0.0006$). Because of the large number of pairwise comparisons (276 comparisons), all differences were adjusted for multiple comparisons using false discovery rate adjustment.[3] All statistical analyses were conducted in SAS analytics software.

General procedure for $^{15}N/^{1}H$ HSQC NMR Titrations: All protein NMR experiments were conducted in 50 mM sodium phosphate (pH 6.6), 100 mM sodium chloride, 5% D_2O with 500 µL of sample in a 5 mm NMR tube unless otherwise noted. Spectra were recorded at 298 K on a Bruker AVANCE III 600 MHz spectrometer equipped with a 5 mm TCI cryoprobe with z-axis gradients. ^{1}H, ^{15}N heteronuclear single quantum correlation (HSQC) spectra were collected with the *hsqcfpf3gpphwg* Bruker sequence. Spectra were processed and plotted using Topspin 3.2.

For titration studies, 500 μL of a 100 μM sample of recombinant ^{15}N enriched OSM in NMR Buffer was titrated with a 20 mM stock solution of SMI in d_6-dimethyl sulfoxide. The SMI stock solution was added in 1 or 2 μL increments corresponding to 20, 40, 80, and 120 μM SMI delivered. An additional 100 μM sample of ^{15}N OSM was prepared with 8 μL d_6-dimethyl sulfoxide as a control.

Computational Studies

General procedure for pharmacophore weighted density map: Using the human OSM crystal structure (PDB ID: 1EVS), the AutoLigand program was used to scan the protein surface for potential SMI binding sites and to calculate energy to volume ratios of binding sites.[4-7] A subset of 10,000 small molecules randomly selected from a ~22M compound library were docked against OSM site 3 using AutoDock Vina 4.2.[8] Using the resulting lowest-energy docking pose of each molecule, the spatial distributions of pharmacophore features, i.e. hydrogen bond acceptors/donors, aromatic carbons, and halogens, were mapped with respect to the OSM structure. To create the distribution density maps of pharmacophore features, a 3-dimensional density grid was generated about the OSM site 3 binding pocket, with a grid resolution of 0.1 Å (corresponding to 10^{-3} Å^3 volume elements).

General procedure for computational docking: All molecular docking studies were performed using AutoDock Vina 4.2 and the visualized were visualized using UCSF Chimera.[8, 9] SMILES codes of potential SMI candidates were generated using

PerkinElmer Chemdraw 16.0 and imported into the Chimera software. Small molecule energies were minimized and charges were added using the Amber Antechamber module utilizing the default ff14SB force field.[10] Molecules were then docked into Site 3 of the human OSM crystal structure (PDB ID: 1EVS) (Center: [10, 35, 25]; Size: [30, 30, 30]) and the docking results were interpreted directly without further optimization of torsion angles and atomic positions.

Chemistry

General: Reagents were purchased at the highest commercial quality and used without further purification. Unless otherwise noted, reactions were conducted using oven-dried glassware under an inert atmosphere of N_2 gas. Anhydrous reaction solvents were obtained via prolonged storage of commercially available solvent over 4Å Linde-type molecular sieves (ca. 20% v/v). Routine ^1H and ^{13}C NMR spectra were recorded on a Bruker AVANCE III 600 MHz spectrometer equipped with a 5 mm TCI cryoprobe with z-axis gradients or a Bruker AVANCE III 300 MHz spectrometer. Spectra were obtained at 298K using reagent grade $CDCl_3$ (99.9 % D atom) stored over 4Å Linde-type molecular sieves as the solvent and the residual $CHCl_3$ signal at $\delta(H) = 7.26$ ppm and the central resonance of the $CDCl_3$ triplet appearing at $\delta(C) = 77.16$ ppm were used to reference ^1H and ^{13}C NMR spectra, respectively. ^1H NMR data are recorded as follows: chemical shift (δ), multiplicity, coupling constant(s) J (Hz), relative integral] where multiplicity is denoted as: s = singlet; d = doublet; t = triplet; q = quartet; hept = heptet; sept = septet; m = multiplet or combinations thereof. NMR spectra were analyzed using Bruker TopSpin and plotted in MestreNova. All HPLC experiments were conducted using an Agilent 1100 Series HPLC system with a Phenomenex Synergi Fusion reverse-phased C18 column with polar endcapping as the stationary phase and 95:5 acetonitrile/0.1% aqueous trifluoracetic acid as the mobile phase. All biologically evaluated compounds were determined to have a purity >95% as determined by HPLC peak area and ^{1}H NMR analyses. Unless otherwise noted, reactions were monitored by TLC (glass-backed, 250 mm silica gel)using short-wave UV light as the visualizing agent, and aqueous $KMnO_4$ with heat as the developing agent. Flash column chromatography was performed using 60 Å, 230-400 mesh silica gel. Melting points were recorded on a Vernier Melt Station MLT-BTA and are uncorrected. High resolution mass spectra were recorded on a Bruker Daltonics maXis Q-TOF Mass Spectrometer using positive ionization mode.

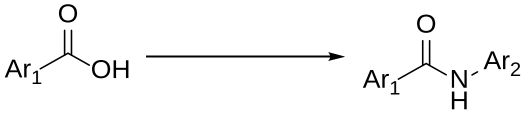

General procedure for amidation reactions: To a flask was added acid (1 eq) and dissolved in anhydrous dichloromethane (~0.5 M). The flask was sealed, purged with N_2 gas, and thionyl chloride (3 eq) was added under an inert atmosphere while stirring. The resulting solution was allowed to reflux at 80 °C for 2 hours. The reaction solution was cooled to room temperature and concentrated under reduced pressure, re-dissolved in anhydrous dichloromethane (~0.5 M), and cooled to 0 °C in an ice-water bath. To the reaction flask under a N_2 atmosphere was added triethylamine (2 eq) and aniline (1 eq) dropwise. Following addition, the ice/water bath is removed and the reaction is allowed warm to room temperature and stir overnight. The reaction mixture was washed with D.I. water (25 mL) and extracted twice with dichloromethane (10 mL). The combined organic layers were then washed with 1M HCl (2 x 20 mL), 1M NaOH (2 x 20 mL), and brine (1 x 25 mL), dried over $MgSO_4$, filtered, and concentrated under reduced pressure to afford a solid. N-Phenylbenzamides were used directly in the next step without further purification. In the case of quinazoline-4-carboxamides, the resulting solid was then suspended in 1 mL of heptane and 1-2 drops of dichloromethane, and the suspension was filtered and the solids were collected to afford the purified amidation product.

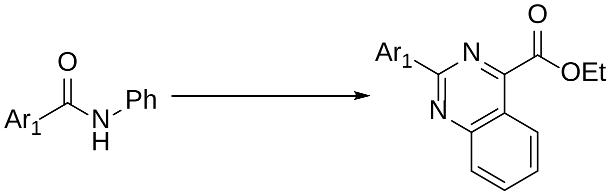

General procedure for Meerwein quinazoline cyclization:[11] N-Phenylbenzamide (1 eq) was added to an appropriately sized round bottom flask and dissolved in anhydrous toluene (~0.1 M), followed by the addition of phosphorus pentachloride (1.2 eq) while stirring. The reaction was maintained under a N_2 atmosphere and was heated to 85 °C for 4 hours. The reaction was then concentrated under reduced pressure, dissolved in chlorobenzene (~0.1 M), and purged with N_2 gas. To the reaction flask was then added ethyl cyanoformate (2.0 eq) and tin (IV) chloride (1.7 eq) while stirring under a N_2 atmosphere. The reaction was heated to 125 °C overnight. The reaction was then cooled to room temperature, concentrated under reduced pressure, dissolved in ethyl acetate (25 mL), and washed with D.I. water (2 x 25 mL) and brine (1 x 25 mL). The organic layer was dried over Na_2SO_4, filtered, and concentrated under reduced pressure. The thick black oil is then purified by flash column chromatography (SiO_2, hexanes/ethyl acetate elution) and the appropriate fractions were combined and concentrated under reduced pressure to afford the purified cyclized product.

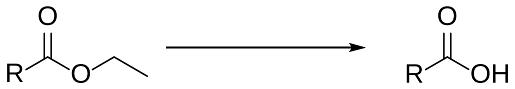

General procedure for saponification reactions: Ethyl ester (1 eq) was added to an appropriately sized round bottom flask and dissolved in ethanol (~0.05 M), followed by the addition of 6M NaOH (5 eq) in one portion. The reaction was allowed to stir at room temperature for 45 minutes, upon which the reaction mixture was concentrated under reduced pressure, re-dissolved in 15 mL of D.I. water, and adjusted to a pH of 2-3 using 6M HCl. The precipitated solids were then collected and dried by vacuum filtration to afford the saponified product.

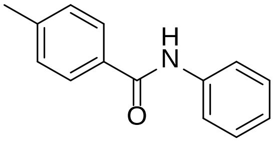

4-methyl-N-phenylbenzamide

Prepared according to the general amidation procedure to afford a shiny tan solid (80% yield). ^{1}H NMR (300 MHz, CDCl$_3$) δ 7.85 (s, 1H), 7.83 – 7.74 (m, 2H), 7.72 – 7.61 (m, 2H), 7.45 – 7.34 (m, 2H), 7.34 – 7.26 (m, 2H), 7.23 – 7.11 (m, 1H), 2.45 (s, 3H).

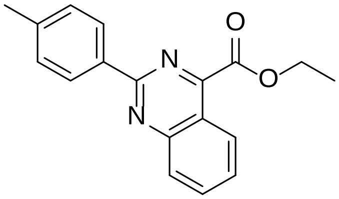

ethyl 2-(p-tolyl)quinazoline-4-carboxylate

Prepared according to the general Meerwein quinazoline cyclization procedure to afford an orange solid (30% yield). ^{1}H NMR (300 MHz, CDCl$_3$) δ 8.58 – 8.49 (m, 2H), 8.43 (ddd, J = 8.5, 1.4, 0.7 Hz, 1H), 8.12 (ddd, J = 8.6, 1.3, 0.7 Hz, 1H), 7.92 (ddd, J = 8.5, 6.9, 1.4 Hz, 1H), 7.63 (ddd, J = 8.3, 6.9, 1.2 Hz, 1H), 7.39 – 7.29 (m, 2H), 4.63 (q, J = 7.1 Hz, 2H), 2.45 (s, 3H), 1.54 (t, J = 7.1 Hz, 3H). 13C NMR (75 MHz, CDCl$_3$) δ 165.49, 160.49, 157.82, 152.58, 141.36, 134.83, 134.45, 129.57, 129.30, 128.83, 128.07, 125.97, 62.69, 21.72, 14.45. MP: 90.8 - 93.1 °C.

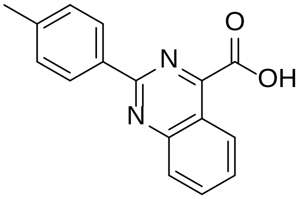

27A0

2-(p-tolyl)quinazoline-4-carboxylic acid

Prepared according to the general saponification procedure to afford a pale yellow solid (98% yield). ^{1}H NMR (300 MHz, CDCl$_3$) δ 9.31 (d, J = 8.6 Hz, 1H), 8.36 (s, 1H), 8.33 (s, 1H), 8.13 (d, J = 8.6 Hz, 1H), 7.98 (t, J = 8.5 Hz, 1H), 7.71 (, J = 8.3, 1H), 7.29 (d, J = 7.8 Hz, 2H), 2.42 (s, 3H). ^{13}C NMR (75 MHz, CDCl$_3$) δ 158.57, 153.75, 141.93, 135.40, 133.22, 129.64, 129.37, 128.94, 128.25, 127.10, 120.60. MP: 139.3 -142.4 °C. HRMS m/z: [M + H]+ Calcd. for $C_{16}H_{12}N_2O_2$ 265.0972; Found 265.0978, Error 2.40 ppm. HPLC: T_R = 3.062 min, peak area = 91.5%.

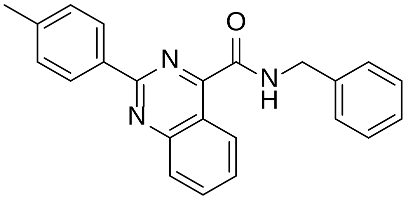

27A1

N-benzyl-2-(p-tolyl)quinazoline-4-carboxamide

Prepared according to the general amidation procedure to afford a white solid (69% yield). ^{1}H NMR (600 MHz, CDCl3) δ 9.49 (dd, J = 8.6, 1.3 Hz, 1H), 8.66 (t, J = 6.1 Hz, 1H), 8.46 (d, J = 8.0 Hz, 2H), 8.12 (dd, J = 8.5, 1.1 Hz, 1H), 7.94 (ddt, J = 8.4, 6.8, 1.1 Hz, 1H), 7.68 (ddd, J = 8.3, 6.9, 1.1 Hz, 1H), 7.50 – 7.40 (m, 4H), 7.40 – 7.33 (m, 3H), 4.82 (d, J = 6.1 Hz, 2H), 2.47 (s, 3H). ^{13}C NMR (151 MHz, CDCl3) δ 164.96, 159.03, 155.38, 153.37, 141.23, 137.99, 134.41, 128.86, 128.79, 128.36, 128.28, 128.24, 127.98, 127.74, 127.74, 127.63, 77.24, 77.03, 76.82, 43.56, 21.53. MP: 185.8-188.3 °C. HRMS m/z: [M + H]+ Calcd. for $C_{23}H_{19}N_3O$ 354.1615; Found 354.1615, Error 3.99 ppm. HPLC: T_R = 3.756 min, peak area = 99.6%.

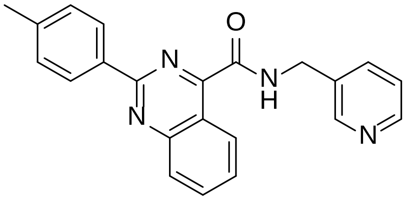

27A2

N-(pyridin-3-ylmethyl)-2-(p-tolyl)quinazoline-4-carboxamide

Prepared according to the general amidation procedure to afford a beige solid (68% yield). ^{1}H NMR (600 MHz, $CDCl_3$) δ 9.42 (d, J = 10.0 Hz, 1H), 8.76 – 8.67 (m, 2H), 8.57 (dd, J = 4.7, 1.6 Hz, 1H), 8.45 – 8.40 (m, 2H), 8.10 (dd, J = 8.5, 1.2 Hz, 1H), 7.92 (ddd, J = 8.4, 6.8, 1.4 Hz, 1H), 7.79 (dt, J = 7.9, 2.0 Hz, 1H), 7.66 (ddd, J = 8.4, 6.8, 1.2 Hz, 1H), 7.35 – 7.29 (m, 3H), 4.79 (d, J = 6.3 Hz, 2H), 2.44 (s, 3H). ^{13}C NMR (151 MHz, $CDCl_3$) δ 165.29, 153.50, 149.36, 149.26, 141.47, 135.65, 135.64, 134.67, 134.47, 133.77, 129.63, 128.95, 128.44, 127.67, 123.86, 121.13, 41.20, 21.68. MP: 191.4 - 194.5 °C. HRMS m/z: [M + H]+ Calcd. for $C_{22}H_{18}N_4O$ 355.1553; Found 355.1569, Error 4.37 ppm. HPLC: T_R = 4.266 min, peak area = 39.8%

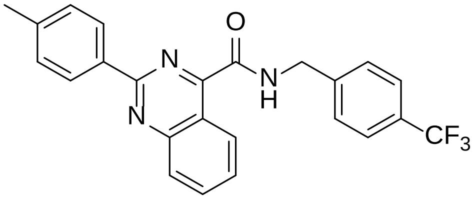

27A3

2-(p-tolyl)-N-(4-(trifluoromethyl)benzyl)quinazoline-4-carboxamide

Prepared according to the general amidation procedure to afford a white solid (69% yield). ^{1}H NMR (600 MHz, CDCl$_3$) δ 9.44 (dd, J = 8.6, 1.4 Hz, 1H), 8.75 (t, J = 6.2 Hz, 1H), 8.46 – 8.42 (m, 2H), 8.11 (dd, J = 8.5, 1.2 Hz, 1H), 7.93 (ddd, J = 8.4, 6.8, 1.4 Hz, 1H), 7.70 – 7.62 (m, 3H), 7.56 (d, J = 8.0 Hz, 2H), 7.33 (d, J = 8.0 Hz, 2H), 4.84 (d, J = 6.3 Hz, 2H), 2.45 (s, 3H). ^{13}C NMR (151 MHz, CDCl$_3$) δ 165.16, 159.04, 154.97, 153.44, 141.34, 134.52, 134.44, 129.51, 128.85, 128.38, 128.34, 127.81, 127.60, 125.83, 125.80, 125.78, 121.05, 43.07, 21.52. MP: 208.9 – 210.5 °C. HRMS m/z: [M + H]+ Calcd. for $C_{24}H_{18}F_3N_3O$ 422.1475; Found 422.1484, Error 2.29 ppm. HPLC: T_R = 3.714 min, peak area = 98.8%.

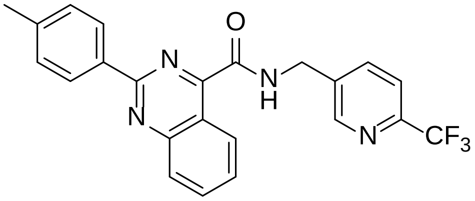

27A4

2-(p-tolyl)-N-((6-(trifluoromethyl)pyridin-3-yl)methyl)quinazoline-4-carboxamide

Prepared according to the general amidation procedure to afford a white solid (75% yield). ^{1}H NMR (600 MHz, CDCl$_3$) δ 9.44 (d, J = 8.6 Hz, 1H), 8.86 (s, 2H), 8.47 (d, J = 7.7 Hz, 2H), 8.15 (d, J = 8.5 Hz, 1H), 8.01 (d, J = 8.1 Hz, 1H), 7.97 (t, J = 7.7 Hz, 1H), 7.75 – 7.67 (m, 2H), 7.38 (d, J = 7.8 Hz, 2H), 4.90 (d, J = 6.3 Hz, 2H), 2.48 (s, 3H). ^{13}C NMR (151 MHz, CDCl$_3$) δ 165.38, 159.07, 154.59, 153.48, 149.35, 147.73, 147.50, 147.27, 141.43, 137.05, 136.69, 134.63, 129.53, 128.91, 128.34, 127.43,120.98, 121.51 (q, $J_{C,F}$ = 273.4 Hz), 120.54 (q, $J_{C,F}$ = 2.8 Hz), 40.76, 21.52. MP: 215.1 – 217.8 °. HRMS m/z: [M + H]+ Calcd. for $C_{23}H_{17}F_3N_4O$ 423.1427; Found 423.1427, Error 0 ppm. HPLC: T_R = 3.376 min, peak area = 96.4%.

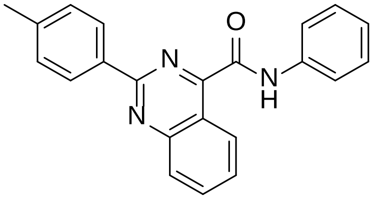

27A5

N-phenyl-2-(p-tolyl)quinazoline-4-carboxamide

Prepared according to the general amidation procedure to afford a light yellow solid (76% yield). ^{1}H NMR (600 MHz, $CDCl_3$) δ 10.29 (s, 1H), 9.53 (dd, J = 8.6, 1.4 Hz, 1H), 8.52 – 8.47 (m, 2H), 8.12 (dt, J = 8.4, 0.9 Hz, 1H), 7.94 (ddd, J = 8.4, 6.8, 1.4 Hz, 1H), 7.87 – 7.82 (m, 2H), 7.68 (ddd, J = 8.3, 6.8, 1.3 Hz, 1H), 7.49 – 7.43 (m, 2H), 7.38 (d, J = 7.9 Hz, 2H), 7.23 (tt, J = 7.4, 1.2 Hz, 1H), 2.47 (s, 3H). ^{13}C NMR (151 MHz, $CDCl_3$) δ 162.59, 158.78, 154.97, 153.61, 141.45, 137.35, 134.63, 134.35, 129.62, 129.27, 128.92, 128.50, 128.34, 127.65, 124.99, 121.17, 120.14, 21.61. MP: 166.7-168.5 °C. HRMS m/z: [M + H]+ Calcd. for $C_{22}H_{17}N_3O$ 340.1444; Found 340.1458, Error 3.91 ppm. HPLC: T_R = 4.283 min, peak area = 97.3%.

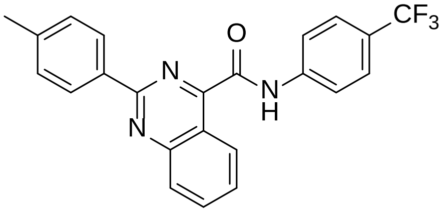

27A6

2-(p-tolyl)-N-(4-(trifluoromethyl)phenyl)quinazoline-4-carboxamide

Prepared according to the general amidation procedure to afford a white solid (67% yield). ^{1}H NMR (600 MHz, $CDCl_3$) δ 10.47 (s, 1H), 9.48 (d, J = 8.4 Hz, 1H), 8.48 (d, J = 7.9 Hz, 2H), 8.13 (d, J = 8.5 Hz, 1H), 7.98 (s, 1H), 7.98 – 7.93 (m, 2H), 7.73 – 7.66 (m, 3H), 7.38 (d, J = 7.8 Hz, 2H), 2.48 (s, 3H). ^{13}C NMR (151 MHz, $CDCl_3$) δ 162.82, 158.77, 154.24, 153.70, 141.60, 140.34, 134.80, 134.17, 129.66, 129.02, 128.75, 128.31, 127.40, 126.96, 126.79, 126.75, 126.55, 126.52, 126.50, 126.47, 126.31, 124.99, 123.19, 121.06, 119.75, 21.62. MP: 218.5 – 219.7 °C. HRMS m/z: [M + H]+ Calcd. for $C_{23}H_{16}F_3N_3O$ 408.1318; Found 408.1318, Error 0 ppm. HPLC: T_R = 4.442 min, peak area = 97.6%.

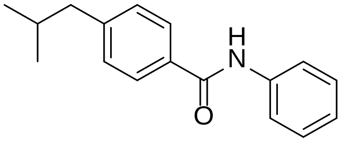

4-isobutyl-N-phenylbenzamide

Prepared according to the general amidation procedure to afford a shiny light brown solid (88% yield). ^{1}H NMR (600 MHz, CDCl$_3$) δ 7.92 (s, 1H), 7.78 (d, J = 8.0 Hz, 2H), 7.64 (d, J = 8.0 Hz, 2H), 7.36 (t, J = 7.8 Hz, 2H), 7.24 (d, J = 7.9 Hz, 2H), 7.14 (t, J = 7.4 Hz, 1H), 2.54 (d, J = 7.2 Hz, 2H), 1.90 (sept, J = 6.8 Hz, 1H), 0.92 (d, J = 6.7 Hz, 6H). ^{13}C NMR (151 MHz, CDCl$_3$) δ 165.95, 146.22, 138.17, 132.50, 129.61, 129.60, 129.34, 129.18, 127.05, 124.53, 120.30, 45.36, 30.30, 22.44. MP: 139.3 – 144.3 °C.

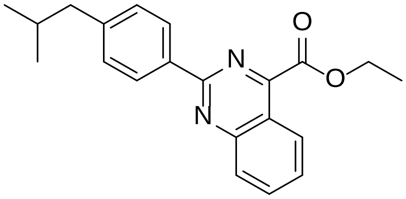

Ethyl 2-(4-isobutylphenyl)quinazoline-4-carboxylate

Prepared according to the general Meerwein quinazoline cyclization procedure to afford a yellow oil (26% yield). ^{1}H NMR (600 MHz, CDCl$_3$) δ 8.55 – 8.51 (m, 2H), 8.44 (dd, J = 8.4, 1.6 Hz, 1H), 8.15 – 8.10 (m, 1H), 7.93 (ddd, J = 8.5, 6.9, 1.4 Hz, 1H), 7.64 (ddd, J = 8.3, 6.9, 1.2 Hz, 1H), 7.31 (d, J = 7.9 Hz, 2H), 4.62 (q, J = 7.3 Hz, 2H), 2.57 (d, J = 7.2 Hz, 2H), 1.93 (hept, J = 6.8 Hz, 1H), 1.54 (t, J = 7.2 Hz, 3H), 0.93 (dd, J = 6.6, 1.6 Hz, 6H). ^{13}C NMR (151 MHz, CDCl$_3$) δ 165.35, 152.46, 145.03, 134.98, 134.36, 131.99, 129.86, 129.54, 129.17, 128.56, 127.98, 125.86, 120.27, 62.59, 45.43, 30.30, 22.40, 22.27, 14.33. MP: N/A

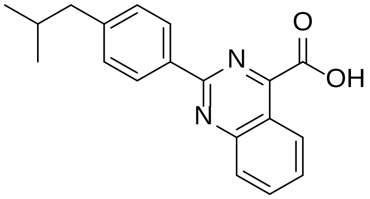

27B0

2-(4-isobutylphenyl)quinazoline-4-carboxylic acid

Prepared according to the general saponification procedure to afford an orange/brown solid (81% yield). ^{1}H NMR (600 MHz, CDCl$_3$) δ 11.82 (s, 1H), 9.37 (d, J = 8.5 Hz, 1H), 8.45 (d, J = 7.8 Hz, 2H), 8.17 (d, J = 8.4 Hz, 1H), 8.00 (t, J = 7.7 Hz, 1H), 7.74 (t, J = 7.3 Hz, 1H), 7.34 (d, J = 7.5 Hz, 2H), 2.59 (d, J = 7.4 Hz, 2H), 1.95 (sept, J = 6.7 Hz, 1H), 0.95 (d, J = 6.7 Hz, 6H). ^{13}C NMR (151 MHz, CDCl$_3$) δ 163.82, 158.89, 153.95, 145.87, 135.57, 133.74, 132.11, 129.98, 129.87, 129.54, 129.16, 129.11, 128.34, 127.28, 124.64, 120.74, 45.47, 30.37, 22.39. MP: 119.7 – 122.3 °C. HRMS m/z: [M + H]+ Calcd. for $C_{19}H_{18}N_2O_2$ 307.1441; Found 307.1451, Error 3.30 ppm. HPLC: T_R = 3.546 min, peak area = 89.1%.

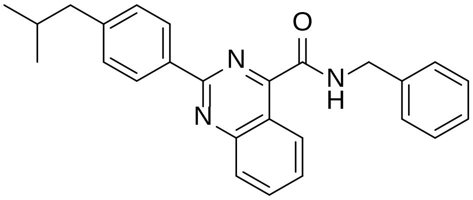

27B1

N-benzyl-2-(4-isobutylphenyl)quinazoline-4-carboxamide

Prepared according to the general amidation procedure to afford a white solid (88% yield). ^{1}H NMR (600 MHz, CDCl$_3$) δ 9.40 (dd, J = 8.6, 1.4 Hz, 1H), 8.63 (t, J = 6.1 Hz, 1H), 8.41 – 8.37 (m, 2H), 8.04 (d, J = 8.5 Hz, 1H), 7.85 (ddd, J = 8.4, 6.8, 1.5 Hz, 1H), 7.58 (ddd, J = 8.4, 6.8, 1.3 Hz, 1H), 7.40 (d, J = 7.1 Hz, 2H), 7.34 (t, J = 7.7 Hz, 2H), 7.27 (t, J = 7.3 Hz, 1H), 7.24 (s, 1H), 7.23 (s, 1H), 4.73 (d, J = 6.2 Hz, 2H), 2.51 (d, J = 7.3 Hz, 2H), 1.89 (sept, J = 6.8 Hz, 1H), 0.89 (d, J = 6.7 Hz, 6H). ^{13}C NMR (151 MHz, CDCl$_3$) δ 164.98, 159.09, 155.37, 153.33, 138.00, 134.76, 134.43, 129.57, 128.80, 128.26, 127.72, 127.70, 127.65, 121.07, 45.39, 43.56, 30.29, 30.29, 22.44. MP: 141.2 – 143.5 °C. HRMS m/z: [M + H]+ Calcd. for $C_{26}H_{25}N_3O$ 396.2070; Found 396.2074, Error 0.97 ppm. HPLC: T_R = 4.611 min, peak area = 93.0%.

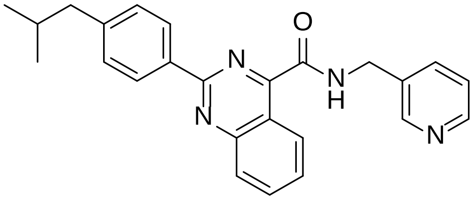

27B2

2-(4-isobutylphenyl)-N-(pyridin-3-ylmethyl)quinazoline-4-carboxamide

Prepared according to the general amidation procedure to afford a pale orange solid (74% yield). ^{1}H NMR (600 MHz, CDCl$_3$) δ 9.38 (d, J = 8.7 Hz, 1H), 8.77 (t, J = 6.3 Hz, 1H), 8.69 (d, J = 2.4 Hz, 1H), 8.57 – 8.53 (m, 1H), 8.41 (d, J = 7.9 Hz, 2H), 8.07 (d, J = 8.5 Hz, 1H), 7.89 (ddd, J = 8.4, 6.8, 1.4 Hz, 1H), 7.76 (dt, J = 8.0, 2.1 Hz, 1H), 7.65 – 7.59 (m, 1H), 7.28 (t, J = 8.9 Hz, 3H), 4.76 (d, J = 6.3 Hz, 2H), 2.54 (d, J = 7.3 Hz, 2H), 1.91 (septet, J = 6.7 Hz, 1H), 0.92 (d, J = 6.6 Hz, 6H). ^{13}C NMR (151 MHz, CDCl$_3$) δ 165.24, 159.15, 155.08, 153.40, 149.32, 149.19, 145.18, 135.55, 134.70, 134.58, 133.73, 129.63, 128.89, 128.88, 128.42, 128.28, 127.57, 123.77, 121.01, 45.41, 41.13, 30.32, 30.31, 22.46. MP: 130.7 – 132.3 °C. MP: 130.7 - 132.3 °C. HRMS m/z: [M + H]+ Calcd. for $C_{25}H_{24}N_4O$ 397.2023; Found 397.2028, Error 1.31 ppm. HPLC: T_R = 7.105 min, peak area = 98.6%.

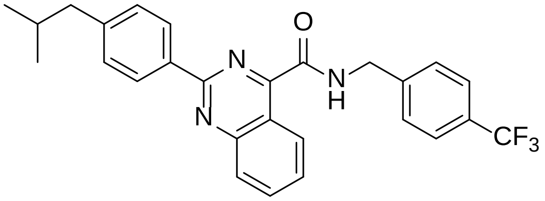

27B3

2-(4-isobutylphenyl)-N-(4-(trifluoromethyl)benzyl)quinazoline-4-carboxamide

Prepared according to the general amidation procedure to afford a white solid (67% yield). ^{1}H NMR (600 MHz, CDCl$_3$) δ 9.45 (d, J = 8.6 Hz, 1H), 8.78 (t, J = 6.4 Hz, 1H), 8.45 (d, J = 8.0 Hz, 2H), 8.12 (d, J = 8.5 Hz, 1H), 7.94 (ddd, J = 8.5, 6.8, 1.5 Hz, 1H), 7.70 – 7.64 (m, 2H), 7.64 (s, 1H), 7.56 (d, J = 8.0 Hz, 2H), 7.32 (d, J = 7.9 Hz, 2H), 4.84 (d, J = 6.3 Hz, 2H), 2.57 (d, J = 7.2 Hz, 2H), 1.94 (sept, J = 6.8 Hz, 1H), 0.94 (d, J = 6.6 Hz, 6H). ^{13}C NMR (151 MHz, CDCl$_3$) δ 165.31, 165.29, 159.24, 155.04, 153.57, 145.30, 142.19, 134.81, 134.71, 130.34, 130.13, 129.91, 129.74, 128.99, 128.56, 128.34, 127.94, 127.72, 126.92, 125.97, 125.94, 125.91, 125.89, 125.12, 123.32, 121.16, 45.49, 45.48, 43.18, 30.40, 22.51. MP: 165.4 – 168.3 °C. HRMS m/z: [M + H]+ Calcd. for $C_{27}H_{24}F_3N_3O$ 464.1944; Found 464.1924, Error 4.42 ppm. HPLC: T_R = 4.576 min, peak area = 99.4%.

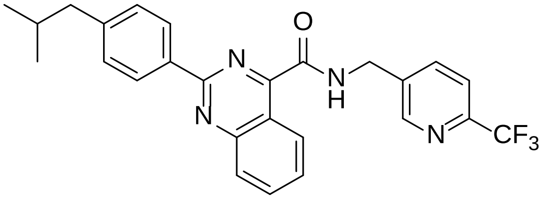

27B4

2-(4-isobutylphenyl)-N-((6-(trifluoromethyl)pyridin-3-yl)methyl)quinazoline-4-carboxamide

Prepared according to the general amidation procedure to afford a white solid (72% yield). ^{1}H NMR (600 MHz, CDCl$_3$) δ 9.42 (d, J = 8.5 Hz, 1H), 8.84 (d, J = 8.1 Hz, 2H), 8.45 (d, J = 7.7 Hz, 2H), 8.13 (d, J = 8.5 Hz, 1H), 7.98 (d, J = 8.1 Hz, 1H), 7.97 – 7.92 (m, 1H), 7.73 – 7.65 (m, 2H), 7.32 (d, J = 7.8 Hz, 2H), 4.87 (d, J = 6.3 Hz, 2H), 2.58 (d, J = 7.2 Hz, 2H), 1.94 (hept, J = 6.7 Hz, 1H), 0.94 (d, J = 6.8 Hz, 6H). ^{13}C NMR (151 MHz, CDCl$_3$) δ 165.51, 154.71, 149.49, 145.38, 137.19, 137.18, 136.85, 134.79, 134.74, 129.75, 129.05, 128.67, 128.35, 127.56, 121.08, 120.71, 120.67, 45.50, 40.88, 30.39, 22.51. MP: 163.3 – 166.8 °C. HRMS m/z: [M + H]+ Calcd. for $C_{26}H_{23}F_3N_4O$ 465.1897; Found 465. 1879, Error 3.88 ppm. HPLC: T$_R$ = 4.059 min, peak area = 98.3%.

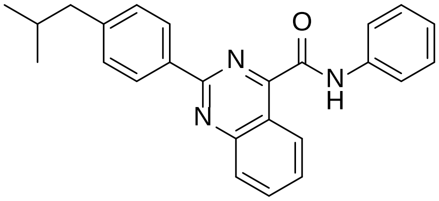

27B5

2-(4-isobutylphenyl)-N-phenylquinazoline-4-carboxamide

Prepared according to the general amidation procedure to afford a white solid (70% yield). ^{1}H NMR (600 MHz, CDCl$_3$) δ 10.32 (s, 1H), 9.54 (d, J = 8.6 Hz, 1H), 8.52 (d, J = 7.8 Hz, 2H), 8.14 (d, J = 8.5 Hz, 1H), 7.95 (t, J = 7.7 Hz, 1H), 7.85 (d, J = 7.9 Hz, 2H), 7.69 (t, J = 7.7 Hz, 1H), 7.46 (t, J = 7.7 Hz, 2H), 7.37 (d, J = 7.9 Hz, 2H), 7.23 (t, J = 7.4 Hz, 1H), 2.60 (d, J = 7.2 Hz, 2H), 1.97 (hept, J = 6.8 Hz, 1H), 0.97 (d, J = 6.6 Hz, 6H). ^{13}C NMR (151 MHz, CDCl$_3$) δ 162.59, 158.90, 154.98, 153.65, 145.25, 137.35, 134.65, 129.71, 129.27, 128.95, 128.53, 128.24, 127.66, 124.99, 121.17, 120.14, 45.41, 30.31, 22.43, 22.43. MP: 132.2 – 133.5 °C. HRMS m/z: [M + H]+ Calcd. for $C_{25}H_{23}N_3O$ 382.1914; Found 382.1903, Error 2.79 ppm. HPLC: T$_R$ = 5.585 min, peak area = 94.2%.

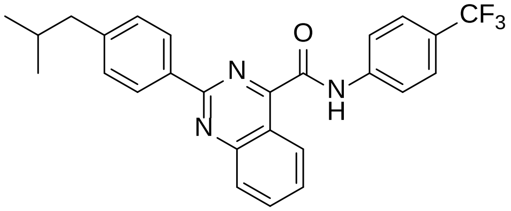

27B6

2-(4-isobutylphenyl)-N-(4-(trifluoromethyl)phenyl)quinazoline-4-carboxamide

Prepared according to the general amidation procedure to afford a light orange solid (73% yield). ^{1}H NMR (600 MHz, $CDCl_3$) δ 10.48 (s, 1H), 9.48 (d, J = 8.5 Hz, 1H), 8.49 (dd, J = 8.2, 1.8 Hz, 2H), 8.12 (d, J = 8.5 Hz, 1H), 7.97 (s, 1H), 7.97 – 7.92 (m, 2H), 7.71 (s, 1H), 7.71 – 7.65 (m, 2H), 7.36 (dd, J = 8.2, 1.8 Hz, 2H), 2.60 (dd, J = 7.3, 1.6 Hz, 2H), 1.97 (hept, J = 6.7 Hz, 1H), 0.97 (dd, J = 6.7, 1.7 Hz, 6H). ^{13}C NMR (151 MHz, $CDCl_3$) δ 162.92, 158.97, 154.33, 153.81, 145.50, 140.46, 134.91, 134.57, 129.85, 129.14, 128.86, 128.32, 127.50, 127.06, 126.90, 126.84, 126.65, 126.63, 126.60, 126.58, 126.41, 125.11, 123.30, 121.14, 119.84, 114.28, 45.52, 30.42, 22.54. MP: 173.5 – 176.0 °C. HRMS m/z: [M + H]+ Calcd. for $C_{26}H_{22}F_3N_3O$ 450.1788; Found 450.1767, Error 4.57 ppm. HPLC: T_R = 5.844 min, peak area = 99.0%.

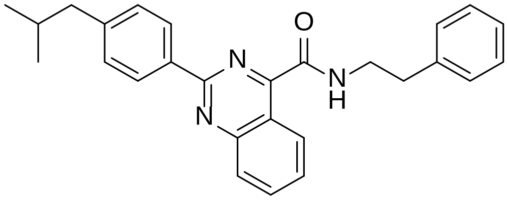

27B7

2-(4-isobutylphenyl)-N-phenethylquinazoline-4-carboxamide

Prepared according to the general amidation procedure to afford a light orange solid (67% yield). ^{1}H NMR (600 MHz, $CDCl_3$) δ 9.44 (dd, J = 8.6, 1.4 Hz, 1H), 8.39 (t, J = 6.1 Hz, 1H), 8.35 (d, J = 7.9 Hz, 2H), 8.09 (d, J = 8.5 Hz, 1H), 7.91 (ddd, J = 8.4, 6.8, 1.4 Hz, 1H), 7.65 (ddd, J = 8.3, 6.8, 1.2 Hz, 1H), 7.43 – 7.28 (m, 7H), 3.85 (q, J = 6.6 Hz, 2H), 3.03 (t, J = 6.8 Hz, 2H), 2.59 (d, J = 7.2 Hz, 2H), 1.96 (hept, J = 6.7 Hz, 1H), 0.96 (d, J = 6.6 Hz, 6H). ^{13}C NMR (151 MHz, $CDCl_3$) δ 164.96, 159.10, 155.44, 153.49, 145.16, 138.94, 134.86, 134.52, 129.64, 129.15, 129.01, 128.89, 128.36, 128.34, 127.82, 126.84, 121.15, 45.52, 40.72, 35.83, 30.44, 22.54. MP: 123.2 – 125.6 °C. HRMS m/z: [M + H]+ Calcd. for $C_{27}H_{27}N_3O$ 410.2227; Found 410.2214, Error 3.23 ppm. HPLC: T_R = 5.355 min, peak area = 98.3%.

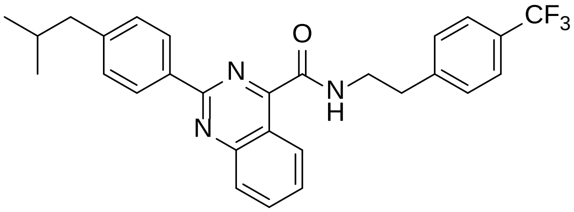

27B8

2-(4-isobutylphenyl)-N-(4-(trifluoromethyl)phenethyl)quinazoline-4-carboxamide

Prepared according to the general amidation procedure to afford a light orange solid (72% yield). ^{1}H NMR (600 MHz, CDCl3) δ 9.42 (dd, J = 8.6, 1.4 Hz, 1H), 8.41 – 8.35 (m, 3H), 8.12 (dd, J = 8.4, 1.1 Hz, 1H), 7.94 (ddd, J = 8.4, 6.7, 1.4 Hz, 1H), 7.70 – 7.64 (m, 3H), 7.49 (d, J = 7.9 Hz, 2H), 7.33 (d, J = 8.1 Hz, 2H), 3.89 (q, J = 6.6 Hz, 2H), 3.12 (t, J = 6.8 Hz, 2H), 2.61 (d, J = 7.2 Hz, 2H), 1.98 (hept, J = 6.8 Hz, 1H), 0.99 (d, J = 6.6 Hz, 6H). ^{13}C NMR (151 MHz, CDCl3) δ 165.09, 159.17, 155.37, 153.55, 145.31, 143.18, 134.83, 134.58, 129.67, 129.53, 129.44, 129.22, 129.01, 128.97, 128.40, 128.28, 127.72, 127.12, 125.92, 125.90, 125.87, 125.85, 125.32, 123.52, 77.37, 77.16, 76.95, 40.48, 35.83, 30.34, 22.49. MP: 148.7 – 149.7 °C. HRMS m/z: [M + H]+ Calcd. for $C_{28}H_{26}F_3N_3O$ 478.2128; Found: TBD. HPLC: T_R = 5.156 min, peak area = 76.9%.

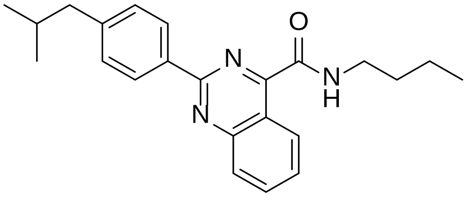

27B9

N-butyl-2-(4-isobutylphenyl)quinazoline-4-carboxamide

Prepared according to the general amidation procedure to afford a white solid (78% yield). ^{1}H NMR (600 MHz, $CDCl_3$) δ 9.45 (ddd, J = 8.6, 1.5, 0.7 Hz, 1H), 8.50 – 8.45 (m, 2H), 8.32 (t, J = 6.1 Hz, 1H), 8.09 (dt, J = 8.5, 1.0 Hz, 1H), 7.91 (ddd, J = 8.4, 6.8, 1.5 Hz, 1H), 7.64 (ddd, J = 8.3, 6.8, 1.2 Hz, 1H), 7.36 – 7.31 (m, 2H), 3.58 (q, J = 7.2 Hz, 2H), 2.59 (d, J = 7.2 Hz, 2H), 1.95 (p, J = 6.8 Hz, 1H), 1.76 – 1.68 (m, 2H), 1.51 (h, J = 7.4 Hz, 2H), 1.02 (t, J = 7.4 Hz, 3H), 0.95 (d, J = 6.6 Hz, 6H). ^{13}C NMR (151 MHz, $CDCl_3$) δ 165.03, 155.76, 153.45, 134.49, 129.71, 128.86, 128.33, 128.30, 127.93, 121.18, 45.51, 39.51, 31.80, 30.41, 22.53, 20.40, 13.98, 13.97. MP: 116.9 – 118.0 °C. HRMS m/z: [M + H]+ Calcd. for $C_{23}H_{27}N_3O$ 362.2254; Found: TBD. HPLC: T_R = 2.037 min, peak area = 99.9%.

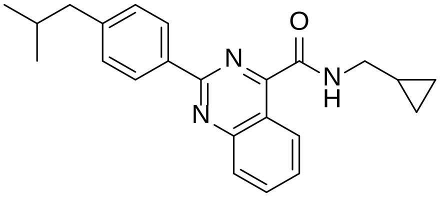

27B10

N-(cyclopropylmethyl)-2-(4-isobutylphenyl)quinazoline-4-carboxamide

Prepared according to the general amidation procedure to afford a white solid (69% yield). ^{1}H NMR (600 MHz, CDCl$_3$) δ 9.42 (dd, J = 8.7, 1.4 Hz, 1H), 8.51 – 8.47 (m, 2H), 8.39 (t, J = 5.8 Hz, 1H), 8.09 (dt, J = 8.4, 0.9 Hz, 1H), 7.90 (ddd, J = 8.4, 6.8, 1.4 Hz, 1H), 7.63 (ddd, J = 8.3, 6.8, 1.3 Hz, 1H), 7.36 – 7.32 (m, 2H), 3.45 (dd, J = 7.2, 5.8 Hz, 2H), 2.59 (d, J = 7.2 Hz, 2H), 1.96 (sept, J = 6.8 Hz, 1H), 1.18 (dddd, J = 15.1, 10.3, 5.2, 2.6 Hz, 1H), 0.95 (d, J = 6.7 Hz, 6H), 0.67 – 0.59 (m, 2H), 0.38 (dt, J = 6.1, 4.6 Hz, 2H). ^{13}C NMR (151 MHz, CDCl$_3$) δ 164.95, 159.18, 155.81, 153.40, 145.13, 134.99, 134.47, 129.70, 128.85, 128.33, 128.27, 127.87, 121.16, 45.50, 44.47, 30.40, 22.52, 10.90, 10.84, 3.68. MP: 132.2 – 134.2 °C. HRMS m/z: [M + H]+ Calcd. for $C_{23}H_{25}N_3O$ 360.2098; Found: TBD. HPLC: T_R = 2.024 min, peak area = 99.9%.

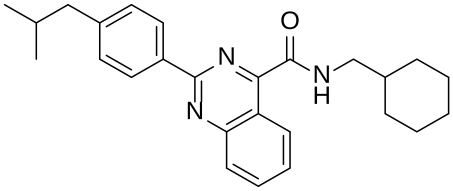

27B11

N-(cyclohexylmethyl)-2-(4-isobutylphenyl)quinazoline-4-carboxamide

Prepared according to the general amidation procedure to afford a white solid (71% yield). ^{1}H NMR (600 MHz, CDCl$_3$) δ 9.45 (ddd, J = 8.6, 1.5, 0.7 Hz, 1H), 8.50 – 8.45 (m, 2H), 8.40 (t, J = 6.4 Hz, 1H), 8.09 (dt, J = 8.5, 1.1 Hz, 1H), 7.91 (ddd, J = 8.4, 6.8, 1.5 Hz, 1H), 7.64 (ddd, J = 8.3, 6.8, 1.2 Hz, 1H), 7.36 – 7.31 (m, 2H), 3.42 (t, J = 6.6 Hz, 2H), 2.59 (d, J = 7.2 Hz, 2H), 1.95 (sept, J = 6.8 Hz, 1H), 1.91 – 1.84 (m, 2H), 1.78 (dt, J = 12.7, 3.5 Hz, 2H), 1.75 – 1.67 (m, 1H), 1.30 (qt, J = 12.5, 3.3 Hz, 2H), 1.21 (qt, J = 12.6, 3.2 Hz, 1H), 1.15 – 1.05 (m, 2H), 0.95 (d, J = 6.6 Hz, 6H). ^{13}C NMR (151 MHz, CDCl$_3$) δ 165.07, 159.12, 155.78, 153.45, 145.14, 141.95, 135.00, 134.49, 129.72, 128.85, 128.31, 128.29, 127.95, 121.20, 45.93, 45.50, 38.28, 31.11, 26.54, 26.44, 26.00, 22.53. MP: 134.8 – 136.3 °C. HRMS m/z: [M + H]+ Calcd. for $C_{26}H_{31}N_3O$ 402.2567; Found: TBD. HPLC: T_R = 2.714 min, peak area = 99.9%.

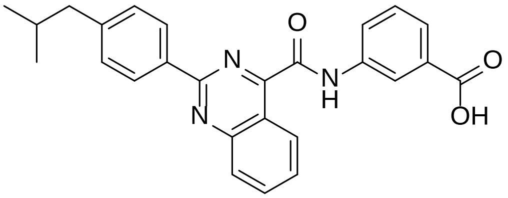

27B12

3-(2-(4-isobutylphenyl)quinazoline-4-carboxamido)benzoic acid

Prepared according to the general amidation procedure directly followed by the general saponification procedure to afford a beige solid (79% yield). ^{1}H NMR (600 MHz, DMSO) δ 13.06 (s, 1H), 11.19 (s, 1H), 8.66 – 8.61 (m, 1H), 8.60 – 8.55 (m, 2H), 8.55 (t, J = 1.9 Hz, 1H), 8.17 – 8.05 (m, 3H), 7.82 – 7.75 (m, 2H), 7.57 (t, J = 7.9 Hz, 1H), 7.40 – 7.36 (m, 2H), 2.56 (d, J = 7.2 Hz, 2H), 1.91 (dq, J = 13.5, 6.8 Hz, 1H), 0.90 (d, J = 6.6 Hz, 6H).^{13}C NMR (151 MHz, DMSO) δ 167.08, 163.73, 159.85, 159.00, 151.71, 144.72, 138.51, 135.20, 131.52, 129.41, 129.18, 128.55, 128.50, 128.41, 126.36, 125.31, 124.63, 121.22, 119.60, 44.49, 39.94, 39.80, 39.66, 39.52, 39.38, 39.24, 39.10, 29.62, 22.15. MP: TBD. HRMS m/z: [M + H]+ Calcd. for $C_{26}H_{23}N_3O_3$ 426.1839; Found: TBD. HPLC: T_R = 2.333 min, peak area = 81.2%.

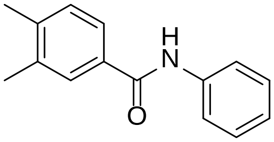

3,4-dimethyl-N-phenylbenzamide

Prepared according to the general amidation procedure to afford a shiny light yellow solid (91% yield). ^{1}H NMR (300 MHz, $CDCl_3$) δ 7.84 (s, 1H), 7.70 – 7.54 (m, 4H), 7.42 – 7.30 (m, 2H), 7.22 (d, J = 7.8 Hz, 1H), 7.21 – 7.08 (m, 1H), 2.32 (s, 6H). ^{13}C NMR (75 MHz, $CDCl_3$) δ 165.95, 141.16, 138.25, 137.36, 132.62, 130.06, 129.19, 128.47, 124.48, 124.46, 120.25, 19.99, 19.94. MP: 107.4 – 111.7 °C.

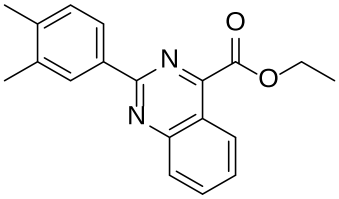

ethyl 2-(3,4-dimethylphenyl)quinazoline-4-carboxylate

Prepared according to the general Meerwein quinazoline cyclization procedure to afford a yellow solid (22% yield). ^{1}H NMR (600 MHz, CDCl$_3$) δ 8.44 – 8.40 (m, 2H), 8.38 (dd, J = 7.8, 1.9 Hz, 1H), 8.12 (dt, J = 8.6, 1.0 Hz, 1H), 7.90 (ddd, J = 8.4, 6.8, 1.4 Hz, 1H), 7.61 (ddd, J = 8.2, 6.9, 1.2 Hz, 1H), 7.30 (d, J = 7.9 Hz, 1H), 4.63 (q, J = 7.2 Hz, 2H), 2.40 (s, 3H), 2.35 (s, 3H), 1.54 (t, J = 7.2 Hz, 3H). ^{13}C NMR (151 MHz, CDCl$_3$) δ 165.44, 160.55, 157.76, 152.48, 140.06, 136.97, 135.04, 134.38, 132.90, 130.34, 130.14, 130.13, 129.74, 129.72, 129.18, 126.42, 126.42, 125.89, 125.89, 120.30, 62.66, 20.22, 20.03, 14.41. MP: 88.4 – 90.1 °C.

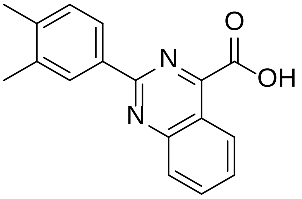

27C0

2-(3,4-dimethylphenyl)quinazoline-4-carboxylic acid

Prepared according to the general saponification procedure to afford yellow solid (89% yield). ^{1}H NMR (600 MHz, CDCl$_3$) δ 11.80 (s, 1H), 9.38 (d, J = 8.5 Hz, 1H), 8.30 (s, 1H), 8.25 (dd, J = 7.9, 1.9 Hz, 1H), 8.17 (d, J = 8.6 Hz, 1H), 8.03 – 7.97 (m, 1H), 7.74 (td, J = 7.8, 7.2, 1.8 Hz, 1H), 7.31 (d, J = 7.9 Hz, 1H), 2.41 (s, 3H), 2.37 (s, 3H). ^{13}C NMR (151 MHz, CDCl$_3$) δ 163.38, 158.73, 153.88, 151.02, 140.72, 137.28, 135.40, 133.58, 130.27, 129.35, 128.97, 127.13, 125.92, 120.63, 19.92, 19.90. MP: 146.7 - 152.6 °C. HRMS m/z: [M + H]+ Calcd. for $C_{17}H_{14}N_2O_2$ 279.1128; Found 279.1130, Error 0.69 ppm. HPLC: T_R = 3.157 min, peak area = 93.0%

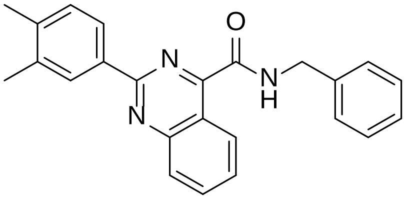

27C1

N-benzyl-2-(3,4-dimethylphenyl)quinazoline-4-carboxamide

Prepared according to the general amidation procedure to afford a white solid (70% yield). ^{1}H NMR (600 MHz, CDCl$_3$) δ 9.46 (d, J = 8.5 Hz, 1H), 8.66 (t, J = 6.2 Hz, 1H), 8.32 (s, 1H), 8.26 (dd, J = 7.8, 1.9 Hz, 1H), 8.11 (d, J = 8.5 Hz, 1H), 7.92 (ddd, J = 8.4, 6.8, 1.4 Hz, 1H), 7.68 – 7.63 (m, 1H), 7.46 (d, J = 7.6 Hz, 2H), 7.40 (t, J = 7.6 Hz, 2H), 7.31 (dd, J = 32.4, 7.6 Hz, 2H), 4.80 (d, J = 6.1 Hz, 2H), 2.39 (s, 3H), 2.35 (s, 3H). ^{13}C NMR (151 MHz, CDCl$_3$) δ 165.11, 159.28, 155.45, 153.47, 140.14, 138.10, 137.15, 134.91, 134.55, 130.20, 129.51, 128.98, 128.87, 128.33, 127.83, 127.76, 126.08, 121.19, 43.65, 20.11, 20.05. MP: 191.8 – 193.7 °C. HRMS m/z: [M + H]+ Calcd. for $C_{24}H_{21}N_3O$ 368.1757; Found 368.1759, Error 0.38 ppm. HPLC: T_R = 3.949 min, peak area = 97.1%.

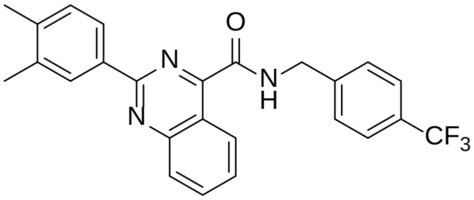

27C3

2-(3,4-dimethylphenyl)-N-(4-(trifluoromethyl)benzyl)quinazoline-4-carboxamide

Prepared according to the general amidation procedure to afford a white solid (67% yield). ^{1}H NMR (600 MHz, CDCl$_3$) δ 9.43 (dd, J = 8.6, 1.4 Hz, 1H), 8.77 (t, J = 6.3 Hz, 1H), 8.32 (d, J = 1.9 Hz, 1H), 8.26 (dd, J = 7.9, 2.0 Hz, 1H), 8.12 (d, J = 8.5 Hz, 1H), 7.93 (ddd, J = 8.4, 6.8, 1.4 Hz, 1H), 7.69 – 7.62 (m, 3H), 7.56 (d, J = 8.0 Hz, 2H), 7.29 (d, J = 7.8 Hz, 1H), 4.84 (d, J = 6.3 Hz, 2H), 2.39 (s, 3H), 2.36 (s, 3H). ^{13}C NMR (151 MHz, CDCl$_3$) δ 165.33, 159.31, 155.06, 142.23, 142.22, 140.25, 137.22, 134.85, 134.67, 130.33, 130.22, 130.11, 129.90, 129.68, 129.49, 128.93, 128.48, 127.91, 127.70, 126.92, 126.07, 125.95, 125.92, 125.90, 125.87, 125.12, 123.31, 121.51, 121.14, 43.18, 20.13, 20.06. MP: 194.4 – 196.6 °C. HRMS m/z: [M + H]+ Calcd. for $C_{25}H_{20}F_3N_3O$ 436.1631; Found 436.1621, Error 2.46 ppm. HPLC: T_R = 3.910 min, peak area = 98.0%

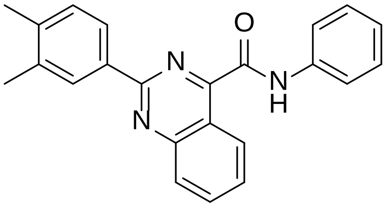

27C5

2-(3,4-dimethylphenyl)-N-phenylquinazoline-4-carboxamide

Prepared according to the general amidation procedure to afford a pale yellow solid (80% yield). ^{1}H NMR (600 MHz, CDCl3) δ 10.49 (s, 1H), 9.50 (d, J = 8.5 Hz, 1H), 8.39 (s, 1H), 8.32 (dd, J = 7.8, 1.9 Hz, 1H), 8.16 (d, J = 8.5 Hz, 1H), 8.01 – 7.95 (m, 3H), 7.74 (s, 1H), 7.74 – 7.69 (m, 2H), 7.36 (d, J = 7.9 Hz, 1H), 2.45 (s, 3H), 2.41 (s, 3H).^{13}C NMR (151 MHz, CDCl3) δ 162.74, 159.07, 155.10, 153.74, 140.27, 137.23, 134.83, 134.65, 130.30, 129.57, 129.37, 129.02, 128.49, 127.77, 126.07, 125.08, 121.27, 120.29, 77.37, 77.16, 76.95, 20.15, 20.04, 0.14. MP: TBD. HRMS m/z: [M + H]+ Calcd. for $C_{23}H_{19}N_3O$ 354.1628; Found: TBD. HPLC: T_R = 2.075 min, peak area = 99.9%.

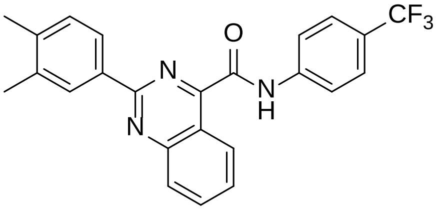

27C6

2-(3,4-dimethylphenyl)-N-(4-(trifluoromethyl)phenyl)quinazoline-4-carboxamide

Prepared according to the general amidation procedure to afford a white solid (76% yield). ^{1}H NMR (600 MHz, CDCl3) δ 10.49 (s, 1H), 9.50 (d, J = 8.5 Hz, 1H), 8.39 (s, 1H), 8.32 (dd, J = 7.8, 1.9 Hz, 1H), 8.16 (d, J = 8.5 Hz, 1H), 8.01 – 7.95 (m, 3H), 7.74 (s, 1H), 7.74 – 7.69 (m, 2H), 7.36 (d, J = 7.9 Hz, 1H), 2.45 (s, 3H), 2.41 (s, 3H). ^{13}C NMR (151 MHz, CDCl3) δ 163.00, 159.12, 154.42, 153.87, 140.55, 140.46, 137.34, 134.87, 134.70, 130.37, 129.59, 129.15, 128.79, 127.55, 126.93, 126.66, 126.64, 126.61, 126.06, 125.14, 123.34, 121.19, 119.91, 77.37, 77.16, 76.95, 20.19, 20.06, 0.14. MP: 220.0 – 222.3 °C. HRMS m/z: [M + H]+ Calcd. for $C_{24}H_{18}F_3N_3O$ 422.1502; Found: TBD. HPLC: T_R = 2.124 min, peak area = 99.8%.

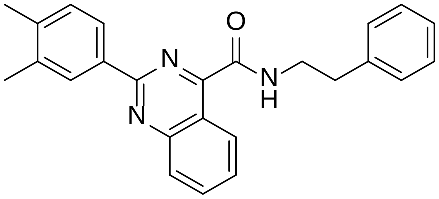

27C7

2-(3,4-dimethylphenyl)-N-phenethylquinazoline-4-carboxamide

Prepared according to the general amidation procedure to afford a white solid (66% yield). ^{1}H NMR (600 MHz, $CDCl_3$) δ 9.43 (dt, J = 8.6, 0.9 Hz, 1H), 8.35 (t, J = 6.2 Hz, 1H), 8.29 – 8.25 (m, 1H), 8.16 (dd, J = 7.9, 1.9 Hz, 1H), 8.09 (dt, J = 8.4, 0.9 Hz, 1H), 7.90 (ddd, J = 8.4, 6.8, 1.5 Hz, 1H), 7.64 (ddd, J = 8.3, 6.8, 1.3 Hz, 1H), 7.41 – 7.26 (m, 6H), 3.86 (q, J = 6.6 Hz, 2H), 3.04 (t, J = 6.8 Hz, 2H), 2.40 (s, 3H), 2.38 (s, 3H). ^{13}C NMR (151 MHz, $CDCl_3$) δ 165.05, 159.23, 155.55, 153.48, 140.07, 139.00, 137.10, 134.98, 134.45, 130.15, 129.47, 129.10, 128.99, 128.87, 128.23, 127.86, 126.87, 126.18, 121.17, 40.80, 35.86, 20.09, 20.04. MP: 151.3 – 152.1 °C. HRMS m/z: [M + H]+ Calcd. for $C_{25}H_{23}N_3O$ 382.1914; Found 382.1908, Error 1.65 ppm. HPLC: T_R = 4.371 min, peak area = 97.3%.

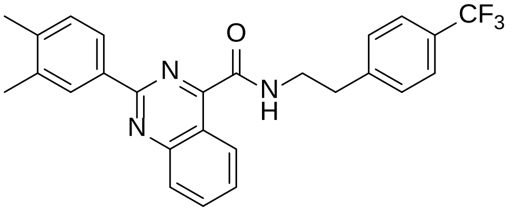

27C8

2-(3,4-dimethylphenyl)-N-(4-(trifluoromethyl)phenethyl)quinazoline-4-carboxamide

Prepared according to the general amidation procedure to afford a white solid (68% yield). ^{1}H NMR (600 MHz, $CDCl_3$) δ 9.39 (dd, J = 8.7, 1.4 Hz, 1H), 8.38 (t, J = 6.3 Hz, 1H), 8.28 (d, J = 1.9 Hz, 1H), 8.14 (dd, J = 7.8, 1.9 Hz, 1H), 8.10 (d, J = 8.3 Hz, 1H), 7.92 (ddd, J = 8.4, 6.8, 1.4 Hz, 1H), 7.65 (td, J = 8.3, 1.5 Hz, 3H), 7.46 (d, J = 7.9 Hz, 2H), 7.27 (d, J = 7.8 Hz, 1H), 3.87 (q, J = 6.7 Hz, 2H), 3.10 (t, J = 6.9 Hz, 2H), 2.39 (s, 3H), 2.37 (s, 3H). ^{13}C NMR (151 MHz, $CDCl_3$) δ 165.14, 159.21, 155.33, 153.47, 143.18, 134.85, 134.57, 130.15, 129.55, 129.46, 129.39, 129.34, 129.12, 128.89, 128.35, 127.69, 127.08, 126.01, 125.89, 125.86, 125.83, 125.81, 125.28, 123.48, 121.67, 121.08, 40.55, 35.82, 20.11, 20.07, 0.14. MP: 192.5 – 194.3 °C. HRMS m/z: [M + H]+ Calcd. for $C_{26}H_{22}F_3N_3O$ 450.1788; Found 450.1787, Error 0.24 ppm. HPLC: T_R = 4.220 min, peak area = 97.1%.

References

1. Charlier, H. A.; Plapp, B. V., Kinetic cooperativity of human liver alcohol dehydrogenase γ2. *J Biol Chem* **2000**. *275*, 11569-11575
2. Motulsky, H., *Analyzing Data with GraphPad Prism*. 1999.
3. Benjamani, Y., Hochberg, Y. Controlling the false discovery rate: a practical and powerful approach to multiple testing. *J Royal Stat Soc* **1995** *57* (1), 289-300.
4. Deller, M. C.; Hudson, K. R.; Ikemizu, S.; Bravo, J.; Jones, E. Y.; Heath, J. K., Crystal structure and functional dissection of the cytostatic cytokine oncostatin M. *Structure* **2000,** *8* (8), 863-74.
5. Harris, R.; Olson, A. J.; Goodsell, D. S., Automated prediction of ligand-binding sites in proteins. *Proteins* **2008,** *70* (4), 1506-17.
6. Chollangi, S.; Mather, T.; Rodgers, K. K.; Ash, J. D., A unique loop structure in oncostatin M determines binding affinity toward oncostatin M receptor and leukemia inhibitory factor receptor. *J Biol Chem* **2012,** *287* (39), 32848-59.
7. Durrant, J. D.; Votapka, L.; Sørensen, J.; Amaro, R. E., POVME 2.0: An Enhanced Tool for Determining Pocket Shape and Volume Characteristics. *J Chem Theory Comput* **2014,** *10* (11), 5047-5056.
8. Morris, G. M.; Huey, R.; Lindstrom, W.; Sanner, M. F.; Belew, R. K.; Goodsell, D. S.; Olson, A. J., AutoDock4 and AutoDockTools4: Automated docking with selective receptor flexibility. *J Comput Chem* **2009,** *30* (16), 2785-91.
9. Pettersen, E. F.; Goddard, T. D.; Huang, C. C.; Couch, G. S.; Greenblatt, D. M.; Meng, E. C.; Ferrin, T. E., UCSF Chimera--a visualization system for exploratory research and analysis. *J Comput Chem* **2004,** *25* (13), 1605-12.
10. Wang, J.; Wang, W.; Kollman, P. A.; Case, D. A., Automatic atom type and bond type perception in molecular mechanical calculations. *J Mol Graph Model* **2006,** *25* (2), 247-60.
11. Aqel, S. I.; Kraus, E. E.; Jena, N.; Kumari, V.; Granitto, M. C.; Mao, L.; Farinas, M. F.; Zhao, E. Y.; Perottino, G.; Pei, W.; Lovett-Racke, A. E.; Racke, M. K.; Fuchs, J. R.; Li, C.; Yang, Y., Novel small molecule IL-6 inhibitor suppresses autoreactive Th17 development and promotes T. *Clin Exp Immunol* **2019,** *196* (2), 215-225.

APPENDIX B

^{1}H and ^{13}C spectra and HPLC Chromatograms

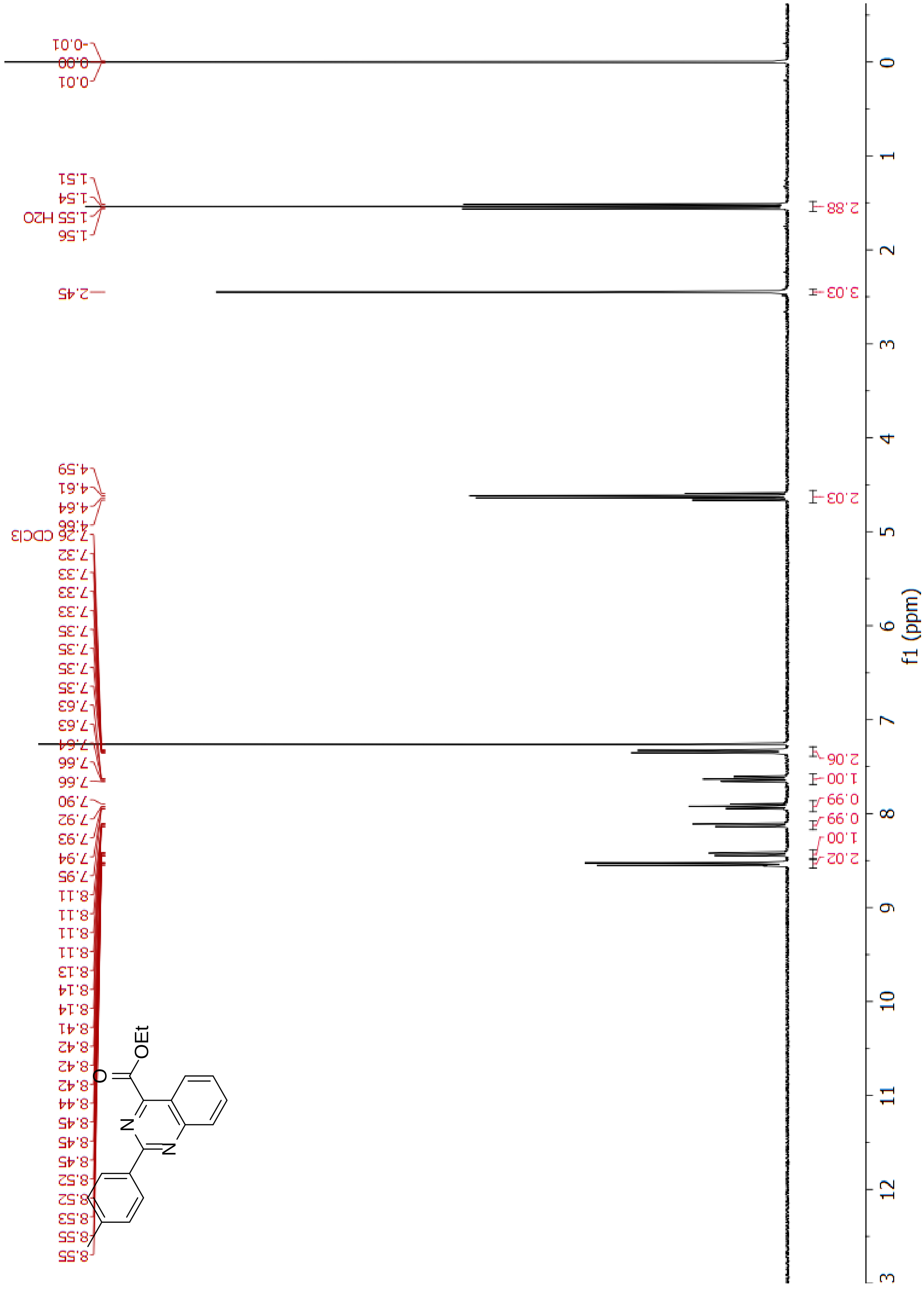
-0.01
0.00
0.01
1.51
1.54
1.55 H2O
1.56
2.45
4.59
4.61
4.64
4.66
7.26 CDCl3
7.32
7.33
7.33
7.33
7.35
7.35
7.35
7.35
7.63
7.63
7.64
7.66
7.66
7.90
7.92
7.93
7.94
7.95
8.11
8.11
8.11
8.11
8.13
8.14
8.14
8.41
8.42
8.42
8.42
8.44
8.45
8.45
8.45
8.52
8.52
8.53
8.55
8.55
O
OEt
N
N
2.88
3.03
2.03
2.06
1.00
0.99
0.99
1.00
2.02
0
1
2
3
4
5
6
7
8
9
10
11
12
13
f1 (ppm)

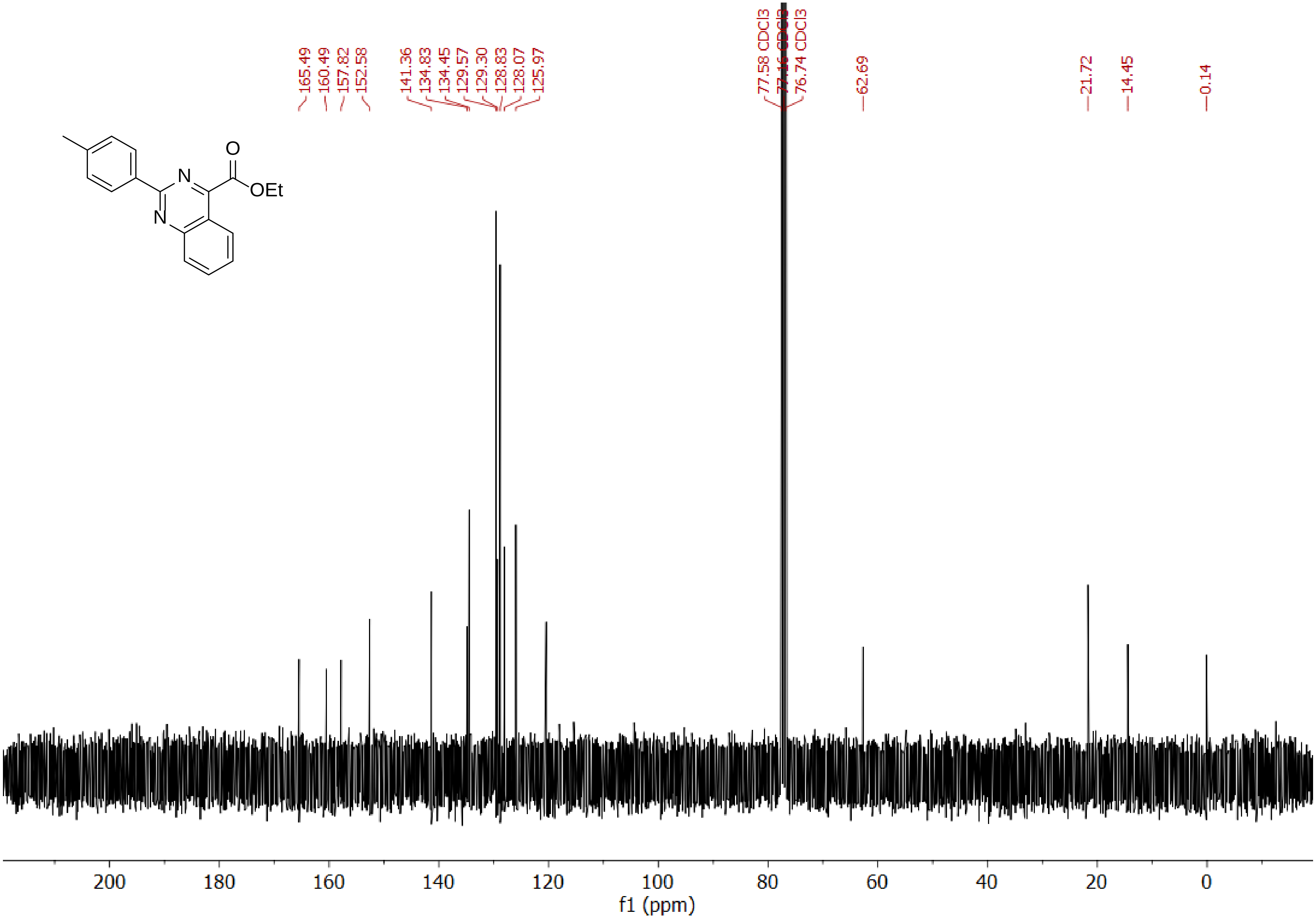
165.49
160.49
157.82
152.58
141.36
134.83
134.45
129.57
129.30
128.83
128.07
125.97
77.58 CDCl3
77.16 CDCl3
76.74 CDCl3
62.69
21.72
14.45
0.14
O
OEt
N
N
200
180
160
140
120
100
80
60
40
20
0
f1 (ppm)

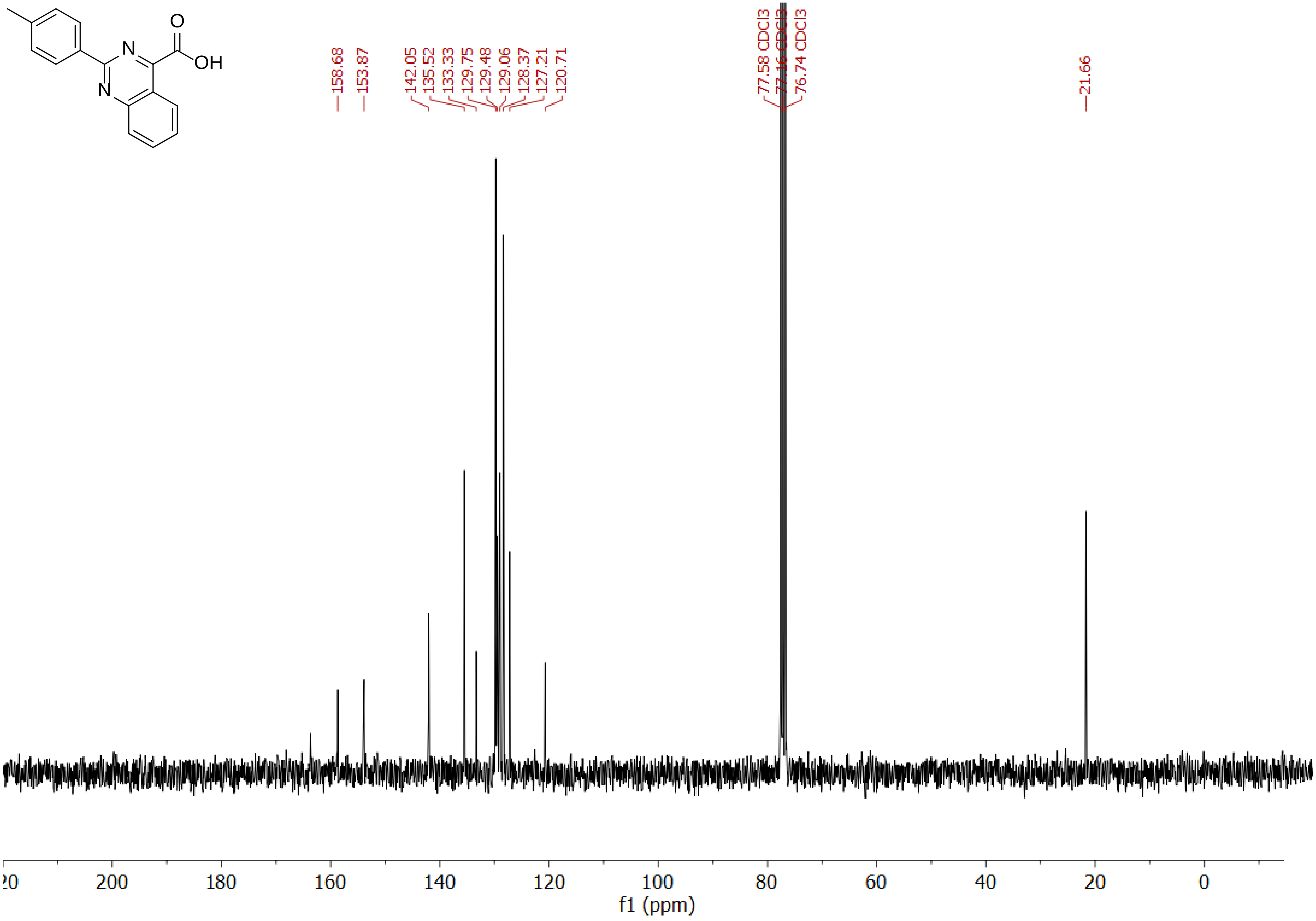
O
OH
N
N
158.68
153.87
142.05
135.52
133.33
129.75
129.48
129.06
128.37
127.21
120.71
77.58 CDCl3
77.16 CDCl3
76.74 CDCl3
21.66
20
200
180
160
140
120
100
80
60
40
20
0
f1 (ppm)

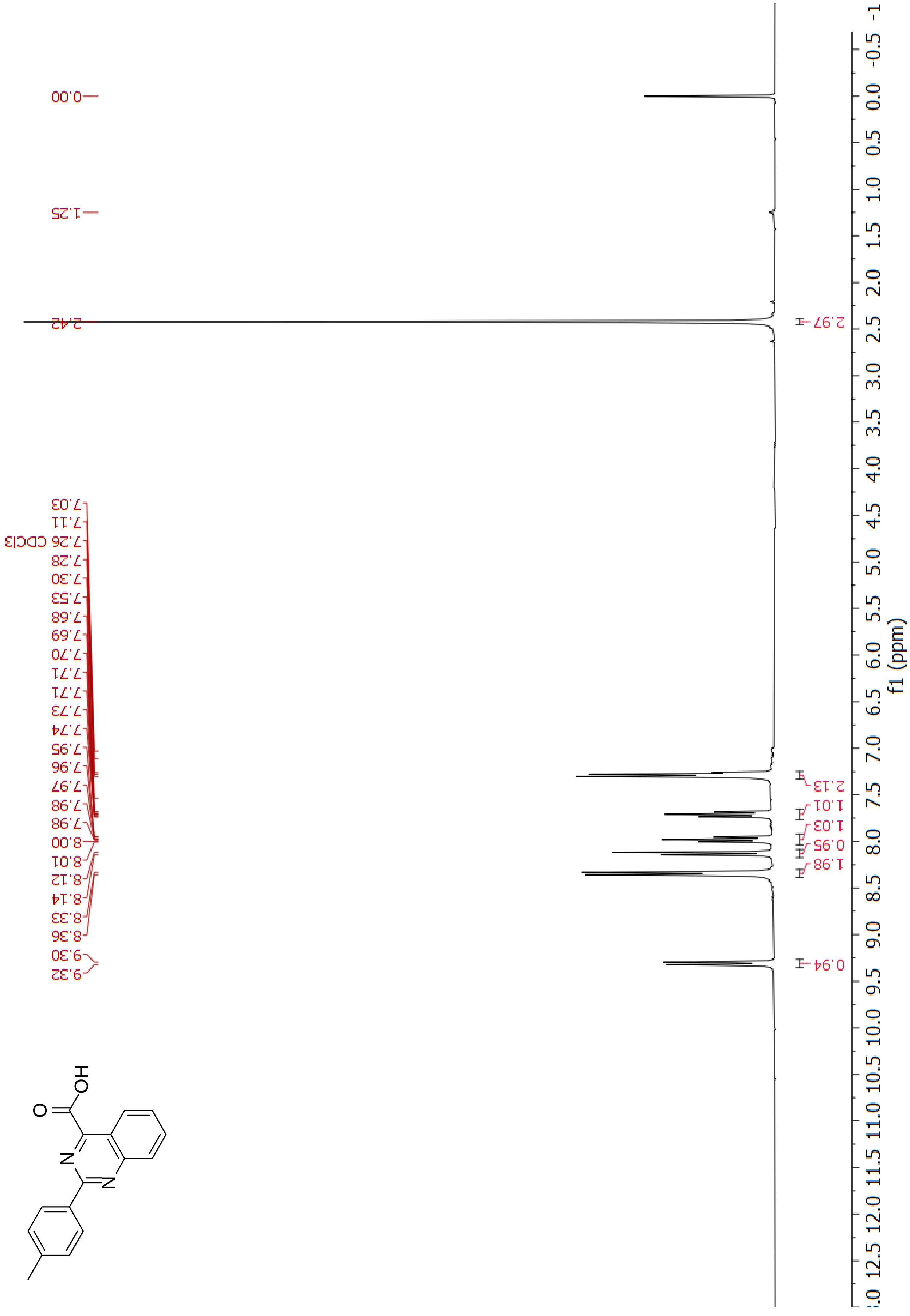
0.00
1.25
2.42
7.03
7.11
7.26 CDCl3
7.28
7.30
7.53
7.68
7.69
7.70
7.71
7.71
7.73
7.74
7.95
7.96
7.97
7.98
7.98
8.00
8.01
8.12
8.14
8.33
8.36
9.30
9.32
2.97
2.13
1.01
1.03
0.95
1.98
0.94
f1 (ppm)
-1
-0.5
0.0
0.5
1.0
1.5
2.0
2.5
3.0
3.5
4.0
4.5
5.0
5.5
6.0
6.5
7.0
7.5
8.0
8.5
9.0
9.5
10.0
10.5
11.0
11.5
12.0
12.5
13.0
O
HO
N
N

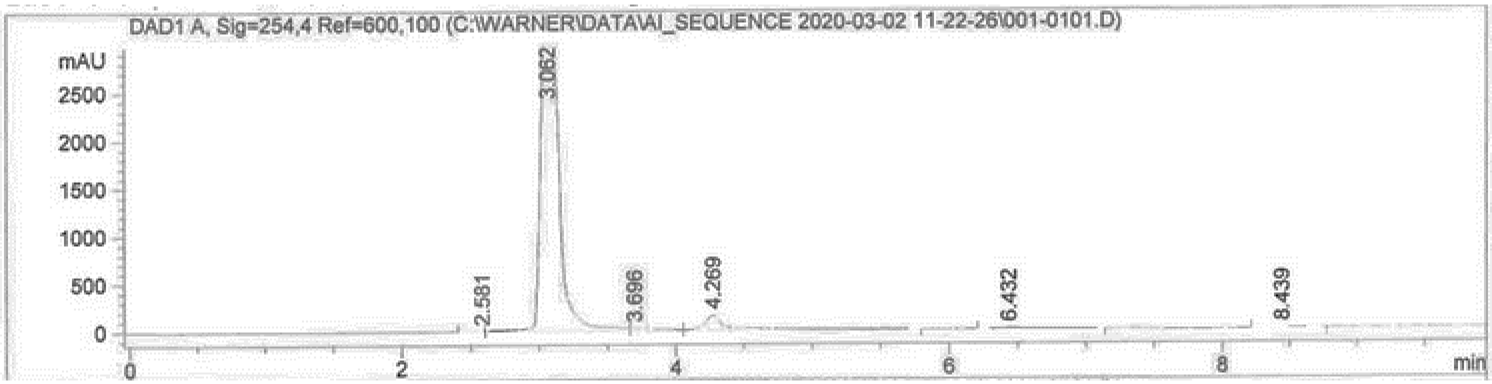

```
Signal 1: DAD1 A, Sig=254,4 Ref=600,100

Peak RetTime Type  Width     Area       Height      Area
  #   [min]        [min]   [mAU*s]      [mAU]        %
----|-------|----|-------|----------|----------|--------|
   1   2.581 BV    0.0674    8.11246    1.59394   0.0257
   2   3.062 VV    0.1630 2.88908e4  2833.55737  91.4783
   3   3.696 VV    0.2065  464.47385   28.74671   1.4707
   4   4.269 VB    0.1747 1951.01611  151.01526   6.1776
   5   6.432 BB    0.3136  227.45409   10.80486   0.7202
   6   8.439 BB    0.1989   40.27509    3.07269   0.1275
```

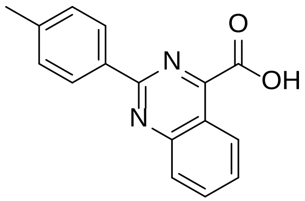

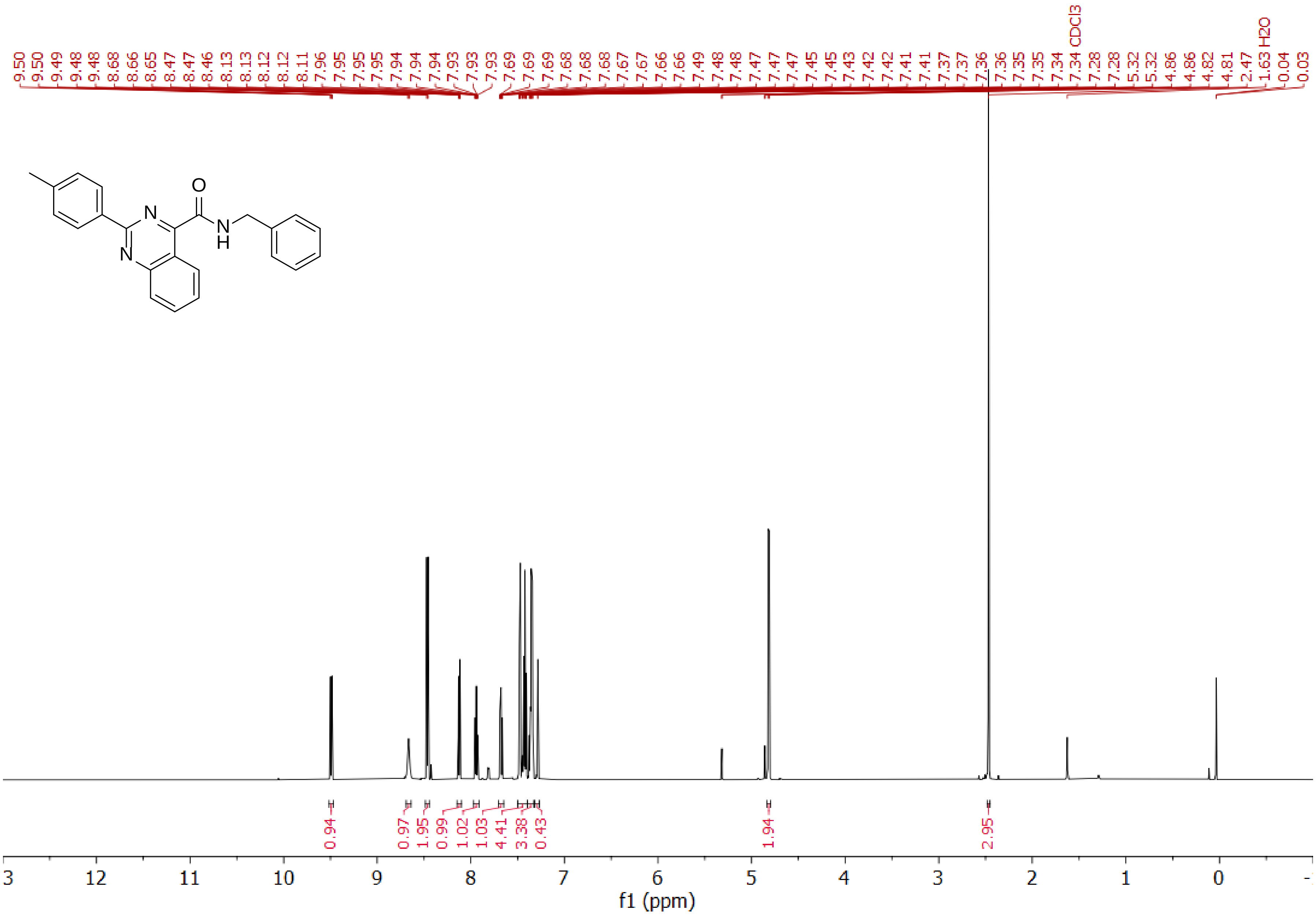
9.50
9.50
9.49
9.48
9.48
8.68
8.66
8.65
8.47
8.47
8.46
8.13
8.13
8.12
8.12
8.11
7.96
7.95
7.95
7.95
7.94
7.94
7.94
7.93
7.93
7.93
7.69
7.69
7.69
7.68
7.68
7.68
7.67
7.67
7.66
7.66
7.49
7.48
7.48
7.47
7.47
7.47
7.45
7.45
7.43
7.42
7.42
7.41
7.41
7.37
7.37
7.36
7.36
7.35
7.35
7.34
7.34 CDCl3
7.28
7.28
5.32
5.32
4.86
4.86
4.82
4.81
2.47
1.63 H2O
0.04
0.03
O
N
N
N
H
0.94
0.97
1.95
0.99
1.02
1.03
4.41
3.38
0.43
1.94
2.95
13
12
11
10
9
8
7
6
5
4
3
2
1
0
-1
f1 (ppm)

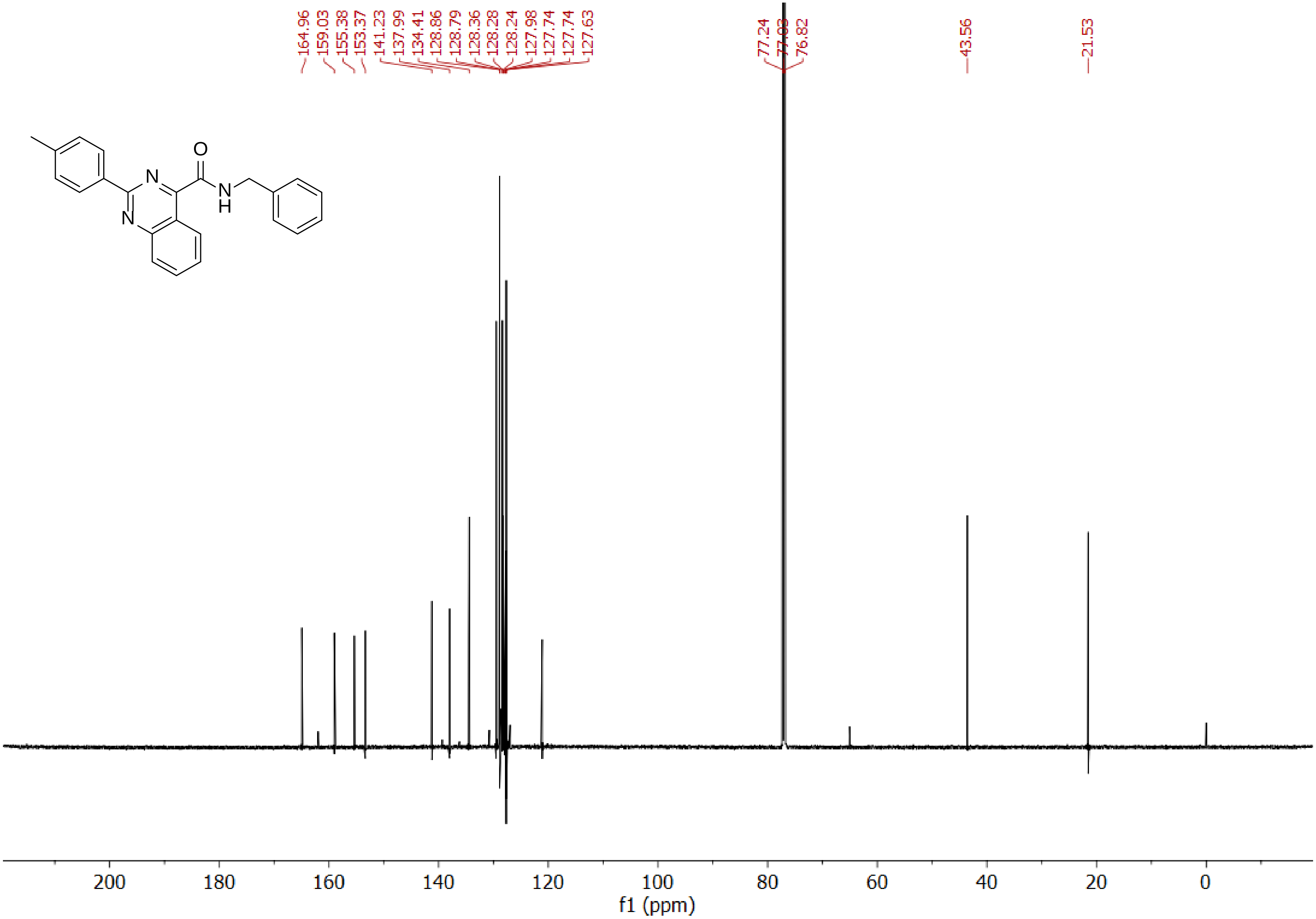
164.96
159.03
155.38
153.37
141.23
137.99
134.41
128.86
128.79
128.36
128.28
128.24
127.98
127.74
127.74
127.63
77.24
77.03
76.82
43.56
21.53
O
N
N
N
H
200
180
160
140
120
100
80
60
40
20
0
f1 (ppm)

HPLC trace

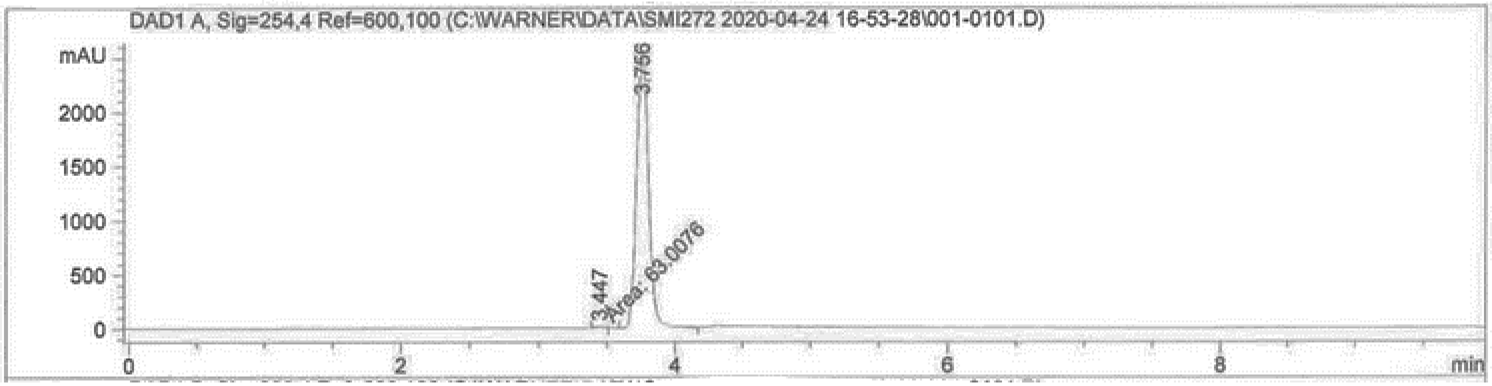

```
Signal 1: DAD1 A, Sig=254,4 Ref=600,100

Peak RetTime Type  Width      Area       Height      Area
  #    [min]        [min]    [mAU*s]      [mAU]        %
----|-------|----|-------|----------|----------|--------|
   1    3.447 MM    0.0914    63.00762    11.48872   0.3976
   2    3.756 VV    0.0992 1.57841e4  2514.00732  99.6024
```

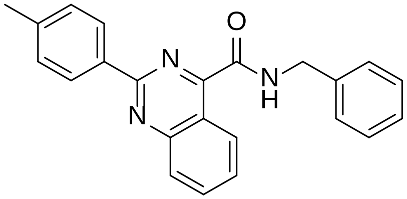

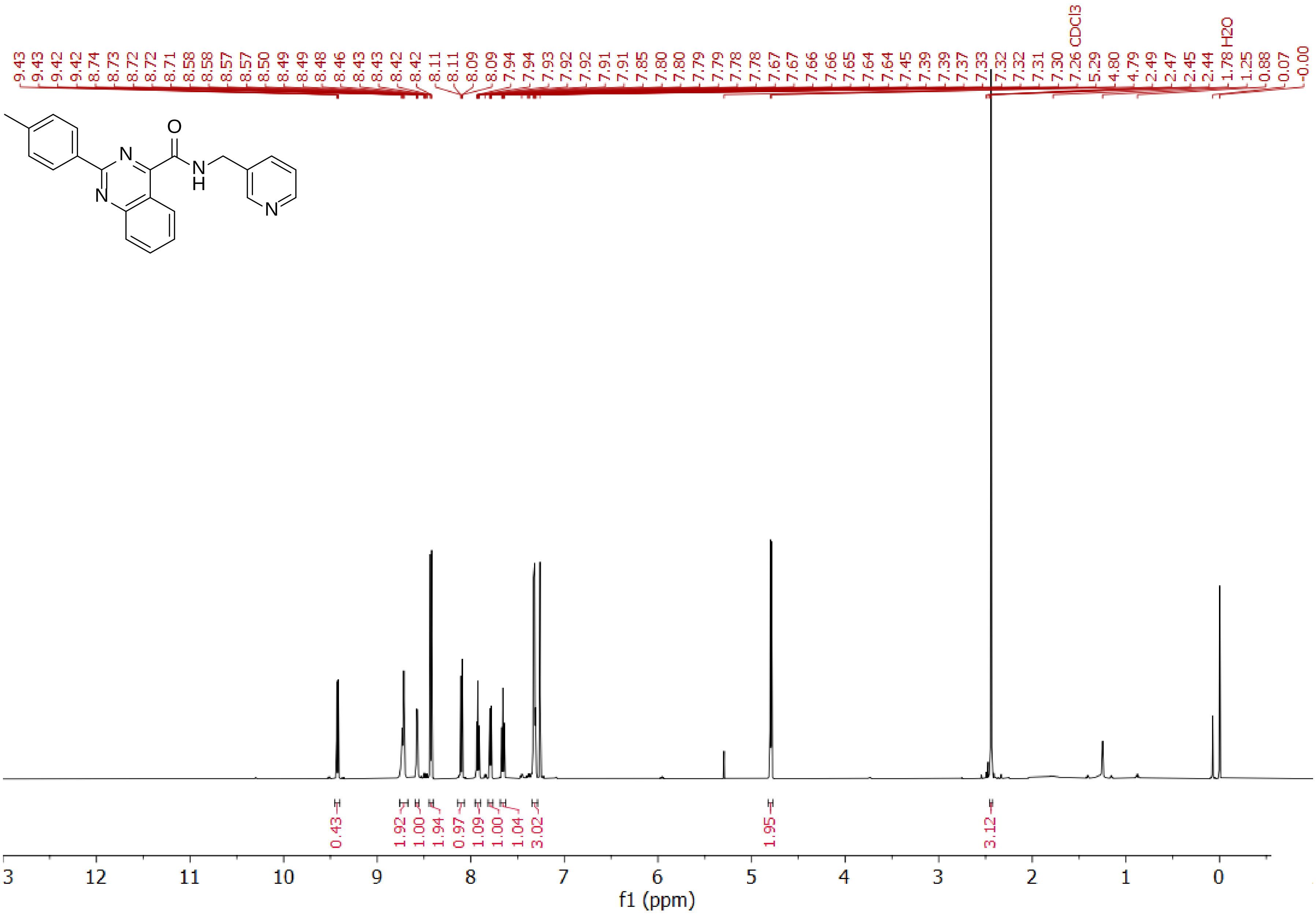
9.43
9.43
9.42
9.42
8.74
8.73
8.72
8.72
8.71
8.58
8.58
8.57
8.57
8.50
8.49
8.49
8.48
8.46
8.43
8.43
8.42
8.42
8.11
8.11
8.09
8.09
7.94
7.94
7.93
7.92
7.92
7.91
7.91
7.85
7.80
7.80
7.79
7.79
7.78
7.78
7.67
7.67
7.66
7.66
7.65
7.64
7.64
7.45
7.39
7.39
7.37
7.33
7.32
7.32
7.31
7.30
7.26 CDCl3
5.29
4.80
4.79
2.49
2.47
2.45
2.44
1.78 H2O
1.25
0.88
0.07
-0.00
O
N
N
N
H
N
0.43
1.92
1.00
1.94
0.97
1.09
1.00
1.04
3.02
1.95
3.12
3
12
11
10
9
8
7
6
5
4
3
2
1
0
f1 (ppm)

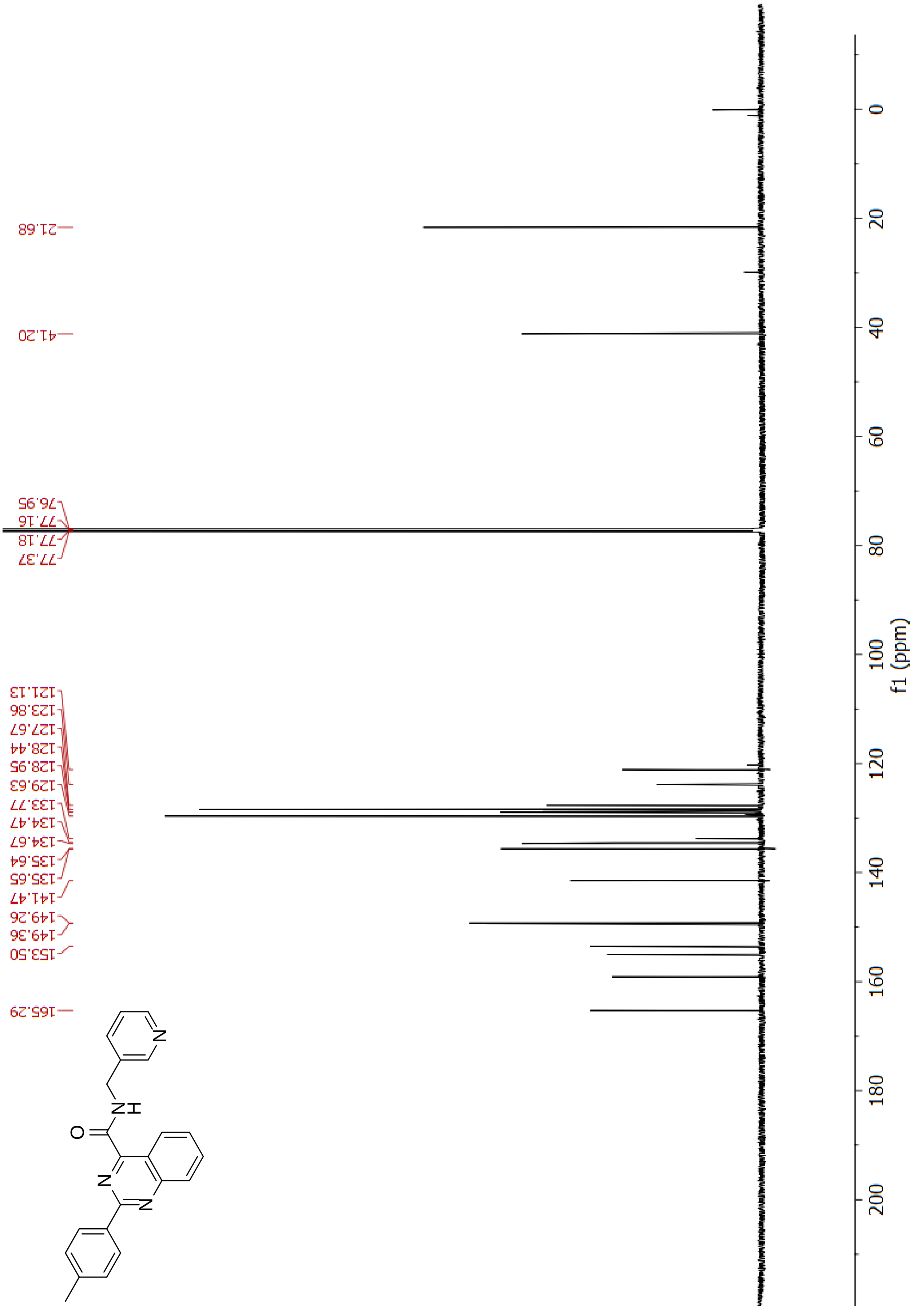
165.29
153.50
149.36
149.26
141.47
135.65
135.64
134.67
134.47
133.77
129.63
128.95
128.44
127.67
123.86
121.13
77.37
77.18
77.16
76.95
41.20
21.68
f1 (ppm)
0
20
40
60
80
100
120
140
160
180
200
N
N
O
NH
N

HPLC trace

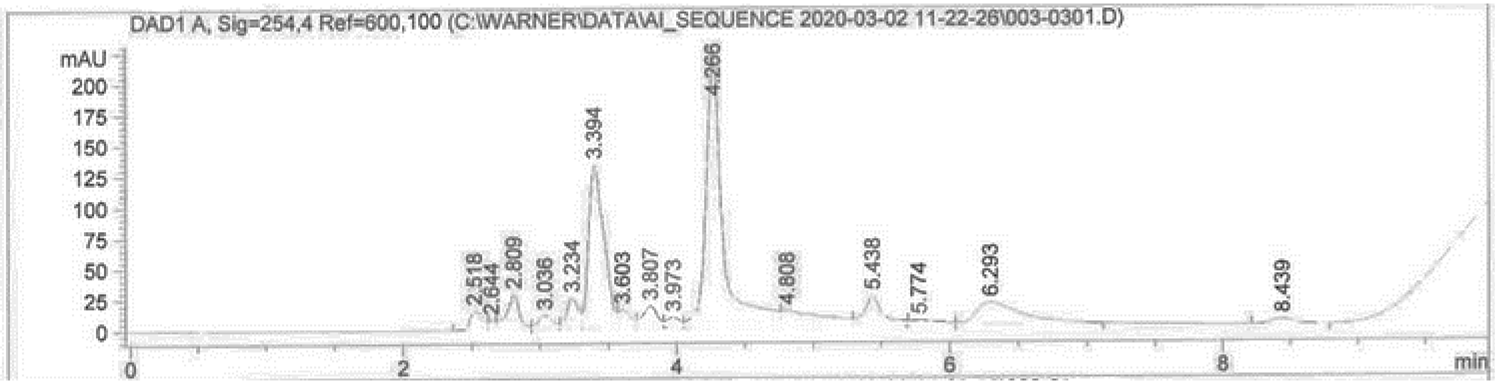

```
Signal 1: DAD1 A, Sig=254,4 Ref=600,100

Peak RetTime Type  Width     Area      Height     Area
  #   [min]        [min]   [mAU*s]     [mAU]        %
----|-------|----|-------|----------|----------|--------|
   1   2.518 BV    0.0933  107.41062   15.79420   2.1723
   2   2.644 VV    0.0487   27.54719    7.90186   0.5571
   3   2.809 VV    0.0958  192.15637   28.82046   3.8863
   4   3.036 VV    0.1196   91.89154   11.44905   1.8585
   5   3.234 VV    0.0920  151.29608   25.21577   3.0599
   6   3.394 VV    0.1171 1060.79968  132.93690  21.4541
   7   3.603 VV    0.0952   97.55929   15.13770   1.9731
   8   3.807 VV    0.1096  133.78520   17.81985   2.7057
   9   3.973 VV    0.1063   58.26308    8.25813   1.1783
  10   4.266 VV    0.1283 1968.87842  220.14485  39.8196
```

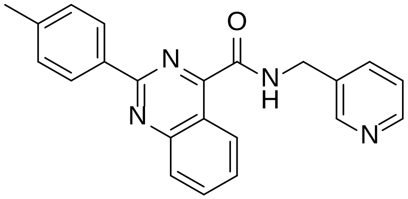

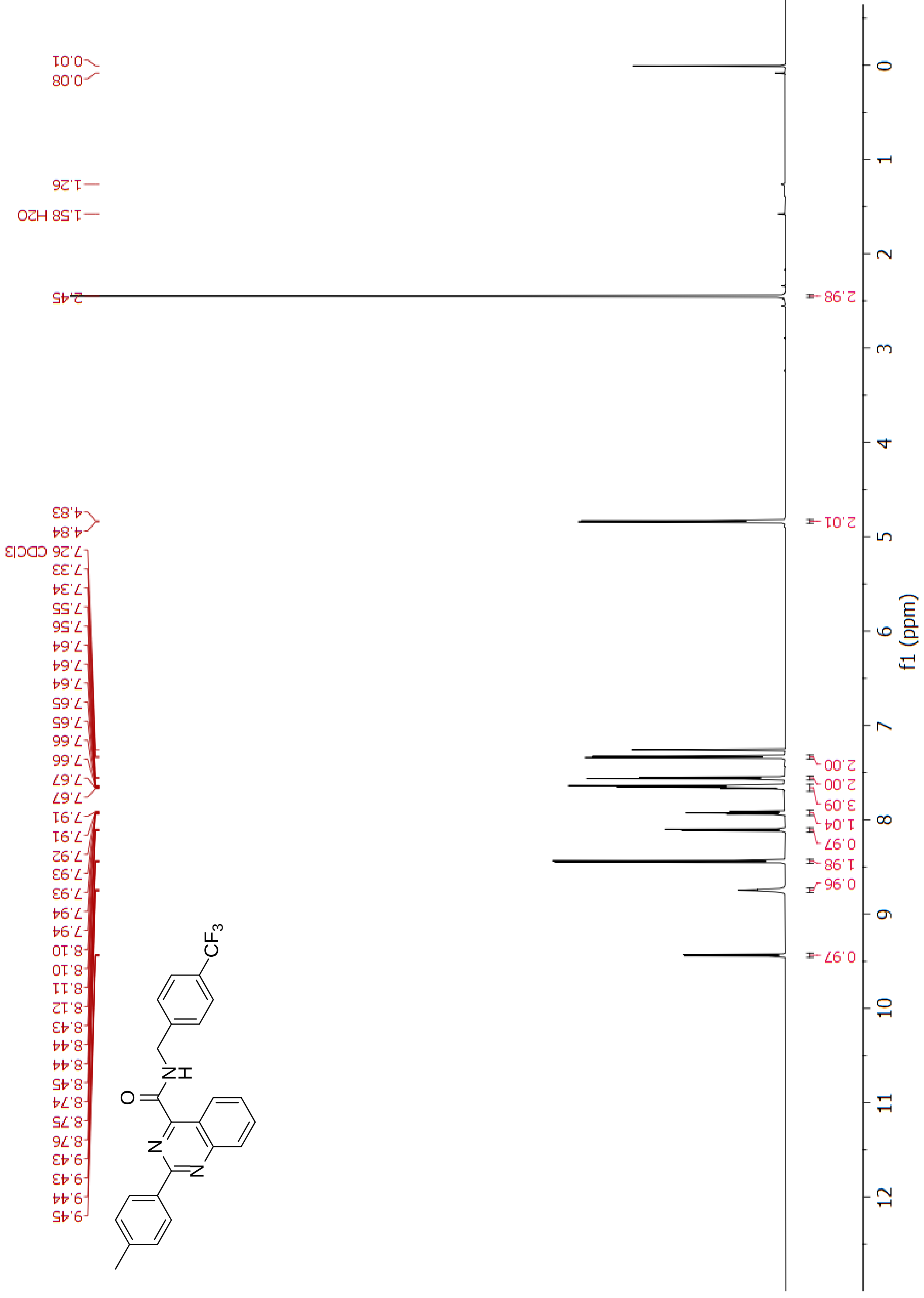

0.01
0.08
1.26
1.58 H2O
2.45
4.83
4.84
7.26 CDCl3
7.33
7.34
7.55
7.56
7.64
7.64
7.64
7.65
7.65
7.66
7.66
7.67
7.67
7.91
7.91
7.92
7.93
7.93
7.94
7.94
8.10
8.10
8.11
8.12
8.43
8.44
8.44
8.45
8.74
8.75
8.76
9.43
9.43
9.44
9.45
2.98
2.01
2.00
2.00
3.09
1.04
0.97
1.98
0.96
0.97
0
1
2
3
4
5
6
7
8
9
10
11
12
f1 (ppm)
N
N
O
NH
CF3

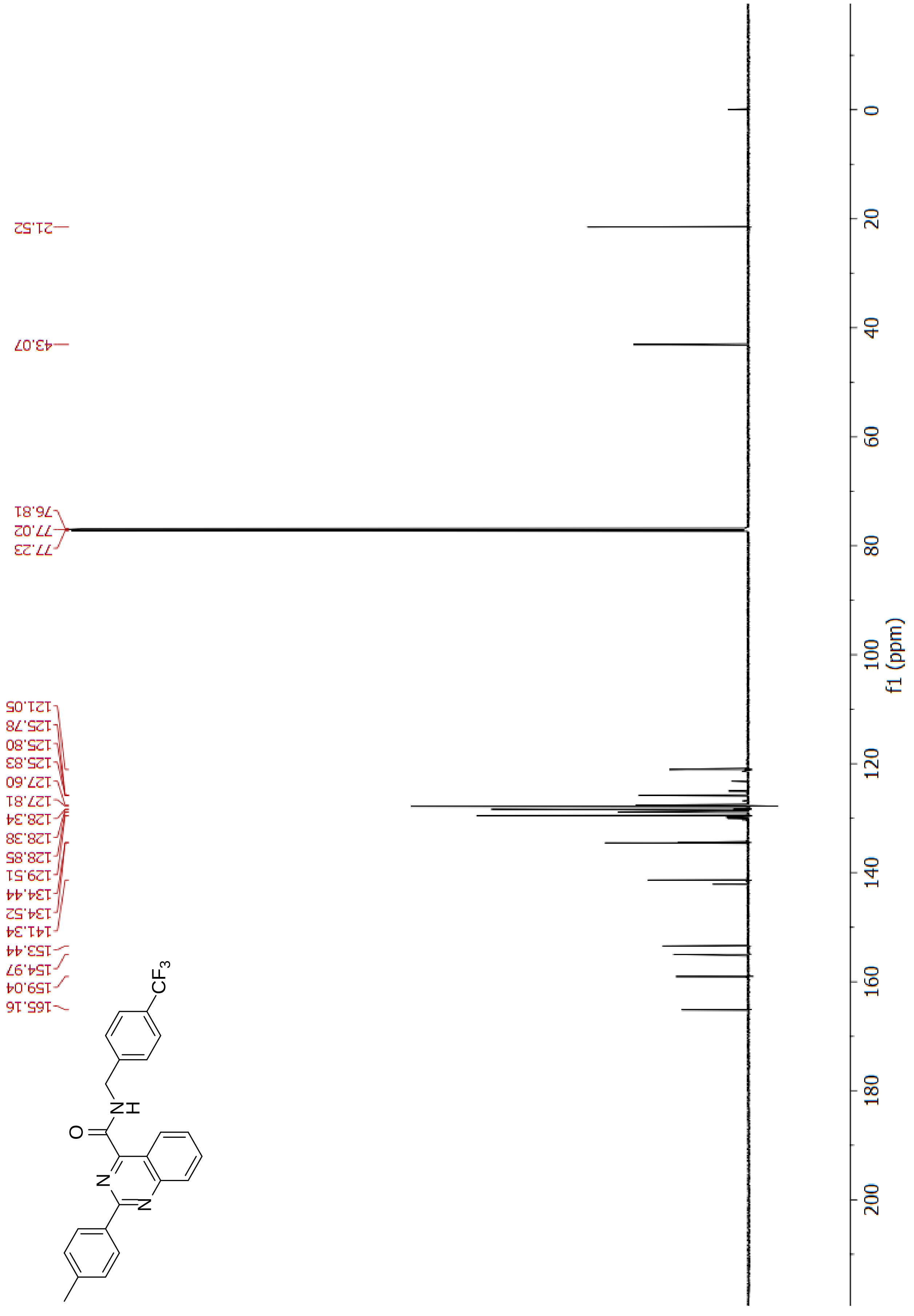
21.52
43.07
76.81
77.02
77.23
121.05
125.78
125.80
125.83
127.60
127.81
128.34
128.38
128.85
129.51
134.44
134.52
141.34
153.44
154.97
159.04
165.16
CF$_3$
NH
O
N
N
0
20
40
60
80
100
120
140
160
180
200
f1 (ppm)

HPLC trace

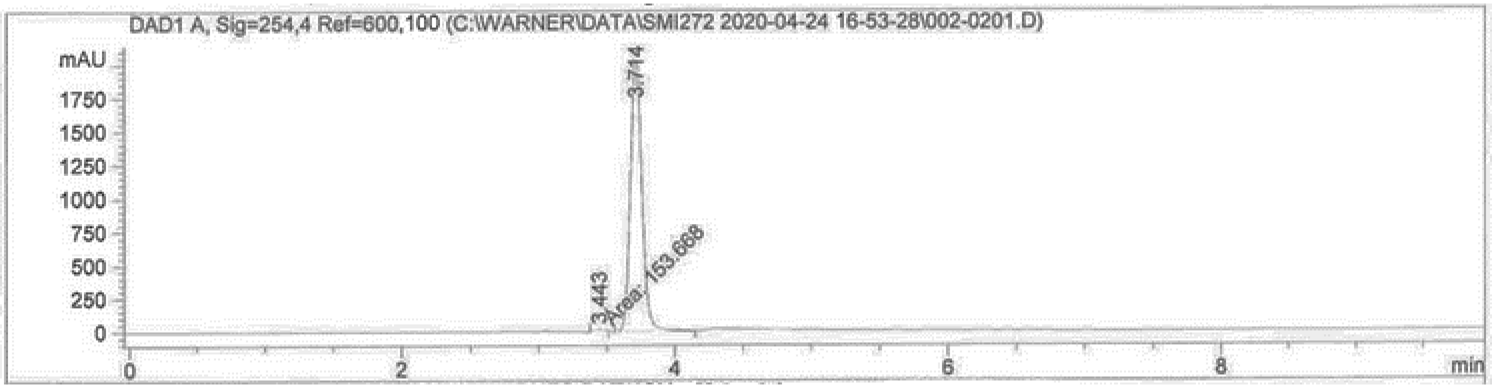

```
Signal 1: DAD1 A, Sig=254,4 Ref=600,100

Peak RetTime Type  Width     Area      Height      Area
  #   [min]        [min]   [mAU*s]     [mAU]        %
----|-------|----|-------|----------|----------|--------|
   1   3.443 MM    0.1129  153.66762   22.68455   1.2585
   2   3.714 VV    0.0928 1.20570e4  2044.42224  98.7415
```

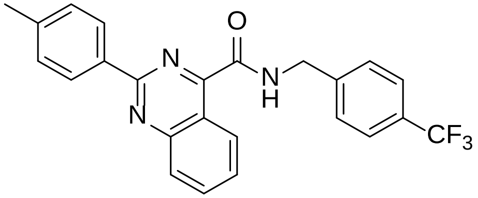

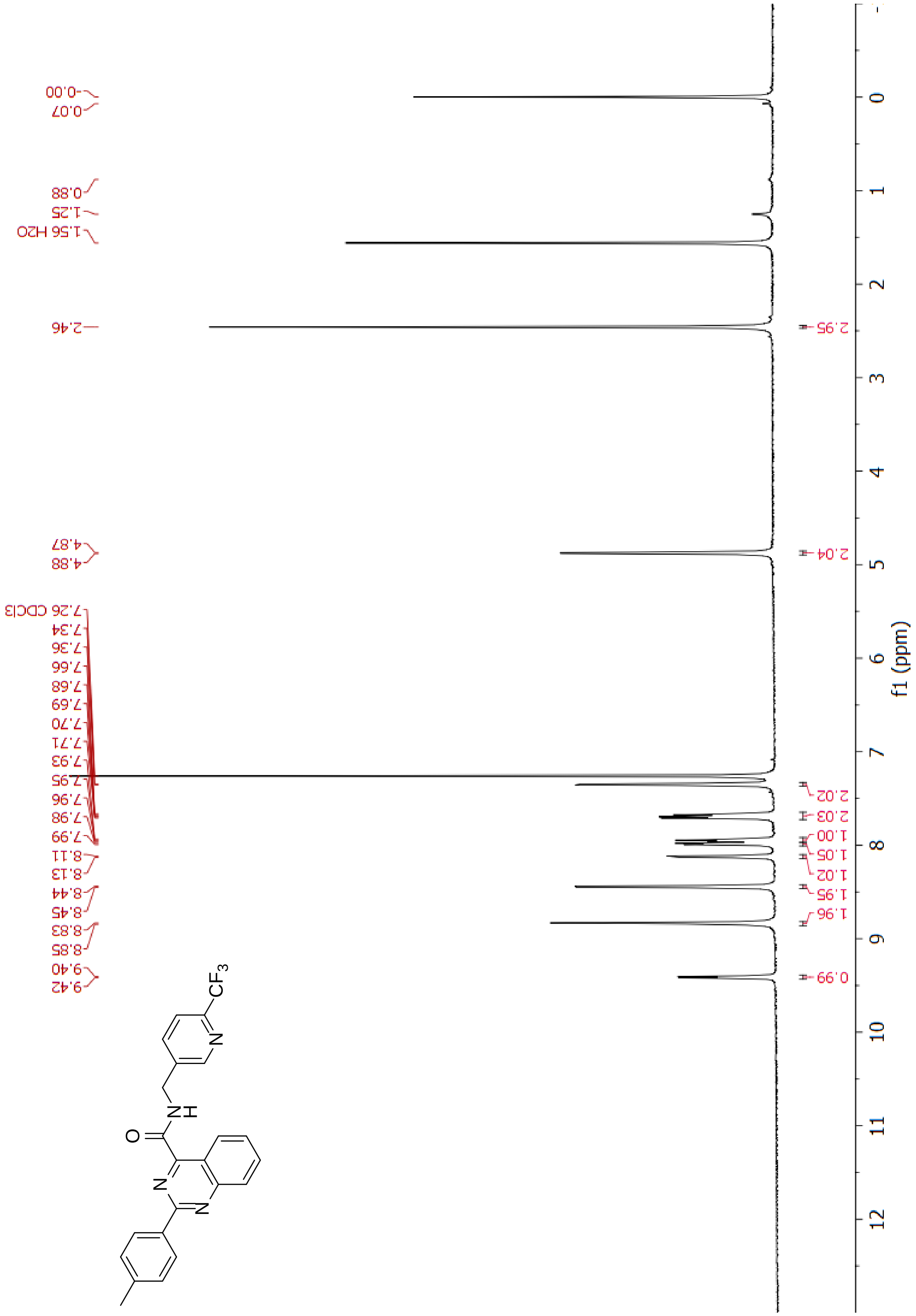
-0.00
0.07
0.88
1.25
1.56 H2O
2.46
4.87
4.88
7.26 CDCl3
7.34
7.36
7.66
7.68
7.69
7.70
7.71
7.93
7.95
7.96
7.98
7.99
8.11
8.13
8.44
8.45
8.83
8.85
9.40
9.42
2.95
2.04
2.02
2.03
1.00
1.05
1.02
1.95
1.96
0.99
0
1
2
3
4
5
6
7
8
9
10
11
12
f1 (ppm)
CF3
N
NH
O
N
N

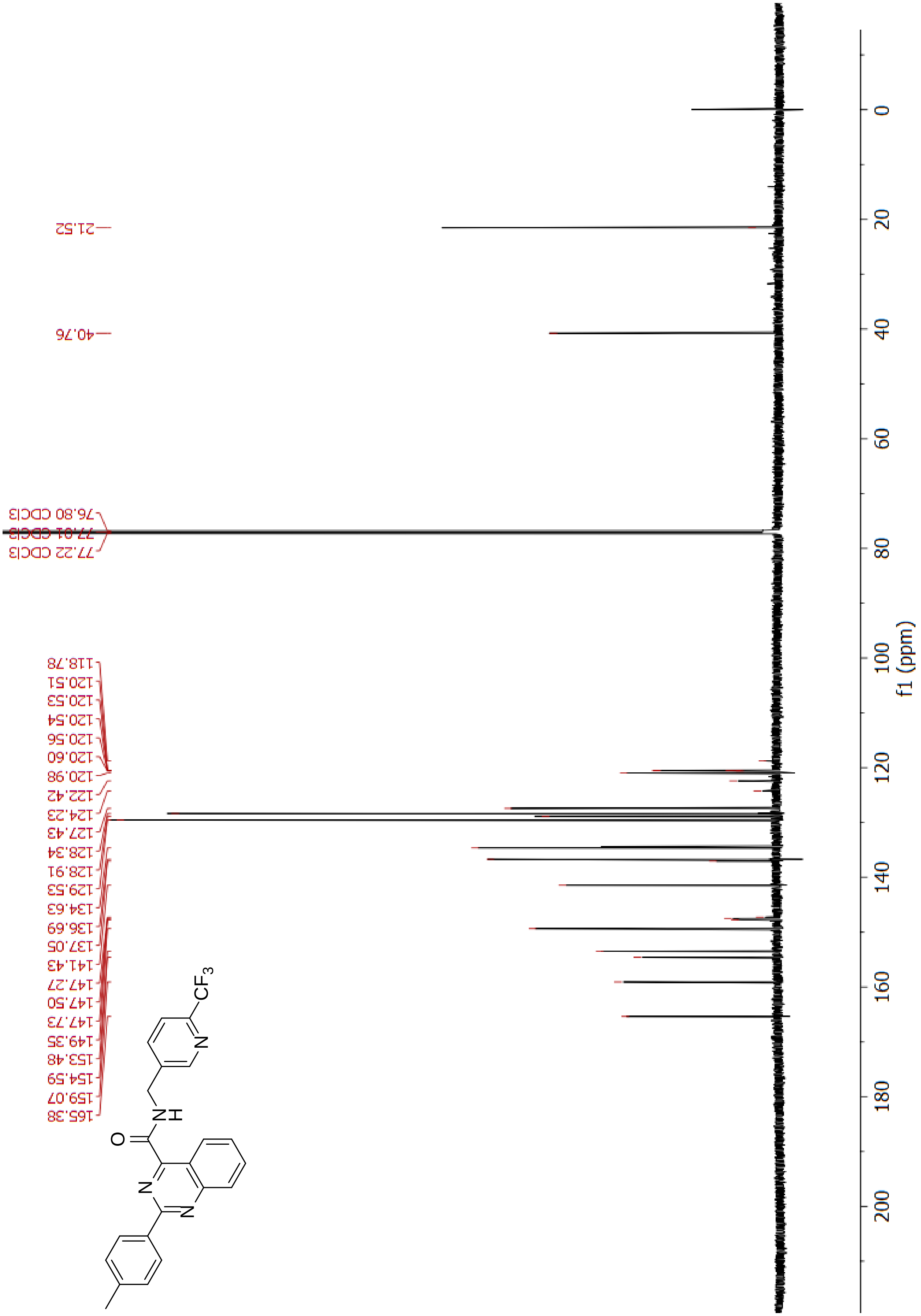
165.38
159.07
154.59
153.48
149.35
147.73
147.50
147.27
141.43
137.05
136.69
134.63
129.53
128.91
128.34
127.43
124.23
122.42
120.98
120.60
120.56
120.54
120.53
120.51
118.78
77.22 CDCl3
77.01 CDCl3
76.80 CDCl3
40.76
21.52
N
N
O
NH
N
CF3
200
180
160
140
120
100
80
60
40
20
0
f1 (ppm)

HPLC trace

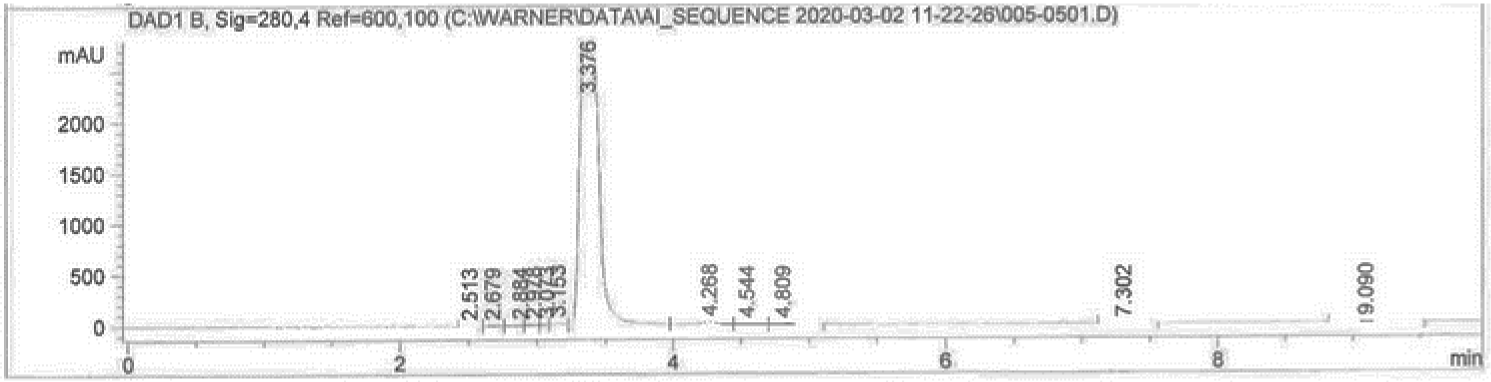

```
Signal 2: DAD1 B, Sig=280,4 Ref=600,100

Peak RetTime Type  Width     Area      Height     Area
  #   [min]        [min]   [mAU*s]     [mAU]       %
----|-------|----|-------|----------|----------|--------|
   1   2.513 BV    0.1096    9.29083    1.11113   0.0332
   2   2.679 VV    0.1111   25.07619    3.52004   0.0897
   3   2.884 VV    0.0867   37.65724    6.04615   0.1347
   4   2.978 VV    0.0750   60.98552   11.67081   0.2182
   5   3.073 VV    0.0504   51.70936   14.91808   0.1850
   6   3.153 VV    0.0945  171.90930   27.66708   0.6151
   7   3.376 VV    0.1640 2.69464e4  2664.00342  96.4209
   8   4.268 VV    0.1934  408.19623   28.11981   1.4606
   9   4.544 VV    0.1536  100.06863    9.14696   0.3581
  10   4.809 VB    0.1602   68.33813    6.02875   0.2445
  11   7.302 BB    0.1531   17.15590    1.73820   0.0614
  12   9.090 BB    0.2540   49.86438    3.09489   0.1784
```

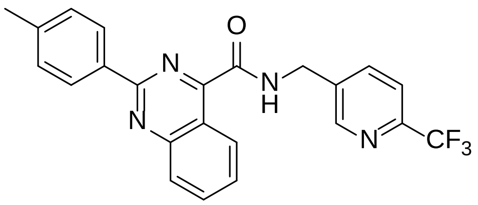

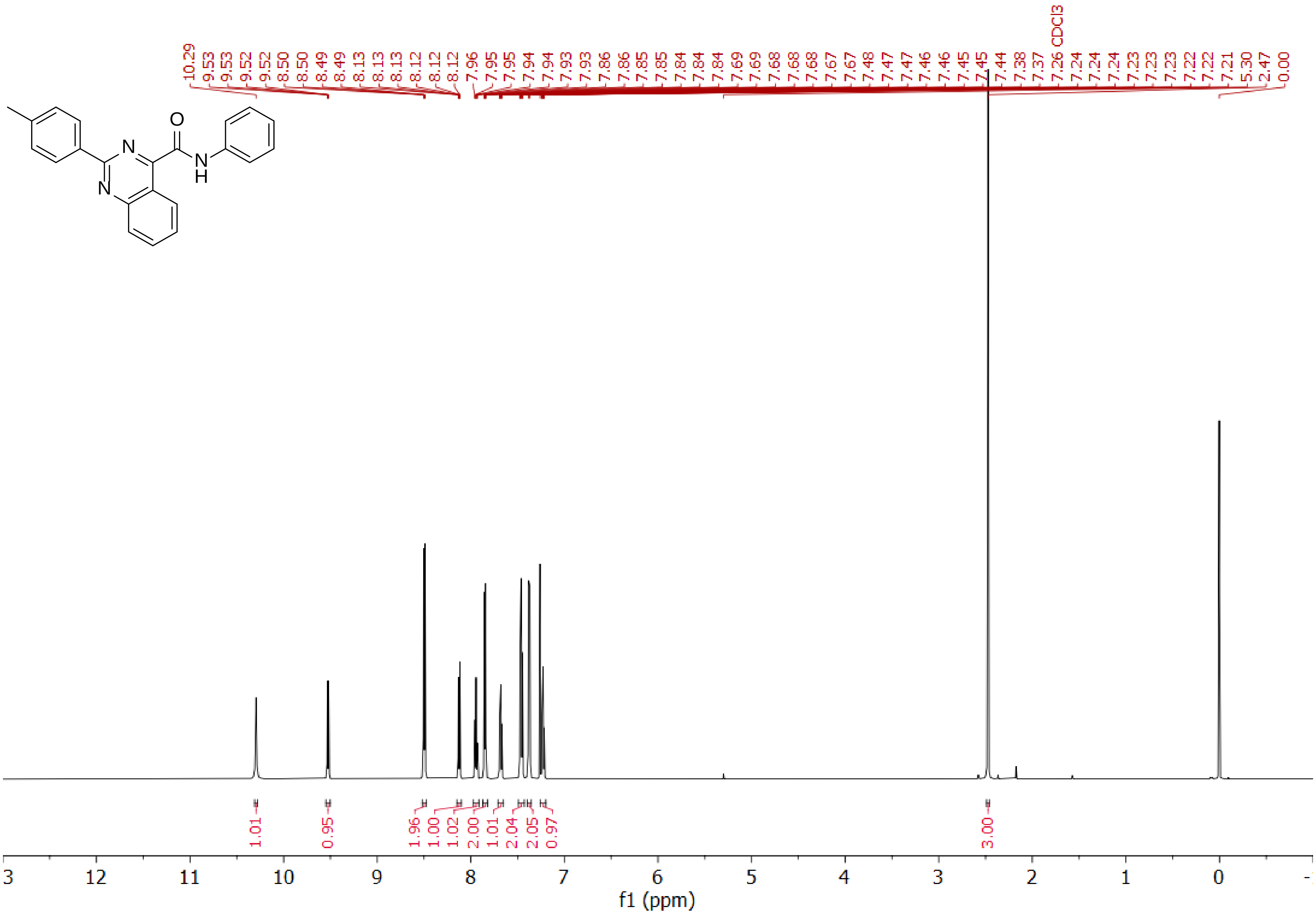
10.29
9.53
9.53
9.52
9.52
8.50
8.50
8.49
8.49
8.13
8.13
8.13
8.12
8.12
8.12
7.96
7.95
7.95
7.94
7.94
7.93
7.93
7.86
7.86
7.85
7.85
7.84
7.84
7.84
7.69
7.69
7.68
7.68
7.68
7.67
7.67
7.48
7.47
7.47
7.46
7.46
7.45
7.45
7.44
7.38
7.37
7.26 CDCl3
7.24
7.24
7.24
7.23
7.23
7.23
7.22
7.22
7.21
5.30
2.47
0.00
O
N
N
N
H
1.01
0.95
1.96
1.00
1.02
2.00
1.01
2.04
2.05
0.97
3.00
13
12
11
10
9
8
7
6
5
4
3
2
1
0
f1 (ppm)

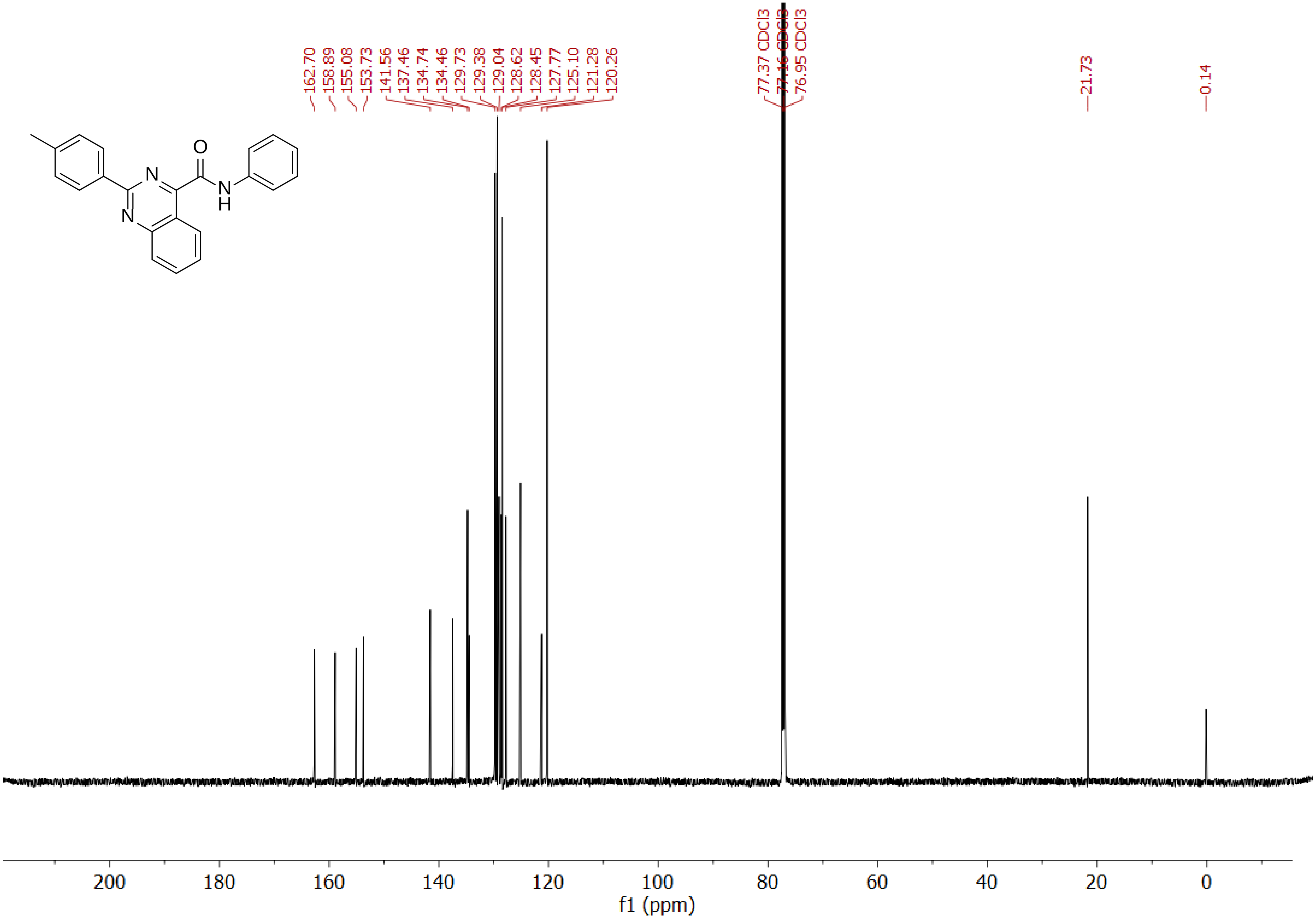
162.70
158.89
155.08
153.73
141.56
137.46
134.74
134.46
129.73
129.38
129.04
128.62
128.45
127.77
125.10
121.28
120.26
77.37 CDCl3
77.16 CDCl3
76.95 CDCl3
21.73
0.14
O
N
N
N
H
200
180
160
140
120
100
80
60
40
20
0
f1 (ppm)

HPLC trace

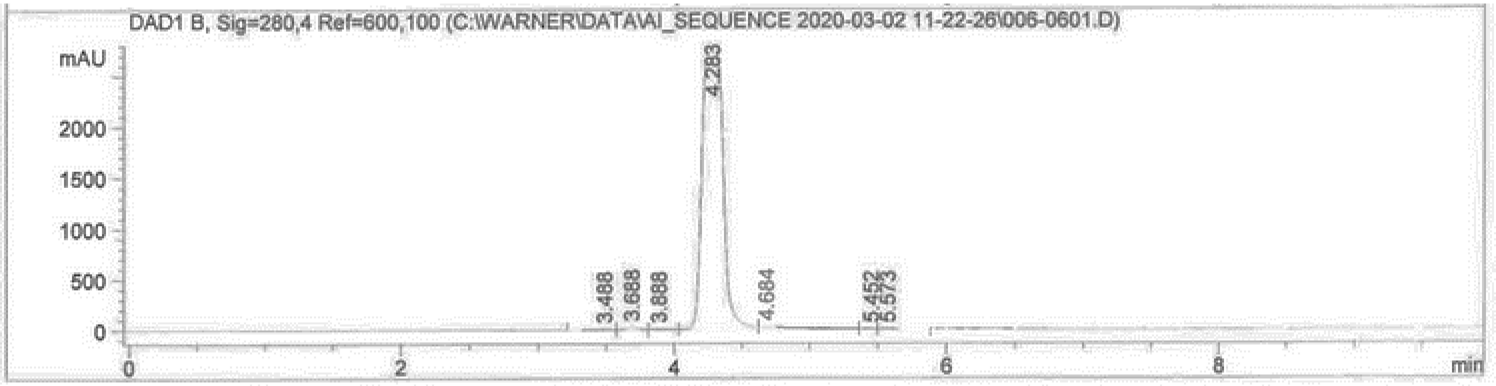

```
Signal 2: DAD1 B, Sig=280,4 Ref=600,100

Peak RetTime Type  Width     Area      Height     Area
  #   [min]        [min]   [mAU*s]     [mAU]        %
----|-------|----|-------|----------|----------|--------|
   1   3.488 BV    0.1119   44.23546    5.87328   0.1471
   2   3.688 VV    0.0927  165.80200   27.36155   0.5512
   3   3.888 VV    0.1041   32.61037    4.63492   0.1084
   4   4.283 VV    0.1776 2.92581e4  2675.36328  97.2632
   5   4.684 VV    0.2580  503.21277   25.08693   1.6728
   6   5.452 VV    0.1045   28.19864    3.89236   0.0937
   7   5.573 VB    0.1450   49.21879    4.82456   0.1636
```

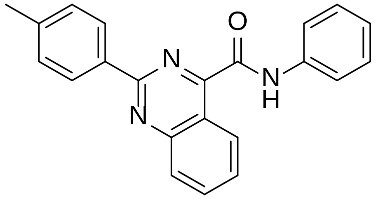

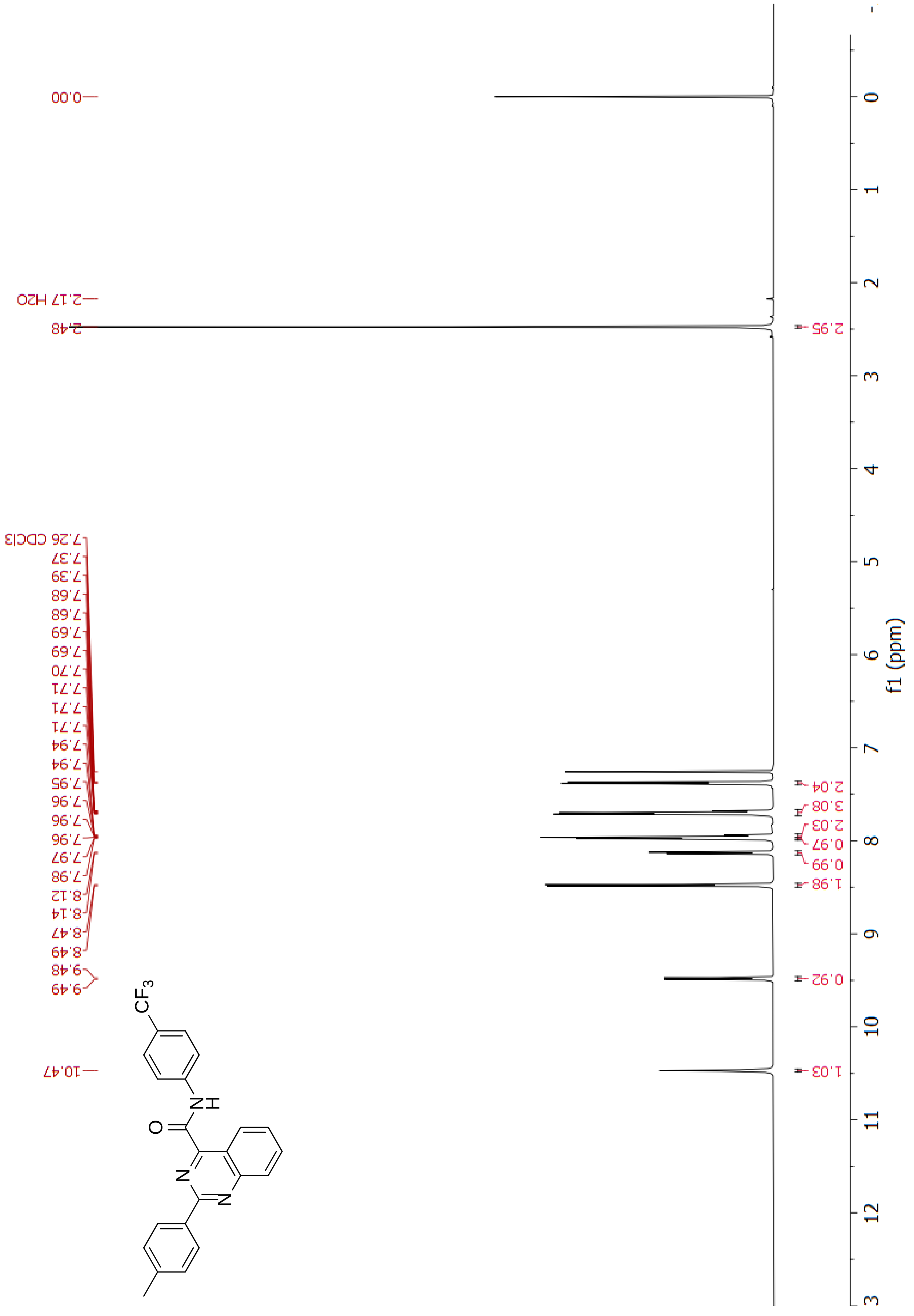
0.00
2.17 H2O
2.48
7.26 CDCl3
7.37
7.39
7.68
7.68
7.69
7.69
7.70
7.71
7.71
7.71
7.94
7.94
7.95
7.96
7.96
7.96
7.97
7.98
8.12
8.14
8.47
8.49
9.48
9.49
10.47
2.95
2.04
3.08
2.03
0.97
0.99
1.98
0.92
1.03
CF3
NH
O
N
N
0
1
2
3
4
5
6
7
8
9
10
11
12
13
f1 (ppm)

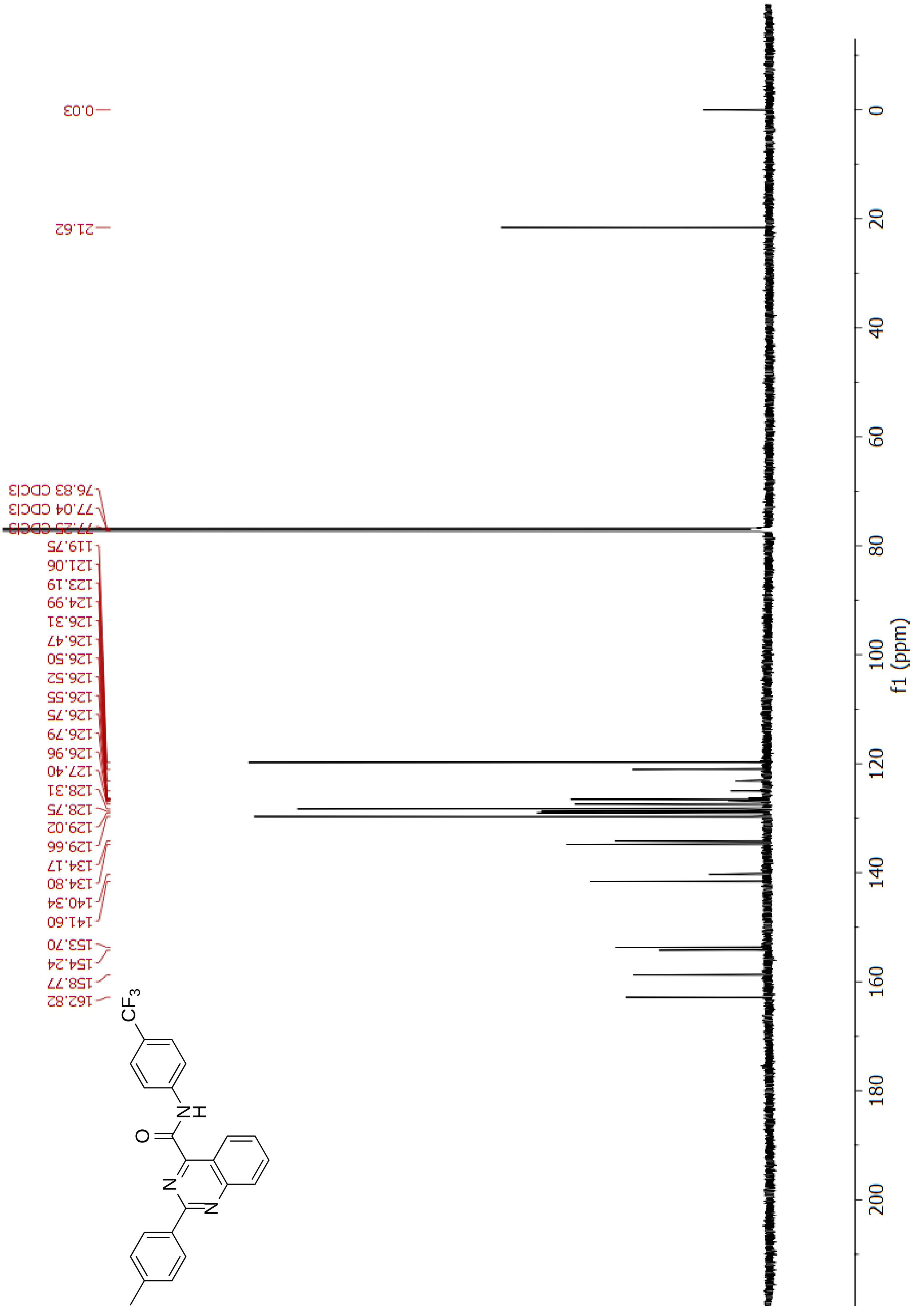

162.82
158.77
154.24
153.70
141.60
140.34
134.80
134.17
129.66
129.02
128.75
128.31
127.40
126.96
126.79
126.75
126.55
126.52
126.50
126.47
126.31
124.99
123.19
121.06
119.75
77.25 CDCl3
77.04 CDCl3
76.83 CDCl3
21.62
0.03
CF3
NH
O
N
N
f1 (ppm)
0
20
40
60
80
100
120
140
160
180
200

HPLC trace

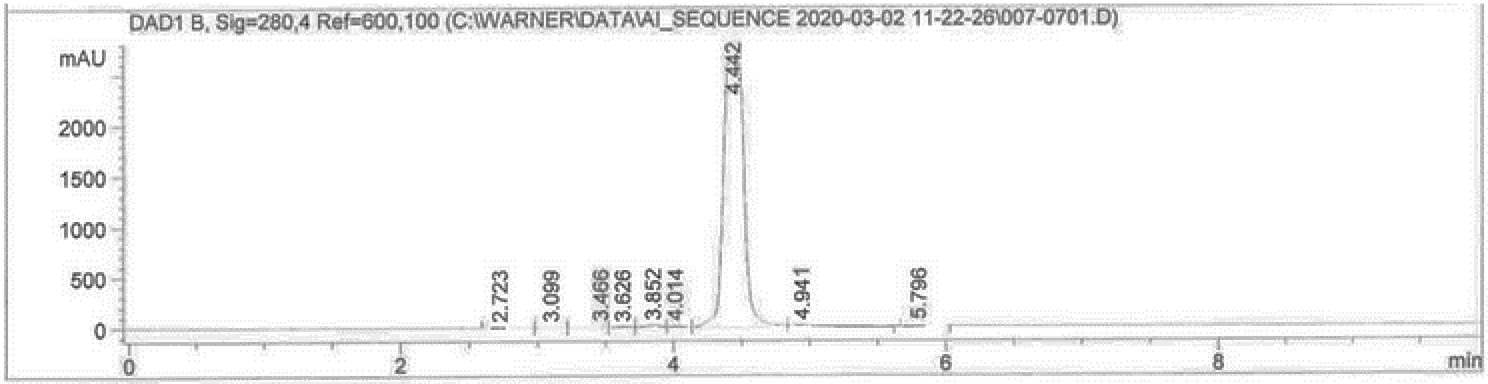

```
Signal 2: DAD1 B, Sig=280,4 Ref=600,100

Peak RetTime Type  Width     Area      Height     Area
  #   [min]        [min]   [mAU*s]     [mAU]        %
----|-------|----|-------|----------|----------|--------|
   1   2.723 BB    0.1683   32.32194    2.89448   0.1138
   2   3.099 BV    0.1508   14.79295    1.26195   0.0521
   3   3.466 VV    0.1738   20.13363    1.50805   0.0709
   4   3.626 VV    0.0991   44.39602    6.71671   0.1563
   5   3.852 VV    0.1086  134.98915   19.06548   0.4752
   6   4.014 VV    0.0904   35.79494    5.76877   0.1260
   7   4.442 VV    0.1669 2.77216e4  2674.85449  97.5831
   8   4.941 VB    0.2633  361.11627   17.75352   1.2712
   9   5.796 BB    0.1641   43.05820    3.69195   0.1516
```

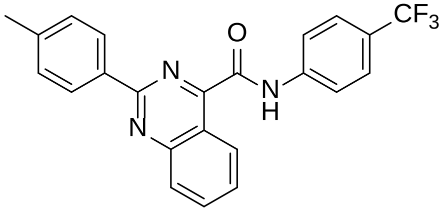

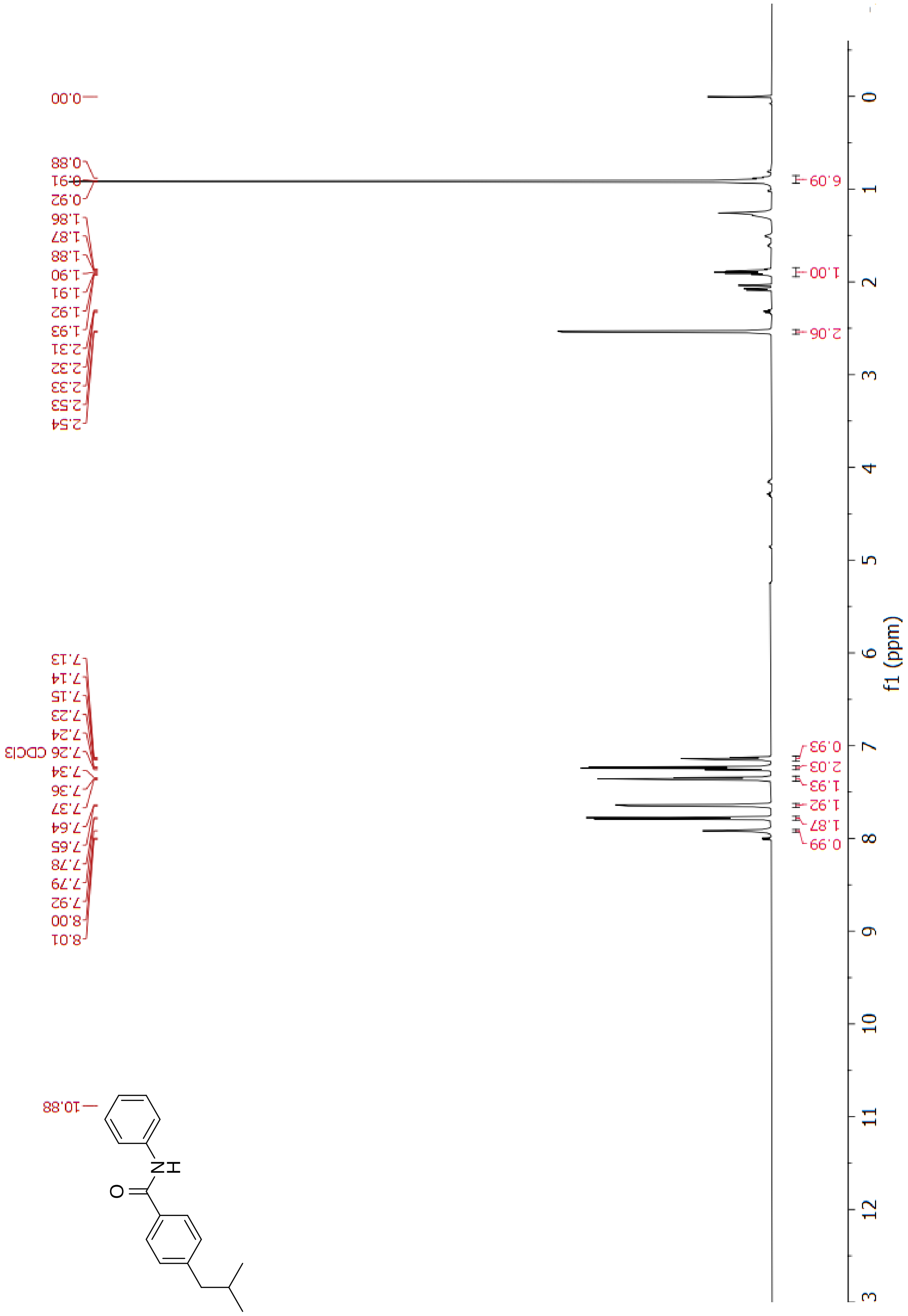
0.00
0.88
0.91
0.92
1.86
1.87
1.88
1.90
1.91
1.92
1.93
2.31
2.32
2.33
2.53
2.54
7.13
7.14
7.15
7.23
7.24
7.26 CDCl3
7.34
7.36
7.37
7.64
7.65
7.78
7.79
7.92
8.00
8.01
10.88
6.09
1.00
2.06
0.93
2.03
1.93
1.92
1.87
0.99
f1 (ppm)
H
N
O

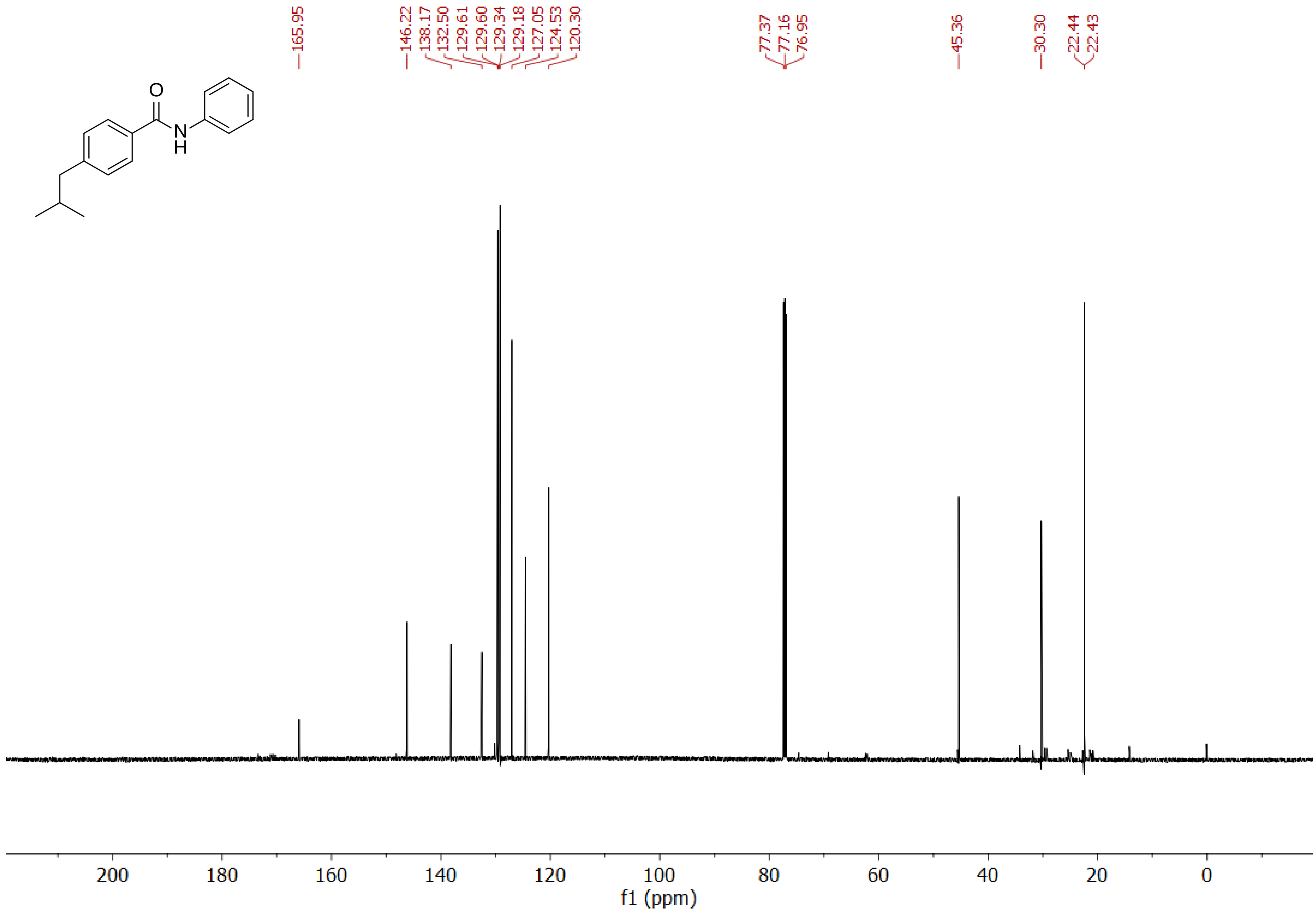

165.95
146.22
138.17
132.50
129.61
129.60
129.34
129.18
127.05
124.53
120.30
77.37
77.16
76.95
45.36
30.30
22.44
22.43
O
N
H
200
180
160
140
120
100
80
60
40
20
0
f1 (ppm)

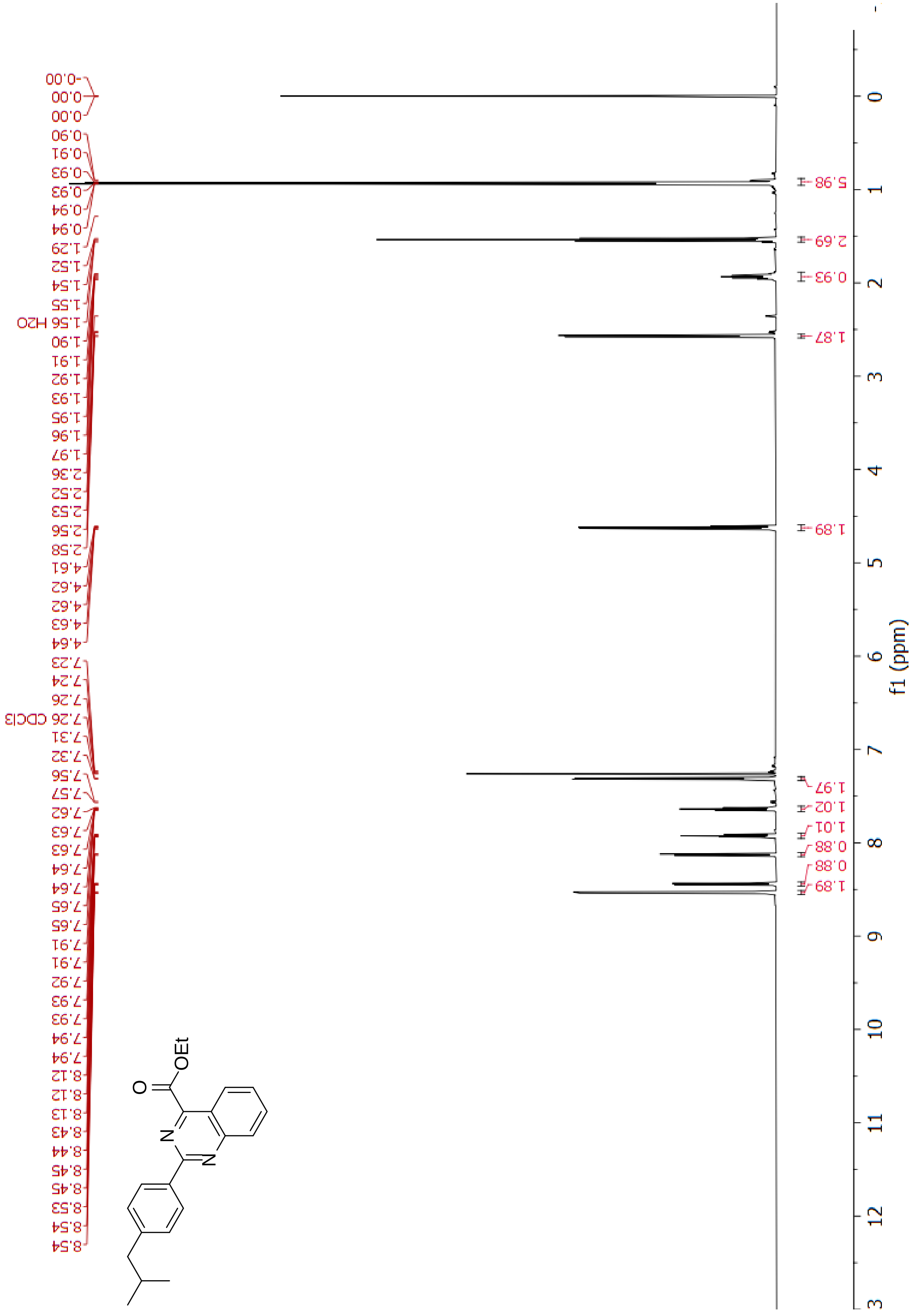
-0.00
0.00
0.00
0.90
0.91
0.93
0.93
0.94
0.94
1.29
1.52
1.54
1.55
1.56 H2O
1.90
1.91
1.92
1.93
1.95
1.96
1.97
2.36
2.52
2.53
2.56
2.58
4.61
4.62
4.62
4.63
4.64
7.23
7.24
7.26
7.26 CDCl3
7.31
7.32
7.56
7.57
7.62
7.63
7.63
7.64
7.64
7.65
7.65
7.91
7.91
7.92
7.93
7.93
7.94
7.94
8.12
8.12
8.13
8.43
8.44
8.45
8.45
8.53
8.54
8.54
5.98
2.69
0.93
1.87
1.89
1.97
1.02
1.01
0.88
0.88
1.89
0
1
2
3
4
5
6
7
8
9
10
11
12
13
f1 (ppm)
O
OEt
N
N

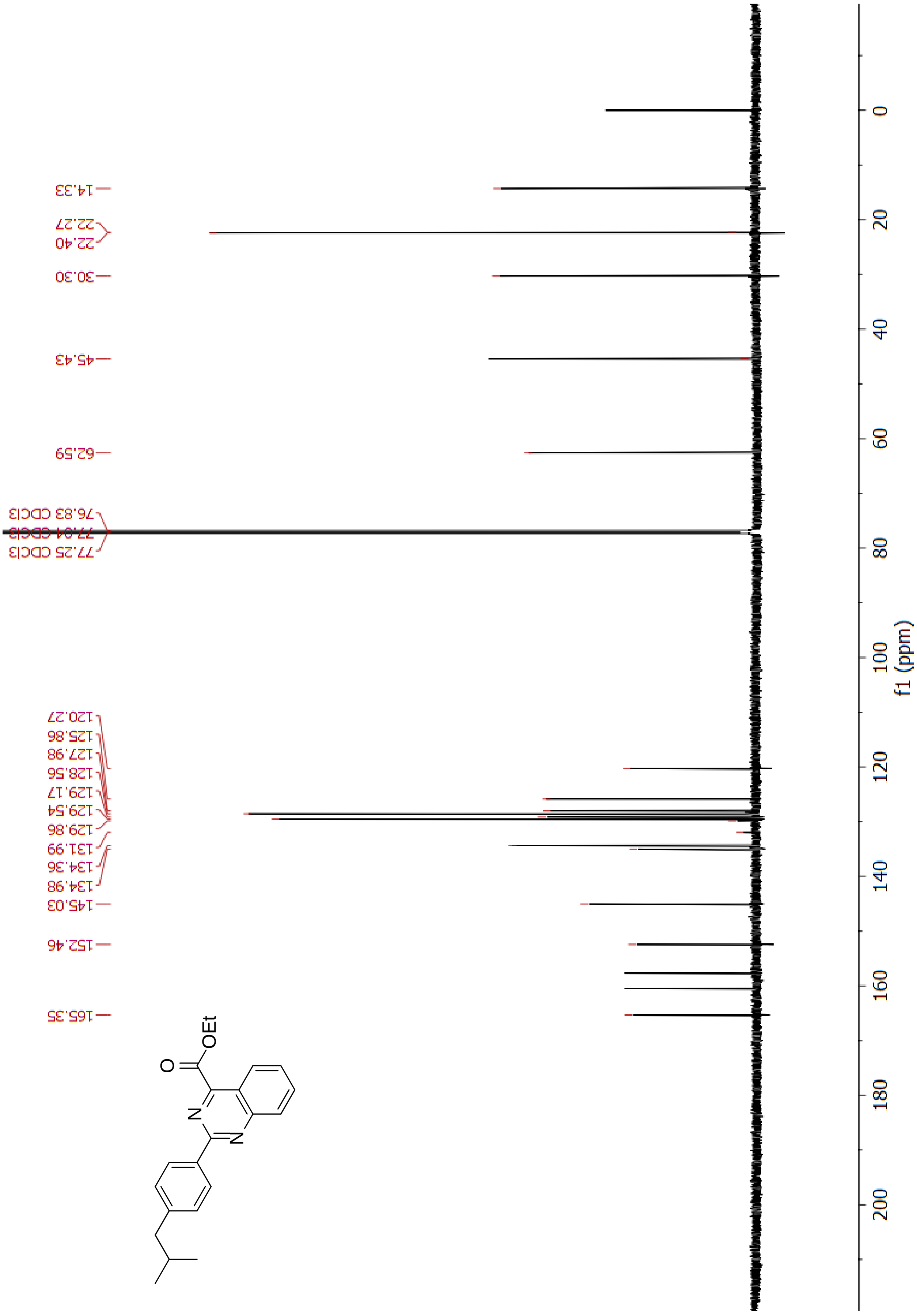
14.33
22.27
22.40
30.30
45.43
62.59
76.83 CDCl3
77.04 CDCl3
77.25 CDCl3
120.27
125.86
127.98
128.56
129.17
129.54
129.86
131.99
134.36
134.98
145.03
152.46
165.35
O
OEt
N
N
0
20
40
60
80
100
120
140
160
180
200
f1 (ppm)

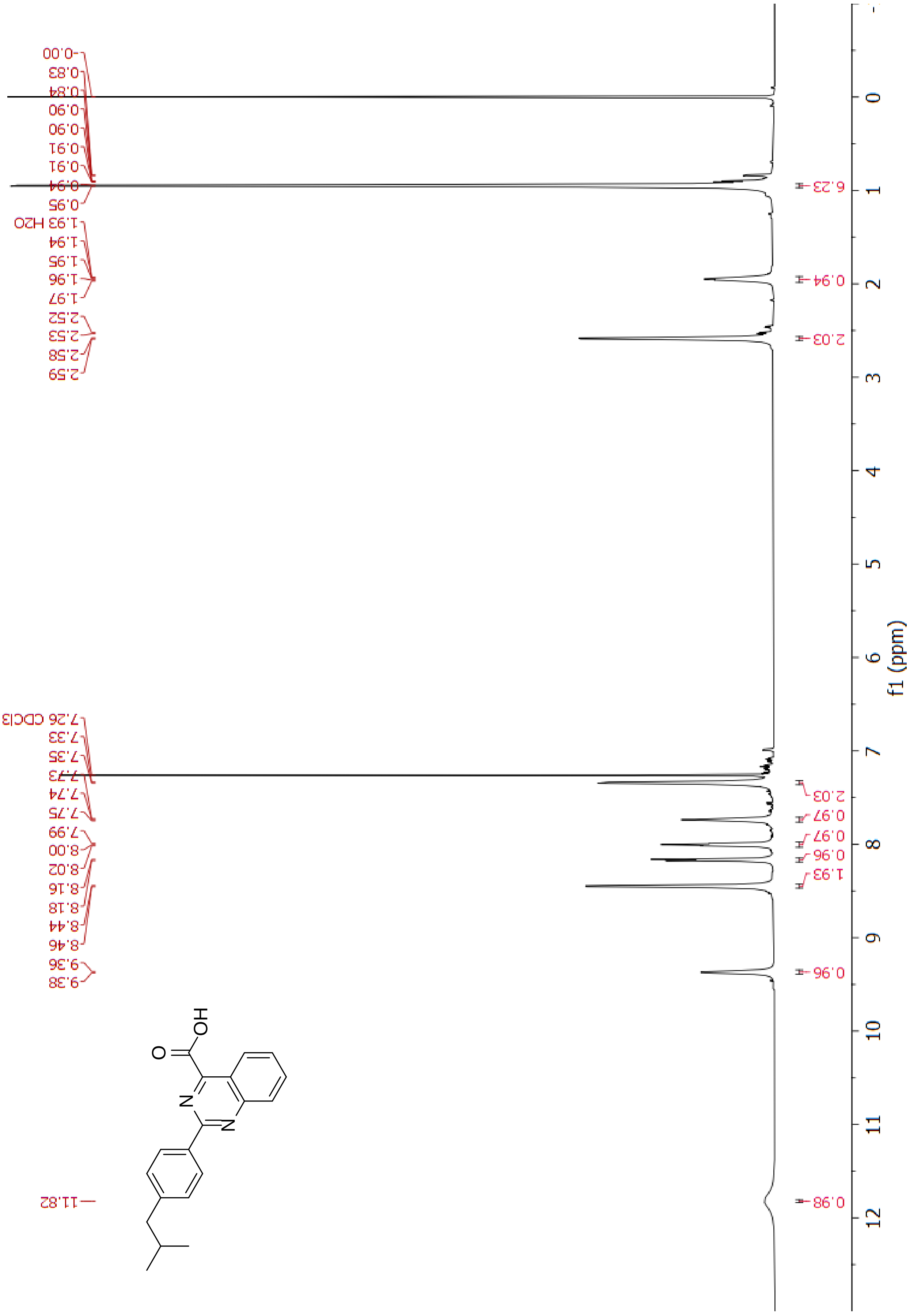
-0.00
0.83
0.84
0.90
0.90
0.91
0.91
0.94
0.95
1.93 H2O
1.94
1.95
1.96
1.97
2.52
2.53
2.58
2.59
7.26 CDCl3
7.33
7.35
7.73
7.74
7.75
7.99
8.00
8.02
8.16
8.18
8.44
8.46
9.36
9.38
11.82
6.23
0.94
2.03
2.03
0.97
0.97
0.96
1.93
0.96
0.98
HO
O
N
N
0
1
2
3
4
5
6
7
8
9
10
11
12
f1 (ppm)

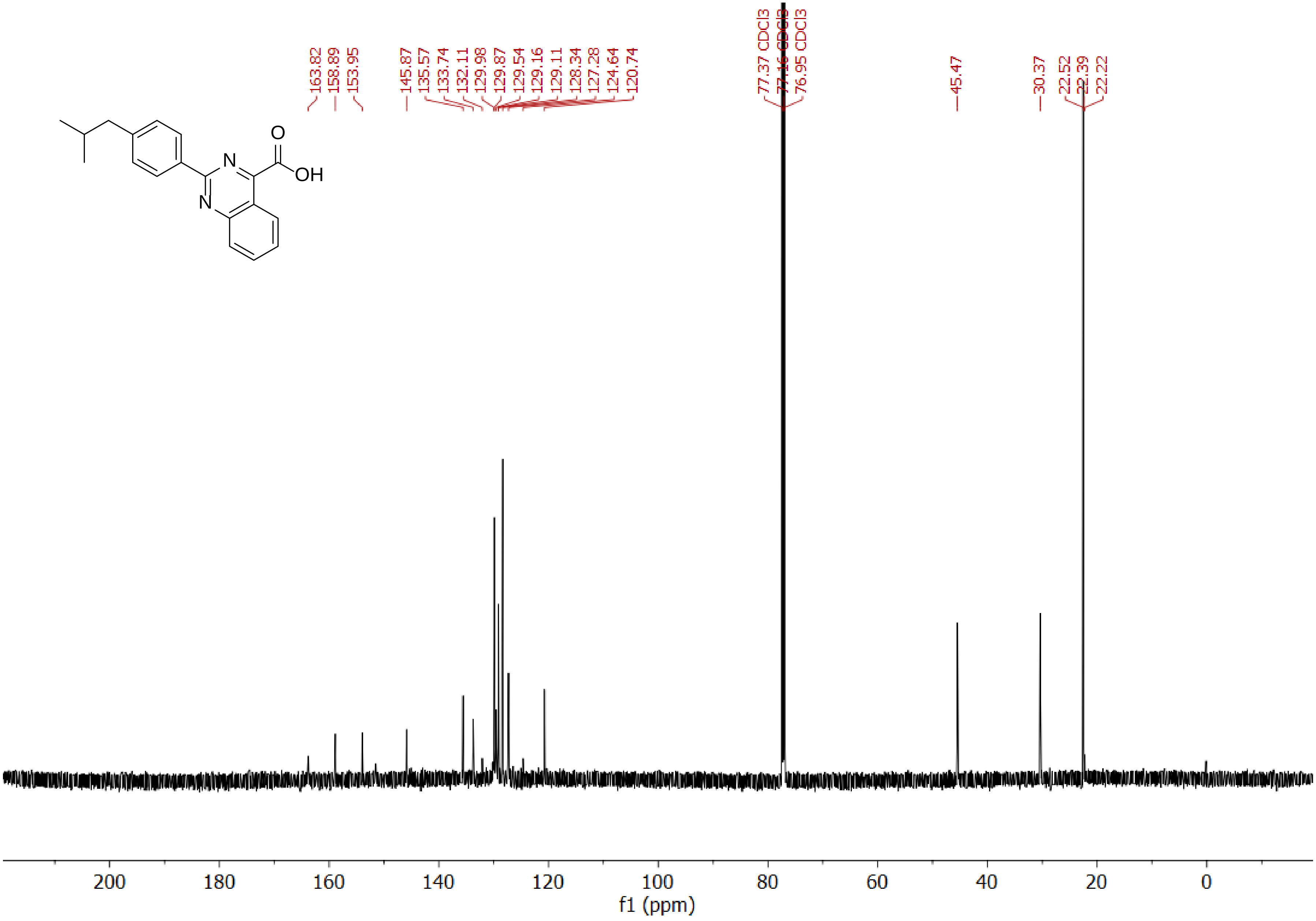
163.82
158.89
153.95
145.87
135.57
133.74
132.11
129.98
129.87
129.54
129.16
129.11
128.34
127.28
124.64
120.74
77.37 CDCl3
77.16 CDCl3
76.95 CDCl3
45.47
30.37
22.52
22.39
22.22
N
N
O
OH
200
180
160
140
120
100
80
60
40
20
0
f1 (ppm)

HPLC trace

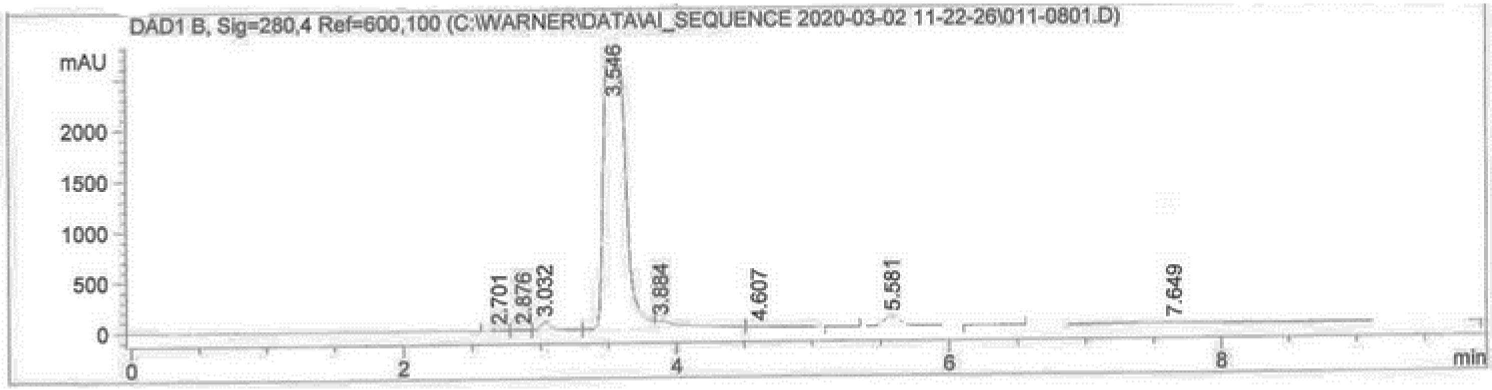

```
Signal 2: DAD1 B, Sig=280,4 Ref=600,100

Peak RetTime Type  Width     Area      Height     Area
  #   [min]        [min]   [mAU*s]     [mAU]        %
----|-------|----|-------|----------|----------|--------|
   1   2.701 BV    0.0989   15.23802    2.65927   0.0444
   2   2.876 VV    0.0932   44.80727    7.13925   0.1306
   3   3.032 VV    0.0846  470.15094   79.96114   1.3700
   4   3.546 VV    0.1855 3.05843e4  2672.19629  89.1237
   5   3.884 VV    0.2142 1193.54944   74.78367   3.4780
   6   4.607 VB    0.2105  173.29723   11.07894   0.5050
   7   5.581 BB    0.1256  805.50928   96.33119   2.3473
   8   7.649 BBA   0.9887 1029.81091   12.85347   3.0009
```

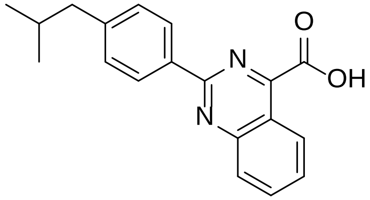

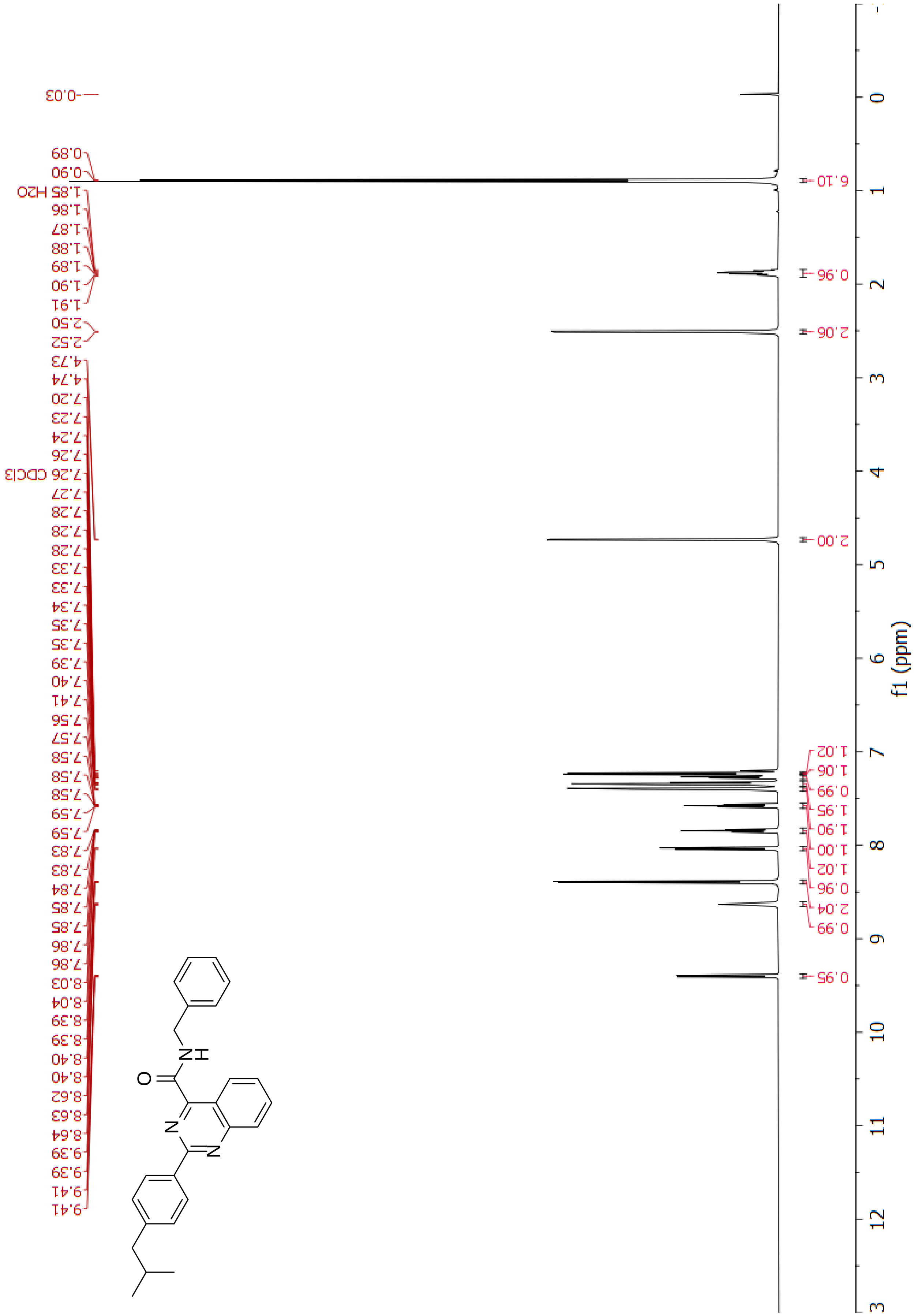
-0.03
0.89
0.90
1.85 H2O
1.86
1.87
1.88
1.89
1.90
1.91
2.50
2.52
4.73
4.74
7.20
7.23
7.24
7.26
7.26 CDCl3
7.27
7.28
7.28
7.28
7.33
7.33
7.34
7.35
7.35
7.39
7.40
7.41
7.56
7.57
7.58
7.58
7.58
7.58
7.59
7.59
7.83
7.83
7.84
7.85
7.85
7.86
7.86
8.03
8.04
8.39
8.39
8.40
8.40
8.62
8.63
8.64
9.39
9.39
9.41
9.41
6.10
0.96
2.06
2.00
1.02
1.06
0.99
1.95
1.90
1.00
1.02
0.96
2.04
0.99
0.95
0
1
2
3
4
5
6
7
8
9
10
11
12
f1 (ppm)
H
N
O
N
N

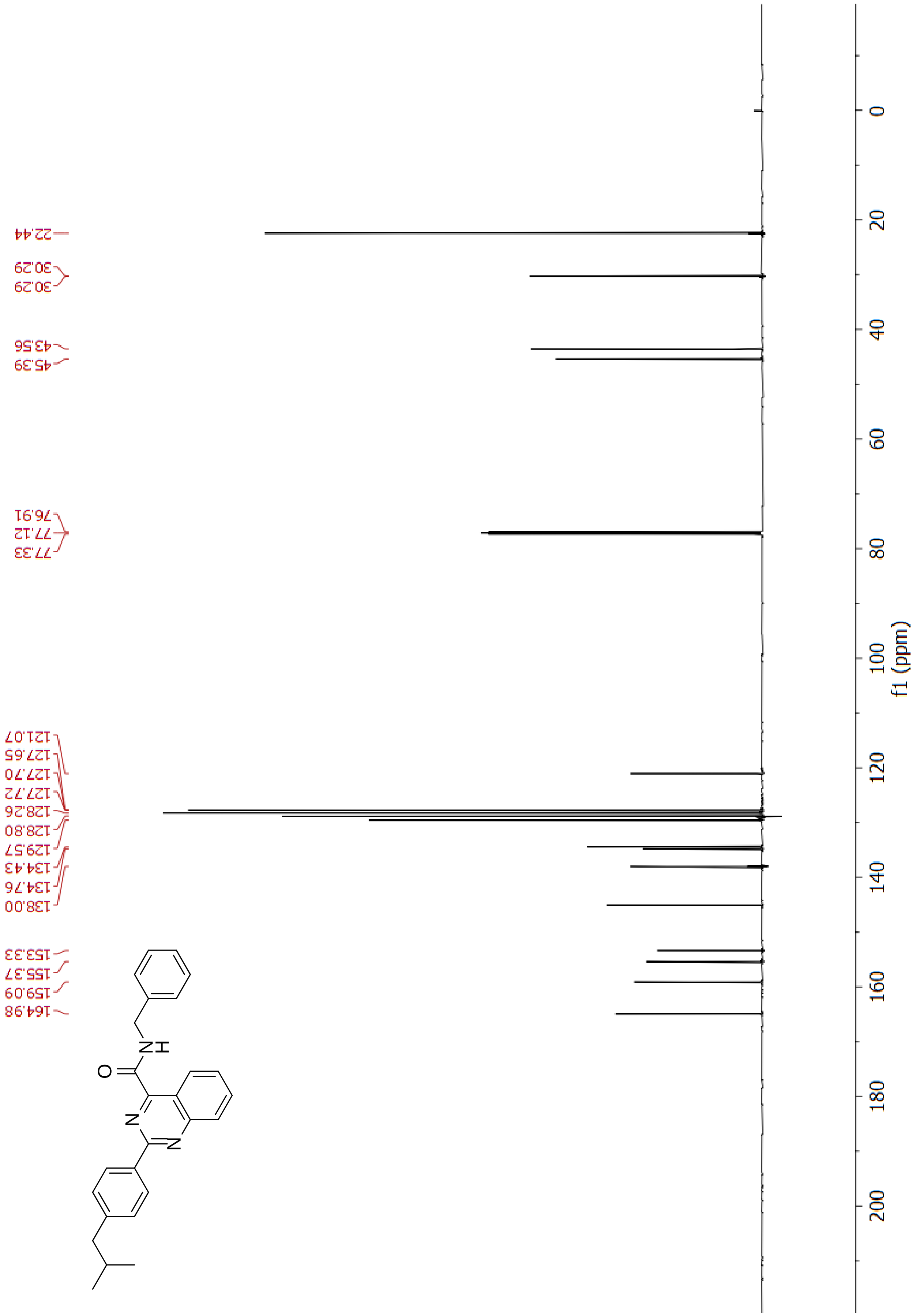
22.44
30.29
30.29
43.56
45.39
76.91
77.12
77.33
121.07
127.65
127.70
127.72
128.26
128.80
129.57
134.43
134.76
138.00
153.33
155.37
159.09
164.98
O
NH
N
N
0
20
40
60
80
100
120
140
160
180
200
f1 (ppm)

HPLC trace

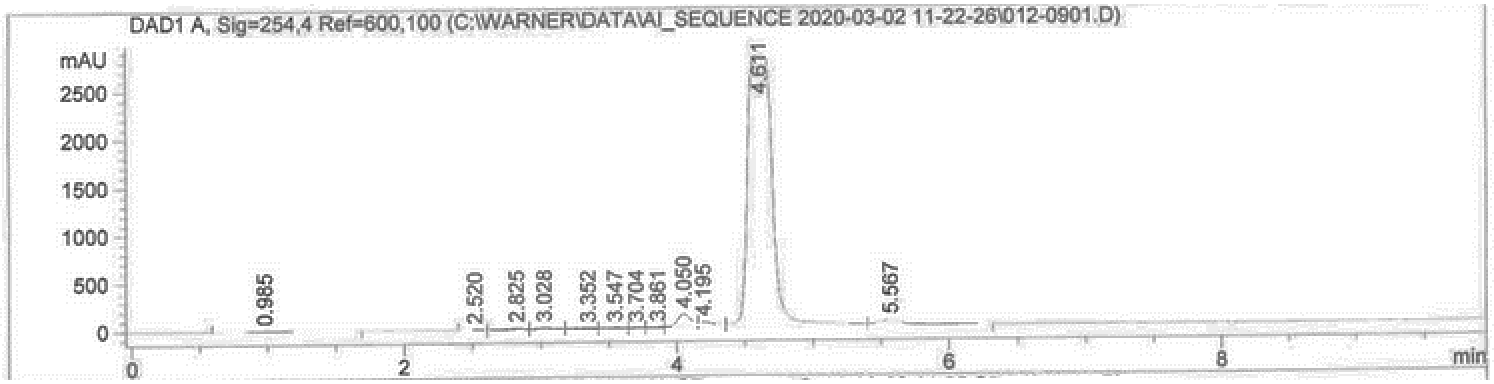

```
Peak RetTime Type  Width     Area      Height     Area
  #   [min]        [min]   [mAU*s]     [mAU]       %
----|-------|----|-------|----------|----------|--------|
  11   4.611 VV    0.2002 3.54515e4 2828.81567 93.0266
  12   5.567 VB    0.1690  628.89630   52.03146  1.6503
```

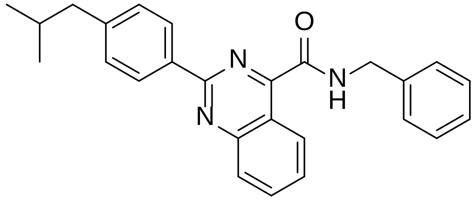

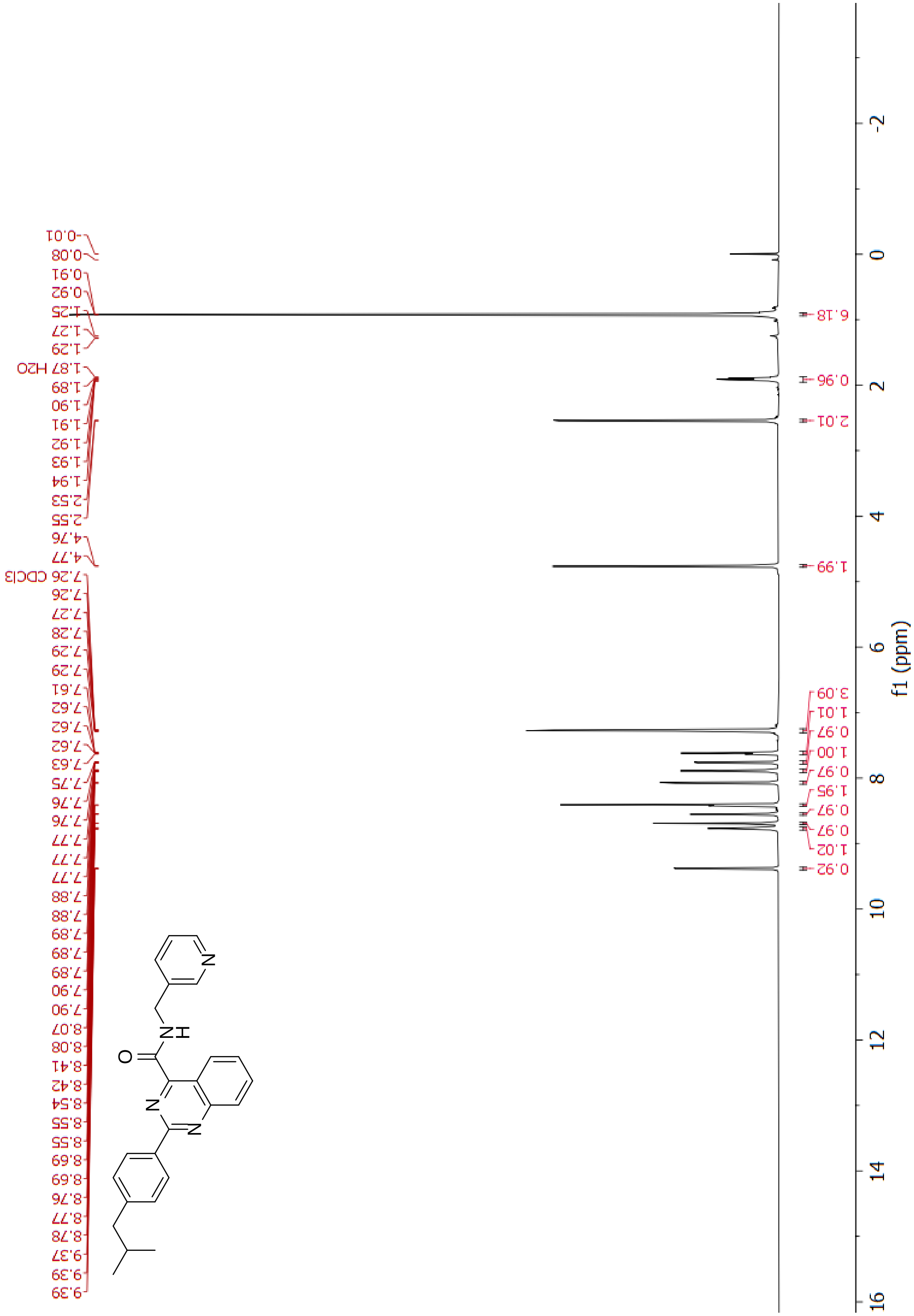
-0.01
0.08
0.91
0.92
1.25
1.27
1.29
1.87 H2O
1.89
1.90
1.91
1.92
1.93
1.94
2.53
2.55
4.76
4.77
7.26 CDCl3
7.26
7.27
7.28
7.29
7.29
7.61
7.62
7.62
7.62
7.63
7.75
7.76
7.76
7.77
7.77
7.77
7.88
7.88
7.89
7.89
7.89
7.90
7.90
8.07
8.08
8.41
8.42
8.54
8.55
8.55
8.69
8.69
8.76
8.77
8.78
9.37
9.39
9.39
6.18
0.96
2.01
1.99
3.09
1.01
0.97
1.00
0.97
1.95
0.97
0.97
1.02
0.92
N
NH
O
N
N
-2
0
2
4
6
8
10
12
14
16
f1 (ppm)

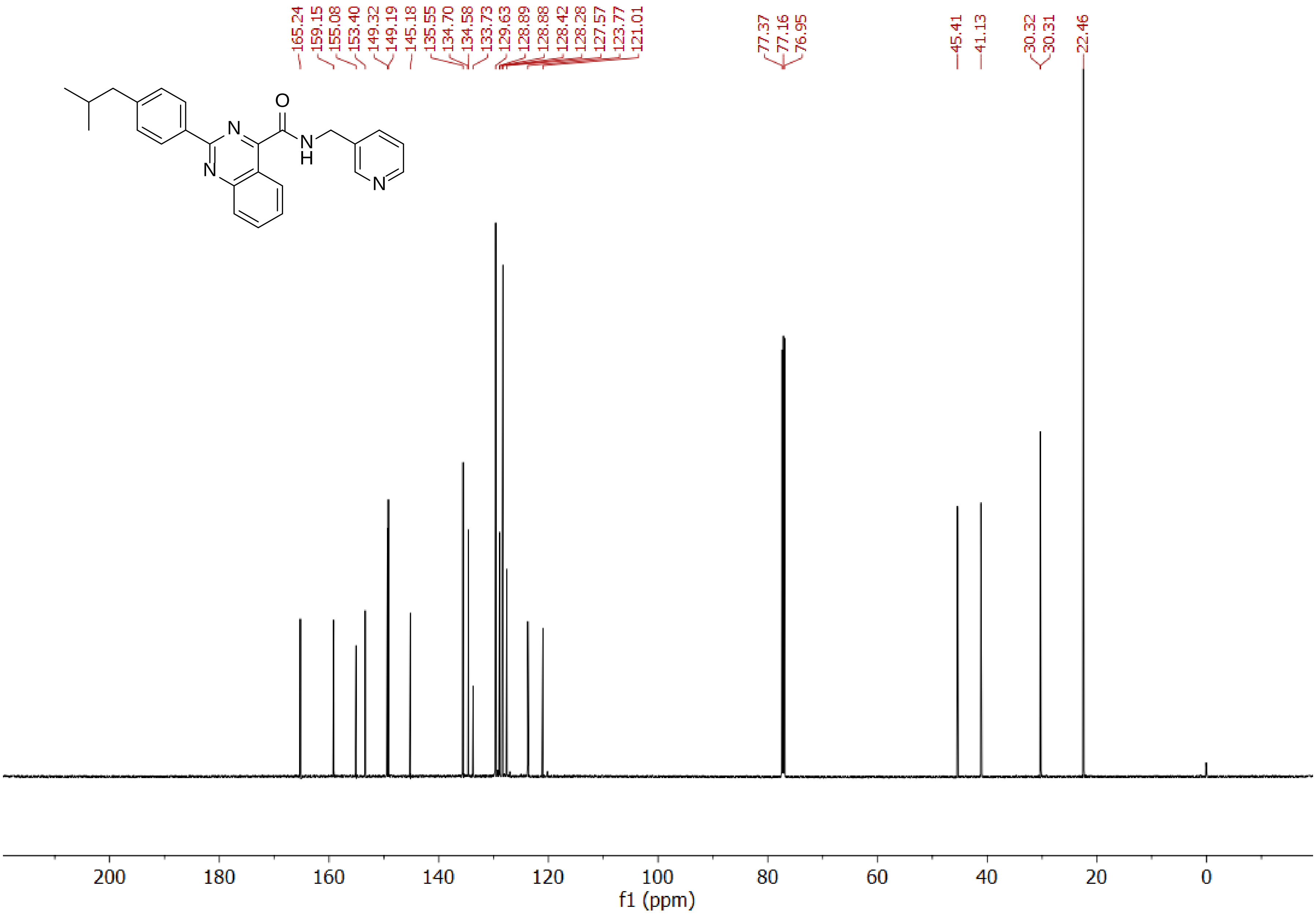
165.24
159.15
155.08
153.40
149.32
149.19
145.18
135.55
134.70
134.58
133.73
129.63
128.89
128.88
128.42
128.28
127.57
123.77
121.01
77.37
77.16
76.95
45.41
41.13
30.32
30.31
22.46
O
N
N
N
H
N
200
180
160
140
120
100
80
60
40
20
0
f1 (ppm)

HPLC trace

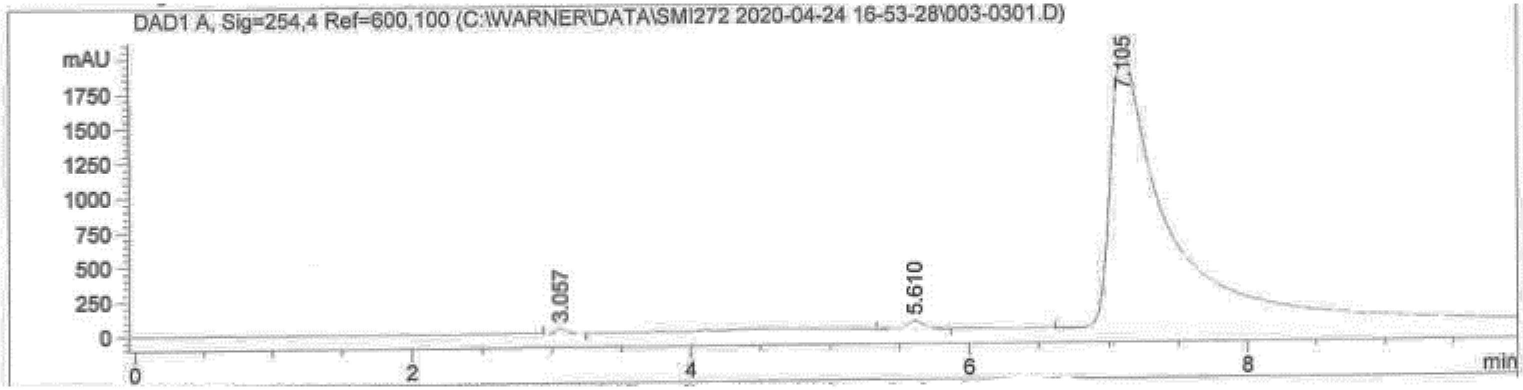

```
Signal 1: DAD1 A, Sig=254,4 Ref=600,100

Peak RetTime Type  Width     Area      Height     Area
  #   [min]        [min]   [mAU*s]     [mAU]        %
----|-------|----|-------|----------|----------|--------|
   1   3.057 VB    0.0824  198.77242   36.02428   0.3149
   2   5.610 VV    0.1512  668.36029   63.29657   1.0587
   3   7.105 VBA   0.4161 6.22618e4  2006.10828  98.6264
```

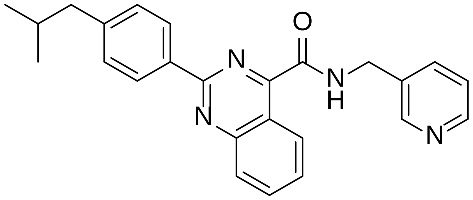

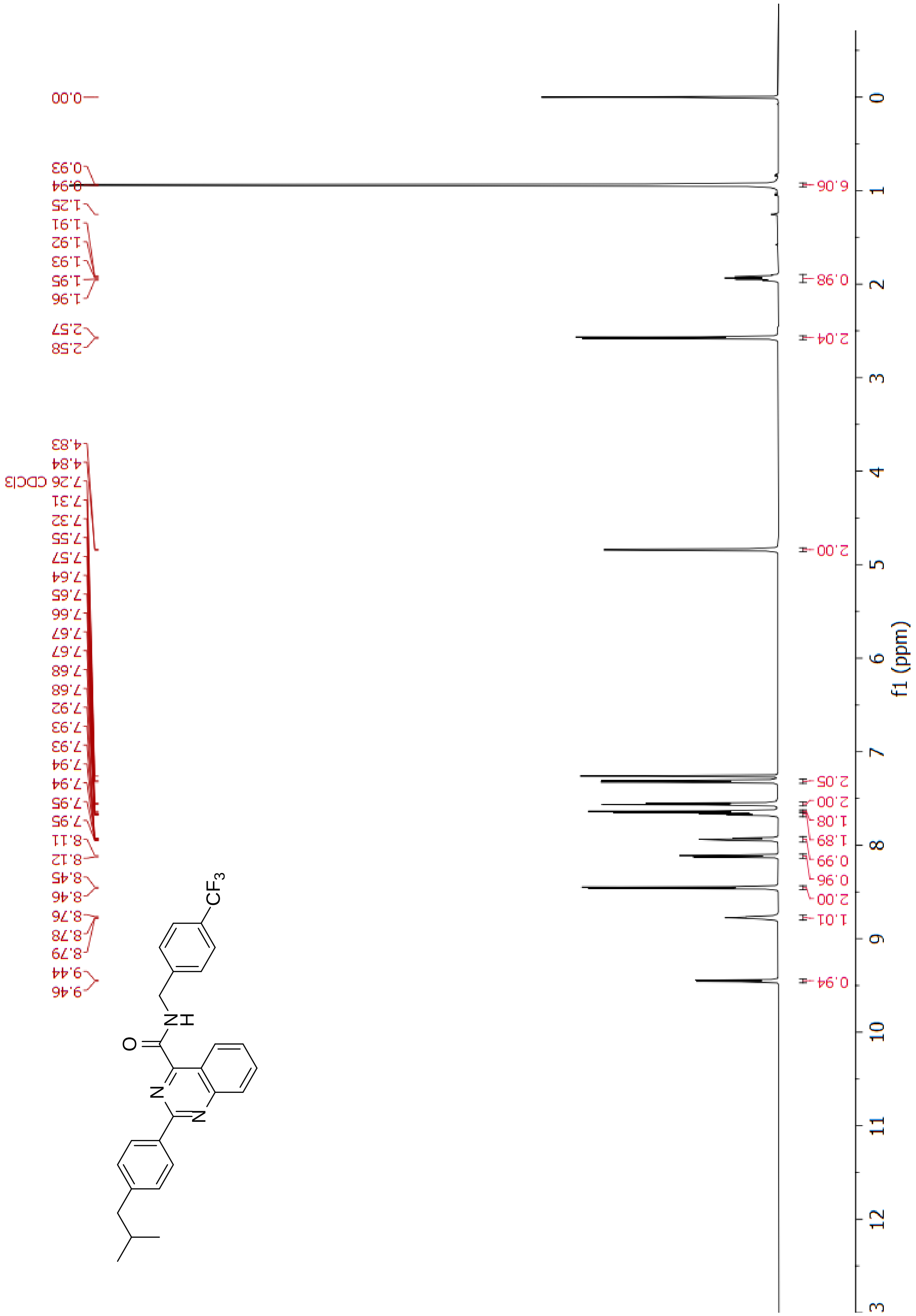

0.00
0.93
0.94
1.25
1.91
1.92
1.93
1.95
1.96
2.57
2.58
4.83
4.84
7.26 CDCl3
7.31
7.32
7.55
7.57
7.64
7.65
7.66
7.67
7.67
7.68
7.68
7.92
7.93
7.93
7.94
7.94
7.95
7.95
8.11
8.12
8.45
8.46
8.76
8.78
8.79
9.44
9.46
6.06
0.98
2.04
2.00
2.05
2.00
1.08
1.89
0.99
0.96
2.00
1.01
0.94
CF3
NH
O
N
N
0
1
2
3
4
5
6
7
8
9
10
11
12
3
f1 (ppm)

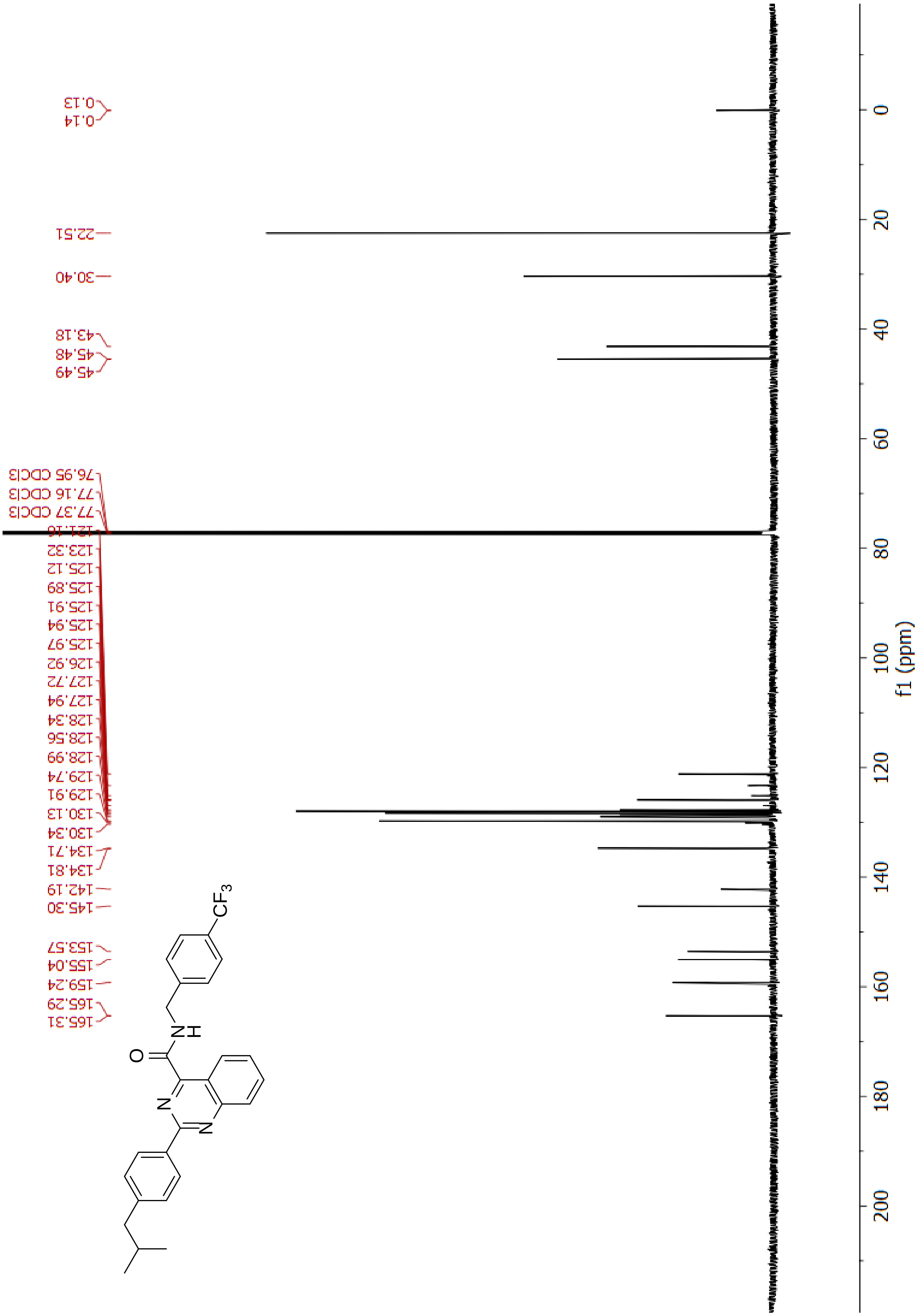
0.13
0.14
22.51
30.40
43.18
45.48
45.49
76.95 CDCl3
77.16 CDCl3
77.37 CDCl3
121.16
123.32
125.12
125.89
125.91
125.94
125.97
126.92
127.72
127.94
128.34
128.56
128.99
129.74
129.91
130.13
130.34
134.71
134.81
142.19
145.30
153.57
155.04
159.24
165.29
165.31
CF3
NH
O
N
N
0
20
40
60
80
100
120
140
160
180
200
f1 (ppm)

HPLC trace

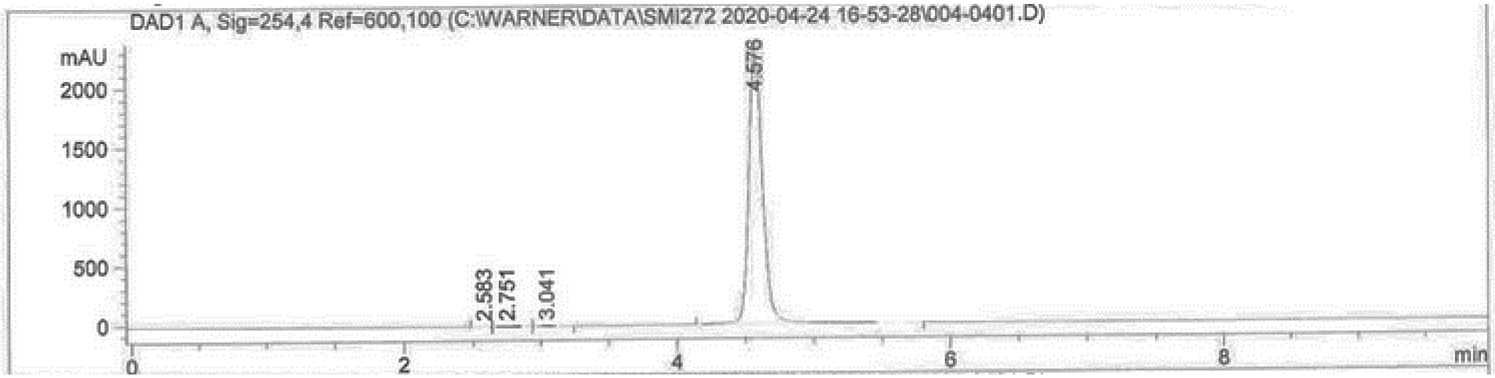

```
Signal 1: DAD1 A, Sig=254,4 Ref=600,100

Peak RetTime Type  Width     Area      Height     Area
  #   [min]        [min]   [mAU*s]     [mAU]        %
----|-------|----|-------|----------|----------|--------|
   1   2.583 BV    0.0914   11.67138    1.90633   0.0711
   2   2.751 VV    0.1646   47.89710    4.41286   0.2917
   3   3.041 VB    0.0961   46.60263    7.14318   0.2839
   4   4.576 BB    0.1090 1.63114e4 2292.87134  99.3533
```

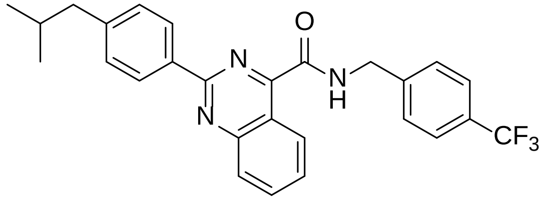

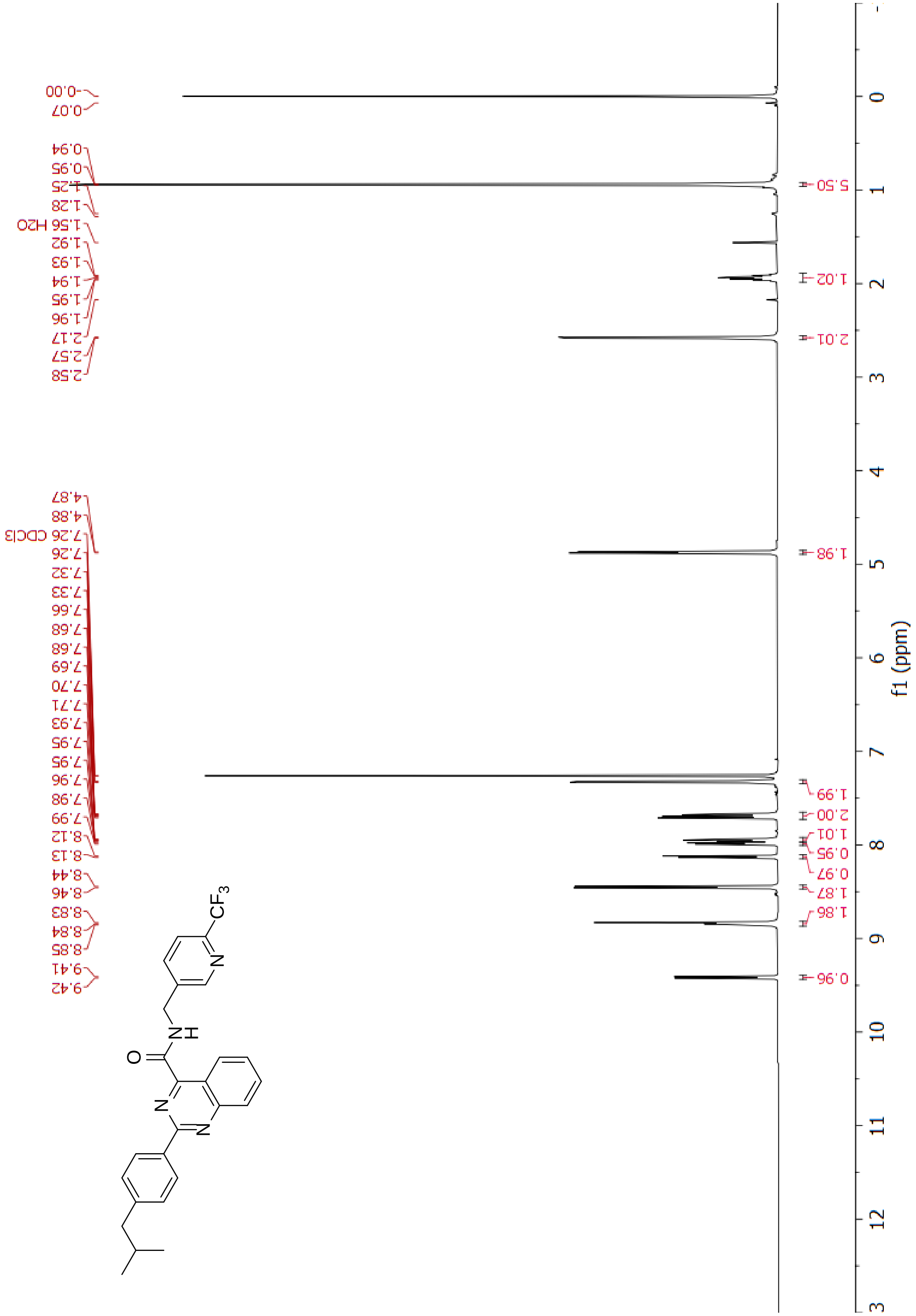
-0.00
0.07
0.94
0.95
1.25
1.28
1.56 H2O
1.92
1.93
1.94
1.95
1.96
2.17
2.57
2.58
4.87
4.88
7.26 CDCl3
7.26
7.32
7.33
7.66
7.68
7.68
7.69
7.70
7.71
7.93
7.95
7.95
7.96
7.98
7.99
8.12
8.13
8.44
8.46
8.83
8.84
8.85
9.41
9.42
5.50
1.02
2.01
1.98
1.99
2.00
1.01
0.95
0.97
1.87
1.86
0.96
f1 (ppm)
0
1
2
3
4
5
6
7
8
9
10
11
12
13
O
NH
N
N
N
CF3

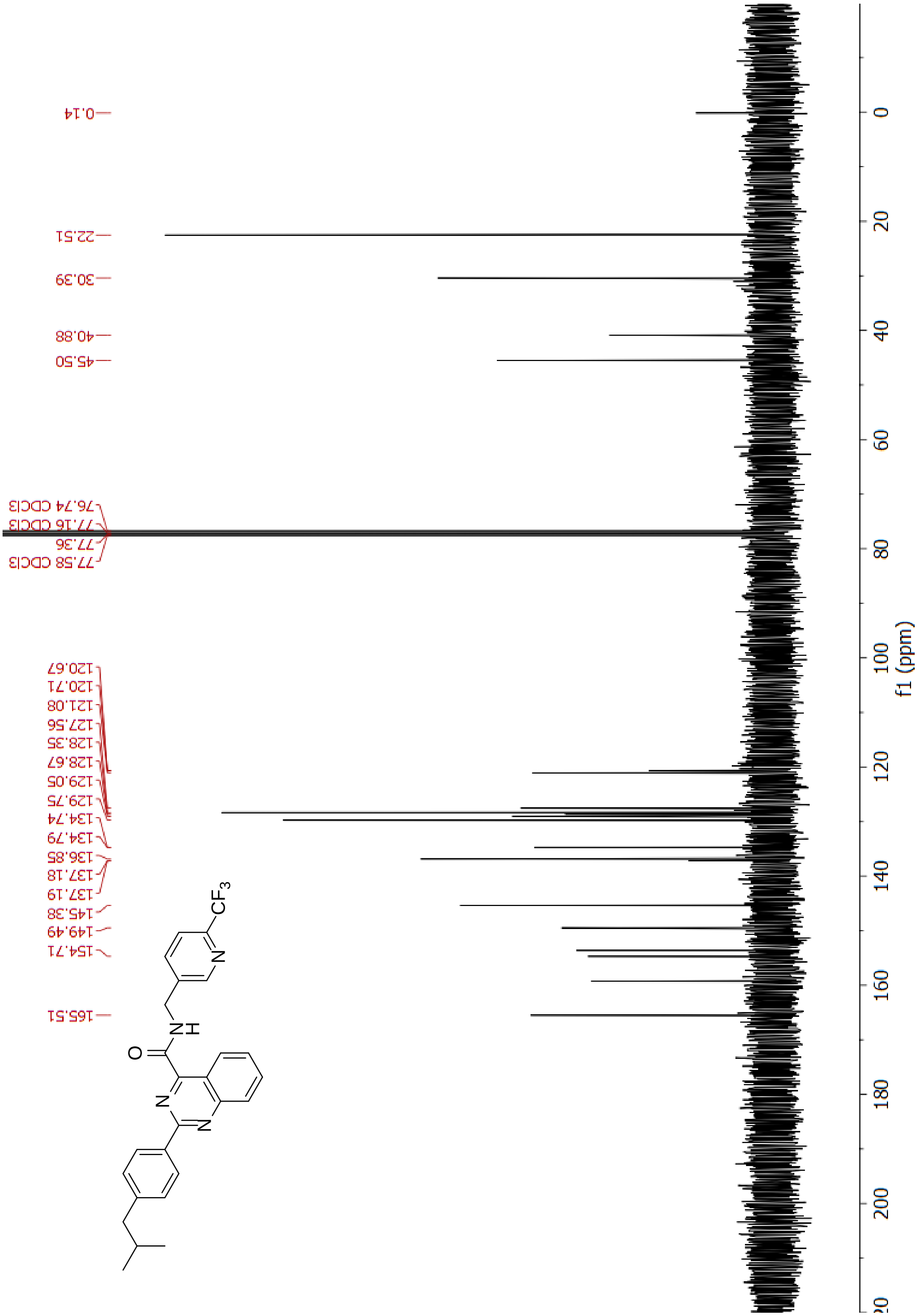
0.14
22.51
30.39
40.88
45.50
76.74 CDCl3
77.16 CDCl3
77.36
77.58 CDCl3
120.67
120.71
121.08
127.56
128.35
128.67
129.05
129.75
134.74
134.79
136.85
137.18
137.19
145.38
149.49
154.71
165.51
CF3
N
NH
O
N
N
0
20
40
60
80
100
120
140
160
180
200
f1 (ppm)

HPLC trace

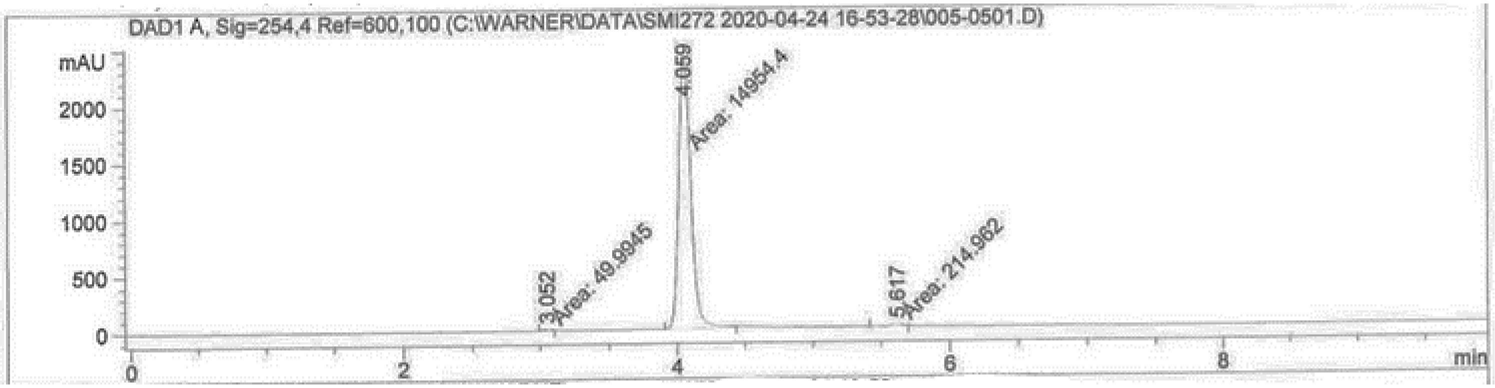

```
Signal 1: DAD1 A, Sig=254,4 Ref=600,100

Peak RetTime Type  Width     Area      Height     Area
  #   [min]        [min]   [mAU*s]     [mAU]       %
----|-------|----|-------|----------|----------|--------|
   1   3.052 MM    0.0734   49.99452   11.35115   0.3285
   2   4.059 MM    0.1039 1.49544e4  2398.74585  98.2591
   3   5.617 MM    0.2076  214.96150   17.25371   1.4124
```

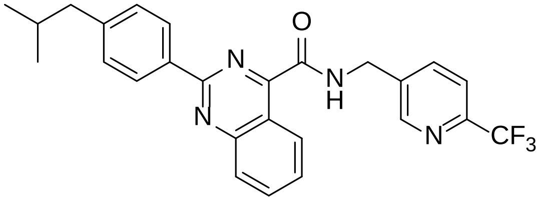

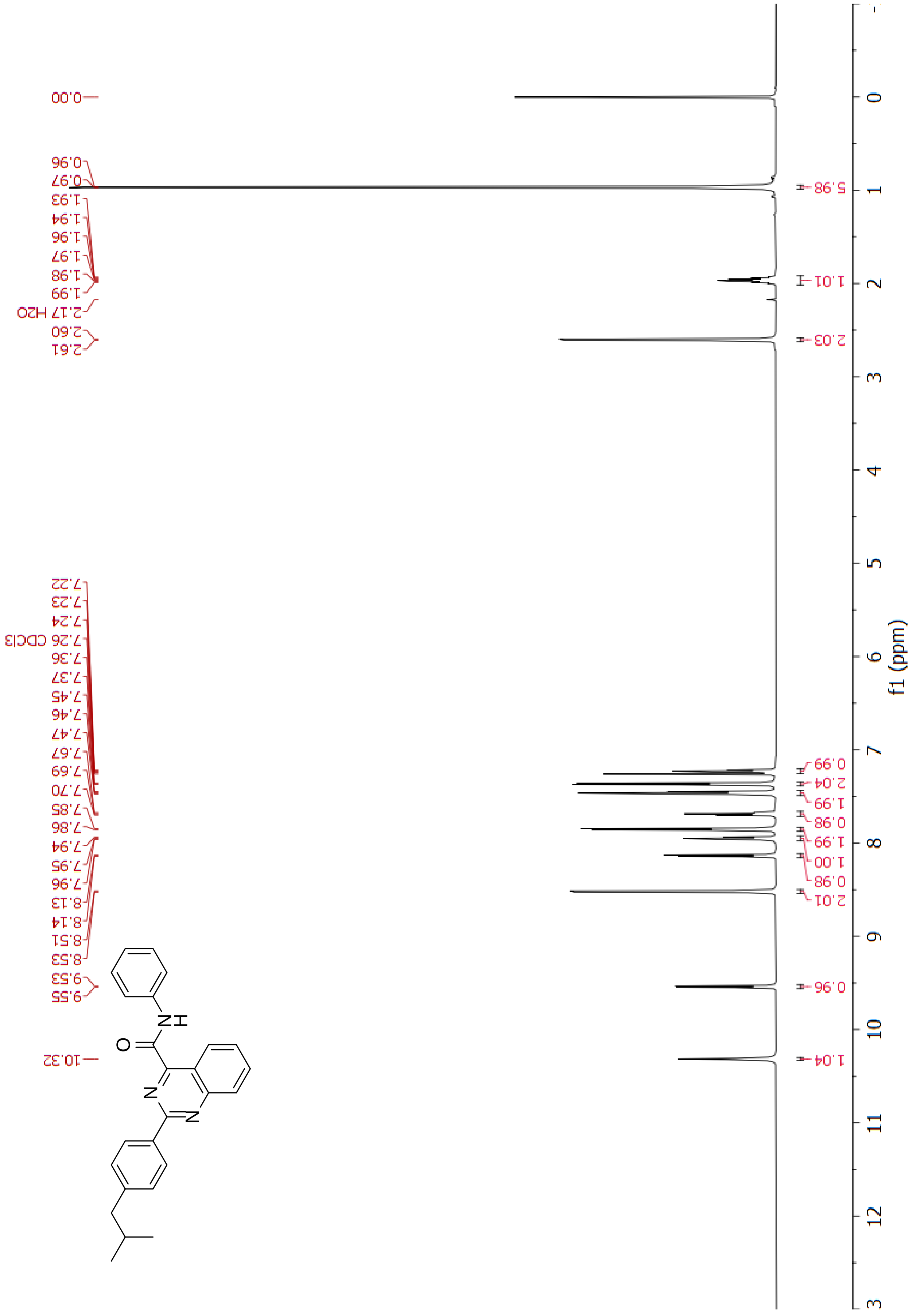

0.00
0.96
0.97
1.93
1.94
1.96
1.97
1.98
1.99
2.17 H2O
2.60
2.61
7.22
7.23
7.24
7.26 CDCl3
7.36
7.37
7.45
7.46
7.47
7.67
7.69
7.70
7.85
7.86
7.94
7.95
7.96
8.13
8.14
8.51
8.53
9.53
9.55
10.32
5.98
1.01
2.03
0.99
2.04
1.99
0.98
1.99
1.00
0.98
2.01
0.96
1.04
H
N
O
N
N
f1 (ppm)
0
1
2
3
4
5
6
7
8
9
10
11
12

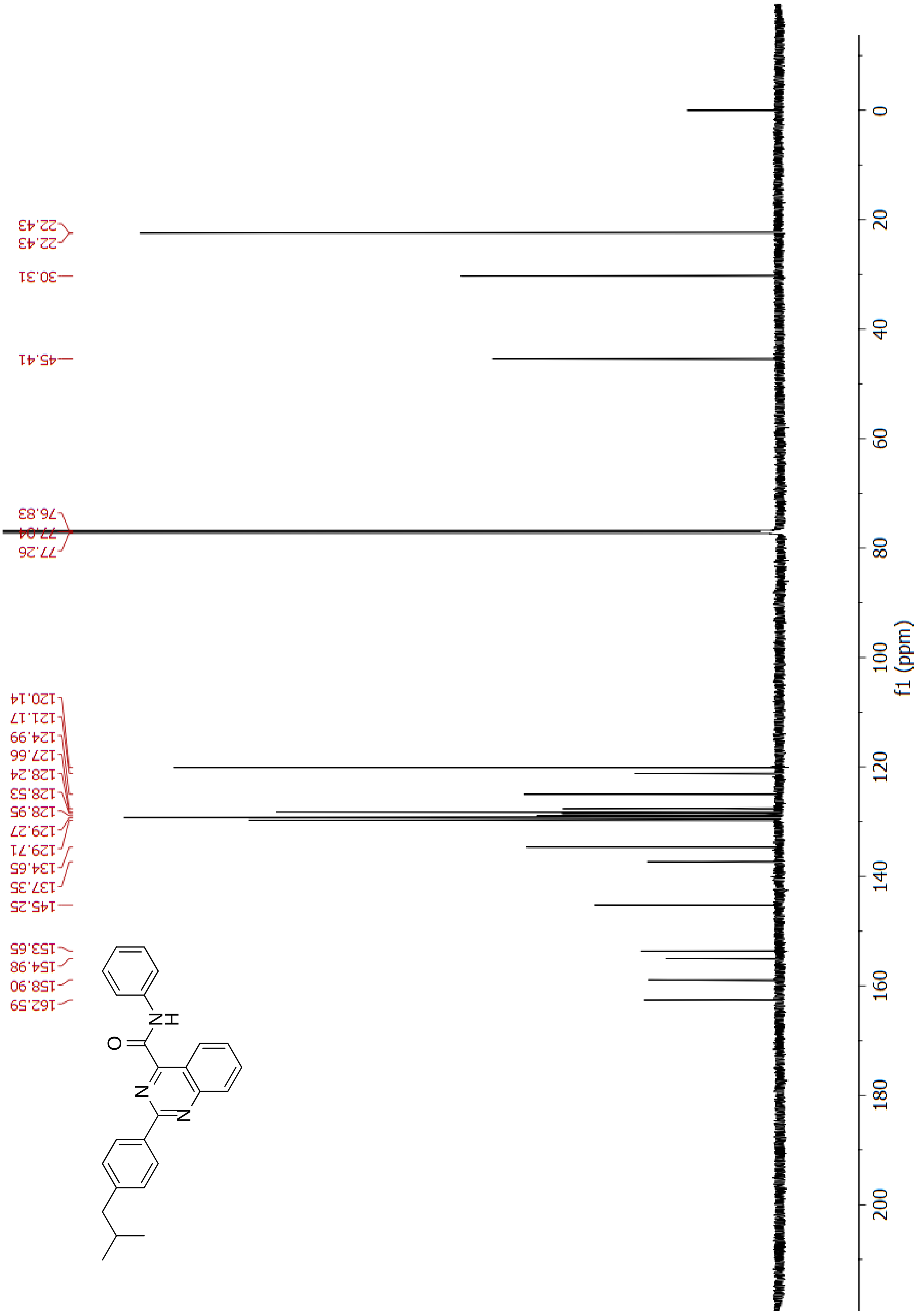
22.43
22.43
30.31
45.41
76.83
77.04
77.26
120.14
121.17
124.99
127.66
128.24
128.53
128.95
129.27
129.71
134.65
137.35
145.25
153.65
154.98
158.90
162.59
O
HN
N
N
0
20
40
60
80
100
120
140
160
180
200
f1 (ppm)

HPLC trace

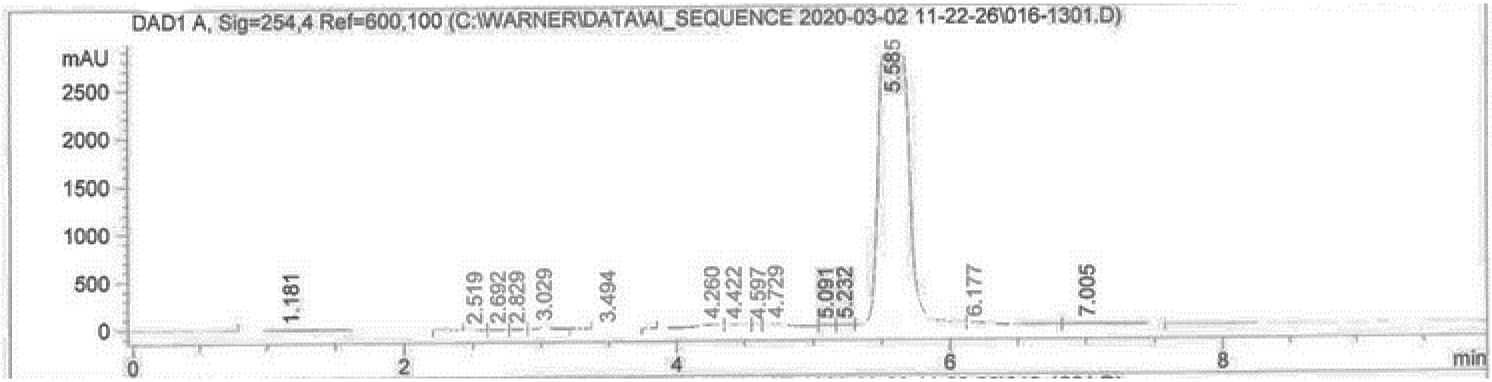

```
Peak RetTime Type  Width      Area      Height     Area
  #   [min]        [min]   [mAU*s]     [mAU]        %
----|-------|----|-------|----------|----------|--------|
  11   5.091 VV    0.1061   79.16255   10.72451   0.1699
  12   5.232 VV    0.1158   87.53796   10.88916   0.1879
  13   5.585 VV    0.1967 4.38828e4  2833.41064  94.1994
  14   6.177 VB    0.2692  702.60431   34.85838   1.5082
  15   7.005 BB    0.2898  229.99538   10.49012   0.4937
```

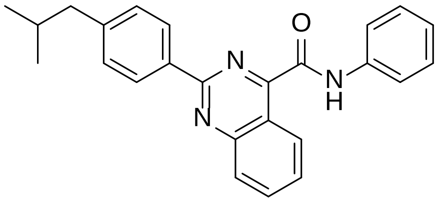

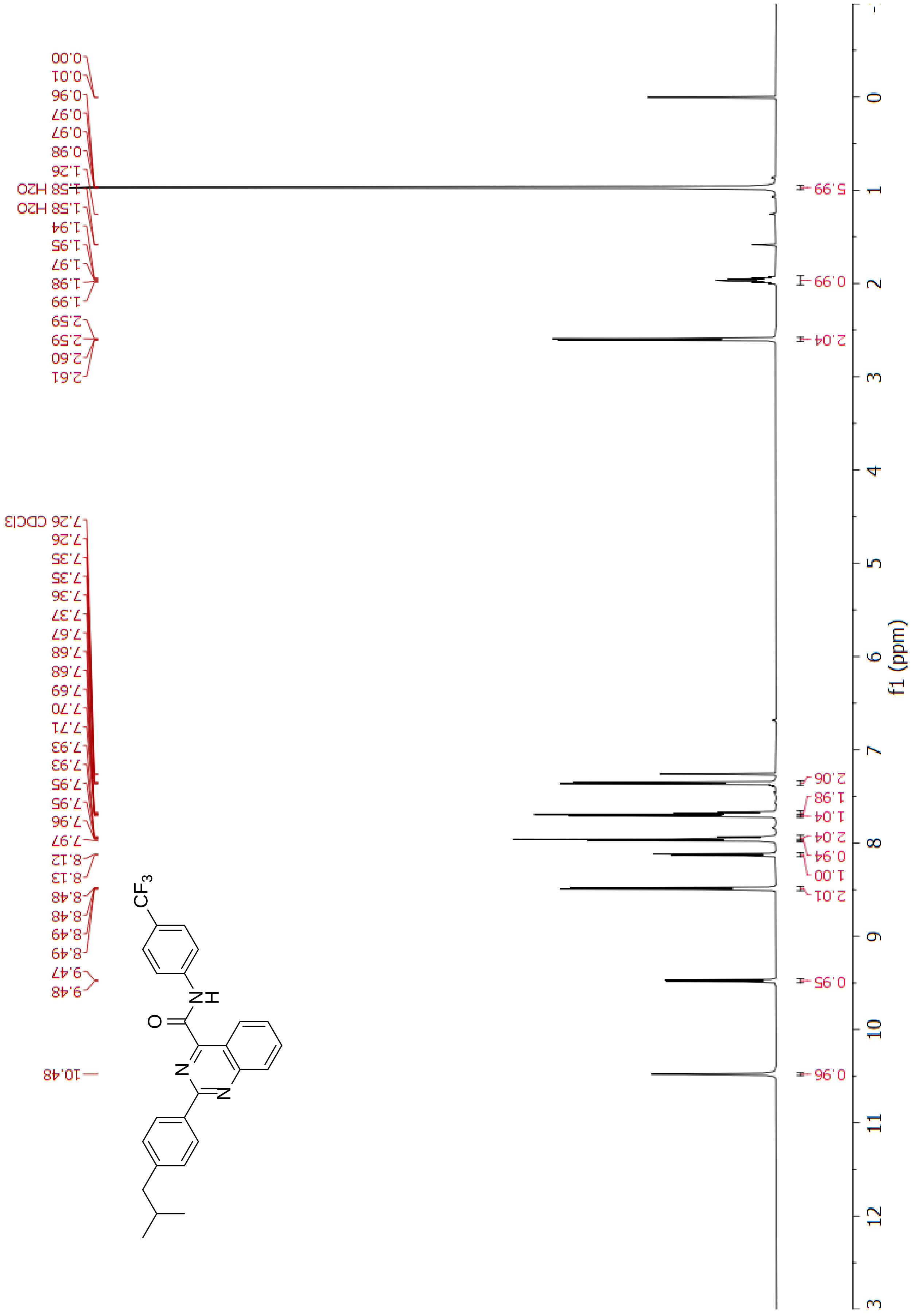

10.48
9.48
9.47
8.49
8.49
8.48
8.48
8.13
8.12
7.97
7.96
7.95
7.95
7.93
7.93
7.71
7.70
7.69
7.68
7.68
7.67
7.37
7.36
7.35
7.35
7.26
7.26 CDCl3
2.61
2.60
2.59
2.59
1.99
1.98
1.97
1.95
1.94
1.58 H2O
1.58 H2O
1.26
0.98
0.97
0.97
0.96
0.01
0.00
0.96
0.95
2.01
1.00
0.94
2.04
1.04
1.98
2.06
2.04
0.99
5.99
CF3
NH
O
N
N
f1 (ppm)
13
12
11
10
9
8
7
6
5
4
3
2
1
0

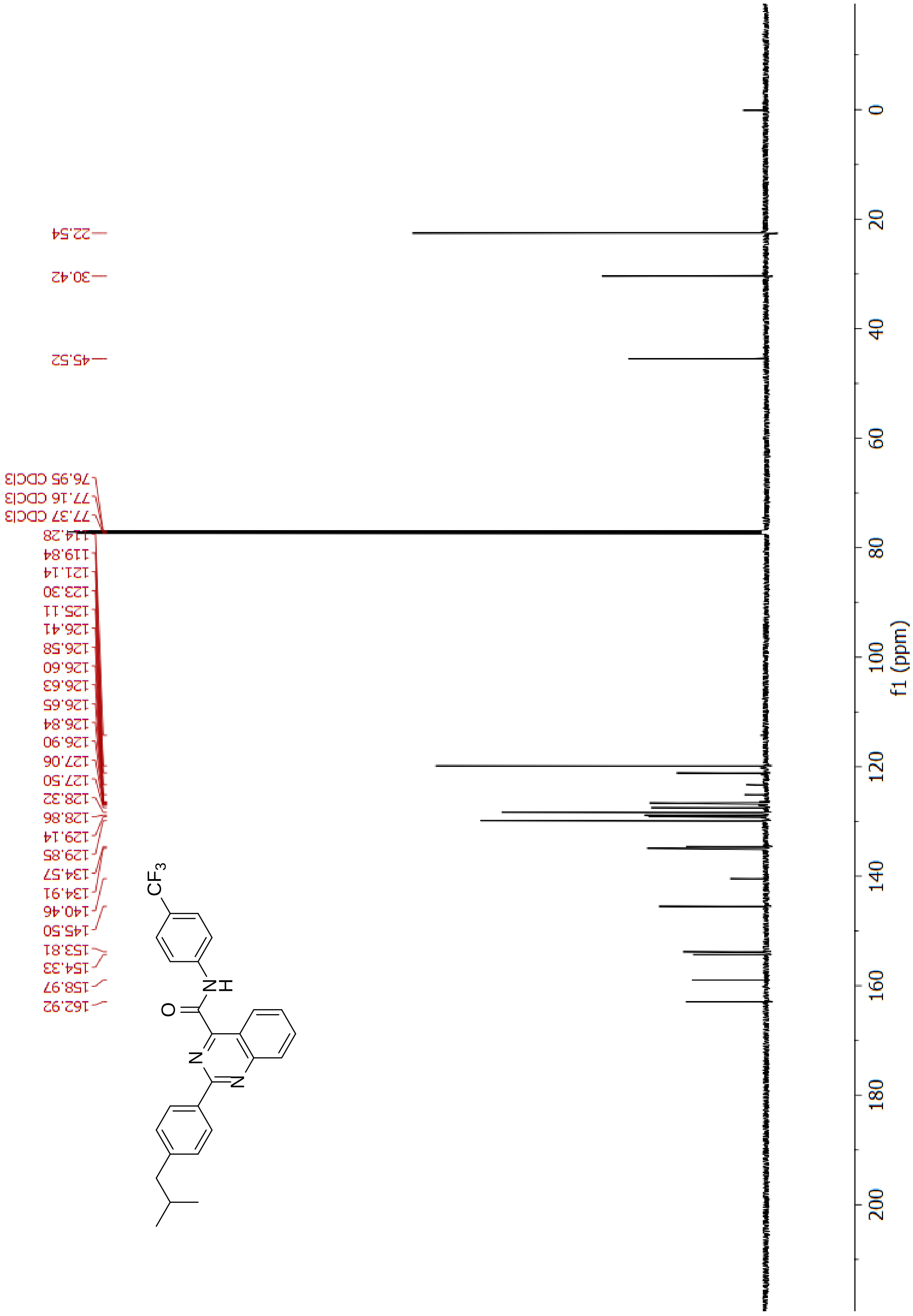
22.54
30.42
45.52
76.95 CDCl3
77.16 CDCl3
77.37 CDCl3
114.28
119.84
121.14
123.30
125.11
126.41
126.58
126.60
126.63
126.65
126.84
126.90
127.06
127.50
128.32
128.86
129.14
129.85
134.57
134.91
140.46
145.50
153.81
154.33
158.97
162.92
CF3
NH
O
N
N
0
20
40
60
80
100
120
140
160
180
200
f1 (ppm)

HPLC trace

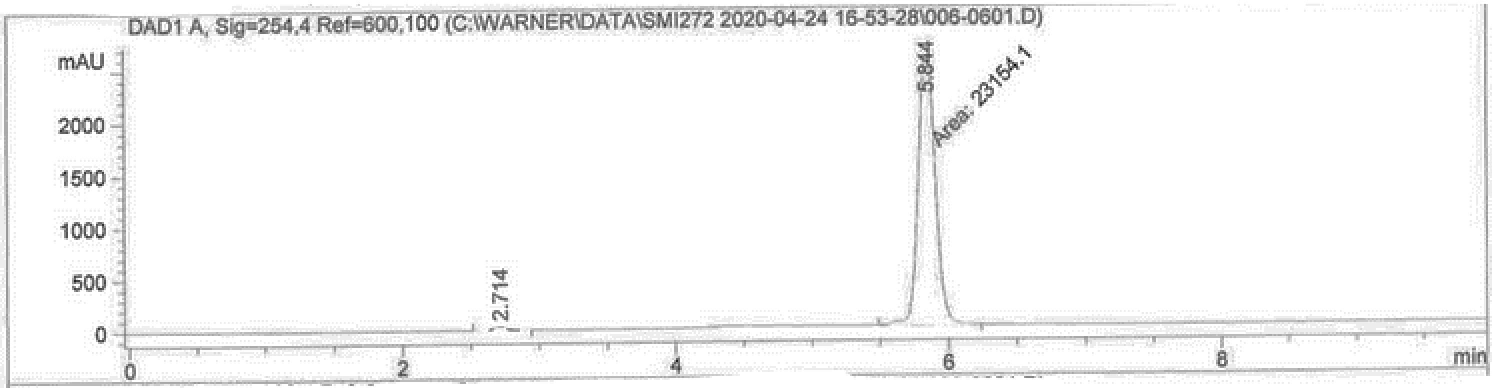

```
Signal 1: DAD1 A, Sig=254,4 Ref=600,100

Peak RetTime Type  Width     Area      Height     Area
  #   [min]        [min]   [mAU*s]     [mAU]       %
----|-------|----|-------|----------|----------|--------|
   1   2.714 BV    0.1112  230.91478   33.18241   0.9874
   2   5.844 MM    0.1480 2.31541e4  2607.95044  99.0126
```

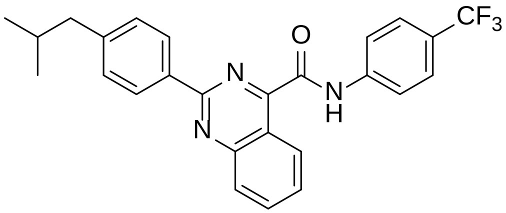

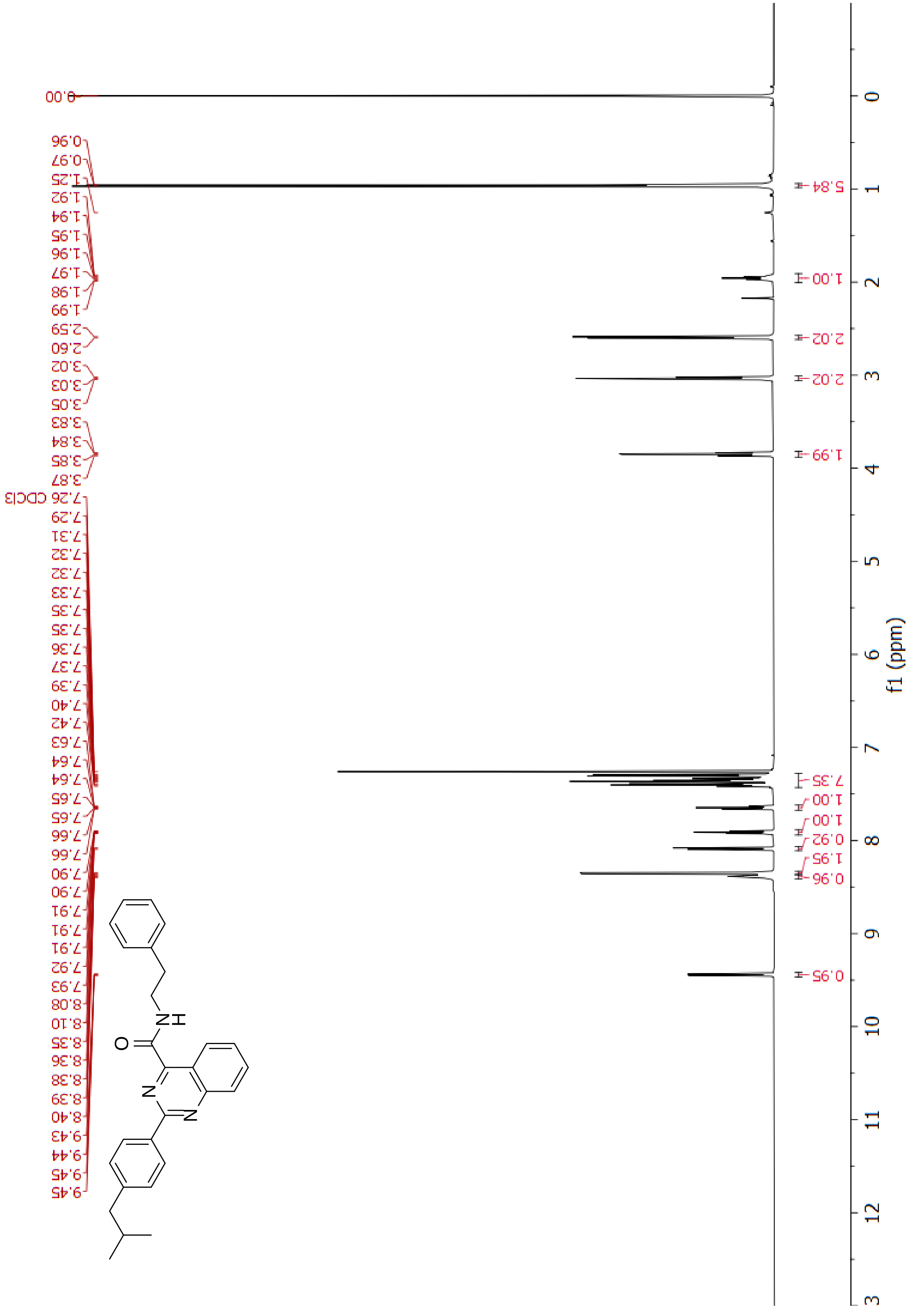
0.00
0.96
0.97
1.25
1.92
1.94
1.95
1.96
1.97
1.98
1.99
2.59
2.60
3.02
3.03
3.05
3.83
3.84
3.85
3.87
7.26 CDCl3
7.29
7.31
7.32
7.32
7.33
7.35
7.35
7.36
7.37
7.39
7.40
7.42
7.63
7.64
7.64
7.65
7.65
7.66
7.66
7.90
7.90
7.91
7.91
7.91
7.92
7.93
8.08
8.10
8.35
8.36
8.38
8.39
8.40
9.43
9.44
9.45
9.45
5.84
1.00
2.02
2.02
1.99
7.35
1.00
1.00
0.92
1.95
0.96
0.95
0
1
2
3
4
5
6
7
8
9
10
11
12
13
f1 (ppm)
O
N
H
N
N

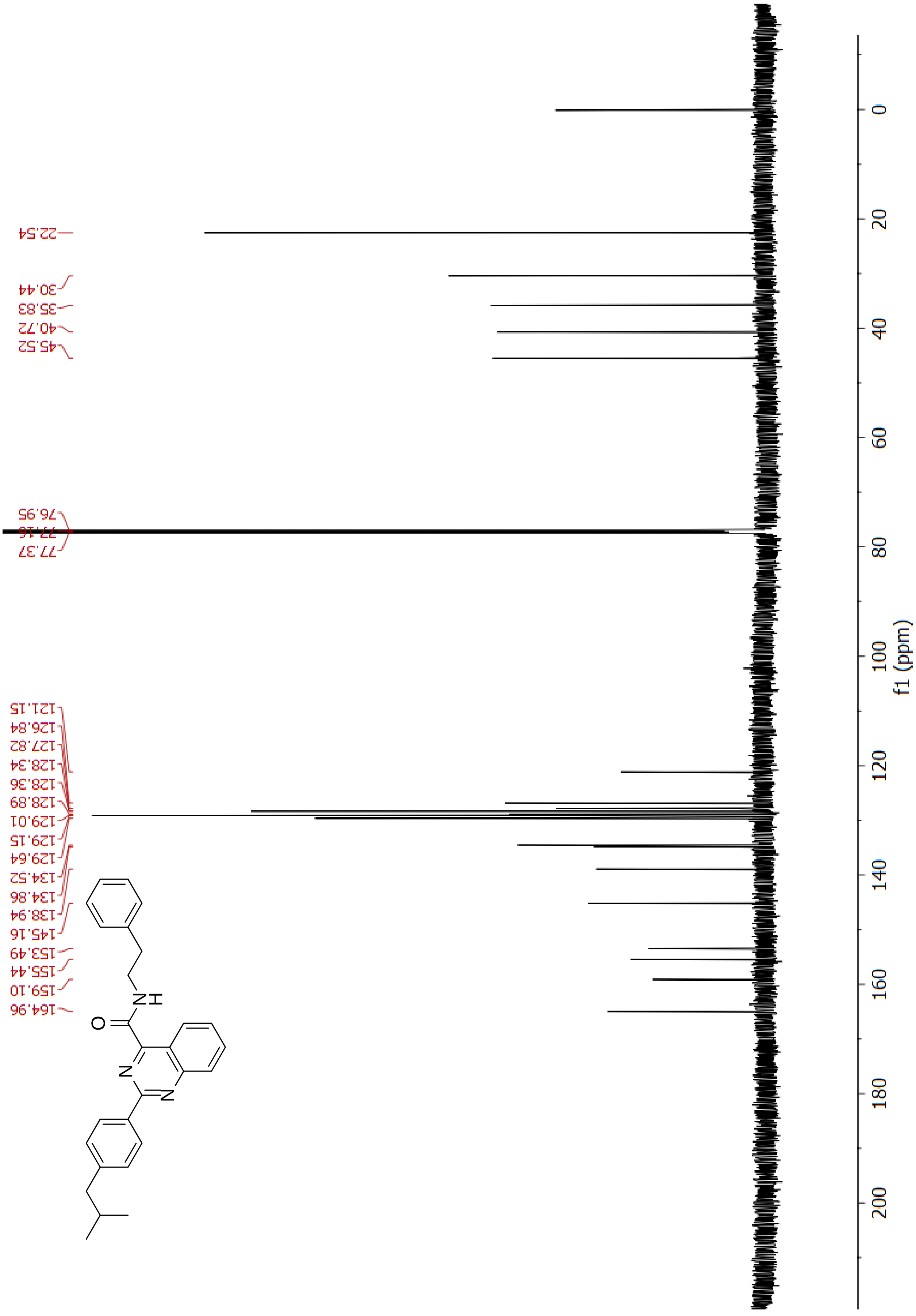
164.96
159.10
155.44
153.49
145.16
138.94
134.86
134.52
129.64
129.15
129.01
128.89
128.36
128.34
127.82
126.84
121.15
77.37
77.16
76.95
45.52
40.72
35.83
30.44
22.54
O
H
N
N
N
0
20
40
60
80
100
120
140
160
180
200
f1 (ppm)

HPLC trace

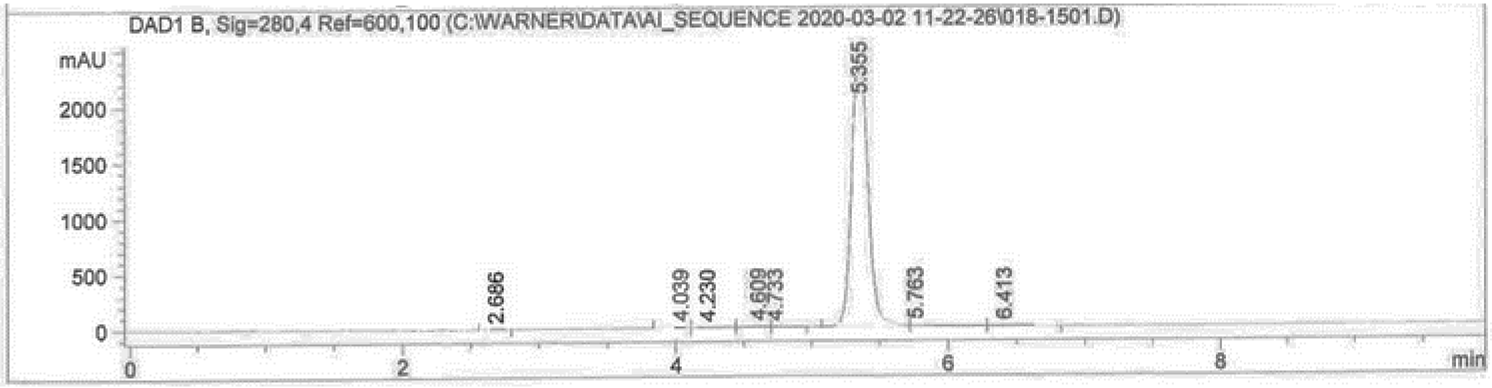

```
Signal 2: DAD1 B, Sig=280,4 Ref=600,100

Peak RetTime Type  Width     Area      Height     Area
  #   [min]        [min]   [mAU*s]     [mAU]        %
----|-------|----|-------|----------|----------|--------|
   1   2.686 BV    0.0816    6.39101    1.71208   0.0308
   2   4.039 BV    0.1071   11.11107    1.52348   0.0535
   3   4.230 VV    0.1798   42.52390    3.14359   0.2049
   4   4.609 VV    0.1309   64.43620    7.03141   0.3104
   5   4.733 VB    0.1285   33.77195    3.63138   0.1627
   6   5.355 BV    0.1320 2.04129e4  2430.25659  98.3387
   7   5.763 VB    0.2156  158.67561    9.76172   0.7644
   8   6.413 BB    0.2153   27.93867    1.77805   0.1346
```

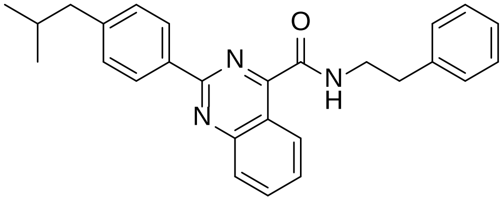

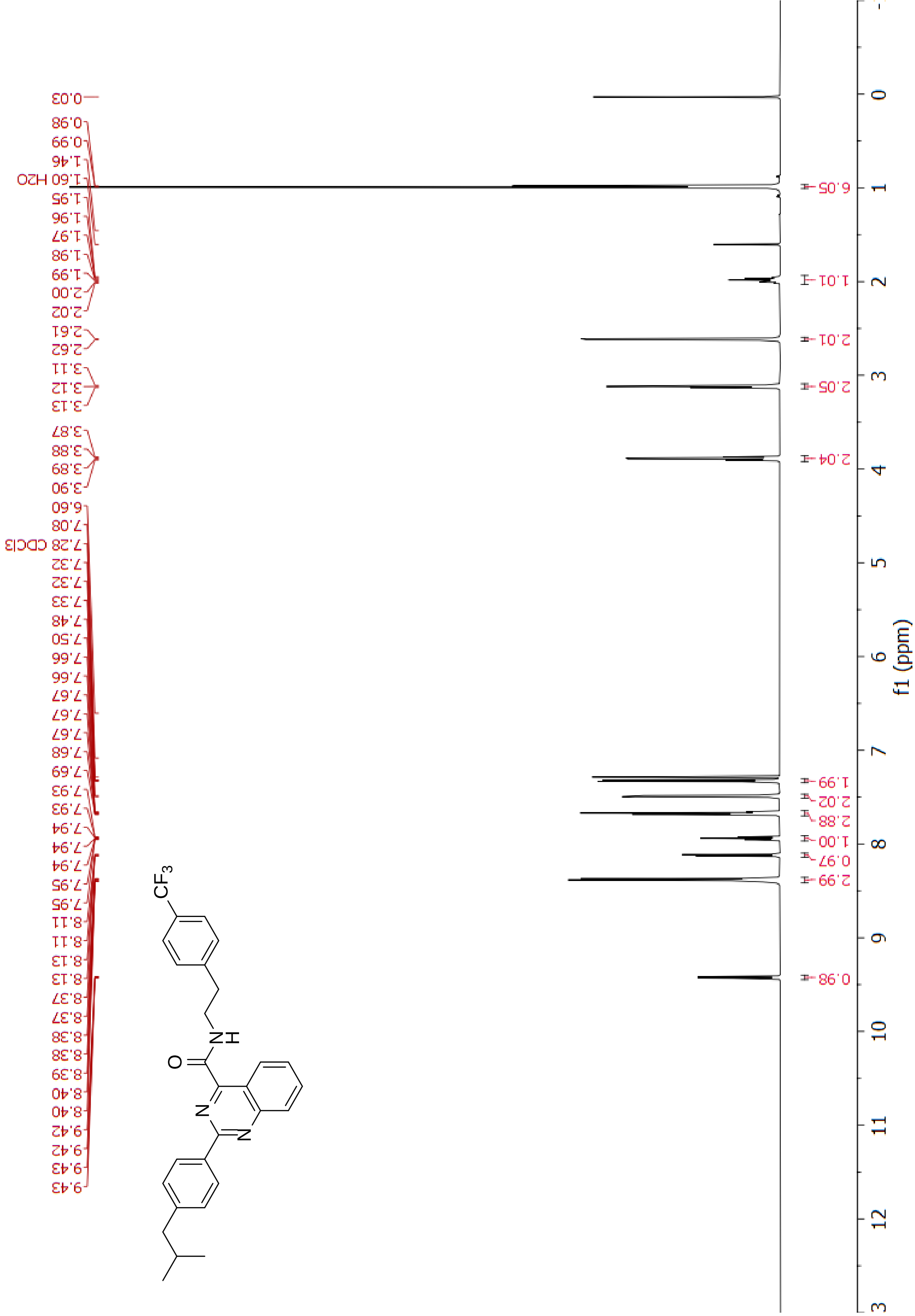

0.03
0.98
0.99
1.46
1.60 H2O
1.95
1.96
1.97
1.98
1.99
2.00
2.02
2.61
2.62
3.11
3.12
3.13
3.87
3.88
3.89
3.90
6.60
7.08
7.28 CDCl3
7.32
7.32
7.33
7.48
7.50
7.66
7.66
7.67
7.67
7.67
7.68
7.69
7.93
7.93
7.94
7.94
7.94
7.95
7.95
8.11
8.13
8.13
8.37
8.37
8.38
8.38
8.39
8.40
8.40
9.42
9.42
9.43
9.43
6.05
1.01
2.01
2.05
2.04
1.99
2.02
2.88
1.00
0.97
2.99
0.98
f1 (ppm)
-1
0
1
2
3
4
5
6
7
8
9
10
11
12
13
CF_3
O
NH
N
N

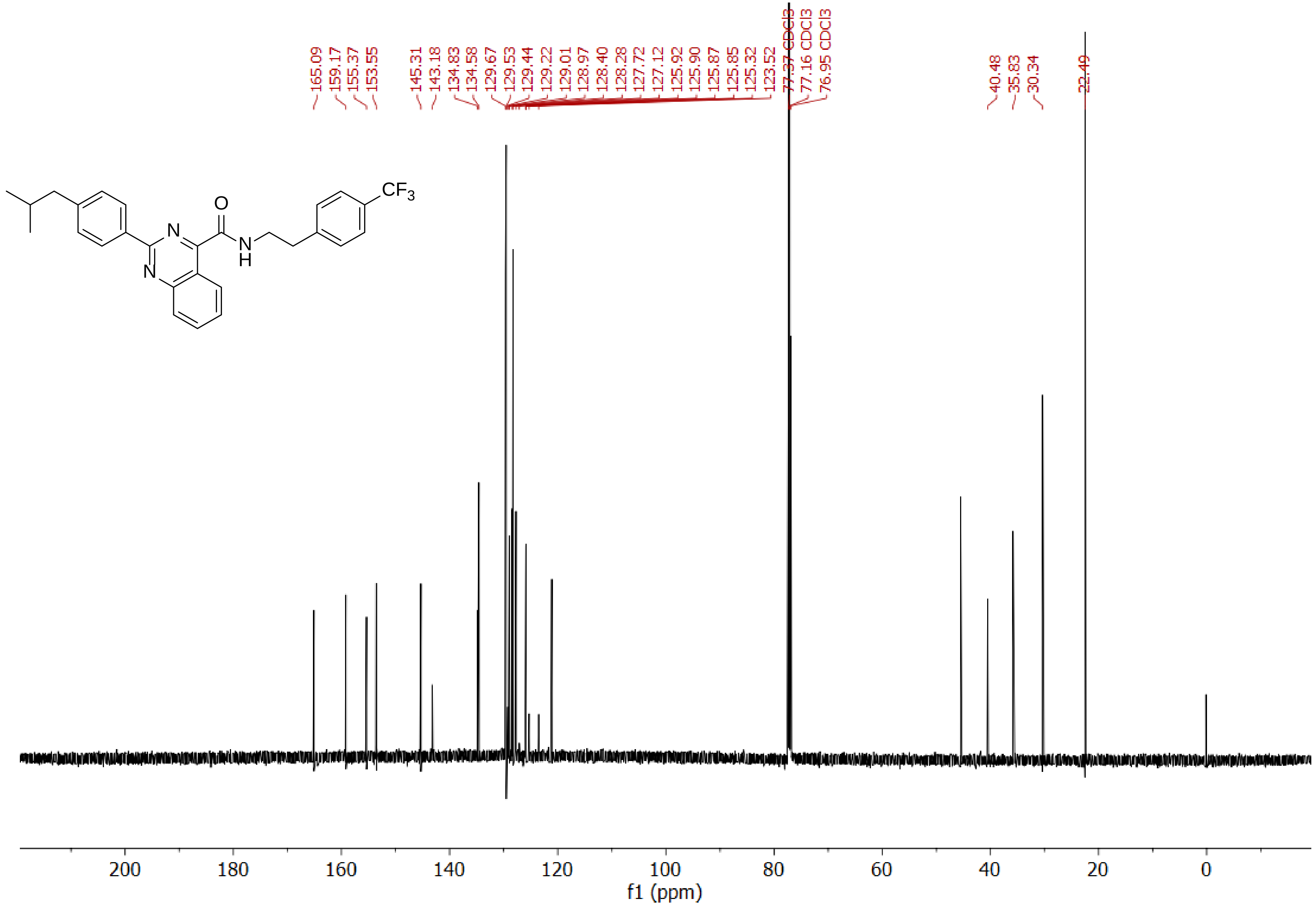
CF3
O
N
N
N
H
165.09
159.17
155.37
153.55
145.31
143.18
134.83
134.58
129.67
129.53
129.44
129.22
129.01
128.97
128.40
128.28
127.72
127.12
125.92
125.90
125.87
125.85
125.32
123.52
77.37 CDCl3
77.16 CDCl3
76.95 CDCl3
40.48
35.83
30.34
22.49
200
180
160
140
120
100
80
60
40
20
0
f1 (ppm)

HPLC trace

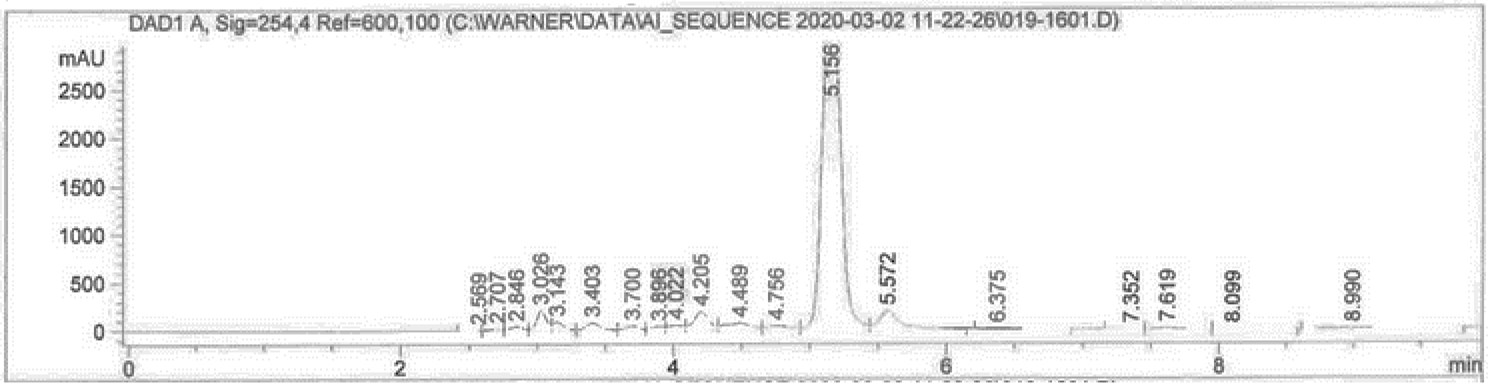

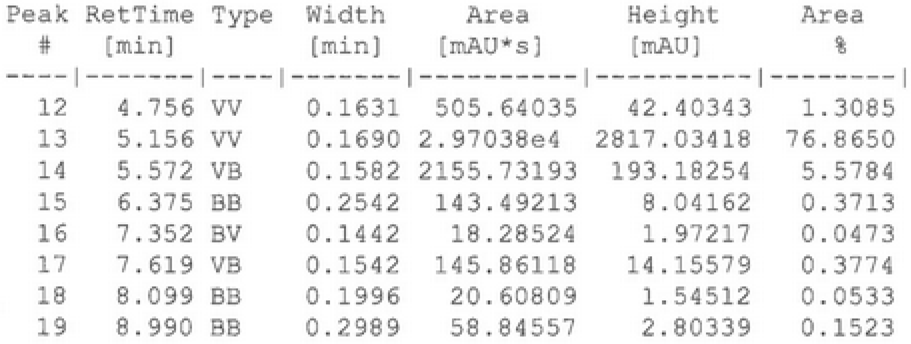

```
Peak RetTime Type  Width     Area      Height     Area
  #   [min]        [min]   [mAU*s]     [mAU]       %
----|-------|----|-------|----------|----------|--------|
  12   4.756 VV    0.1631  505.64035   42.40343   1.3085
  13   5.156 VV    0.1690 2.97038e4  2817.03418  76.8650
  14   5.572 VB    0.1582 2155.73193  193.18254   5.5784
  15   6.375 BB    0.2542  143.49213    8.04162   0.3713
  16   7.352 BV    0.1442   18.28524    1.97217   0.0473
  17   7.619 VB    0.1542  145.86118   14.15579   0.3774
  18   8.099 BB    0.1996   20.60809    1.54512   0.0533
  19   8.990 BB    0.2989   58.84557    2.80339   0.1523
```

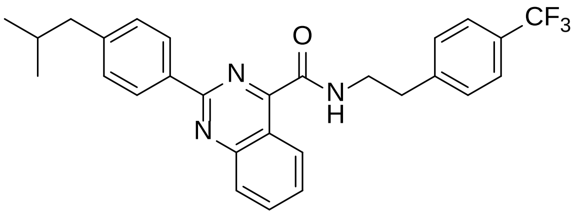

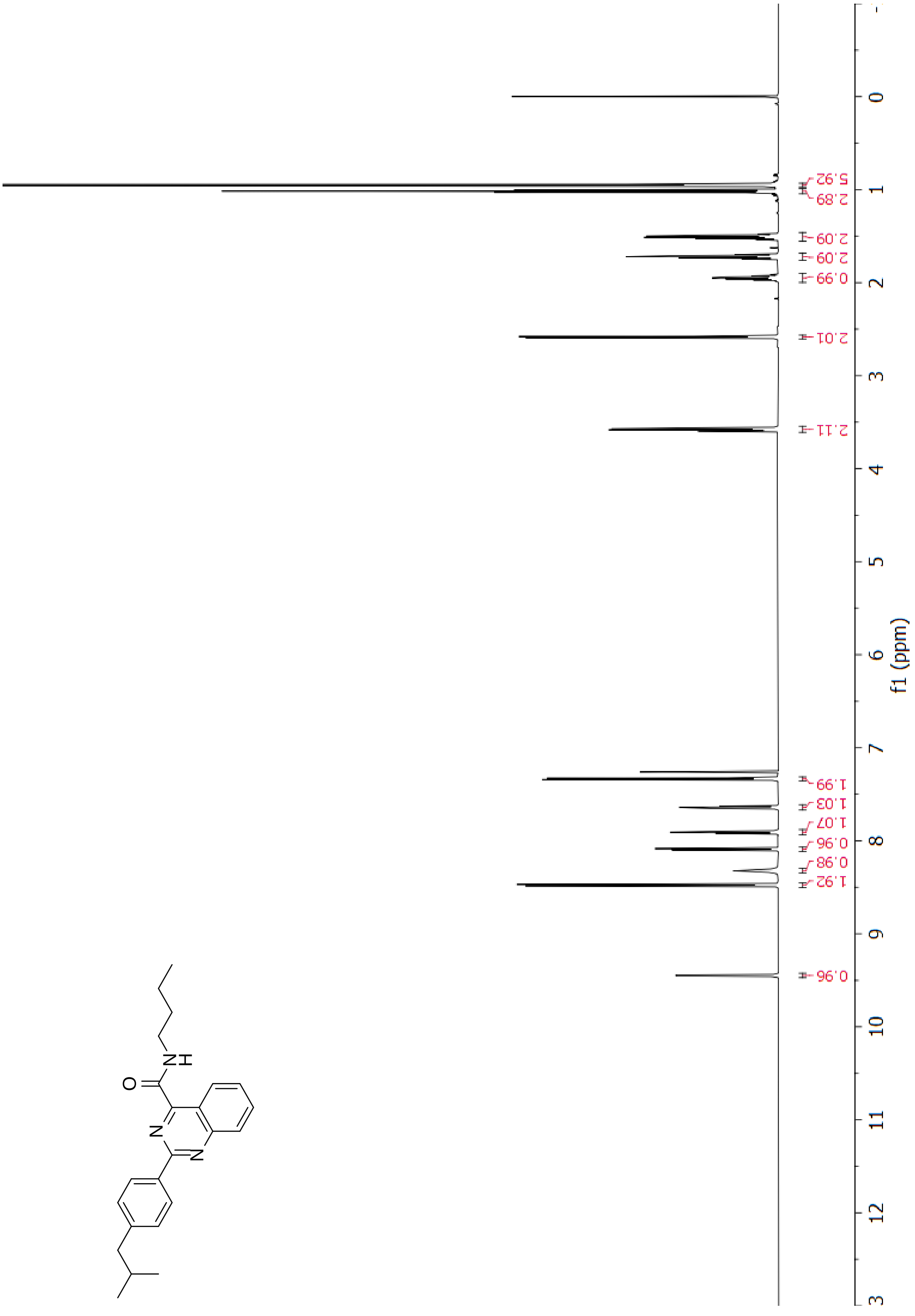
O
NH
N
N
5.92
2.89
2.09
2.09
0.99
2.01
2.11
1.99
1.03
1.07
0.96
0.98
1.92
0.96
0
1
2
3
4
5
6
7
8
9
10
11
12
13
f1 (ppm)

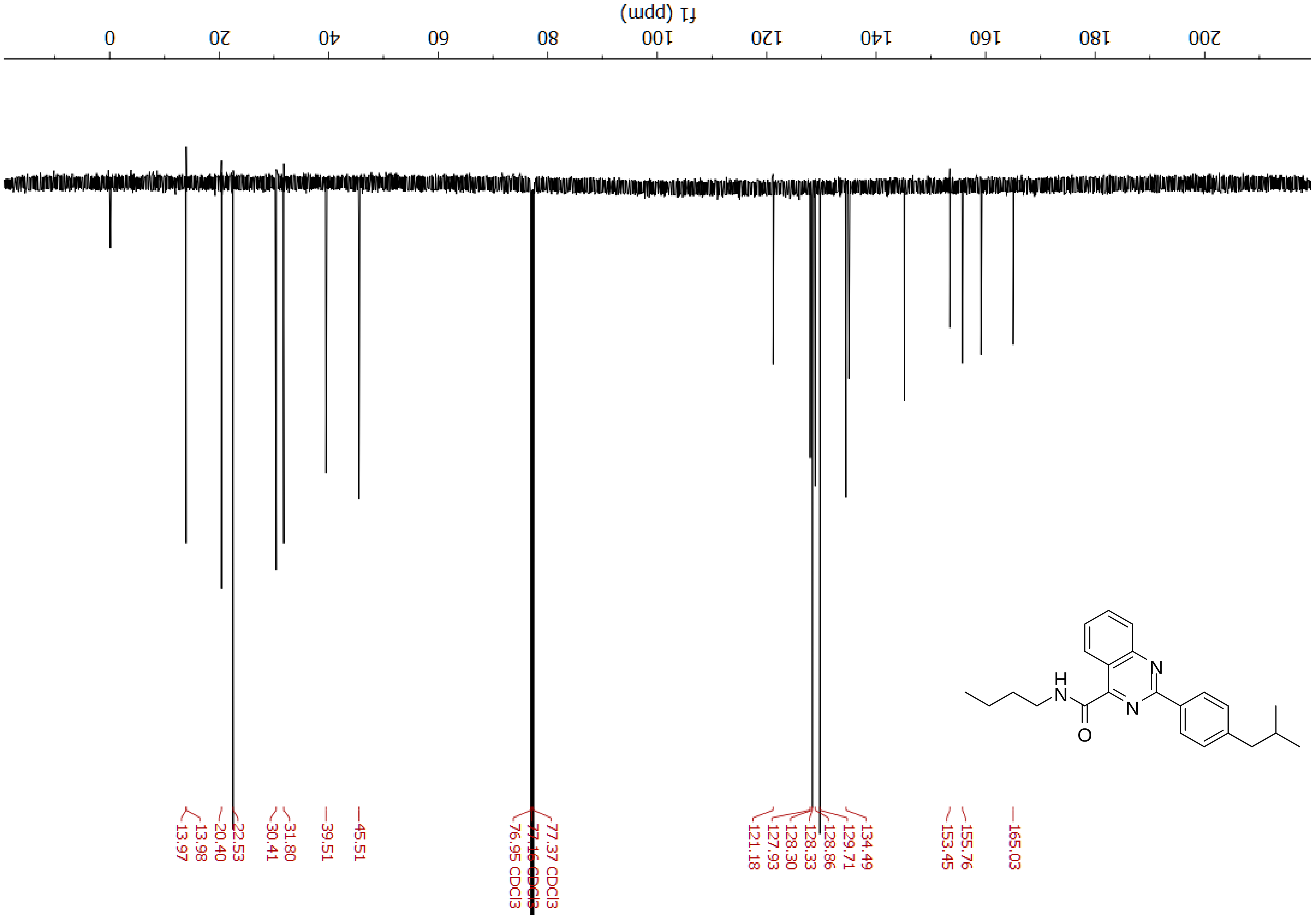
13.97
13.98
20.40
22.53
30.41
31.80
39.51
45.51
76.95 CDCl3
77.16 CDCl3
77.37 CDCl3
121.18
127.93
128.30
128.33
128.86
129.71
134.49
153.45
155.76
165.03
0
20
40
60
80
100
120
140
160
180
200
f1 (ppm)
H
N
O
N
N

HPLC trace

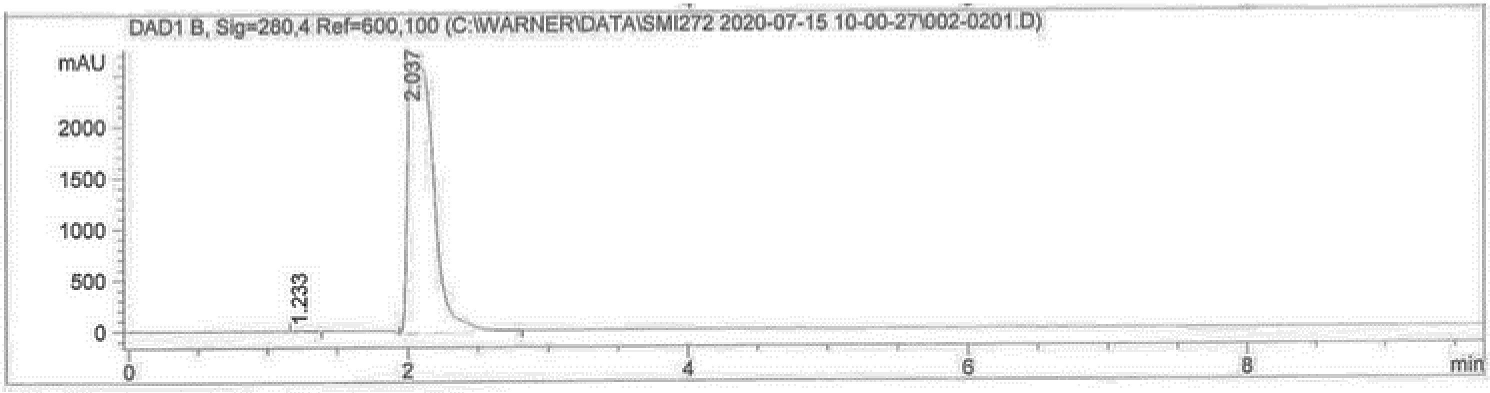

```
Signal 2: DAD1 B, Sig=280,4 Ref=600,100

Peak RetTime Type  Width     Area      Height     Area
  #   [min]        [min]   [mAU*s]     [mAU]        %
----|-------|----|-------|----------|----------|--------|
   1    1.233 BV    0.0597   33.11686    8.09467   0.0968
   2    2.037 BB    0.1666 3.41854e4  2648.09302  99.9032
```

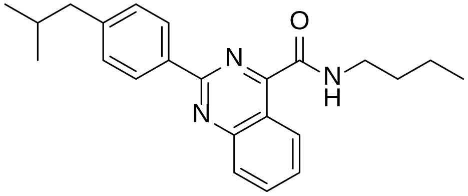

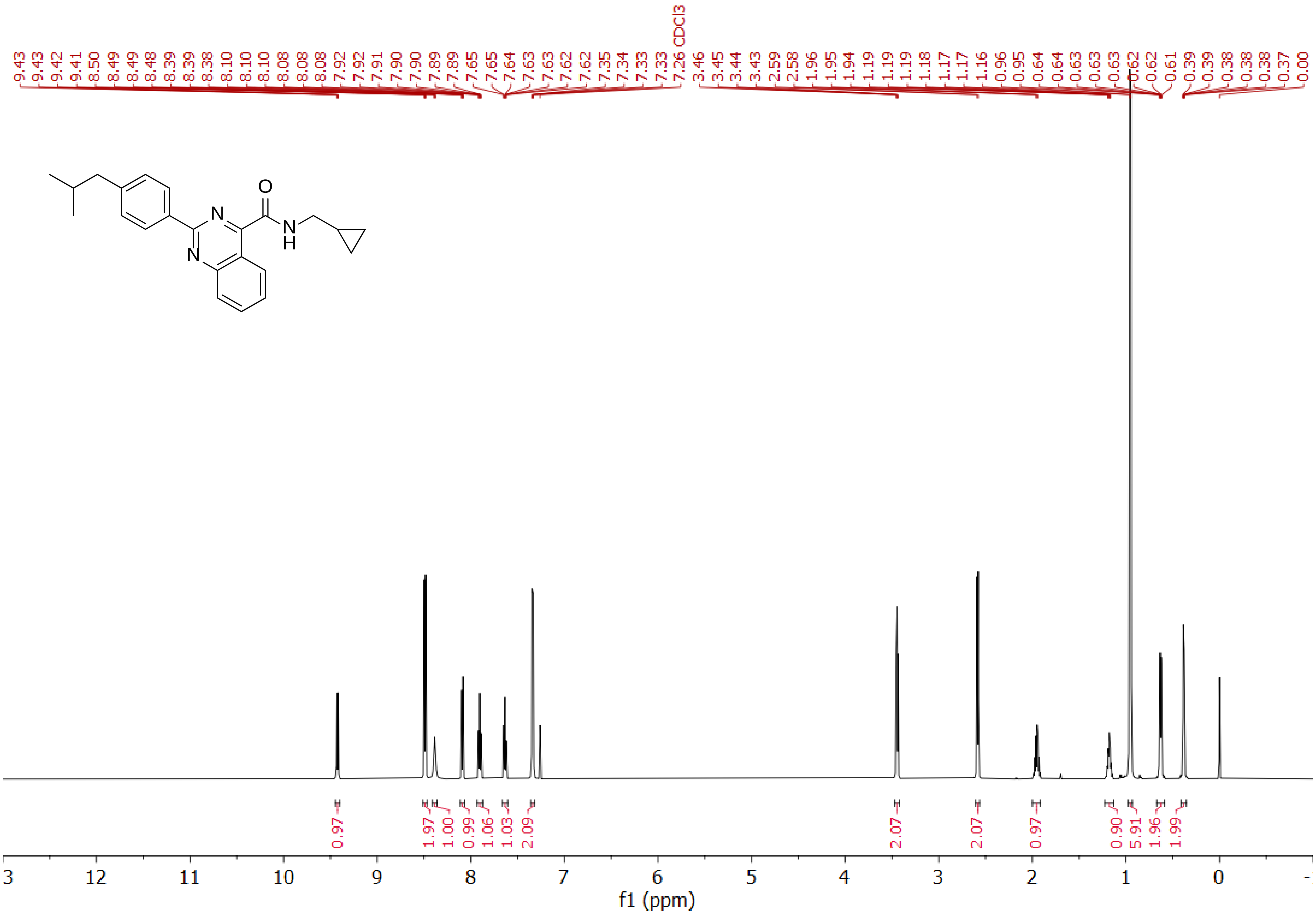
9.43
9.43
9.42
9.41
8.50
8.49
8.49
8.48
8.39
8.39
8.38
8.10
8.10
8.10
8.08
8.08
8.08
7.92
7.92
7.91
7.90
7.90
7.89
7.89
7.65
7.65
7.64
7.63
7.63
7.62
7.62
7.35
7.34
7.33
7.33
7.26 CDCl3
3.46
3.45
3.44
3.43
2.59
2.58
1.96
1.95
1.94
1.19
1.19
1.19
1.18
1.17
1.17
1.16
0.96
0.95
0.64
0.64
0.63
0.63
0.63
0.62
0.62
0.61
0.39
0.39
0.38
0.38
0.38
0.37
0.00
O
N
N
N
H
0.97
1.97
1.00
0.99
1.06
1.03
2.09
2.07
2.07
0.97
0.90
5.91
1.96
1.99
13
12
11
10
9
8
7
6
5
4
3
2
1
0
-1
f1 (ppm)

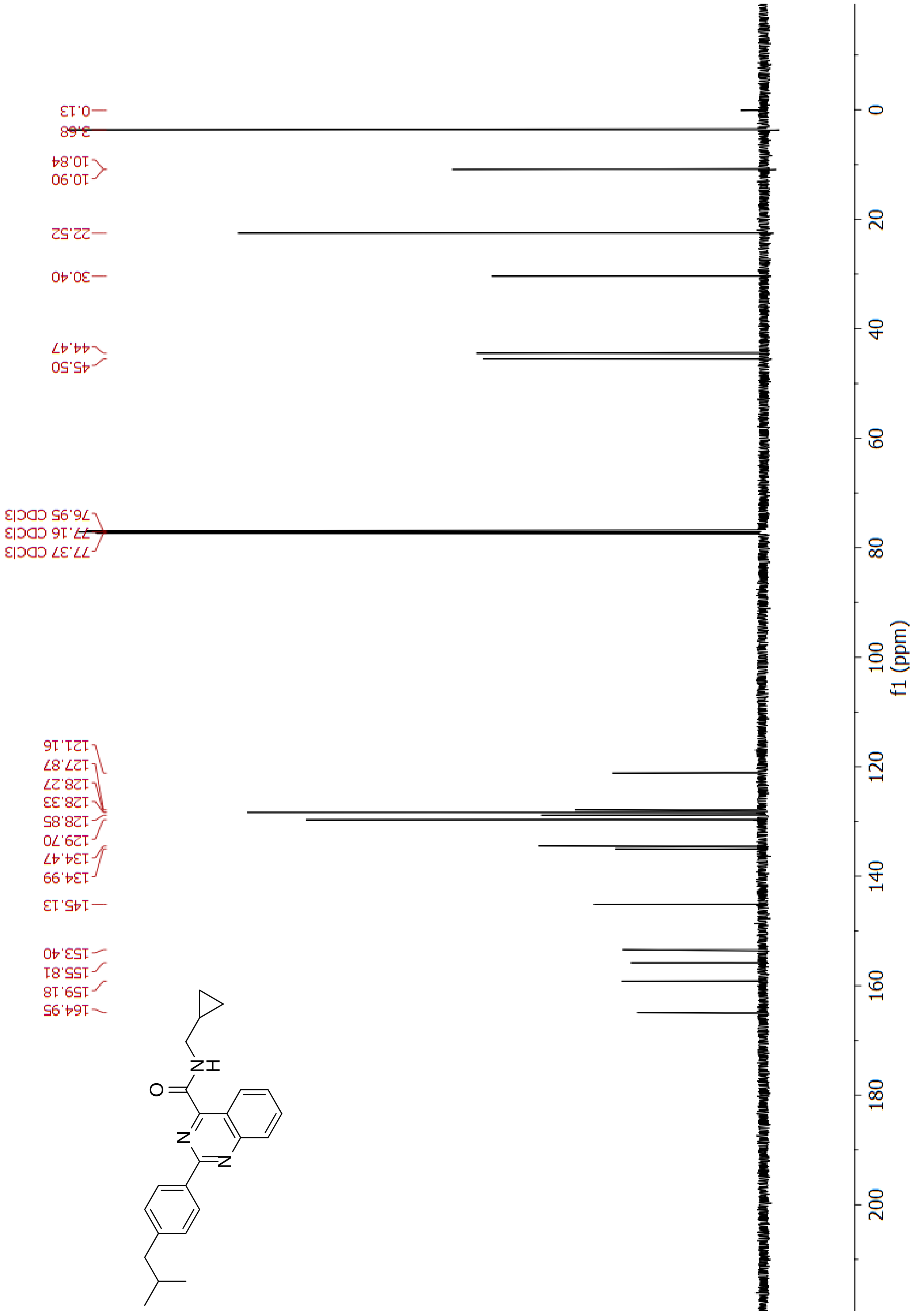
0.13
3.68
10.84
10.90
22.52
30.40
44.47
45.50
76.95 CDCl3
77.16 CDCl3
77.37 CDCl3
121.16
127.87
128.27
128.33
128.85
129.70
134.47
134.99
145.13
153.40
155.81
159.18
164.95
O
NH
N
N
0
20
40
60
80
100
120
140
160
180
200
f1 (ppm)

HPLC trace

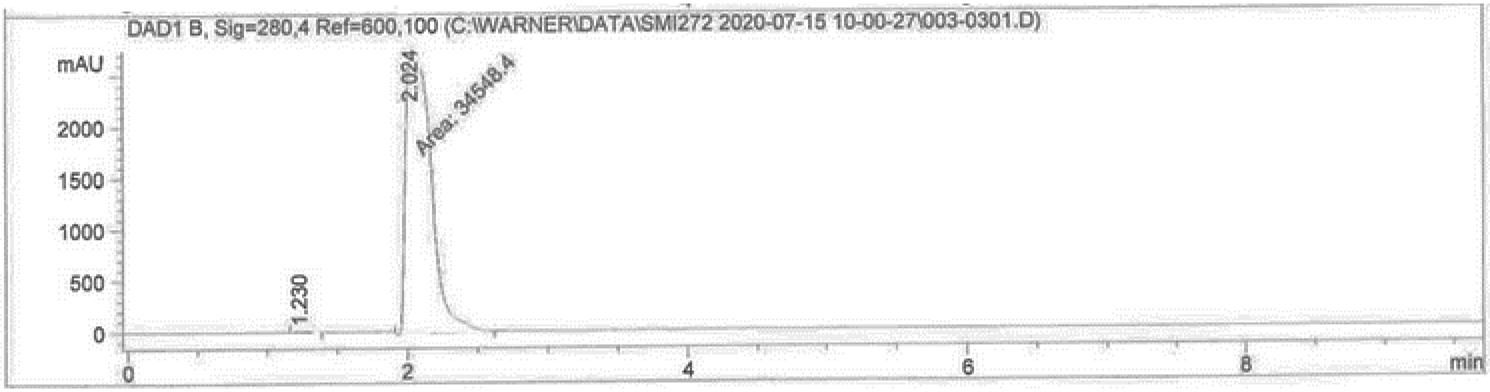

```
Signal 2: DAD1 B, Sig=280,4 Ref=600,100

Peak RetTime Type  Width     Area      Height     Area
  #   [min]        [min]   [mAU*s]     [mAU]        %
----|-------|----|-------|----------|----------|--------|
   1   1.230 BV    0.0622   27.02910    6.54535   0.0782
   2   2.024 MM    0.2174 3.45484e4  2648.44165  99.9218
```

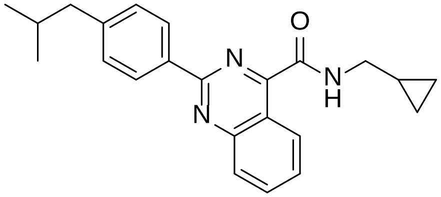

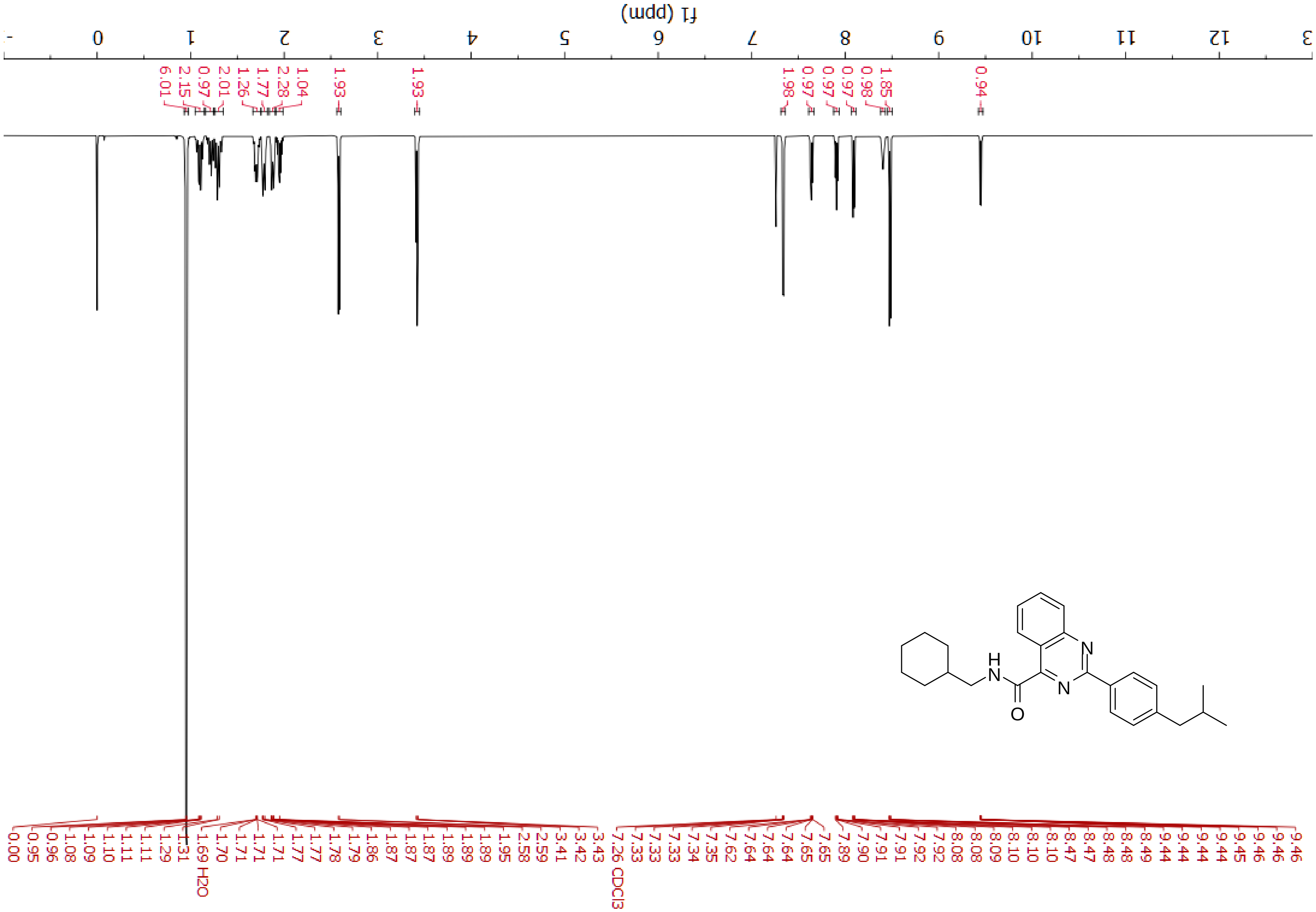
0.00
0.95
0.96
1.08
1.09
1.10
1.11
1.11
1.29
1.31
1.69 H2O
1.70
1.71
1.71
1.71
1.77
1.77
1.78
1.79
1.86
1.87
1.87
1.87
1.89
1.89
1.89
1.95
2.58
2.59
3.41
3.42
3.43
7.26 CDCl3
7.33
7.33
7.33
7.34
7.35
7.62
7.64
7.64
7.64
7.65
7.65
7.89
7.90
7.91
7.91
7.92
7.92
8.08
8.08
8.09
8.10
8.10
8.10
8.47
8.47
8.48
8.48
8.49
9.44
9.44
9.44
9.44
9.45
9.46
9.46
9.46
6.01
2.15
0.97
2.01
1.26
1.77
2.28
1.04
1.93
1.93
1.98
0.97
0.97
0.97
0.98
1.85
0.94
0
1
2
3
4
5
6
7
8
9
10
11
12
3
f1 (ppm)
N
N
H
N
O

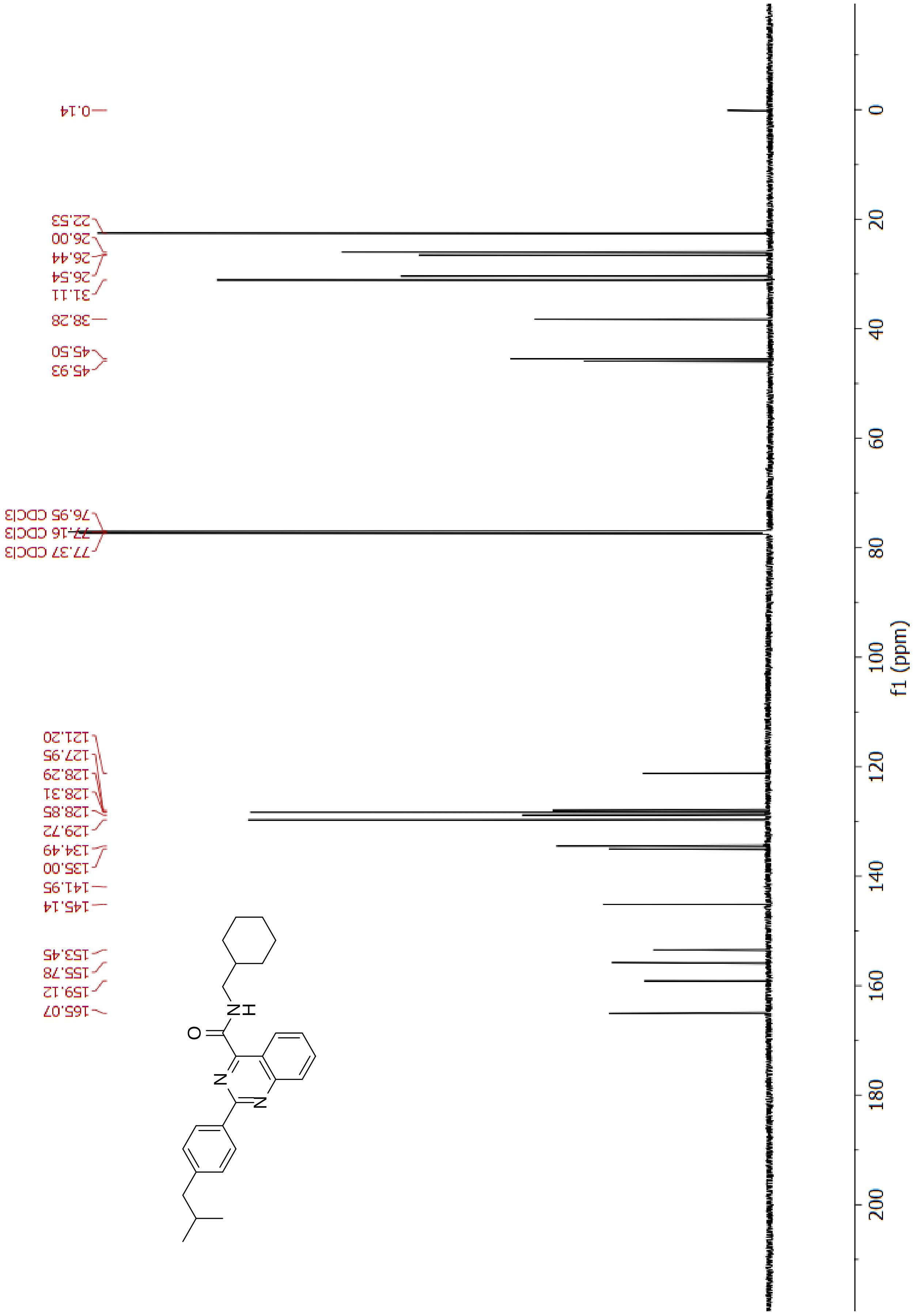
0.14
22.53
26.00
26.44
26.54
31.11
38.28
45.50
45.93
76.95 CDCl3
77.16 CDCl3
77.37 CDCl3
121.20
127.95
128.29
128.31
128.85
129.72
134.49
135.00
141.95
145.14
153.45
155.78
159.12
165.07
NH
O
N
N
0
20
40
60
80
100
120
140
160
180
200
f1 (ppm)

HPLC trace

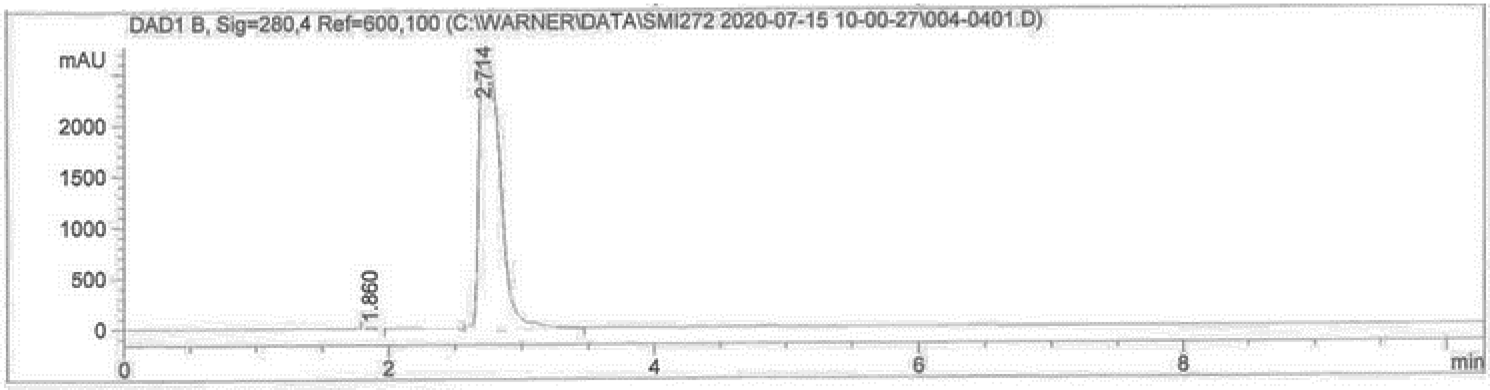

```
Signal 2: DAD1 B, Sig=280,4 Ref=600,100

Peak RetTime Type  Width     Area      Height     Area
  #   [min]        [min]   [mAU*s]     [mAU]        %
----|-------|----|-------|----------|----------|--------|
   1   1.860 BB    0.0601   20.58248    5.20420   0.0675
   2   2.714 BB    0.1854 3.04509e4 2662.19165  99.9325
```

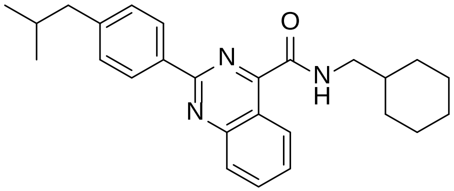

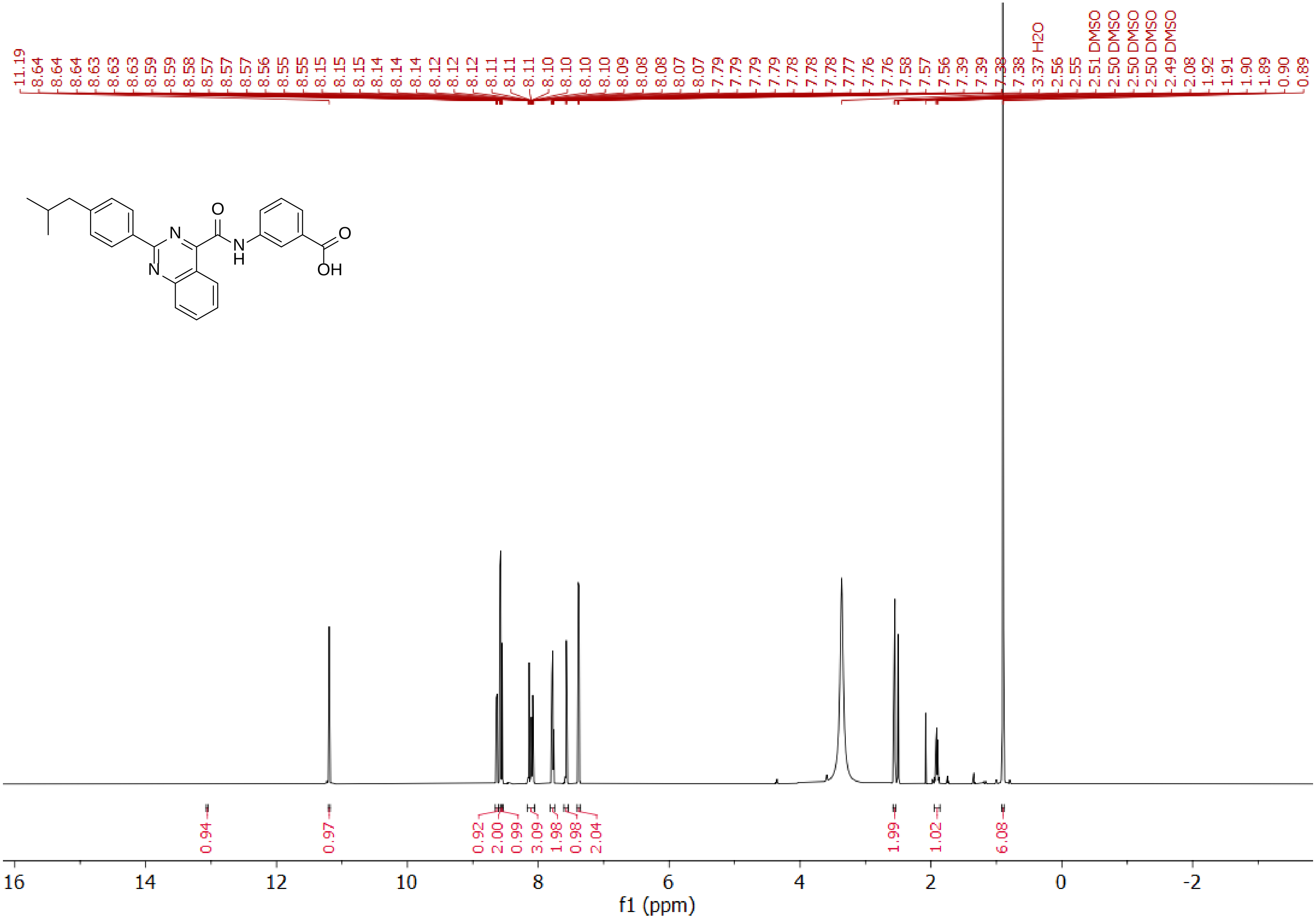
11.19
8.64
8.64
8.64
8.63
8.63
8.63
8.59
8.59
8.58
8.57
8.57
8.57
8.56
8.55
8.55
8.15
8.15
8.15
8.14
8.14
8.14
8.12
8.12
8.12
8.11
8.11
8.11
8.10
8.10
8.10
8.10
8.09
8.08
8.08
8.07
8.07
7.79
7.79
7.79
7.79
7.78
7.78
7.78
7.77
7.76
7.76
7.58
7.57
7.56
7.39
7.39
7.38
7.38
3.37 H2O
2.56
2.55
2.51 DMSO
2.50 DMSO
2.50 DMSO
2.50 DMSO
2.49 DMSO
2.08
1.92
1.91
1.90
1.89
0.90
0.89
O
N
N
H
N
O
OH
0.94
0.97
0.92
2.00
0.99
3.09
1.98
0.98
2.04
1.99
1.02
6.08
16
14
12
10
8
6
4
2
0
-2
f1 (ppm)

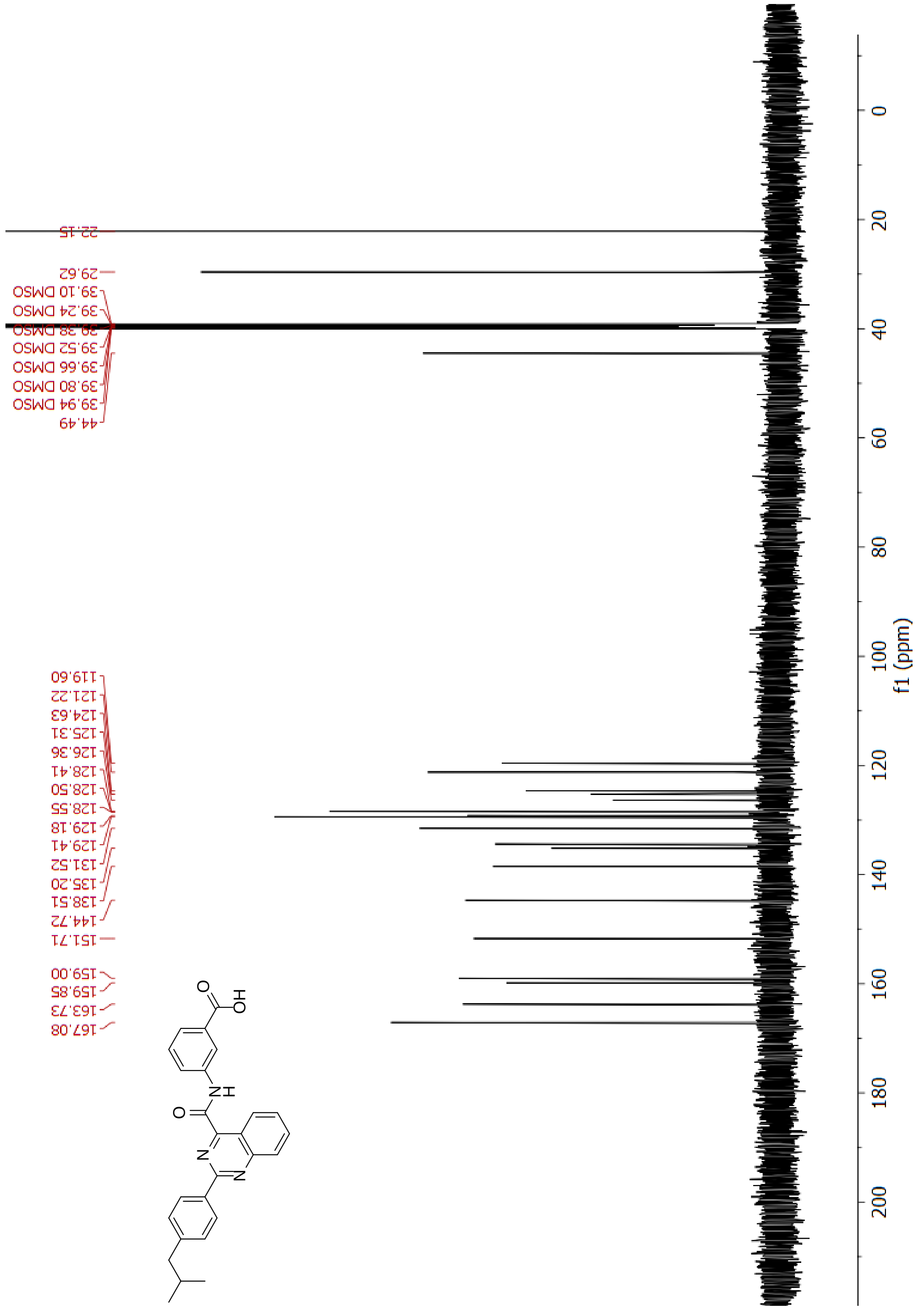
22.15
29.62
39.10 DMSO
39.24 DMSO
39.38 DMSO
39.52 DMSO
39.66 DMSO
39.80 DMSO
39.94 DMSO
44.49
119.60
121.22
124.63
125.31
126.36
128.41
128.50
128.55
129.18
129.41
131.52
135.20
138.51
144.72
151.71
159.00
159.85
163.73
167.08
0
20
40
60
80
100
120
140
160
180
200
f1 (ppm)
N
N
O
H
N
O
OH

HPLC trace

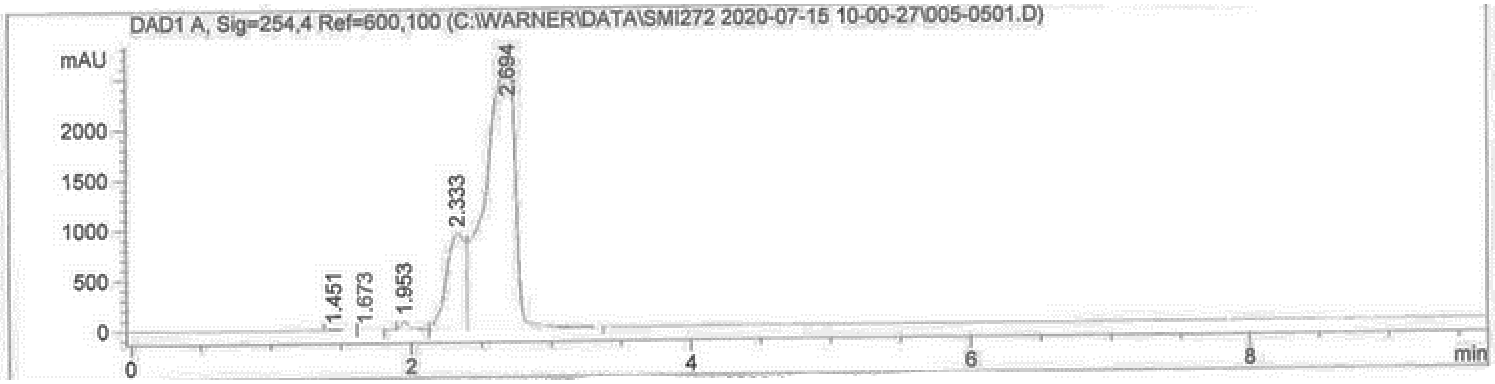

```
Signal 1: DAD1 A, Sig=254,4 Ref=600,100

Peak RetTime Type  Width     Area      Height     Area
  #   [min]        [min]   [mAU*s]     [mAU]       %
----|-------|----|-------|----------|----------|--------|
   1   1.451 BV    0.0731   34.17477    6.74782   0.0705
   2   1.673 VB    0.1266   15.45750    1.69225   0.0319
   3   1.953 BV    0.0569  330.67102   85.95543   0.6822
   4   2.333 VV    0.1411 8750.82129  952.85620  18.0541
   5   2.694 VB    0.2006 3.93390e4  2690.05005  81.1613
```

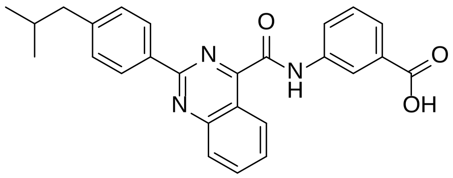

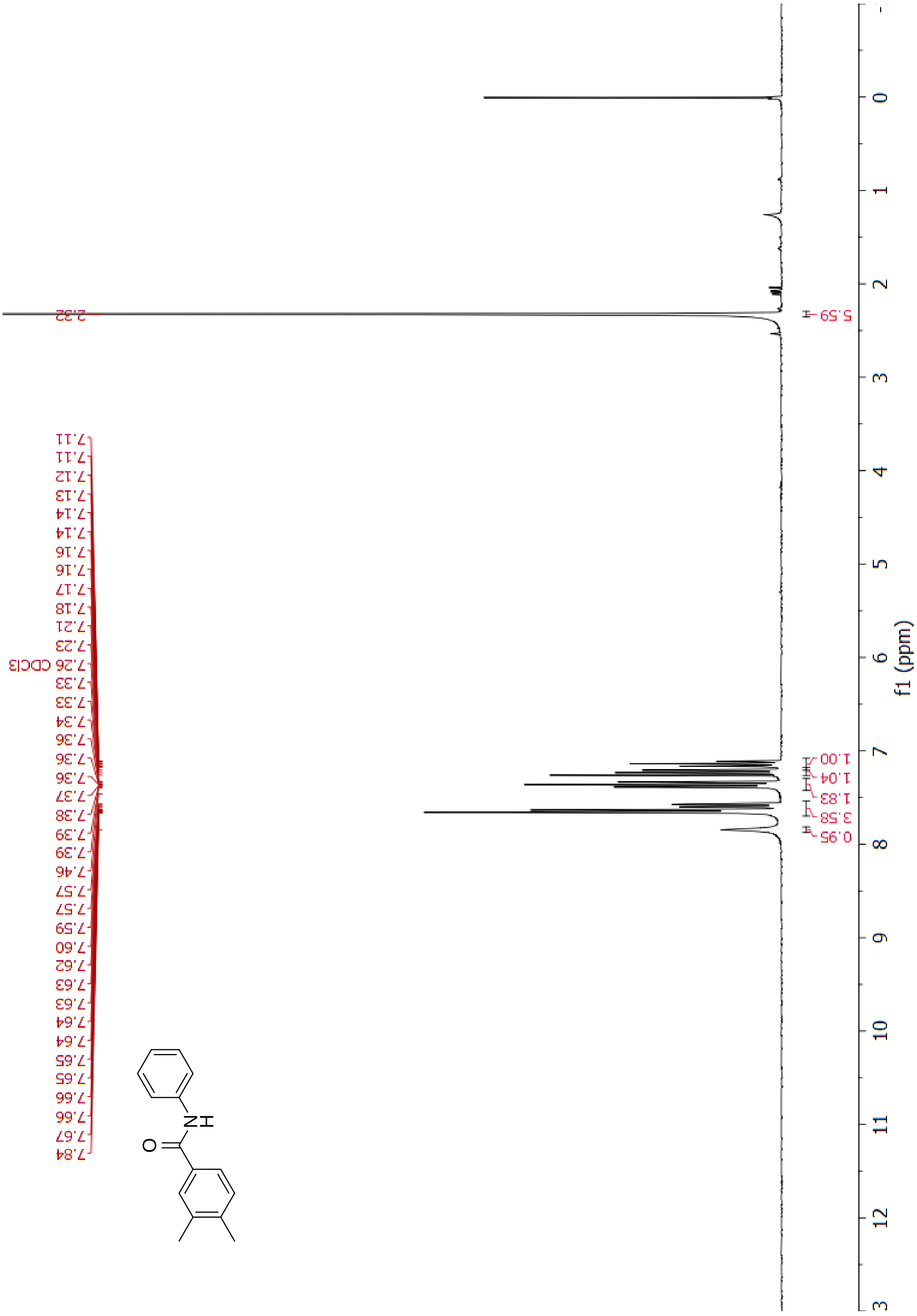
7.84
7.67
7.66
7.66
7.65
7.65
7.64
7.64
7.63
7.63
7.62
7.60
7.59
7.57
7.57
7.46
7.39
7.39
7.38
7.37
7.36
7.36
7.36
7.34
7.33
7.33
7.26 CDCl3
7.23
7.21
7.18
7.17
7.16
7.16
7.14
7.14
7.13
7.12
7.11
7.11
2.32
0.95
3.58
1.83
1.04
1.00
5.59
O
NH
13
12
11
10
9
8
7
6
5
4
3
2
1
0
-1
f1 (ppm)

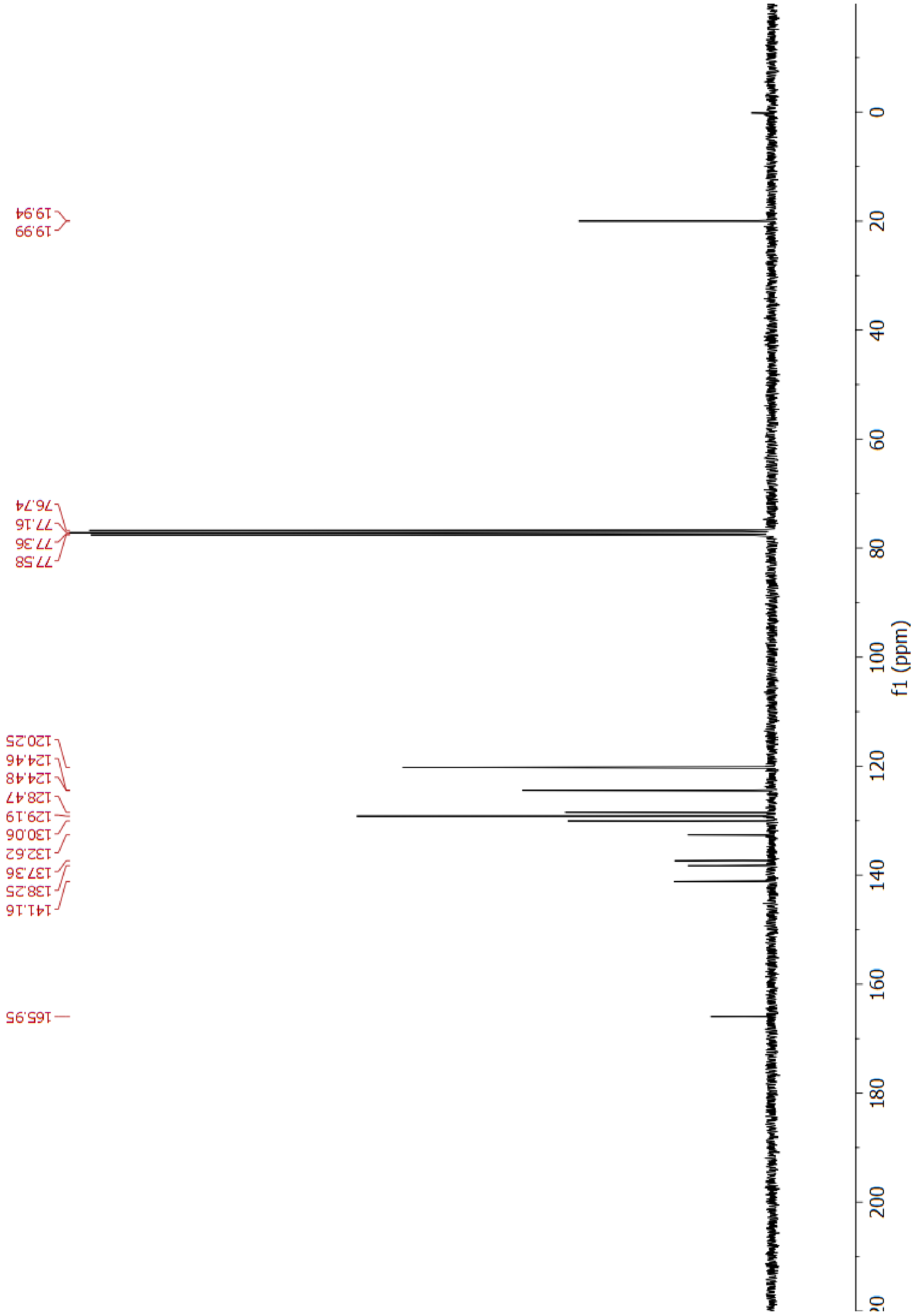
19.94
19.99
76.74
77.16
77.36
77.58
120.25
124.46
124.48
128.47
129.19
130.06
132.62
137.36
138.25
141.16
165.95
0
20
40
60
80
100
120
140
160
180
200
f1 (ppm)

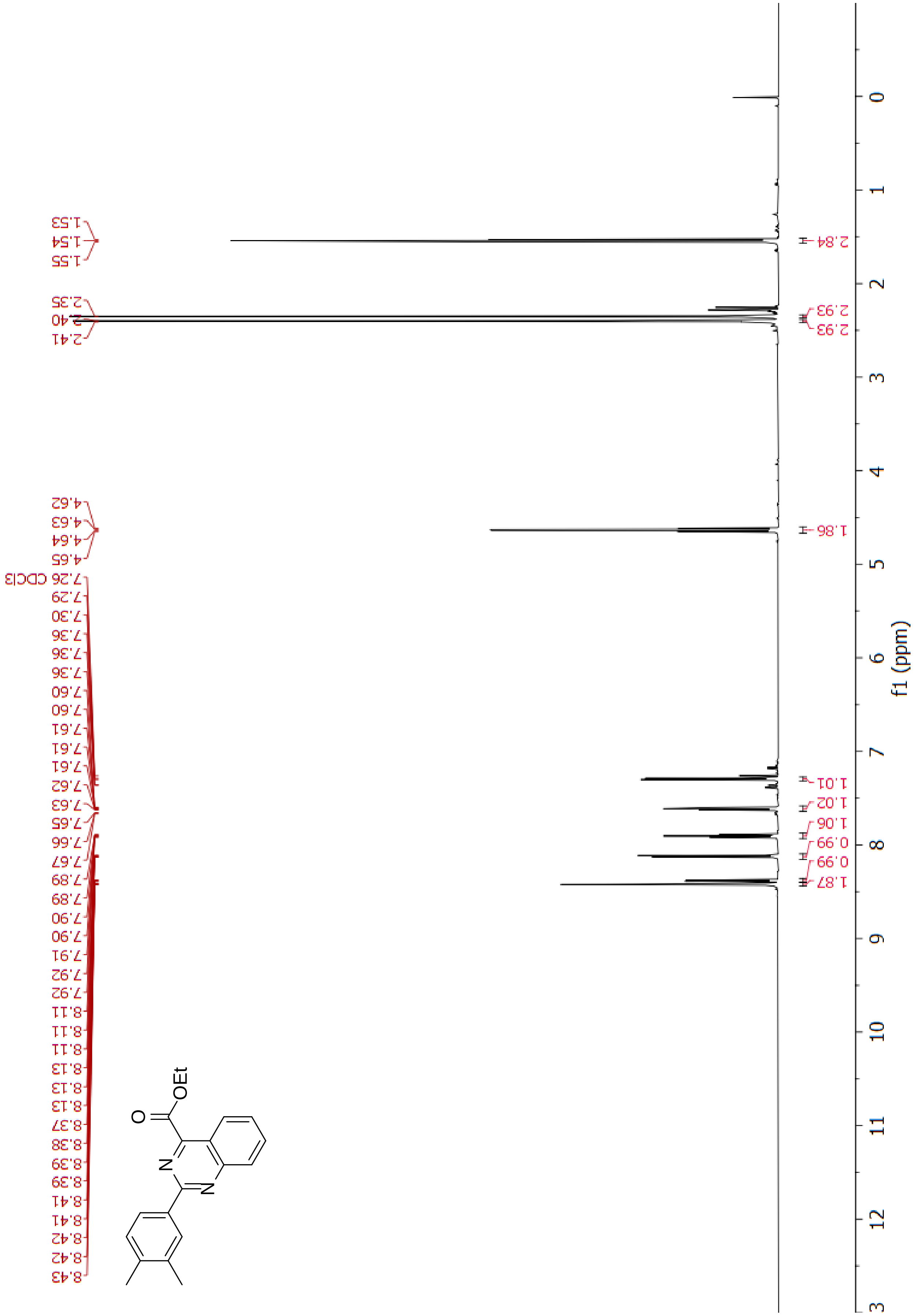
1.53
1.54
1.55
2.35
2.40
2.41
4.62
4.63
4.64
4.65
7.26 CDCl3
7.29
7.30
7.36
7.36
7.36
7.60
7.60
7.61
7.61
7.61
7.62
7.63
7.65
7.66
7.67
7.89
7.89
7.90
7.90
7.91
7.92
7.92
8.11
8.11
8.11
8.13
8.13
8.13
8.37
8.38
8.39
8.39
8.41
8.41
8.42
8.42
8.43
2.84
2.93
2.93
1.86
1.01
1.02
1.06
0.99
0.99
1.87
0
1
2
3
4
5
6
7
8
9
10
11
12
f1 (ppm)
O
OEt
N
N

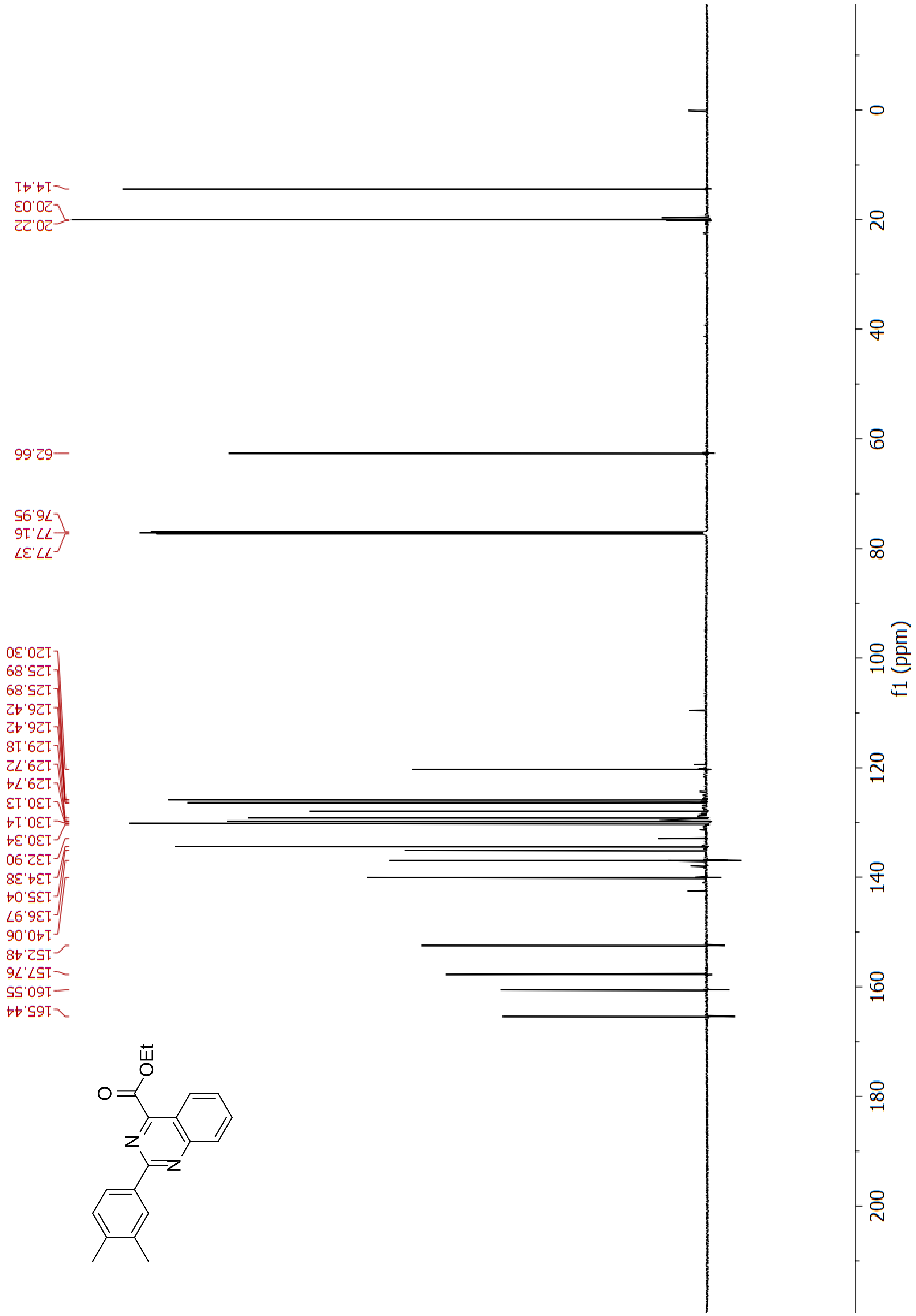
14.41
20.03
20.22
62.66
76.95
77.16
77.37
120.30
125.89
125.89
126.42
126.42
129.18
129.72
129.74
130.13
130.14
130.34
132.90
134.38
135.04
136.97
140.06
152.48
157.76
160.55
165.44
O
OEt
N
N
0
20
40
60
80
100
120
140
160
180
200
f1 (ppm)

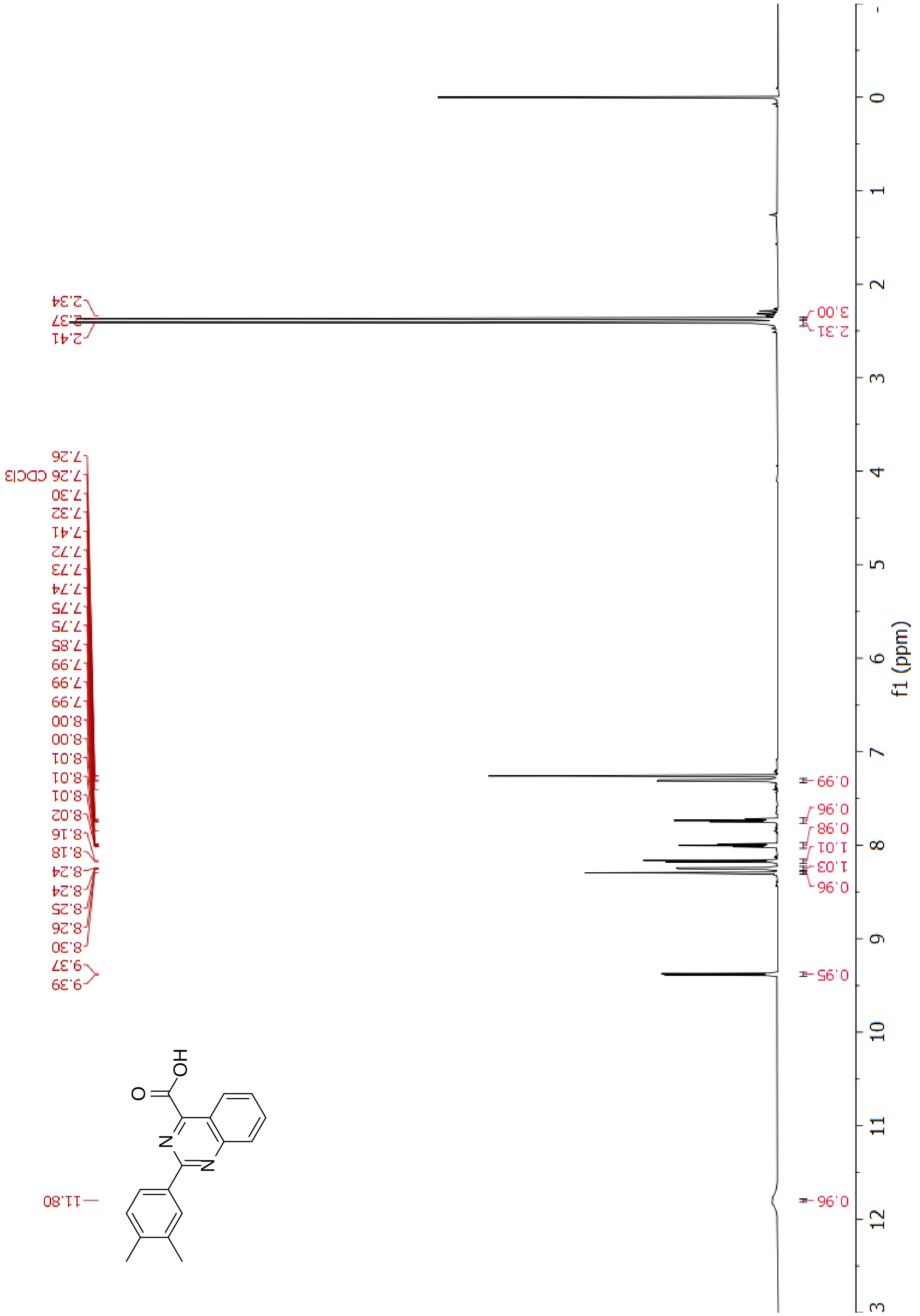
11.80
9.39
9.37
8.30
8.26
8.25
8.24
8.24
8.18
8.16
8.02
8.01
8.01
8.01
8.00
8.00
7.99
7.99
7.99
7.85
7.75
7.75
7.74
7.73
7.72
7.41
7.32
7.30
7.26 CDCl3
7.26
2.41
2.37
2.34
0.96
0.95
0.96
1.03
1.01
0.98
0.96
0.99
2.31
3.00
O
OH
N
N
f1 (ppm)
0
1
2
3
4
5
6
7
8
9
10
11
12

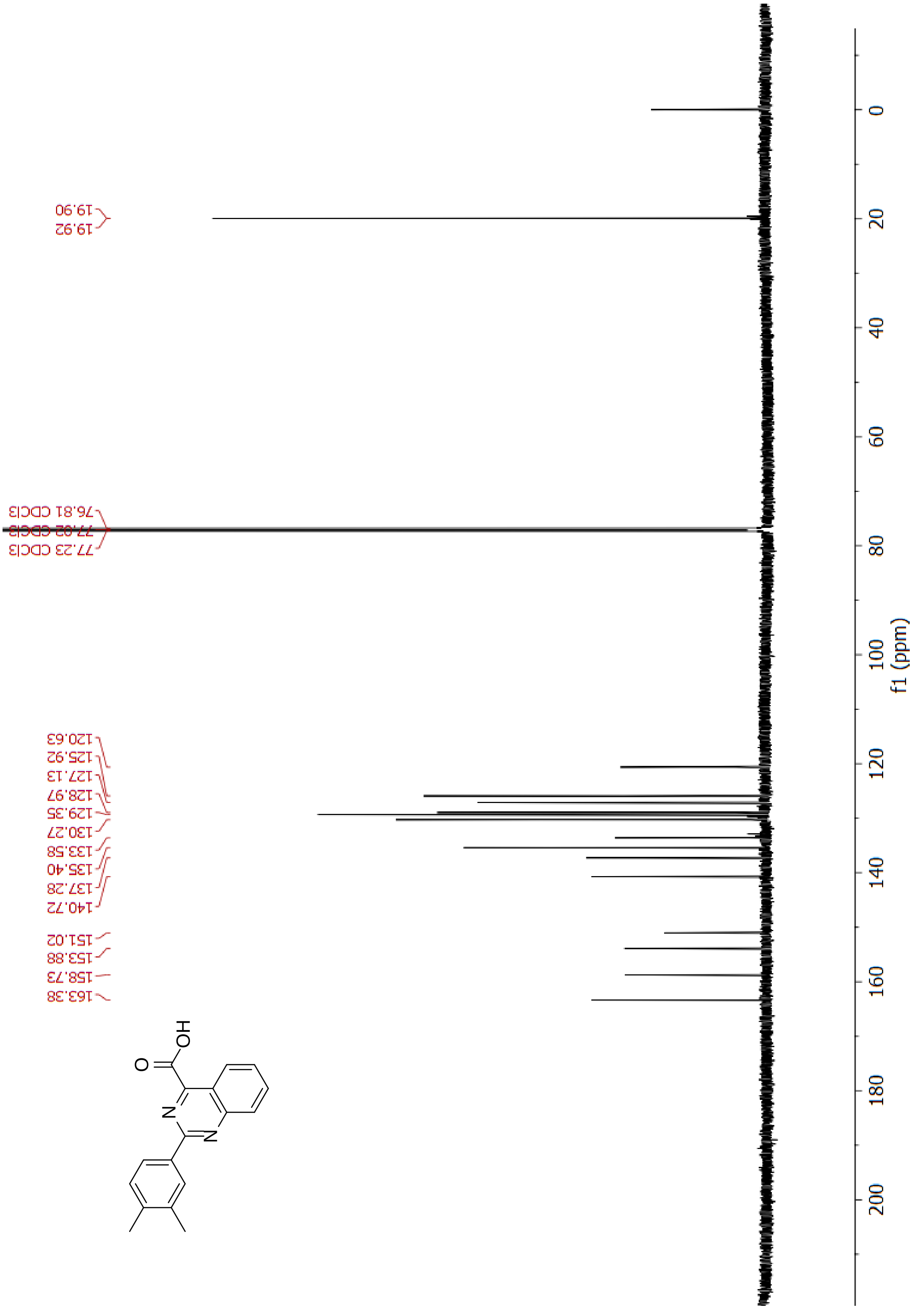
19.90
19.92
76.81 CDCl3
77.02 CDCl3
77.23 CDCl3
120.63
125.92
127.13
128.97
129.35
130.27
133.58
135.40
137.28
140.72
151.02
153.88
158.73
163.38
N
N
O
OH
0
20
40
60
80
100
120
140
160
180
200
f1 (ppm)

HPLC trace

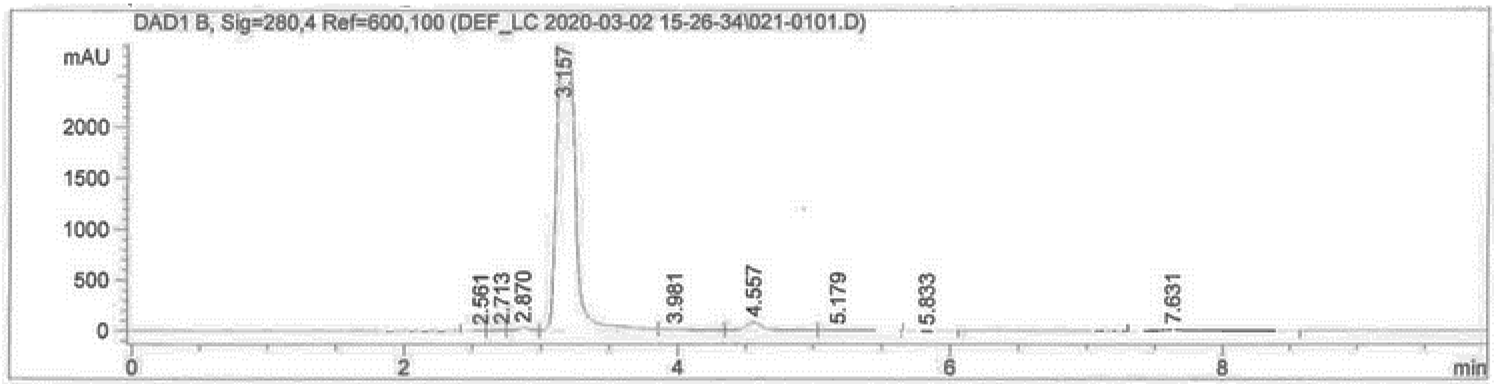

```
Signal 2: DAD1 B, Sig=280,4 Ref=600,100

Peak RetTime Type  Width     Area      Height     Area
  #   [min]        [min]   [mAU*s]     [mAU]        %
----|-------|----|-------|----------|----------|--------|
   1   2.561 BV    0.0823    7.06684    1.24321   0.0248
   2   2.713 VV    0.1091   43.47208    6.57417   0.1525
   3   2.870 VV    0.1064  209.46425   27.03316   0.7346
   4   3.157 VV    0.1598 2.65014e4  2670.42676  92.9409
   5   3.981 VV    0.2230  323.02701   18.74750   1.1329
   6   4.557 VB    0.1415  796.28186   80.45106   2.7926
   7   5.179 BB    0.2771  108.62189    5.04595   0.3809
   8   5.833 BB    0.1852   23.94635    1.82349   0.0840
   9   7.631 BB    0.4730  500.98425   15.26196   1.7570
```

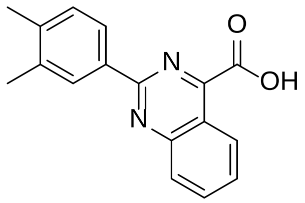

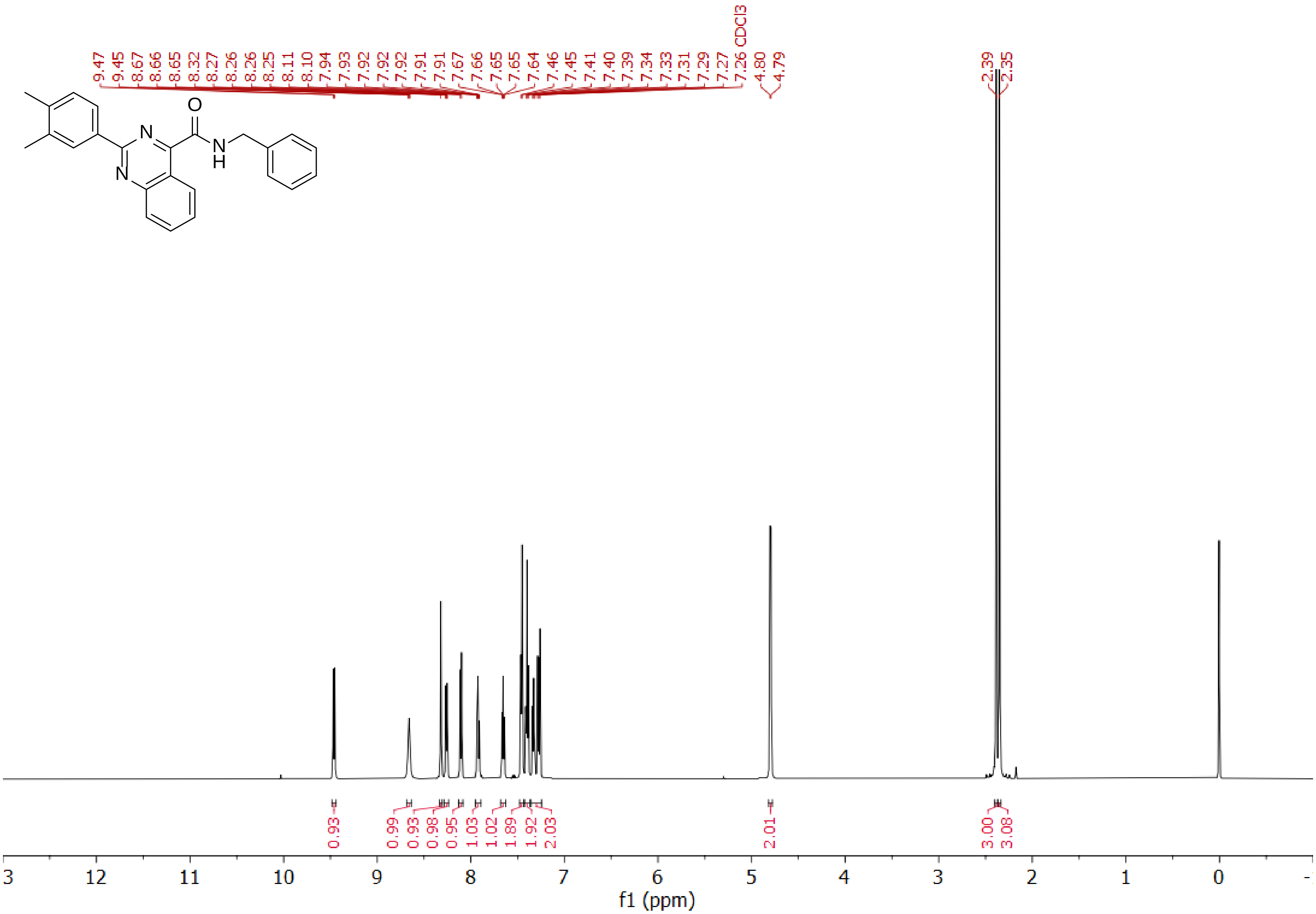
9.47
9.45
8.67
8.66
8.65
8.32
8.27
8.26
8.26
8.25
8.11
8.10
7.94
7.93
7.92
7.92
7.92
7.91
7.91
7.67
7.66
7.65
7.65
7.64
7.46
7.45
7.41
7.40
7.39
7.34
7.33
7.31
7.29
7.27
7.26 CDCl3
4.80
4.79
2.39
2.35
O
N
N
H
0.93
0.99
0.93
0.98
0.95
1.03
1.02
1.89
1.92
2.03
2.01
3.00
3.08
3
12
11
10
9
8
7
6
5
4
3
2
1
0
f1 (ppm)

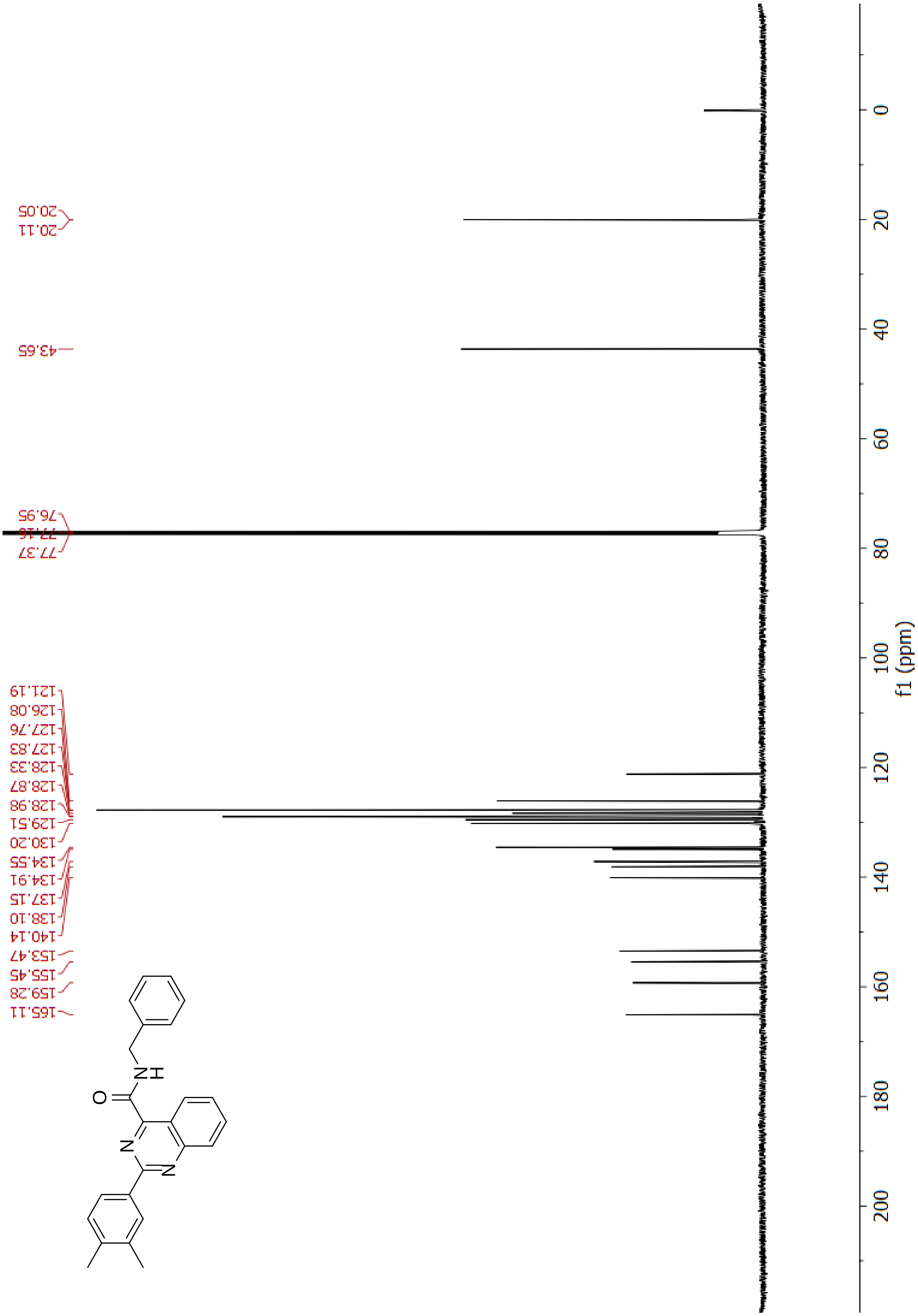
20.05
20.11
43.65
76.95
77.16
77.37
121.19
126.08
127.76
127.83
128.33
128.87
128.98
129.51
130.20
134.55
134.91
137.15
138.10
140.14
153.47
155.45
159.28
165.11
O
NH
N
N
0
20
40
60
80
100
120
140
160
180
200
f1 (ppm)

HPLC trace

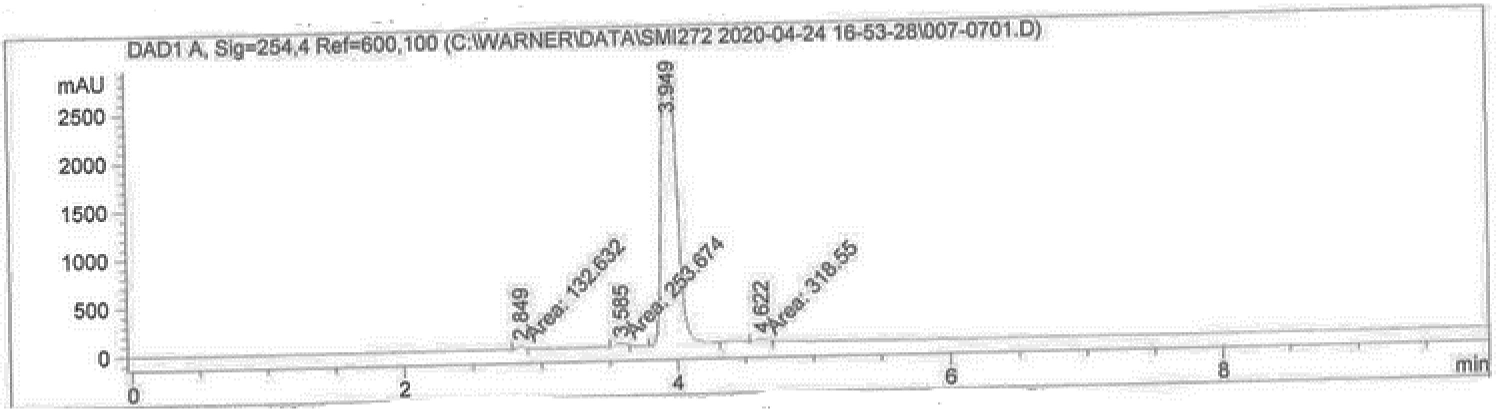

```
Signal 1: DAD1 A, Sig=254,4 Ref=600,100

Peak RetTime Type  Width     Area      Height     Area
  #   [min]        [min]   [mAU*s]     [mAU]        %
----|-------|----|-------|----------|----------|--------|
   1   2.849 MM    0.0702  132.63164   31.47556   0.5541
   2   3.585 MM    0.1019  253.67380   41.49988   1.0597
   3   3.949 VV    0.1326 2.32336e4  2806.16138  97.0556
   4   4.622 MM    0.1254  318.55011   42.32108   1.3307
```

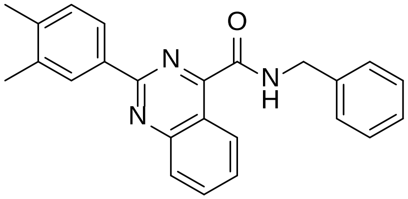

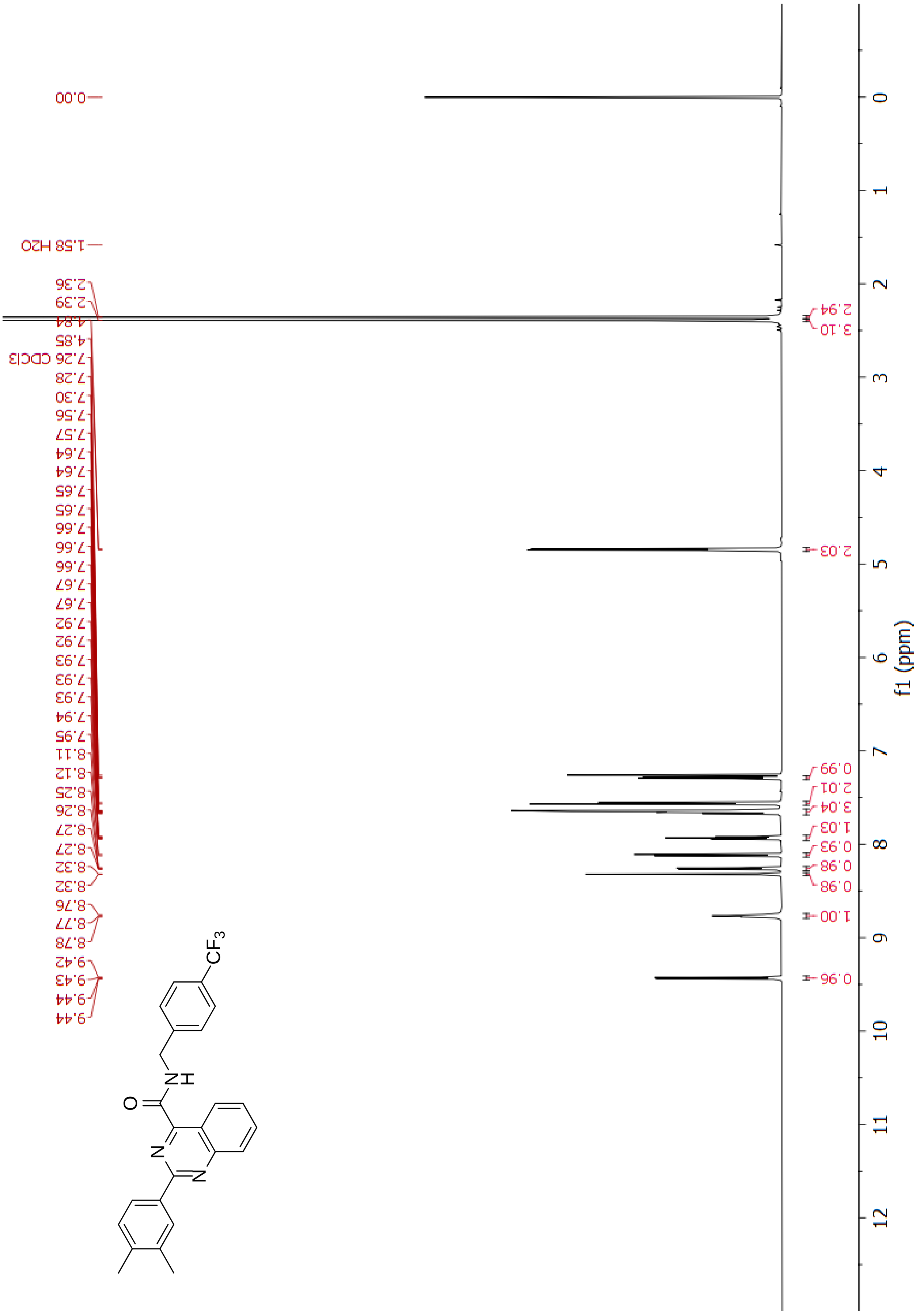
0.00
1.58 H2O
2.36
2.39
4.84
4.85
7.26 CDCl3
7.28
7.30
7.56
7.57
7.64
7.64
7.65
7.65
7.66
7.66
7.66
7.67
7.67
7.92
7.92
7.93
7.93
7.93
7.94
7.95
8.11
8.12
8.25
8.26
8.27
8.27
8.32
8.32
8.76
8.77
8.78
9.42
9.43
9.44
9.44
2.94
3.10
2.03
0.99
2.01
3.04
1.03
0.93
0.98
0.98
1.00
0.96
0
1
2
3
4
5
6
7
8
9
10
11
12
f1 (ppm)
CF3
N
H
O
N
N

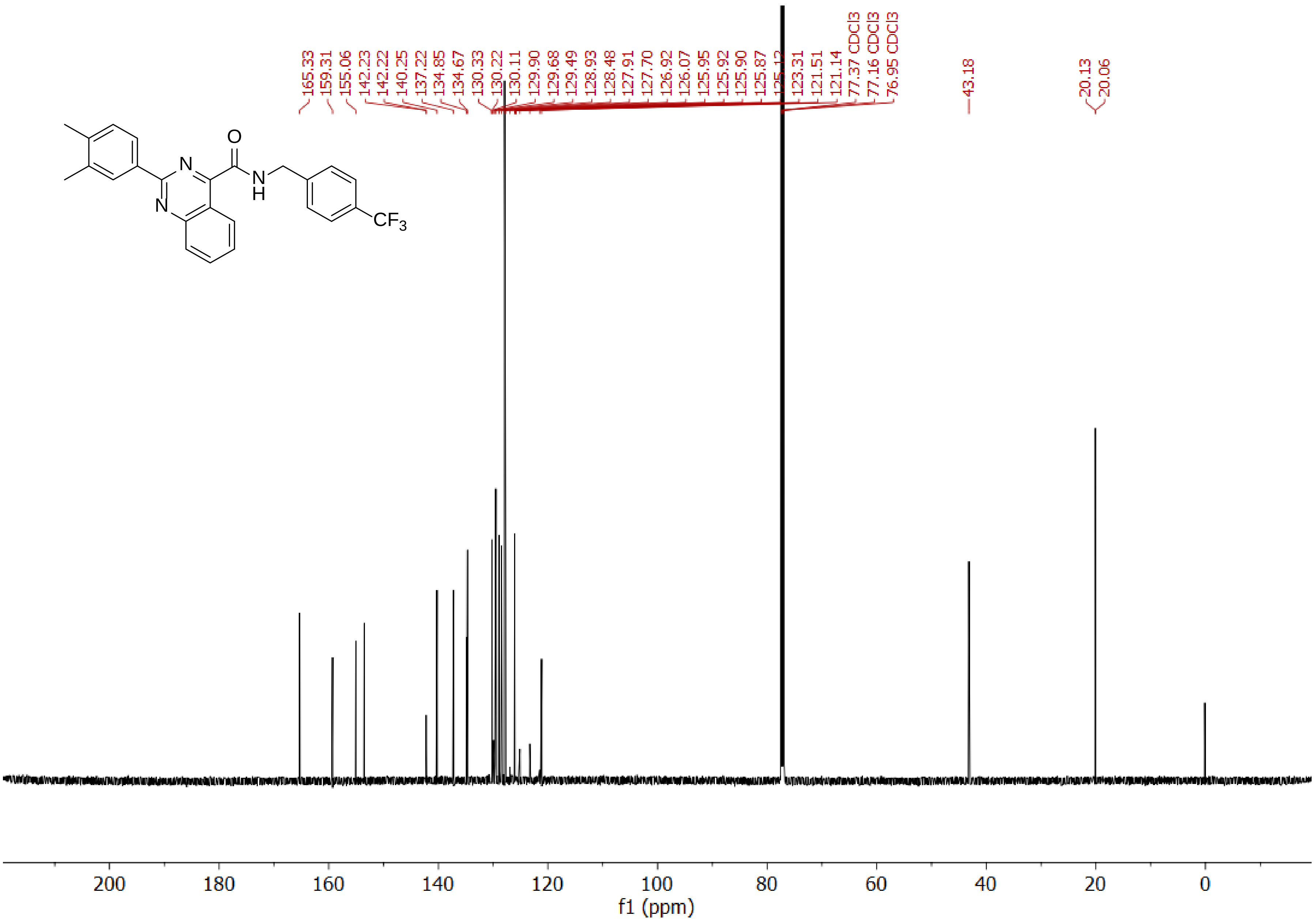
165.33
159.31
155.06
142.23
142.22
140.25
137.22
134.85
134.67
130.33
130.22
130.11
129.90
129.68
129.49
128.93
128.48
127.91
127.70
126.92
126.07
125.95
125.92
125.90
125.87
125.12
123.31
121.51
121.14
77.37 CDCl3
77.16 CDCl3
76.95 CDCl3
43.18
20.13
20.06
N
N
O
N
H
CF_3
200
180
160
140
120
100
80
60
40
20
0
f1 (ppm)

HPLC trace

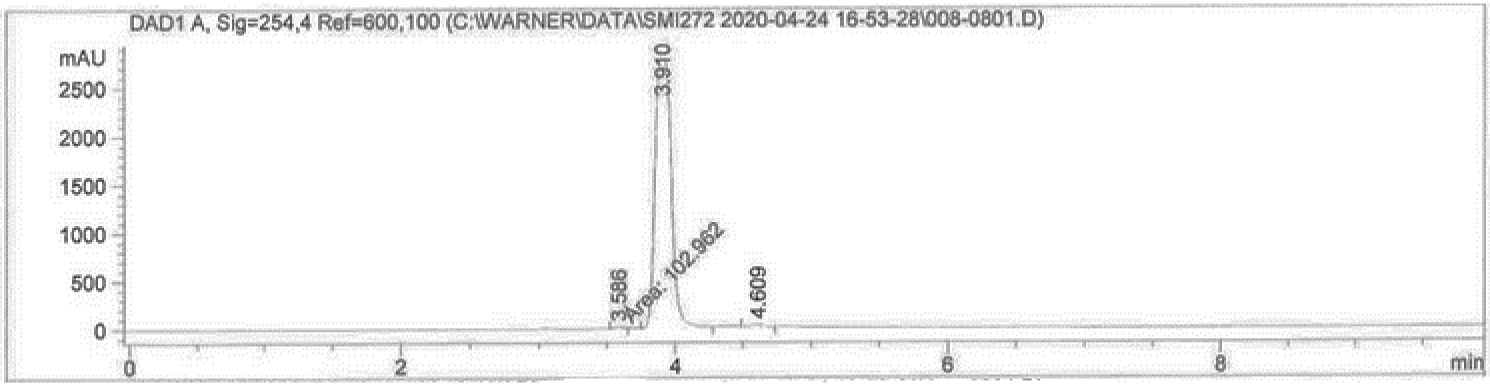

```
Signal 1: DAD1 A, Sig=254,4 Ref=600,100

Peak RetTime Type  Width     Area      Height     Area
  #   [min]        [min]   [mAU*s]     [mAU]        %
----|-------|----|-------|----------|----------|--------|
   1   3.586 MM    0.0952  102.96150   18.02638   0.4343
   2   3.910 VV    0.1325 2.32212e4  2807.19727  97.9434
   3   4.609 VV    0.1441  384.62228   37.98069   1.6223
```

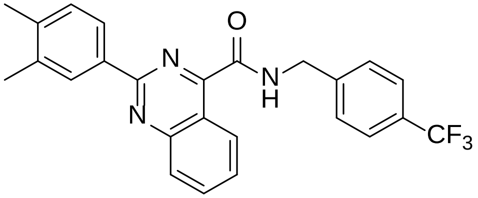

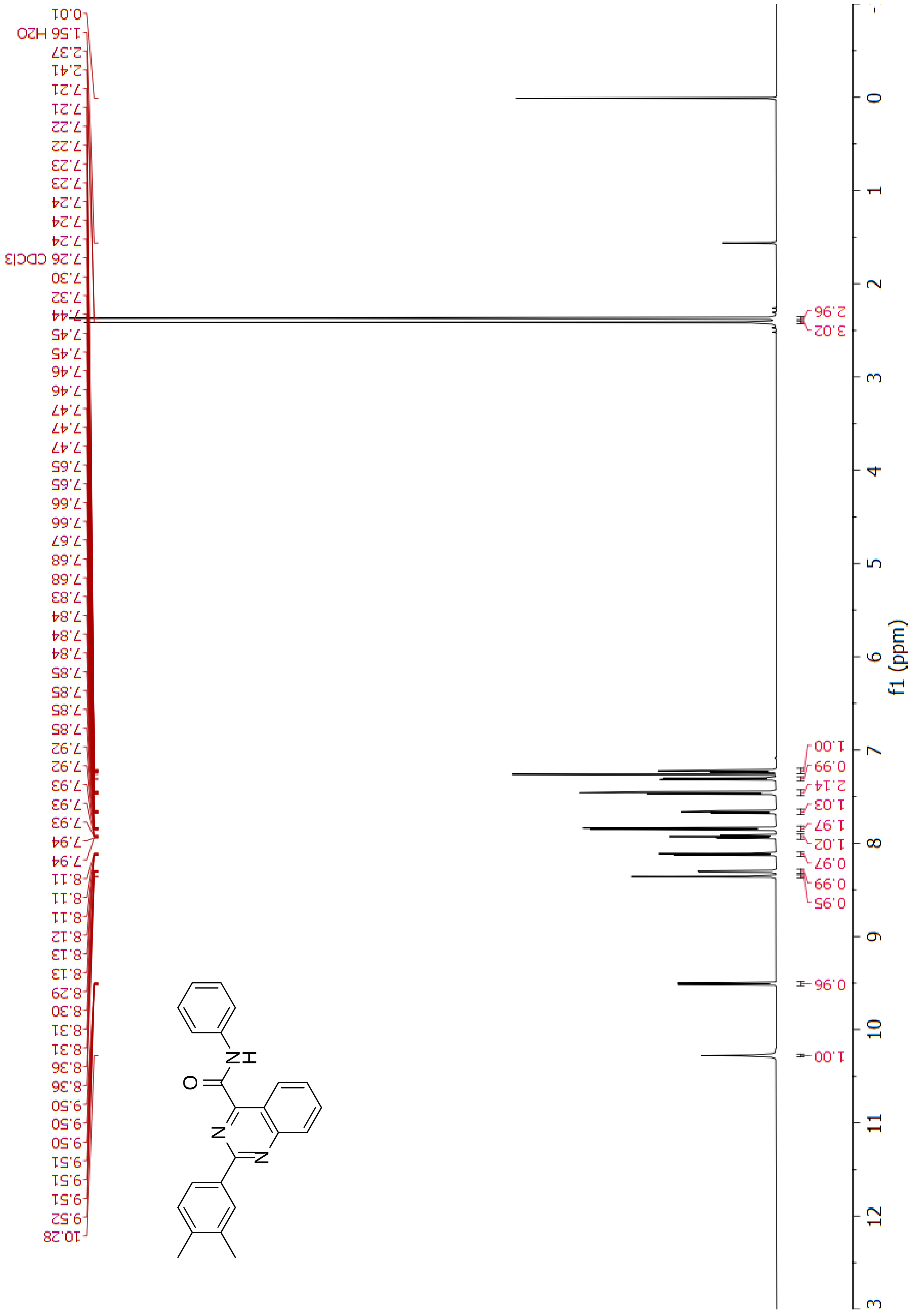
0.01
1.56 H2O
2.37
2.41
7.21
7.21
7.22
7.22
7.23
7.23
7.24
7.24
7.24
7.26 CDCl3
7.30
7.32
7.44
7.45
7.45
7.46
7.46
7.47
7.47
7.47
7.65
7.65
7.66
7.66
7.67
7.68
7.68
7.83
7.84
7.84
7.84
7.85
7.85
7.85
7.85
7.92
7.92
7.93
7.93
7.93
7.94
7.94
8.11
8.11
8.11
8.12
8.13
8.13
8.29
8.30
8.31
8.31
8.36
8.36
9.50
9.50
9.50
9.51
9.51
9.51
9.52
10.28
2.96
3.02
1.00
0.99
2.14
1.03
1.97
1.02
0.97
0.99
0.95
0.96
1.00
-1
0
1
2
3
4
5
6
7
8
9
10
11
12
3
f1 (ppm)
NH
O
N
N

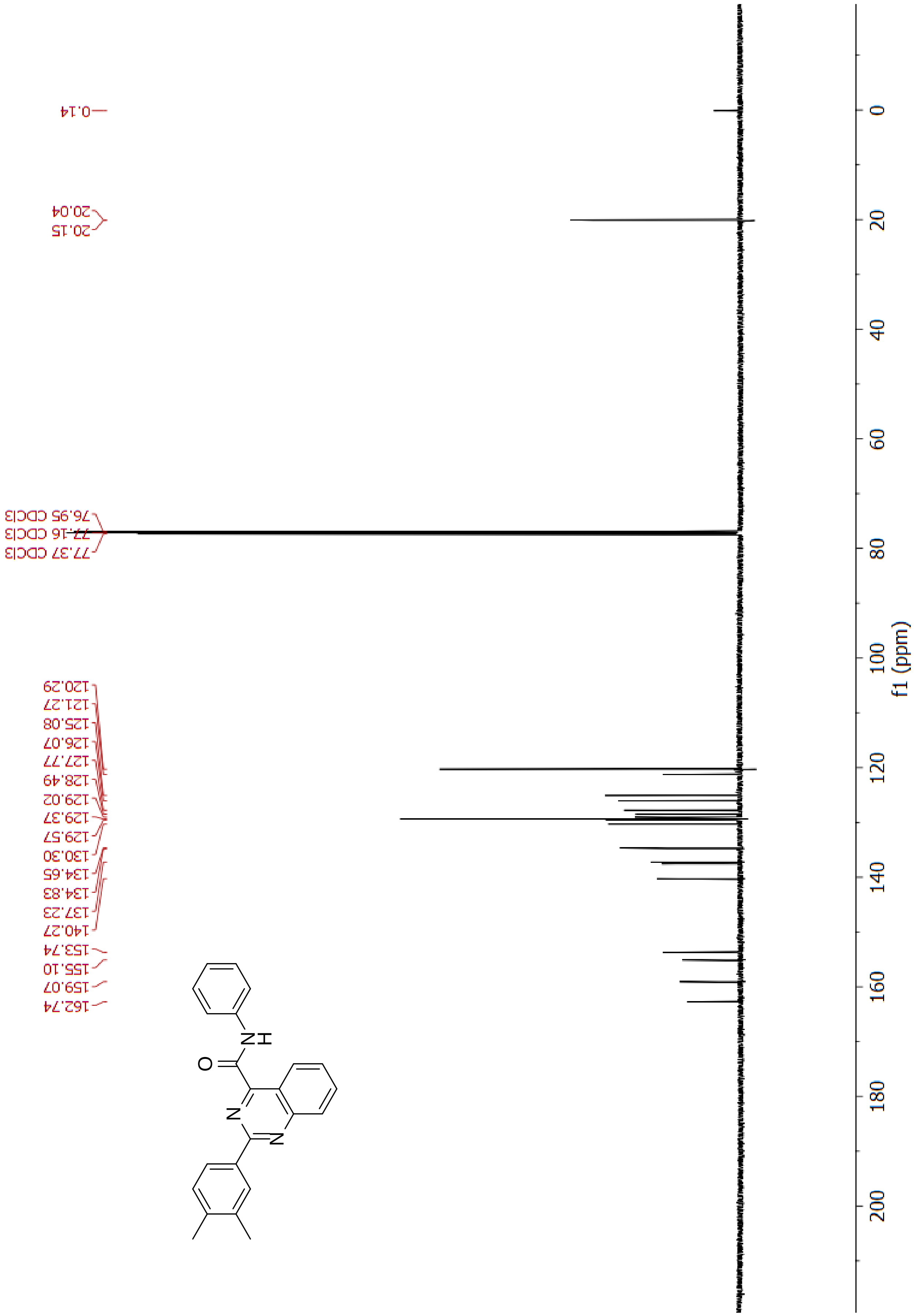
0.14
20.04
20.15
76.95 CDCl3
77.16 CDCl3
77.37 CDCl3
120.29
121.27
125.08
126.07
127.77
128.49
129.02
129.37
129.57
130.30
134.65
134.83
137.23
140.27
153.74
155.10
159.07
162.74
O
NH
N
N
0
20
40
60
80
100
120
140
160
180
200
f1 (ppm)

HPLC trace

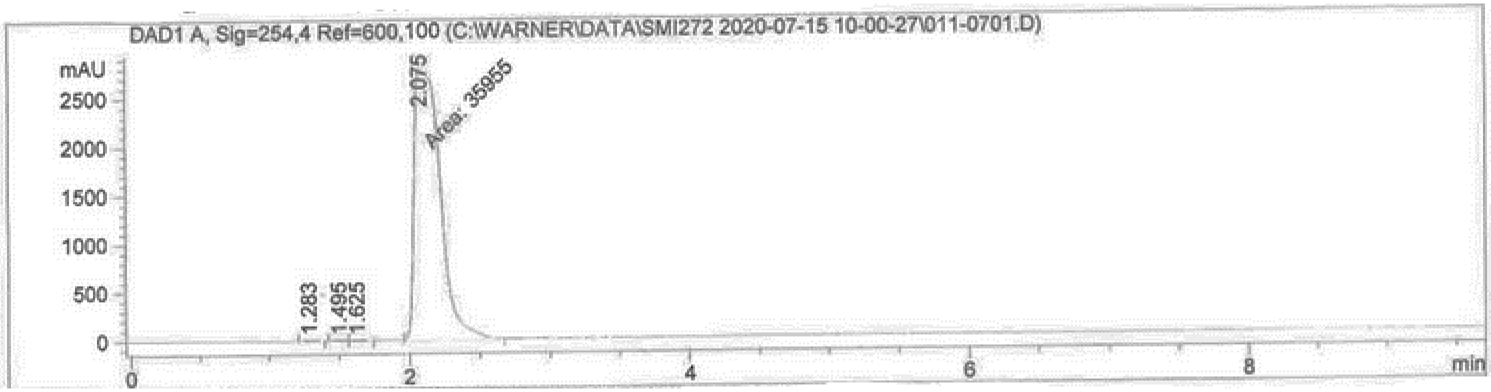

```
Signal 1: DAD1 A, Sig=254,4 Ref=600,100

Peak RetTime Type  Width      Area       Height      Area
  #   [min]        [min]    [mAU*s]      [mAU]        %
----|-------|----|-------|----------|----------|--------|
   1   1.283 BB    0.0635   12.96897    3.05363   0.0360
   2   1.495 BV    0.0678   10.19901    2.21353   0.0283
   3   1.625 VB    0.0669   10.59852    2.33911   0.0294
   4   2.075 MM    0.2128 3.59550e4  2816.52563  99.9062
```

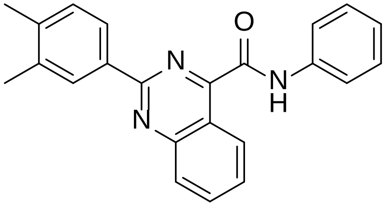

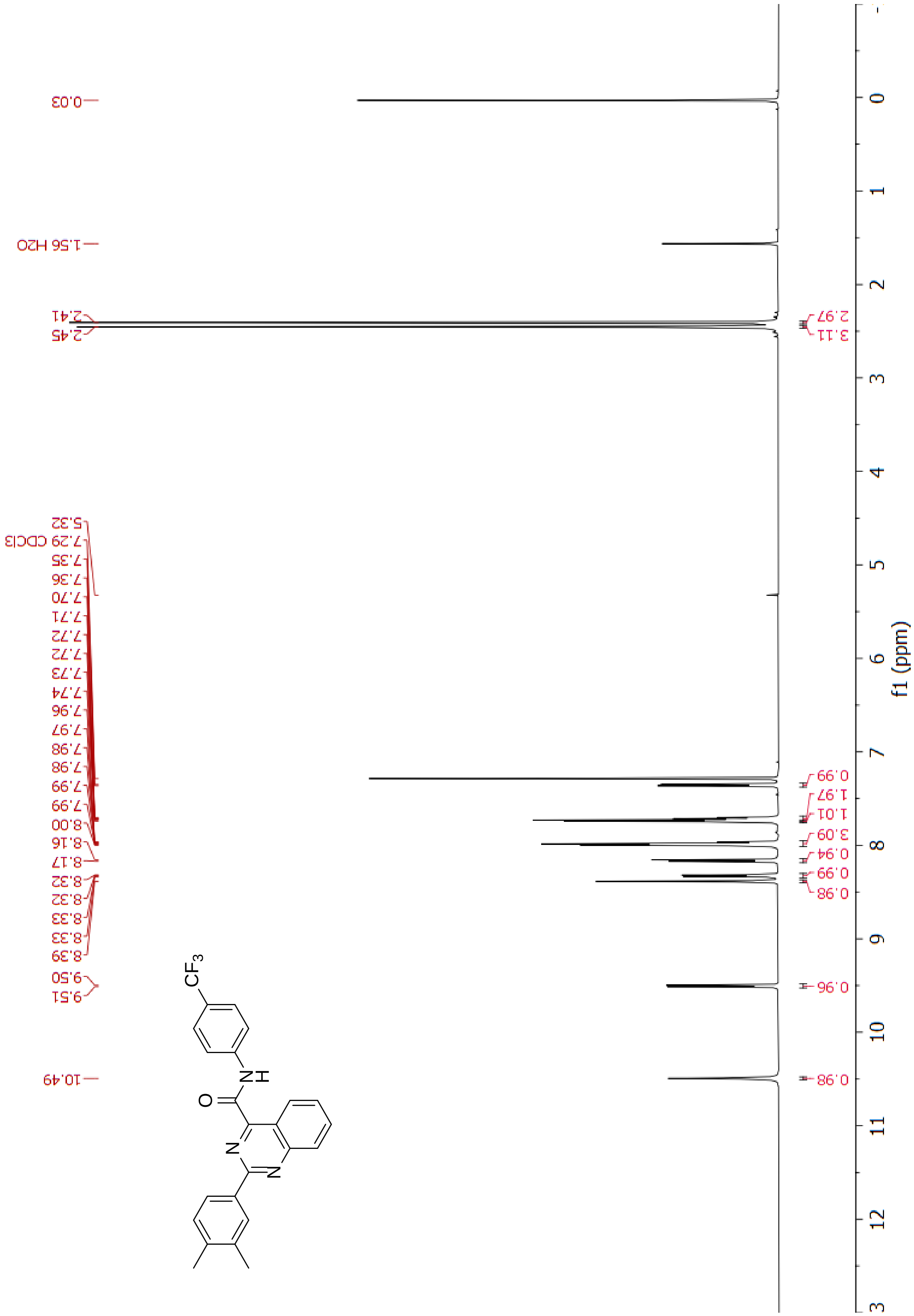

0.03
1.56 H2O
2.41
2.45
5.32
7.29 CDCl3
7.35
7.36
7.70
7.71
7.72
7.72
7.73
7.74
7.96
7.97
7.98
7.98
7.99
7.99
8.00
8.16
8.17
8.32
8.32
8.33
8.33
8.39
9.50
9.51
10.49
2.97
3.11
0.99
1.97
1.01
3.09
0.94
0.99
0.98
0.96
0.98
CF$_3$
NH
O
N
N
f1 (ppm)
13
12
11
10
9
8
7
6
5
4
3
2
1
0
-1

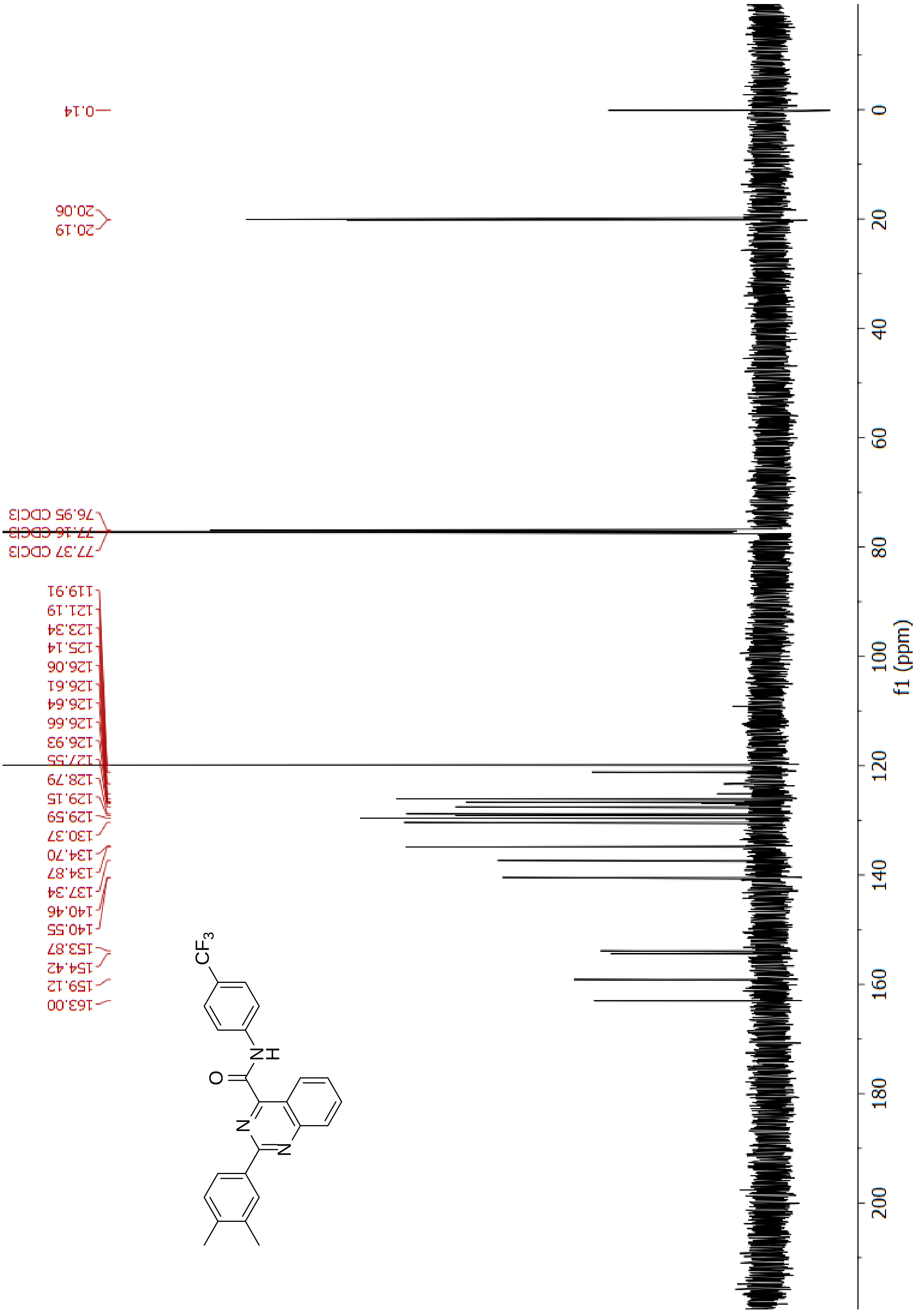
0.14
20.06
20.19
76.95 CDCl3
77.16 CDCl3
77.37 CDCl3
119.91
121.19
123.34
125.14
126.06
126.61
126.64
126.66
126.93
127.55
128.79
129.15
129.59
130.37
134.70
134.87
137.34
140.46
140.55
153.87
154.42
159.12
163.00
CF3
NH
O
N
N
0
20
40
60
80
100
120
140
160
180
200
f1 (ppm)

HPLC trace

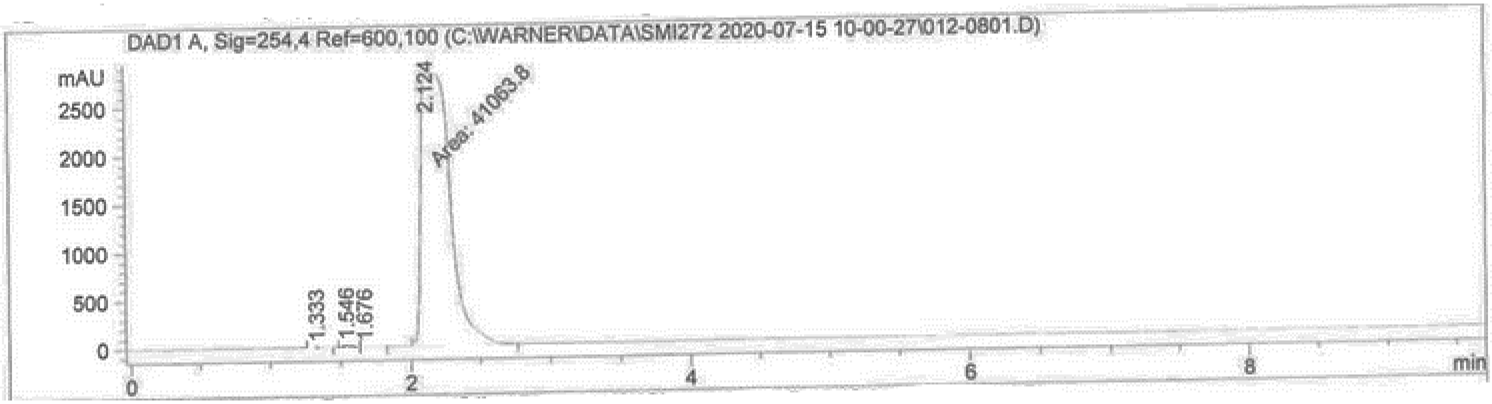

```
Signal 1: DAD1 A, Sig=254,4 Ref=600,100

Peak RetTime Type  Width     Area      Height     Area
  #   [min]        [min]   [mAU*s]     [mAU]        %
----|-------|----|-------|----------|----------|--------|
   1   1.333 BB    0.0671   15.54854    3.41494   0.0378
   2   1.546 BV    0.0605   75.73083   19.01193   0.1839
   3   1.676 VB    0.0973   15.07549    2.11074   0.0366
   4   2.124 MM    0.2422 4.10638e4  2825.19800  99.7417
```

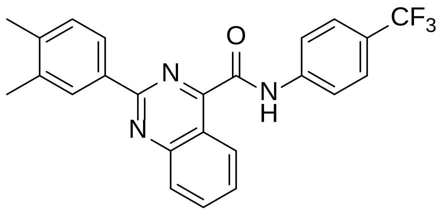

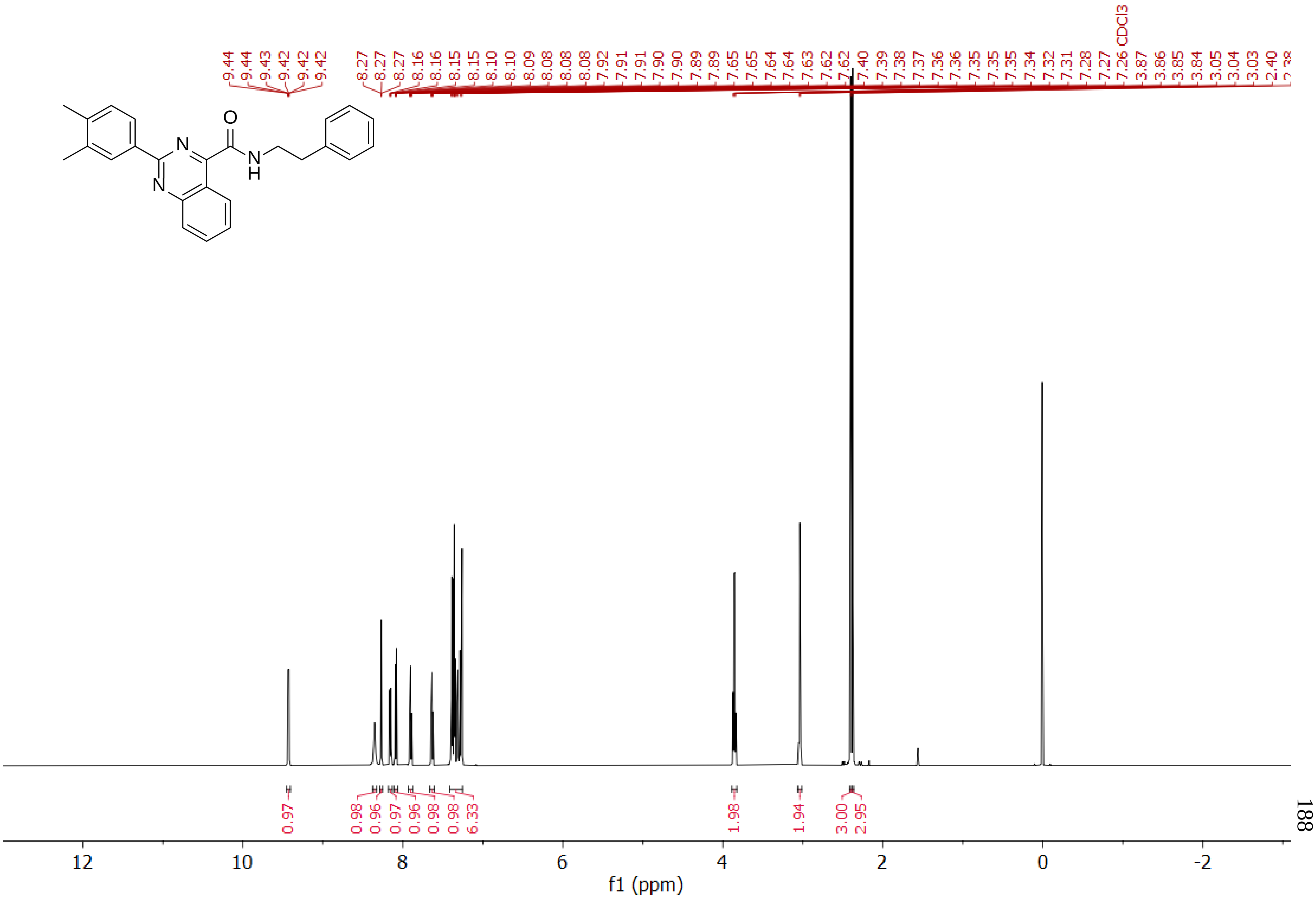
9.44
9.44
9.43
9.42
9.42
9.42
8.27
8.27
8.27
8.16
8.16
8.15
8.15
8.10
8.10
8.09
8.08
8.08
8.08
7.92
7.91
7.91
7.90
7.90
7.89
7.89
7.65
7.65
7.64
7.64
7.63
7.62
7.62
7.40
7.39
7.38
7.37
7.36
7.36
7.35
7.35
7.35
7.34
7.32
7.31
7.28
7.27
7.26 CDCl3
3.87
3.86
3.85
3.84
3.05
3.04
3.03
2.40
O
N
N
N
H
0.97
0.98
0.96
0.97
0.96
0.98
0.98
6.33
1.98
1.94
3.00
2.95
12
10
8
6
4
2
0
-2
f1 (ppm)

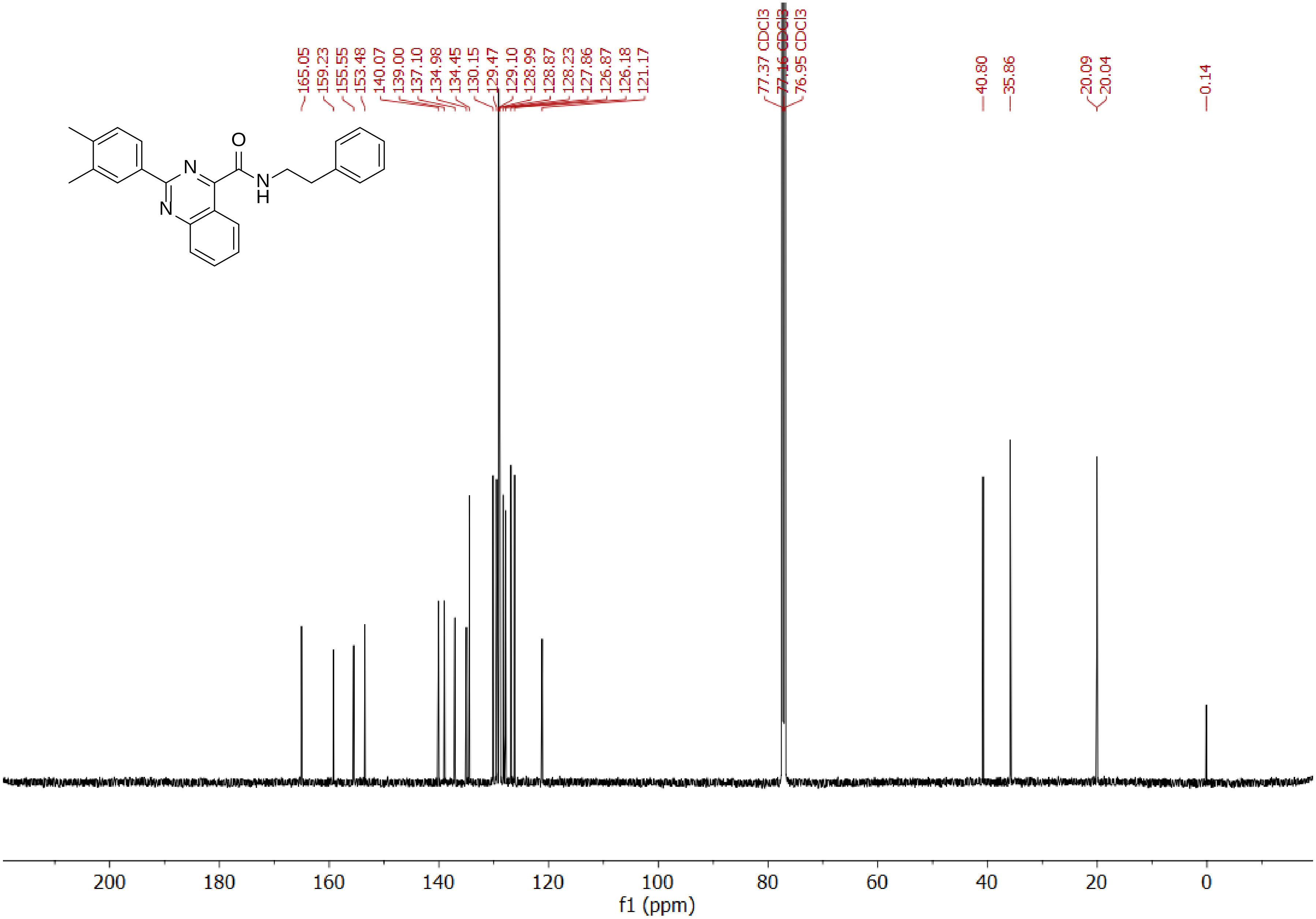
165.05
159.23
155.55
153.48
140.07
139.00
137.10
134.98
134.45
130.15
129.47
129.10
128.99
128.87
128.23
127.86
126.87
126.18
121.17
77.37 CDCl3
77.16 CDCl3
76.95 CDCl3
40.80
35.86
20.09
20.04
0.14
O
N
N
N
H
200
180
160
140
120
100
80
60
40
20
0
f1 (ppm)

HPLC trace

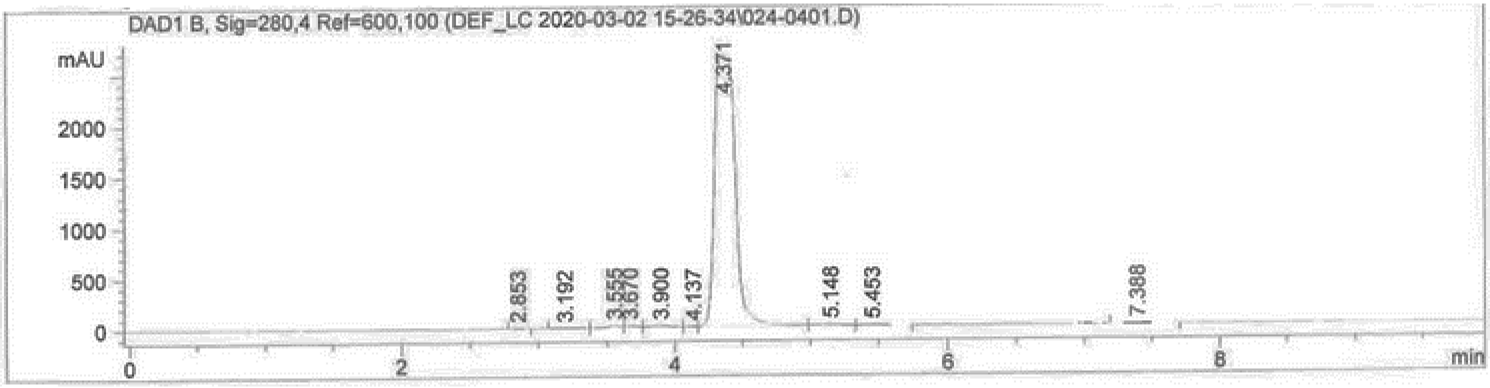

```
Signal 2: DAD1 B, Sig=280,4 Ref=600,100

Peak RetTime Type  Width     Area      Height     Area
  #   [min]        [min]   [mAU*s]     [mAU]        %
----|-------|----|-------|----------|----------|--------|
   1   2.853 VV    0.0875    6.21807    1.14164   0.0212
   2   3.192 VV    0.1570   18.42031    1.59160   0.0628
   3   3.555 VV    0.1095  147.40688   20.60254   0.5029
   4   3.670 VV    0.0910  101.98436   16.76869   0.3479
   5   3.900 VV    0.1369  175.61510   18.14682   0.5991
   6   4.137 VV    0.0689   24.50010    5.21023   0.0836
   7   4.371 VV    0.1709 2.85146e4  2662.81689  97.2782
   8   5.148 VV    0.2127  220.53885   15.80996   0.7524
   9   5.453 VB    0.1496   93.77029    9.30493   0.3199
  10   7.388 BB    0.1416    9.37805    1.05625   0.0320
```

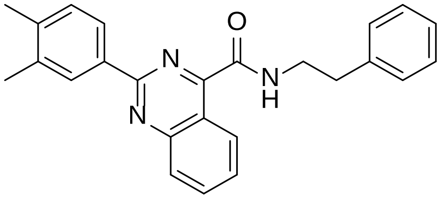

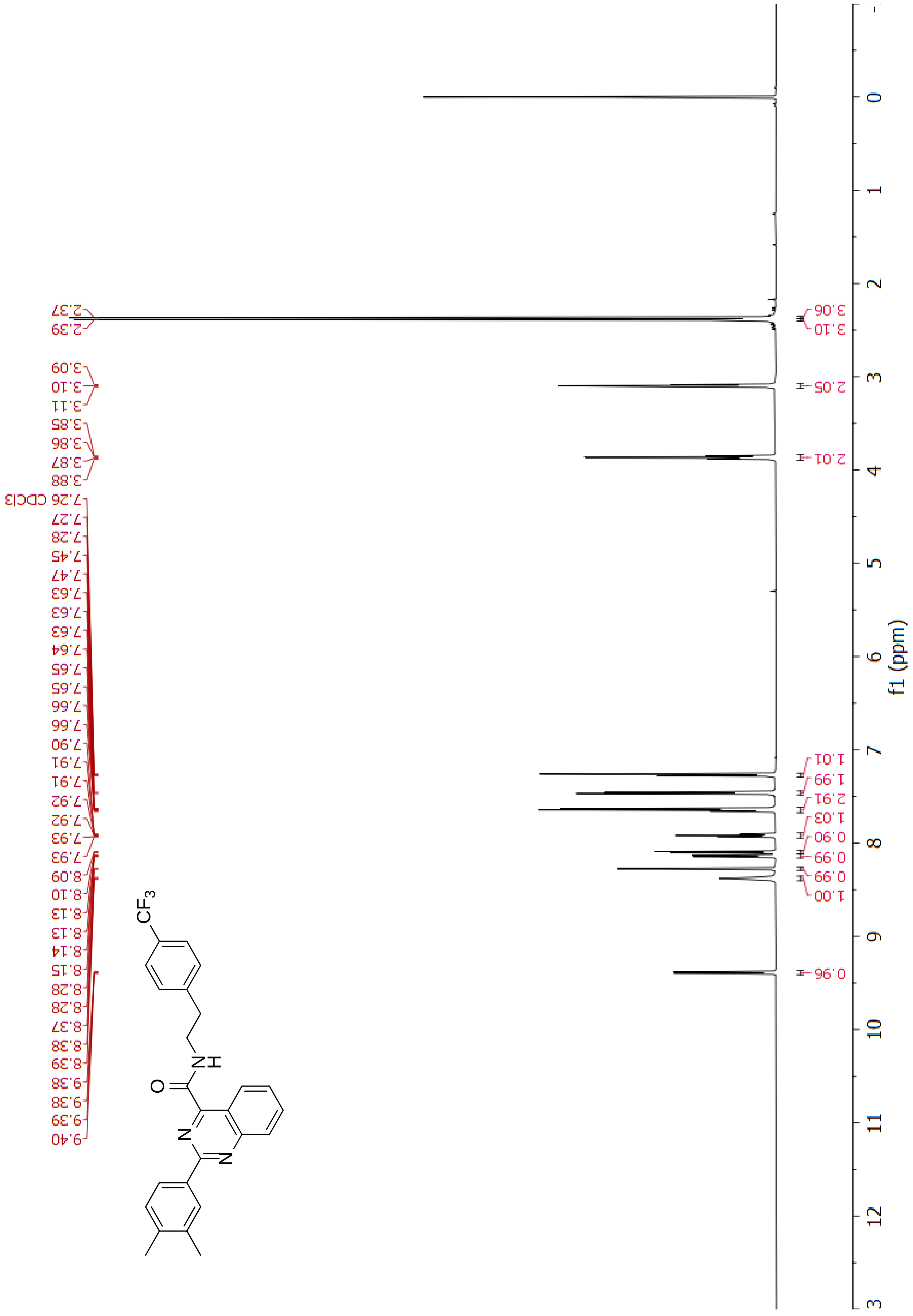
2.37
2.39
3.09
3.10
3.11
3.85
3.86
3.87
3.88
7.26 CDCl3
7.27
7.28
7.45
7.47
7.63
7.63
7.63
7.64
7.65
7.65
7.66
7.66
7.90
7.91
7.91
7.92
7.92
7.93
7.93
8.09
8.10
8.13
8.13
8.14
8.15
8.28
8.28
8.37
8.38
8.39
9.38
9.38
9.39
9.40
3.06
3.10
2.05
2.01
1.01
1.99
2.91
1.03
0.90
0.99
0.99
1.00
0.96
CF3
N
H
O
N
N
0
1
2
3
4
5
6
7
8
9
10
11
12
3
f1 (ppm)

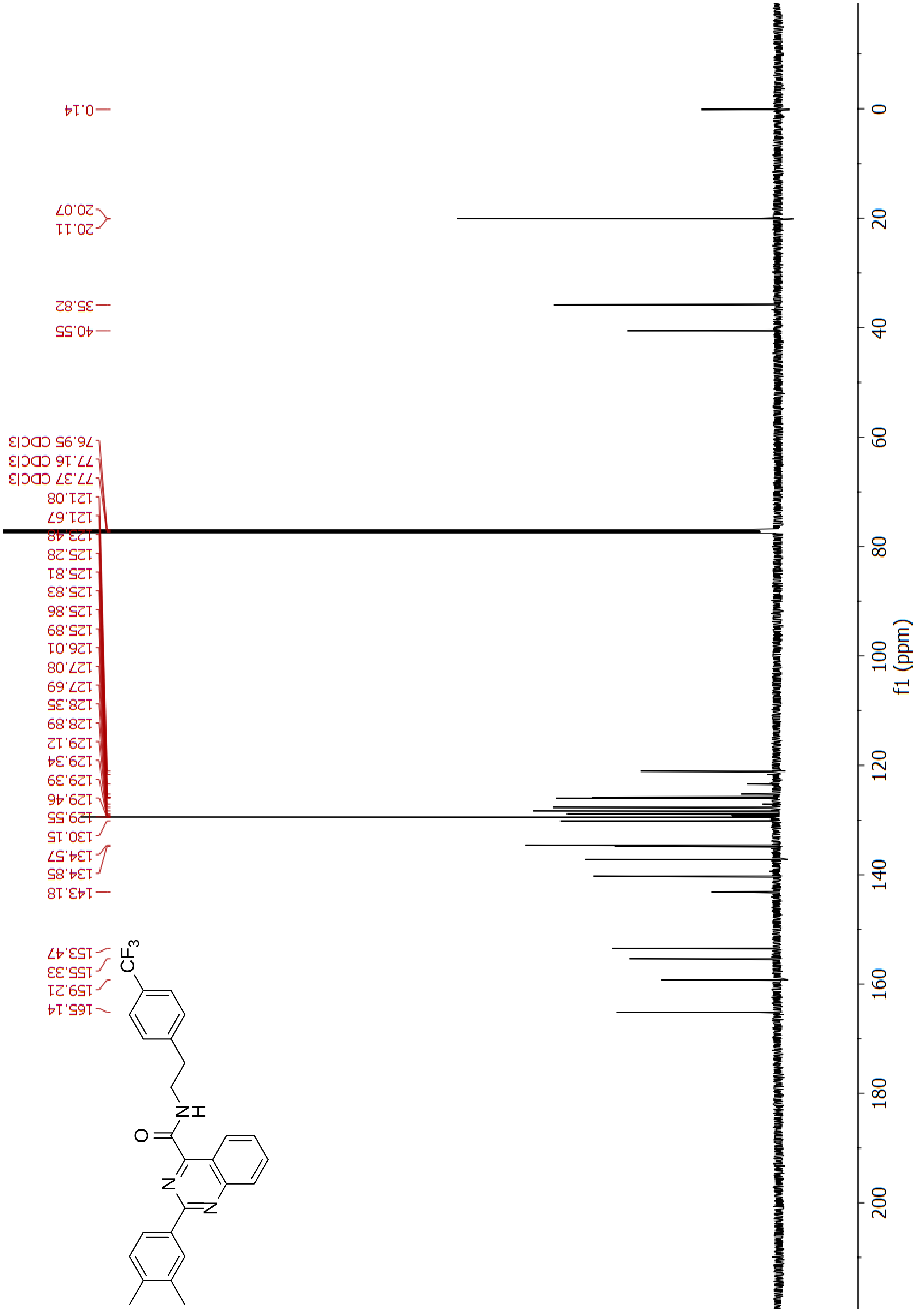
165.14
159.21
155.33
153.47
143.18
134.85
134.57
130.15
129.55
129.46
129.39
129.34
129.12
128.89
128.35
127.69
127.08
126.01
125.89
125.86
125.83
125.81
125.28
123.48
121.67
121.08
77.37 CDCl3
77.16 CDCl3
76.95 CDCl3
40.55
35.82
20.11
20.07
0.14
CF3
NH
O
N
N
200
180
160
140
120
100
80
60
40
20
0
f1 (ppm)

HPLC trace

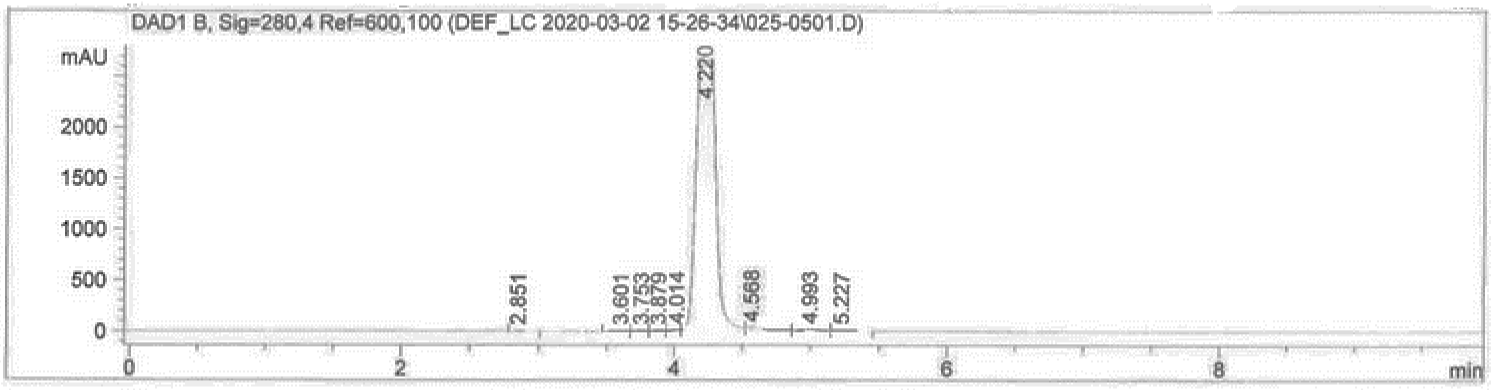

```
Signal 2: DAD1 B, Sig=280,4 Ref=600,100

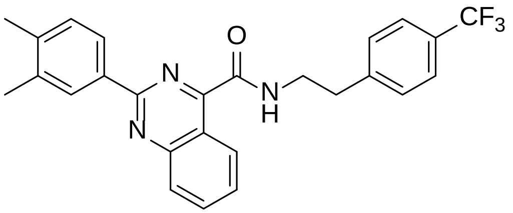Peak RetTime Type  Width     Area      Height     Area
  #   [min]        [min]   [mAU*s]     [mAU]        %
----|-------|----|-------|----------|----------|--------|
   1   2.851 VB    0.0915    6.15903    1.06470   0.0221
   2   3.601 BV    0.0978   31.78654    4.88964   0.1139
   3   3.753 VV    0.0872   42.37677    7.35797   0.1518
   4   3.879 VV    0.0895   54.99839    9.23160   0.1970
   5   4.014 VV    0.0723   80.21304   16.04592   0.2873
   6   4.220 VV    0.1647 2.70949e4  2662.01392  97.0519
   7   4.568 VV    0.1564  359.63678   30.76706   1.2882
   8   4.993 VV    0.1520  184.01021   17.03725   0.6591
   9   5.227 VB    0.1387   63.86432    6.60915   0.2288
```